Eastern Pacific background state and tropical South American climate history during the last 3 million years.

Dissertation
Zur Erlangung des Doktorgrades
Der Naturwissenschaften
- Dr. Rer. Nat. –

Am Fachbereich Geowissenschaften
Der Universität Bremen

Vorgelegt von
Daniel A. Rincón Martínez

Bremen
June 2013

Supervisor:

Prof. Dr. Ralf Tiedemann

Co-supervisor:

Prof. Dr. Dierk Hebbeln

This thesis was accomplished with financial support from the *Deutsche Forschungsgemeinschaft* (DFG) through grants Ha 2756/9-1 and TI240/17-2) and was carried out under the Bremen International Graduate School for Marine Sciences “Global Change in the Marine Realm” (GLOMAR).

KURZFASSUNG

Im tropischen Pazifik reagieren die Konvektion und Windänderungen direkt auf die zonale Verteilung der Oberflächentemperaturen und haben einen tiefgreifenden Einfluss auf Auftrieb, Thermoklinen-Tiefe, Produktivität, Staubdüngung, Fluss-Sedimenteintrag, und kontinentale Aridität der nicht-konvektiven Regionen. Obwohl sich unser Verständnis der heutigen dynamischen Interaktion zwischen Ozean und Atmosphäre im tropischen Pazifik stark verbessert hat, bleiben noch viele Unsicherheiten bestehen. Diese betreffen besonders die Reorganisationen der tropischen Konvektion unter verschiedenen Klimaszenarien der Vergangenheit (z.B. Eiszeiten) und bezüglich der zukünftigen Klimaentwicklung. Gegenstand dieser Dissertation ist eine Verbesserung unserer Kenntnis der Ablagerung von fluviatil transportiertem terrigenem Material in Tiefseesedimenten des östlichen tropischen und subtropischen Pazifik. Diese Eintrag soll in Beziehung mit der Entwicklung der Paläozeangraphie des östlichen tropischen Pazifiks (EEP) und des kontinentalen Klimas entlang der Westküste Südamerikas über das Plio-Pleistozän gebracht werden.

Kapitel 4 beinhaltet die Untersuchung der Artenzusammensetzung und stabilen Sauerstoffisotopie von Foraminiferen an Oberflächensediment-Proben (10°N - 25°S, 100°W - 70°W), um die Lage der äquatorialen Front zu definieren. Das Probenmaterial wurde mittels Multicorer, Boxcorer, Schwerlot- und Kolbenlotkernen gewonnen. Dabei zeigte sich, dass das Verhältnis der Häufigkeit von *G. menardii cultrata* und *N dutertrei* abundances ($R_{c/d}$) sowie die Sauerstoffisotopendifferenz zwischen *G. ruber* und *G. tumida* ($\Delta\delta^{18}O_{G.tumida\text{-}G.ruber}$) und zwischen *P. oliquiloculata* und *G. tumida* ($\Delta\delta^{18}O_{G.tumida\text{-}P.obliquiloculata}$) sehr gute paläozeanographische Werkzeuge für die Rekonstruktion der Breitengradlage der ostpazifischen Äquatorialfront im Gebiet zwischen Cocos und Carnegie Rücken sind.

Kapitel 5 präsentiert eine kombinierte Analyse von Proxydaten zur Rekonstruktion von päläozeangraphischen Änderungen im EEP und Schwankungen des kontinentalen Paläoklimas im angrenzenden Hinterland über die letzten 500 ka. Die Proxy-Daten beruhen auf Proben von Sedimentkernen vor der Küste Ecuadors (ODP Site 1239) und im Panama Becken (Kern MD 02-2529). Die Daten zeigen ausgeprägte Glazial/Interglazialschwankungen im fluviatilen Sedimenteintrag, die humidere Klimabedingungen im Küstenbereich von Ecuador während Warmzeiten dokumentieren. Humidere Interglaziale werden wahrscheinlich durch wärmere Wassertemperaturen in der EEP „cold tongue“ und eine Südverlagerung des EF-ITCZ –Systems gesteuert. Entsprechend zeigt der geringere Eintrag fluviatiler Sedimente während der Glaziale aridere Bedingungen an, die mit größeren SST Gradienten im tropischen Pazifik und einer nördlicheren Lage des EF-ITCZ-Systems übereinstimmen. Die latitudinalen Verschiebungen des EF-ITCZ-Systems könnten lediglich auf den EEP und die Küstengebiete des nordwestlichen Südamerikas beschränkt sein. Die glaziale Abkühlung war besonders im Südost-Pazifik ausgeprägt, welches die Möglichkeit beinhaltet, dass die ITCZ Verschiebungen im Arbeitsgebiet durch eine verstärkte nordwärts-gerichtete Advektion von kalten Wassermassen des Humboldt Stromsystems kontrolliert wurden. Über dem pazifikfernen südamerikanischen Kontinent, bestimmen die Anden und das Amazonasbecken die atmosphärischen Zirkulationsmuster. Deshalb sind hier Südverlagerungen der ITCZ während Glazialzeiten aufgetreten.

Kapitel 6 behandelt molekulare Fossilien von marinen und terrestrischen Organismen, um Umweltbedingungen im hochproduktiven Küstenauftriebsgebiet von Peru (ODP Site 1229) während des letzten Interglazials im Vergleich zum späten Holozän zu rekonstruieren. Die Ergebnisse geben Hinweise auf erhöhten Regen und Flusseintrag am Nordrand der Atacama-Wüste in Peru während des letzten Interglazials. Die warmen Oberflächenwasser, erhöhte

Wassersäulen-Stratifizierung, geringere Primärproduktion und feuchteren Klimabedingungen während des letzten Interglazials waren wahrscheinlich mit einer langfristen Erwärmung des Klimazustands im tropischen Pazifik verbunden.

Im **Kapitel 7** rekonstruieren wir den äolischen Sedimenteintrag in den Südost-Pazifik (ODP Site 1237) über die letzten 500 ka. Dabei benutzen wir verschiedene Proxy-Datensätze. Diese beinhalten Korngrößenverteilungen, Th-Isotope und die geochemischen Zusammensetzung der Sedimente, die eine Differenzierung zwischen Änderungen der Windintensitäten und Klimaänderungen in den Herkunftsgebieten (Atacama Wüste und aride Küstengebiete in Peru) vorzunehmen. Die Ergebnisse dieser Studie zeigen, dass das westliche Südamerika, südlich des Golf von Guayaquil arider während der Glaziale und humider während der Interglaziale der letzten 500 ka war. Diese Ergebnisse unterstützen die allgemeine Idee von global „staubigeren“ Glazialen gegenüber humideren Interglazialen.

Im **Kapitel 8** werden Oberflächenwasser-Temperaturen und marine Produktivität basierend auf dem Alkenon-Biomarker, Biogen-Opal, organischem Kohlenstoff, Gesamtstickstoffgehalt und Stickstoffisotope für den Plio-Pleistozänen Klima-Übergang rekonstruiert (ODP Site 1239), um die verschiedenen Regulationsprozesse von Produktivitätsänderungen im äquatorialen Pazifik aufzuschlüsseln. Wir fanden, dass das Produktivitätsmaximum während der letzten 3 Ma zwischen 2,4 und 1,6 Ma auftrat. Abgeschwächte Produktivität charakterisierte die spätpliozäne/pleistozäne Abkühlung und das mittlere und späte Pleistozän.

SUMMARY OF THIS RESEARCH

Nowadays reorganizations of tropical Pacific convection and wind variability respond to the zonal distribution of sea surface temperatures and have a profound effect on the Pacific Ocean's upwelling, thermocline depth, productivity, dust fertilization, riverine sediment loads, and continental dryness of the non-convective regions. Though much progress has been made in the understanding of the present dynamical interaction between the ocean and the atmosphere, many uncertainties remain concerning tropical reorganizations of convection under different climatic scenarios, such as future global warming and ice ages. The subject of this thesis is to gain deeper insights into the deposition of windblown and fluvially transported terrigenous material in deep-sea sediments of the easternmost tropical and subtropical Pacific Ocean and its relationship to the evolution of the eastern tropical Pacific background state and the continental climate of the west coast of South America over Plio-Pleistocene time.

In **Chapter 4** a set of surface sediment samples (10°N - 25°S, 100°W - 70°W) was analyzed to define the location of the equatorial front in the Pacific, based on foraminifer's census and stable isotope data. The sample material was obtained by means of multi-corers, box-corers, gravity or piston corers. We propose that the ratio between *G. menardii cultrata* and *N dutertrei* abundances ($R_{c/d}$) as well as the oxygen isotopic difference between *G. ruber* and *G. tumida* ($\Delta\delta^{18}O_{G.tumida\text{-}G.ruber}$) and between *P. oliquiloculata* and *G. tumida* ($\Delta\delta^{18}O_{G.tumida\text{-}P.obliquiloculata}$) are useful paleoceanographic tools for reconstructing the latitudinal position of the eastern Pacific Equatorial Front in an area delimited by the Cocos and Carnegie ridges.

Chapter 5 provides a combined analysis of proxy data that allude to paleoceanographic changes in the EEP and concomitant continental paleoclimate variations onshore during the past 500 kyr. The proxy profiles are derived from samples obtained from sediment cores off the coast of Ecuador (ODP Site 1239) and in the Panama Basin (core MD02-2529). We find prominent glacial-interglacial changes of fluvial sediment input that reflects more humid conditions along the Ecuadorian coast during interglacials. A warmer interglacial EEP cold tongue and a southward shift of the EF-ITCZ system likely control these humid interglacial conditions. Conversely, reduced fluvial input during glacials suggests more arid conditions coinciding with larger tropical Pacific SST gradients and a more northward location of the EF-ITCZ system. The glacial-interglacial latitudinal shifts of the EF-ITCZ system suggested by our data may be restricted to the EEP and the coastal area of northwest South America. Glacial cooling is particularly pronounced in the Southeast Pacific, which suggests a possibility that ITCZ migration in the region may be controlled by the northward advection of cold waters with the Humboldt Current system. Over the South American continent, away from the coast, the Andes and Amazon Basin impact atmospheric circulation patterns, allowing larger southward migrations of the ITCZ during glacial periods.

In **Chapter 6** we deal with molecular fossils of marine and terrestrial organisms to reconstruct environmental changes in the highly productive Peruvian coastal upwelling region (ODP Site 1229) comparing the last interglacial vs. the late Holocene. Our results provide evidence of increased rainfall and river runoff over the northern extension of the Atacama Desert (Peru) during the last interglacial. The warm surface waters, enhanced water column stratification, lower primary productivity and wetter conditions of the last interglacial were probably associated with a long-term warming of the tropical Pacific mean state.

In **Chapter 7** we reconstruct eolian input into the southeast Pacific (ODP Site 1237) covering the last 500 ka. By doing so, we used multiple proxies, including grain-size distributions, Th-

isotopes, and the geochemical composition of the sediment allowing us to differentiate between changes in wind intensities and climatic changes in the source areas (Atacama Desert and the arid coasts of Peru). The results of this study demonstrate that western South America, south of the Gulf of Guayaquil, was more arid during glacials and more humid during interglacials of the past 500 ka, corroborating the general idea of globally dustier glacials vs. more humid interglacials.

In **Chapter 8** sea surface temperatures and marine productivity based on the alkenone biomarker, biogenic opal, total organic carbon, total nitrogen and nitrogen isotopes are reconstructed for the Plio-Pleistocene climatic transition to disentangle the different processes regulating the eastern equatorial Pacific productivity record (ODP Site 1239). We found that for the last 3 Ma the maxima in productivity occurred between 2.4 and 1.6 Ma, while weakened productivity characterized the late Plio/Pleistocene cooling and the mid-to-late Pleistocene.

ACKNOWLEDGEMENT

Yo creo que la verdad es perfecta para las
matemáticas, la química, la filosofía,
pero no para la vida. En la vida,
la ilusión, la imaginación, el deseo,
la esperanza cuentan más.

I believe that truth is perfect
for maths, chemistry and philosophy,
but not for life. In life,
aspiration, imagination, yearning
and hope are by far more important.

Ernesto Sabato

This thesis benefited from help, contribution and support I received from many (ex) colleagues, friends and my family.

First of all, I would like to thank my supervisor Prof. Dr. Ralf Tiedemann and my co-supervisor Dr. Frank Lamy for their constant support over the last years, for giving me the opportunity in the Alfred Wegener Institute (AWI), for all the fruitful discussion, reviews on the various abstracts, presentations, and papers over the years. I appreciate a lot that I was always free, to a certain degree, to pursue my own interest within my Ph.D. Project.

Secondly, I thank my second co-promotor Prof. Dr. Dierk Hebbeln for providing me a dedicated research-training program through the graduate school GLOMAR. All the training courses and meetings will have an ever-lasting effect on me. I would like to thank all the GLOMAR Staff especially for their endless support during the years in Bremen.

I particularly would like to thank all my (ex-) colleagues at the Alfred Wegener Institute, especially David, Cornelia, Ines, Micha and Magaly for the stimulating work atmosphere. In addition, I would like to thank all my fellow Ph.D. students at the AWI over the years who are not mentioned above but whom made my time in Bremerhaven much more fun. I thank Lisa for her friendship and support, and David for our morning-to-evening chats on various subjects, be it science, work or whatever the topic you brought up – I will miss them. Cristiano Chiessi, and Rik Tjallingii, from Bremen, thanks for the discussions about paleoceanography, especially XRF. Silke Steph is thanked for her help with writing the first manuscript, and providing constructive comments on oxygen isotope analysis.

My short research stay in Kiel would not have been possible without the funding of GLOMAR and the support of Prof. Dr. Raplh Schneider. During those months at *Christian Albrechts Universität zu Kiel* I made friends with the French speaking crew: Johan Etourneau, Guillaume Leduc and Nabil Khélifi who made my stay much more enjoyable and made me feel welcomed. Thank you guys for the nicest summer I spent in Germany. Special thanks also go to Dr. Thomaz Blanz, who helped me with the laboratory work in Kiel.

I thank Prof. Dr. Henry Hooghiemstra, whom hosted me twice at the University of Amsterdam

and offered a great deal of scientific and moral support. I had the chance to interact with other colleagues that widen my scientific vision and offered enormous support. Thank you.

I am very grateful to all my colleagues and co-authors, who contributed with their enthusiasm and specific knowledge to my chapters/publications. Prof. Dr. Andreas Mackensen (AWI) for helpful discussions in Chapter 4. I also would like to thank Prof. Dr. Reiner Schlitzer for making available Ocean Data View and for teaching me how to handle it; Sergio Contreras for showing up with this nice idea of measuring taraxerol in Chapters 5 and 6; Guillaume Leduc for his rocket-science comments in Chapter 5, Johan Etourneau for being a solid partner for three years, building together our own projects.

I very much acknowledge the help I received from Lisa Schönborn at AWI (for mass spectrometer measurements), Silvia Koch at CAU (for alkenone measurements), Susanne Wiebe, Rita Fröhlking, Ute Bock, Ingrid Stimac, and Ilsetraut Stölting Reza Ahi and all the Colombian girls at AWI (for technical help and assistance with sample preparation). The IODP core repository staff at the MARUM in Bremen made sampling-life very easy.

I also like to thank Dr. Ignacio Martinez, my former supervisor at the Universidad EAFIT, who initially introduced me to the world of Palaceanography and micropaleontology, for his continuous enthusiasm, support and interest in me and my research over the last 10 years.

Finally I would like to thank friends and family for the interest, concern and support over the years. I extremely value the long friendships I have with Sergio and Juancho who were always there for me, particularly when I needed to drink. Even though I have lived far, or not so far, away from them, it never made any difference to our friendship. This is true brotherhood.

I am very grateful to my family who gave me the opportunity to have the education that brought me to Germany. I appreciate a lot that they were never holding me back but supporting every step, every decision I took. Without their loving support, I would not have been able to achieve this. Thank you very, very much!

Last but not least I would like to thank Yina for his never-ending support, patience and unconditioned love during those years in Germany. You were really always there for me, at 8 o'clock in the morning, at 8 o'clock in the evening, at midnight, or whenever I came home and make me feel a better man.

CONTENTS

LIST OF FIGURES AND TABLES

CHAPTER 1

INTRODUCTION

1.1 Research foci and objectives

The tropics are often the focus of the discussion of climate change, owing to the fact that the global atmospheric circulation is highly sensitive to tropical Pacific sea surface temperature (SST) anomalies. Though much progress has been made in the understanding of the present dynamical interaction between the ocean and the atmosphere, many uncertainties remain concerning tropical reorganizations of convection under different climatic scenarios, such as future global warming and ice ages (Mechoso et al., 2005). Nowadays reorganizations of tropical Pacific convection and wind variability respond to the zonal distribution of SSTs and have a profound effect on the Pacific Ocean's upwelling, thermocline depth, productivity, dust fertilization, riverine sediment loads, and continental dryness of the non-convective regions. Moreover, the atmospheric teleconnections associated with SST anomalies in the equatorial Pacific alter the air temperature, humidity, winds, and clouds far from the equatorial Pacific.

In the tropics, changes in precipitation/aridity are dynamically linked to SSTs through the El Niño–Southern Oscillation (ENSO) phenomenon (E.g., Wyrtki 1975; Rasmusson and Carpenter 1982), which represents the leading mode of variability for both precipitation and SST (E.g., Dai and Wigley 2000). For instance a number of studies have identified the key role played by ENSO on rainfall anomalies found over most of the South American region, including the Ecuador–Peru coast, Colombia, Venezuela, southern Brazil, Uruguay and northeastern Argentina (E.g. Ropelewski and Halpert, 1987; Chu, 1991; Pisciottano *et al*., 1994; Diaz et al., 1998; Grimm et al., 1998). To what extent there is a robust signature of continental precipitation/aridity in response to tropical SSTs on timescales longer than instrumental record has not been explicitly addressed. Paleoclimate reconstructions of tropical Pacific SST fields and continental precipitation anomalies have a unique and critical role to play in improving our understanding of the range of tropical climate variability and sensitivity and in developing a predictive knowledge of the role that the tropics play in global climate change. Thus, paleoclimatic reconstructions offer the only source of information on long-term changes in tropical variability and its teleconnections, but they require the perspective of instrumental data for process understanding, and deriving a broader context when interfaced with numerical simulations of the ocean and atmosphere.

Through the combined use of bulk geochemical parameters, molecular biomarkers, and stable isotopes, the general scope of this thesis is to gain deeper insights into the deposition of windblown and fluvially transported terrigenous material in deep-sea sediments of the easternmost tropical and subtropical Pacific Ocean and its relationship to the evolution of the eastern tropical Pacific background state and the continental climate of the west coast of South America over Plio-Pleistocene time. The main objectives of this thesis are to:

- Reconstruct the modern spatial pattern of planktonic foraminifera oxygen isotopes variability in the southeast Pacific from surface sediment samples.
- Characterize the "primary signature" of cold-saline and warm-less saline waters in oxygen isotopes of planktonic foraminifera from surface sediment samples collected over the southeast Pacific.
- Reconstruct changes in terrigenous input during the Late Pleistocene, based on the analysis of different organic and inorganic proxies.
- Compare the different proxy records to assess how different proxies reflect terrigenous input.
- Determine possible sources and transport processes of terrigenous material deposited in marine sediments off South American west coast.
- Reconstruct paleo-sea surface temperatures and relate the results to the eastern Pacific background state.

• Reconstruct oceanic productivity, based on organic geochemistry and relate the results to nutrient supply, thermocline depth and the mean background state of the tropical Pacific.
• Relate the proxy records to paleo-environmental changes in the location and area of the convective moisture source region and to changes in the intensity of trade winds during the last 3 million years.

1.2. Terrigenous sources, transport and signal in deep-sea sediments

Terrigenous sediments are those that accumulate from rock fragments, grains of clastic minerals and argillaceous materials and are transported to the marine environment mainly through fluvial or eolian pathways. The type and amount of terrigenous material on marine sediments reflect the climatic conditions affecting adjacent continental regions, and/or the oceanic and atmospheric circulation at the time of deposition (E.g. McManus, 1970; Kolla et al., 1979). The terrigenous sediments most likely to reach the deep sea are the clays, which arrive at the ocean margins in suspension, either in the air over the oceans or in surface waters, and may be transported by wind and ocean currents thousands of kilometers from their terrestrial source. The type and amount of terrigenous material depend on climatic conditions on the continent.

About 84% of terrigenous material in the ocean reaches by the rivers of by direct continental runoff (Lisitzin, 1996), providing the crucial transfer of mass between terrestrial and marine realms. Gravel and sand, being larger, usually settle near shore. Muds (silt- and clay-sized sediments) are carried in suspension by moving water and begin to settle out soon after the river water meets the ocean, though finer clay particles remain in suspension for years, allowing them to be conveyed far out into the ocean before settling to the bottom. Eliminating influences due to bedrock geology, riverine sediment loads are controlled by those factors that control erosion and sediment delivery, such as local topography (mean gradient, relief, elevation), soil properties, climate (precipitation trends, temperature), catchment vegetation cover, catchment morphology, drainage network characteristics, and land use (Hovius, 1998). These factors may be most adequate at describing the influence of weathering, hill slope erosion and fluvial transport on the rate of denudation, but they only explain half of the observed variance of that rate. It is demonstrated that rate of uplift of rock is a control on regional denudation rates of an importance similar to, or greater than that of climatic and topographic factors (Hovius, 1998).

The tropical rivers across the globe drain a variety of geologic–geomorphologic settings: (a) orogenic mountains belts, (b) sedimentary and basaltic plateau/platforms, (c) cratonic areas, (d) lowland plains in sedimentary basins and (e) mixed terrain. All of them show clearly high but variable peak discharges during the rainy season and a period of low flow when rainfall decreases. Some tropical rivers show two flood peaks, a principal and a secondary one, during the year in accordance to the annual precipitation cycle (Latrubesse et al., 2005). Tropical drainage basins situated in high relief, active orogenic belts have very high sediment production. Rivers draining the Andes of South America transport a large quantity of sediments. For instance with a drainage area of 257,000 km^2, the Magdalena, which drains the Colombian Andes, contributes 144 to 220 million tons of suspended sediment to the Caribbean sea (E.g. Milliman and Meade, 1983; Restrepo and Kjerfve, 2000). In South America, the Andes act as an orographic barrier to the incoming air masses from the east, thereby increasing rainfall along the Eastern Andes slope from Venezuela to Argentina. High relief and heavy concentrated precipitation produce high sediment yield in mountainous basins: rainfall can reach more than 6000 mm/year in some parts of the subandean zones of Equator, Peru and Bolivia (Latrubesse et al., 2005). Rivers draining platforms, cratonic areas or a combination of different geological domains in savannas or mixed savanna/forest environments, for example

the Araguaia-Tocantins, Paraná and Orinoco rivers, show lower sediment yields when compared to tropical mountain rivers but higher values when compared with rainforest cratonic/plateau rivers.

The fine-grained sediments that reach the deep-sea in regions remote from direct terrigenous sources are predominantly windblown, which makes up for more than 7% of terrigenous material in the ocean (Lisitzin, 1996). Wind-borne mineral aerosol (dust) includes volcanic ash and terrigenous silts and clays. Particles from each of these sources can tell something about the provenance from which they came. Concentrations and fluxes of terrigenous material have proved to be change greatly in association with rapid climate change in the Quaternary, for instance, in the transitions from glacial to interglacial regimes. The linkage of the climate system and the dust cycle makes eolian dust as retrieved from natural archives a valuable proxy to learn about past climatic variability, especially changes in atmospheric circulation patterns. Dust accumulation rates provide information on changes in the dust cycle, comprising dust source, transport and deposition.

Generation and transport of dust are extremely sensitive to climate. At the present day, the removal of sedimentary material from land surfaces by wind and its transport through the atmosphere for great distances is possible wherever a cover of vegetation does not protect the surfaces of the soil or rocks. Therefore, the main sources of aerosols are deserts and semiarid regions, where de soil cover is absent. The large changes in dust emissions and transport seen from the palaeo-dust record may reflect a variety of processes: changes in sources and source conditions; changes in vegetative cover; sub-aerial erosion of emergent continental shelves; deflation from periglacial deposits; variations in wind speed and gustiness; changed wind patterns linking sources to deposition areas; changes in deposition along the dust transport path (E.g. Jickells et al., 2005; Maher et al., 2010).

Investigation of various proxies observed in terrigenous material deposited in marine sediments of the easternmost tropical and subtropical Pacific could elucidate our knowledge about paleo-environmental conditions. Specific organic compounds (lipid biomarkers) and pollen records can also help identifying terrigenous input, especially from higher plants (e.g. certain steroids, lignin or long-chain odd-carbon-numbered n-alkanes and n-alkanols), and climatic conditions over the land masses. For instance Heusser and Shackleton (1994) and Gonzalez et al. (2006) reconstructed the paleoclimatic conditions (e.g. precipitation) and vegetation of western South America based on pollen records. Similar to pollen, biomarkers of unambiguous terrestrial origin are also common in marine sediments and can even be dominant in coastal regions with high fluvial inputs (E.g. Hu et al., 2009) or open ocean settings where aeolian terrestrial inputs are greater than pelagic ones (E.g. Pagani et al., 2000).

Geochemical element concentrations and element ratios are useful tools to gain information about changes in the sediment provenance, transport and deposition. Elemental fluxes depend upon the weathering intensity, which in turn is controlled by the vegetation coverage on the continents. However, the interpretation of sedimentary signals depends of how many sources should be taken in account and how far from the continent the samples are taken from. For instance, on the continental margins, and as part of the essentially fine-grained particles transported by the river, one can include Fe particles (resultant from the weathering of continental rocks and soils). Therefore, the Fe content of the sediments has been used as a simple chemical proxy for the input of land-derived materials and Fe variations are considered to be a direct measure of rainfall and river input by several authors such as Haug et al. (2001) and Pattan et al. (2012). On the other hand, in many open-ocean regions the input of new iron to the surface sediments is dominated by the atmospheric deposition of particulate and soluble iron in mineral aerosols (E.g., Fung et al., 2000; Sarthou et al., 2003; Jickells et al.,

2005) and hence its content can be interpreted on terms of changes in the dust cycle, related primarily to aridity and vegetation cover at the source, the atmospheric structure, wind speed, and precipitation that regulate its entrainment and removal (E.g. Jickells et al., 2005).

Grain-size distribution of siliciclastic marine sediments has been used as indicators of changes in wind strength and/or changes in the distance of the deposited dust from the source area (E.g., Sarnthein et al., 1981; Rea, 1994; Prins and Weltje, 1999) and in few cases to distinguish between fluvial and eolian transport (E.g., Stuut et al., 2002; Holz et al., 2004). Using eolian grain size as a paleoclimate proxy for changing wind strength is based on the assumption that mineral aerosol size distribution tend to stabilize after transport distances of several thousand kilometers because larger grains have already settled out due to gravitational fallout (Prospero et al., 1985). Thus, downcore changes composition of dust and its grain size distribution at a certain location will probably record changes in wind strength, depending on the dust event and its transport path (E.g. Rea, 1994; Clemens, 1998; Hovan, 1995).

Accordingly, in this study, siliciclastic, iron, aluminium and titanium accumulation rates were generated to represent the variability in terrigenous supply to the easternmost tropical and subtropical Pacific to draw inferences about changes in western South American continental climate. The high terrigenous flux suggests intensive hydrolysis resulting in enhanced erosion due to increased precipitation. Continental derived biomarker proxies were examined to check the source of terrestrial organic matter. Additionally, grain-size distributions of the lithogenic fraction were analyzed to reconstruct relative changes in southeast trade-wind strength. Major attention was turned on the coherence between different (inorganic and organic) proxies in marine sediments deposited during the past 3 Million years.

1.3. Tropical Pacific background state

Nowadays, the background state of the tropical Pacific Ocean is characterized by large zonal and meridional SST asymmetries, with a warm pool in the west, an eastern equatorial cold tongue (EECT), and a northern intertropical convergence zone (ITCZ). The warm surface waters of the western Pacific warm pool give rise to atmospheric convection, driving easterly trade winds at the surface, and promoting a zonal circulation cell denominated Walker circulation (Bjerknes, 1969; Figure 1.1). Simultaneously, in the vicinity of the equator, warm tropical air rises and flows toward the poles until it reaches the subtropics where it descends and returns towards the equator in the surface layers as the trade winds, forming what is known as Hadley Circulation. On the global scale, the ITCZ constitutes the rising branch of the Hadley circulation, known as ITCZ, and is characterized by a belt of low-level convergence and upper-level divergence with strong upward motion, frequent cloudiness, and intense rainfall (Sansom, 1965). The modern ITCZ is at latitude close to the insolation induced SST peak (Chao, 2000). The latent heat released in the convective clouds of the ITCZ plays a central role in maintaining tropical circulation, transporting heat and momentum poleward, and balancing water and energy in the troposphere (Waliser and Gautier, 1993). Displacements of the ITCZ have been suggested as the main way for the tropics to respond during climate change on a variety of time scales. Over the eastern-central Pacific and Atlantic Oceans, the ITCZ is mostly in the Northern Hemisphere (between 5°N and 20°N), and exhibits a distinct annual cycle in its strength and latitudinal locations, being farthest from the equator in July and closest to the equator in January (E.g. Mitchell and Wallace 1992; Xie 1994).

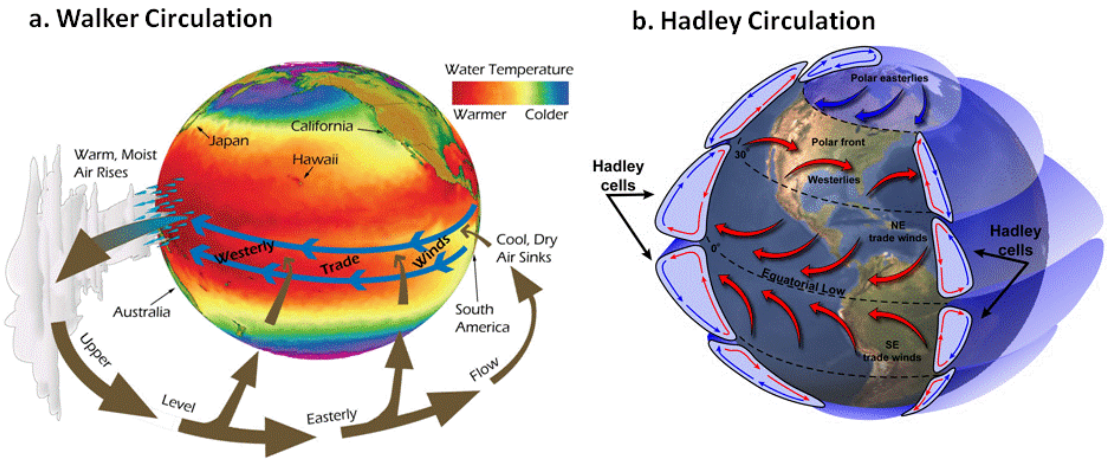

Figure 1. 1 Sketch illustrating the tropical atmospheric circulation. (a) This is a three-dimensional view of the Walker circulation, which consists of trade winds blowing from east to west across the tropical Pacific Ocean (blue arrow), bringing moist surface air to the west. In the western tropical Pacific, the moist air rises, forming clouds. The rising air becomes drier as much of its moisture falls to the surface as rain. Winds a few miles high blow from west to east, moving the now drier air toward South America. The air returns back to the surface in the eastern tropical Pacific, dry and relatively cloud free, completing the circulation loop. Changes under warming are exaggerated for emphasis. (b) Hadley circulation: three major convective cells between the equator and the pole. Easterly winds predominate near the equator and in the lower atmosphere at the poles. Elsewhere westerlies are dominant. Illustration credit: Gabriel A. Vecchi, NOAA Geophysical Fluid Dynamics.

Despite a solar radiation forcing at the top of the atmosphere that is zonally uniform and nearly symmetrical about the equator in the annual mean, the asymmetric SST features of the tropical Pacific background state are generated and maintained by complex ocean–atmosphere-land interactions (Takahashi and Battisti, 2004). The easterly trade winds advect warm surface waters to the tropical west Pacific and cause deeper, colder waters to upwell off the west coast of South America, therefore maintaining the zonal surface temperature gradient. The great height and continuity of the Andes Cordillera forms a sharp barrier to zonal flow, resulting in strong southerly winds parallel to the coasts of Chile and Peru, promoting vigorous coastal upwelling (Garreaud and Muñoz, 2005). As a result, the coastal Chilean and Peruvian upwelling waters are seasonally advected into the EECT (Fiedler and Talley, 2006). The cold surface water of the later, in combination with warm, dry air aloft, supports the largest and most persistent subtropical stratocumulus deck in the world (Klein and Hartmann, 1993). Philander et al. (1996) and Philander et al. (1999) pointed out that stratocumulus clouds off Peru contribute decisively to the meridional asymmetries in the climate of the tropical eastern Pacific, where SSTs are colder in the Southern Hemisphere than in the Northern Hemisphere. The colder ocean surface underlying the stratocumulus resulted in increased zonal and meridional SST gradients and enhanced Walker and Hadley circulations. Consistently, there was increased surface evaporation and cooler SSTs immediately to the north of the region with artificially increased clouds. Oceanic advection propagated the cooling toward and along the equator. Thus all the above-mentioned interactions give rise to a background state which is self-reinforcing, but which represents a state of unstable equilibrium.

One of the most important sources of year-to-year natural climatic variability is the El Niño-Southern Oscillation (ENSO). On a timescale of two to seven years, the eastern tropical Pacific climate varies between anomalously cold (La Niña) and warm (El Niño) conditions (Figure 1.2). These swings in SST are accompanied by changes in the structure of the subsurface ocean; variability in the strength of the equatorial easterly trade winds; shifts in the position of atmospheric convection; and global teleconnection patterns associated with these changes that lead to variations in rainfall and weather patterns in many parts of the world (E.g. Wyrtki,

1975; Hamilton and Garcia, 1986; Alexander and Scott, 2002; Alexander et al., 2002; Haylock et al., 2006; McPhaden et al., 2006; Wang and Fiedler, 2006). During El Niño events the trade winds weaken along the equator as atmospheric pressure rises in the western Pacific and falls in the eastern Pacific. Anomalous warming in the central and eastern Pacific ensues and the weakening of the Walker atmospheric circulation across the tropical Pacific is accompanied by a deepening of the thermocline by 5–10 m in much of the eastern tropical Pacific, especially along the equator, but shoaling towards the west along the equator and in the subtropics (E.g. Wyrtki, 1975; Fiedler and Talley, 2006; McPhaden et al., 2006; Wang and Fiedler, 2006).

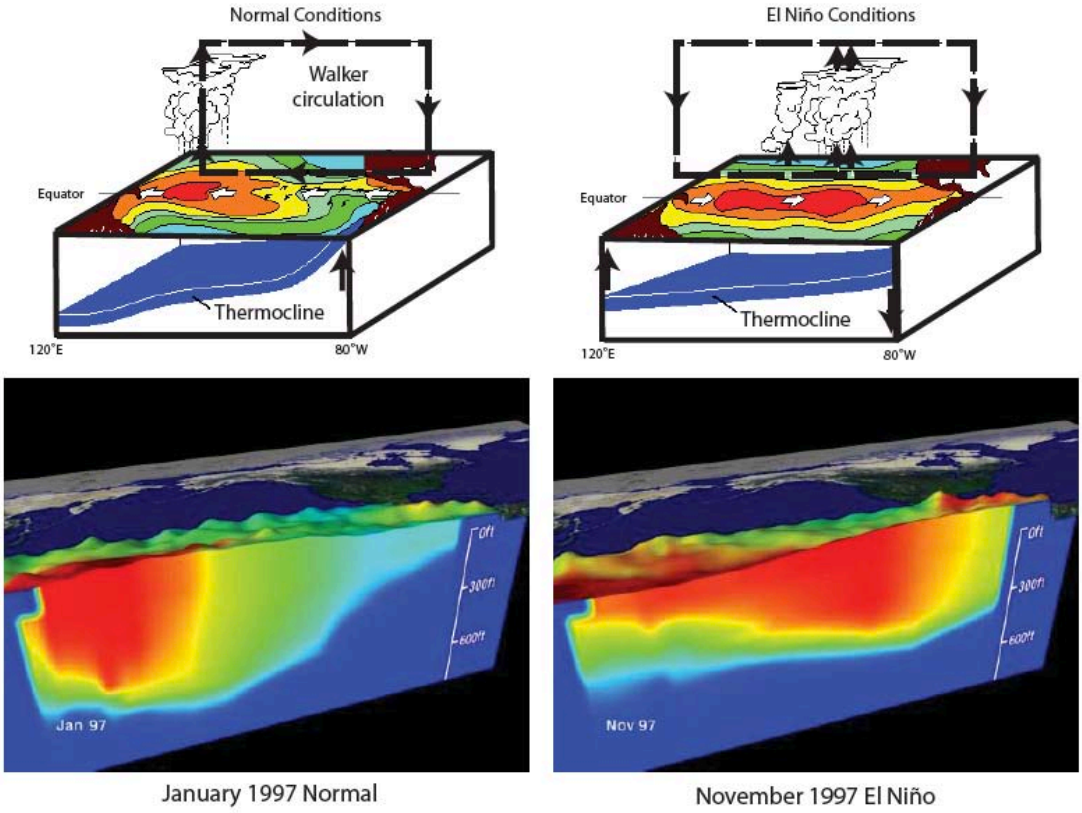

Figure 1. 2 Comparison of normal and El Niño conditions in the modern ocean, from Ravelo (2006). Schematic of normal conditions includes strong Walker circulation or convective loop, and strong east-west temperature gradient and thermocline tilt (upper left); schematic of El Niño conditions includes weakened Walker circulation, temperature gradient, and thermocline tilt (upper right). Equatorial Pacific cross sections of temperature prior to El Niño (January 1997), when sub-surface temperature gradient is relatively large (lower left), and during an El Niño (November 1997), when sub-surface temperature gradient is relatively small (lower right). Sea surface height is represented by bumps. Temperature range is from 30°C (red) to 8°C (blue). The thermocline is at approximately the 20°C isotherm (the border between dark blue and cyan).

ENSO-related impacts on precipitation in the eastern equatorial Pacific (EEP) are strongly linked to meridional adjustments of the ITCZ (E.g., Deser and Wallace 1990). During El Niño the reduction of off-shore upwelling, and the spatial extent of the EECT permits the southward shift of the ITCZ, resulting in an anomalously strong local meridional (Hadley) circulation and abnormally heavy rainfall over the ordinarily arid coastal region of Ecuador and Peru and over Southern Brazil, Paraguay and northern Argentina (E.g. Hastenrath, 1978; Hamilton and Garcia, 1986; Aceituno, 1988; Waylen and Poveda, 2002; Haylock et al., 2006), and a reduction in seasonal mean rainfall over much of Central America, the Caribbean and the northern portion of South America (E.g. Hastenrath, 1978; Aceituno, 1988; Waylen and Poveda, 2002; Haylock et al., 2006). During La Niña the ITCZ shifts northward, with attendant weakening of the local Hadley circulation and causing the opposite effect on precipitation patterns. The strong

correlation between the precipitation frequency/intensity and SST variability in western South America (E.g. Rossel et al., 1996; Bendix and Bendix, 2006; Haylock et al., 2006) suggests that precipitation proxy records located in major loading and discharging regions such as offshore South America will have high skill in reconstructing past ENSO conditions.

For the purpose of this study, we may define the terms "El Niño-like" and "La Niña-like" climate change to denote patterns of mean change (or trend) in the equatorial Pacific, which resemble at the ocean surface and in the atmosphere, a present day El Niño or La Niña event. El Niño–like convey nothing more than a warming in the eastern equatorial Pacific and a lower SST gradient between the eastern equatorial Pacific and western equatorial Pacific WEP condition, but this does not, by any means, imply a that permanent or perennial El Niño state. An ENSO analogy is invoked for interpreting tropical Pacific climate change because if an external forcing introduces some east-west asymmetry, this asymmetry can be amplified in the same way, as interannual perturbations are, through the positive ocean-atmosphere feedback.

1.4. Plio-Pleistocene climate and the tropical Pacific paleoceanography

The past 5 million years of Earth history are part of the Cenozoic era and encompass three relatively recent climate intervals: the globally warm climate of the Early and Middle Pliocene epoch, the transition from an ice-free planet to the onset of the glacial–interglacial cycles during the Late Pliocene, and the Quaternary Period with dramatic and frequent changes in global climate, alternating warm interglacials with cold ice ages (Figure 1.3a). Mean annual temperatures during and early Pliocene (4.0–4.2 Ma) and the middle Pliocene (3.0–3.3 Ma) were 4°C and 2.5°C, warmer than preindustrial conditions, respectively (E.g. Haywood and Valdez, 2004; Brierley, 2009; Haywood et al., 2009a). The greatest warming appears to have been in the high latitudes where temperatures were often elevated enough to prevent continental glaciers in the northern hemisphere (Haywood et al., 2009) and references therein). Greenland and North Canada were forested, with possible small glacier outlets and terrestrial summer temperatures between 5 and 4 Ma were 19°C warmer than today (E.g. Ballantyne et al., 2006; 2009). Global sea-level (eustatic) estimates with a peak of ~22 m higher than present for the Pliocene interval 2.7–3.2 Ma (E.g. Miller et al., 2012), perhaps higher, which would have inundated many low-lying coastal regions and suggest a significant reduction of Antarctic continental ice volume. Atmospheric CO_2 estimates for the warm Pliocene (E.g., Pagani et al., 2010 and references therein) are not well constrained (330–425 ppmv), but appear comparable to 390 ppmv measured in 2011 and higher than pre-anthropogenic levels (280 ppmv). The CO_2 increases and associated feedbacks reconstructed for the Pliocene would imply a very high Earth-system climate sensitivity, which would explain the warmth of the Pliocene globally but not regionally (Haywood et al., 2009b). Therefore to explain the regional changes in surface temperature suggested by palaeoclimate proxies (E.g. Crowley, 1996) additional mechanisms working independently or combined with variations in CO_2 concentrations in the atmosphere are required to drive and maintain the warming over longer timescales (E.g. Haywood et al., 2009b; Pagani et al., 2010). Roughly at 3 Ma, the global scenario changed progressively (Figure 1.3a). At this time, the closure of the Panama and Indonesia corridors in the tropical oceans was complete (E.g. Keigwin et al., 1982; Coates et al., 1992; Haug and Tiedemann, 1998; Srinivasan and Sinha, 1998; Cane and Molnar, 2001; Karas et al., 2009), especially affecting deep thermohaline circulation, thus contributing to a substantial reorganization of the oceanic and atmospheric system. The tectonically driven closure of the Panama seaway, led to an increase of the salinity contrast between the Pacific and Atlantic oceans, increased oceanic northward heat transport, and warmer and more evaporative surface water masses in the North Atlantic (E.g. Keigwin, 1982; Burton et al., 1997; Mikolajewicz and Crowley, 1997; Haug and Tiedemann, 1998; Haug et al., 2001b; Steph et al., 2010). This led to increased atmospheric moisture in the Arctic, greater snowfall over

Greenland and ultimately an increase in ice volume. This hypothesis is supported by the coincidental timing of changes in salinity gradient between the Caribbean basin and the east Pacific, and pulses of increased ice rafted debris on the Icelandic Plateau (Figure 1.3b; E.g. Bartoli et al., 2005). On the other hand, the restricted Indonesian Gateway might led to a switch in Indonesian throughflow source waters from initially South Pacific to cooler North Pacific subsurface waters (E.g. Cane and Molnar, 2001; Karas et al., 2009). The associated changes in the thermocline might have preconditioned the cooling of the Benguela upwelling system and contributed to the global cooling of the thermocline. In the same way, Karas et al. (2009) suggest that the addition of a larger portion of subantarctic mode water into the equatorial undercurrent supported the final formation of the equatorial eastern Pacific cold tongue.

The onset of intensive glaciations on Greenland, Scandinavia, and North America occurred during the Pliocene epoch between 3.6 and 2.7 Ma, and mechanisms of the gradual amplification of glacial cycles since the Late Pliocene, remains a subject of persistent discussion (see the review of Raymo and Huybers, 2008). However, a recent modeling study suggested that a decrease in atmospheric CO_2 from a Pliocene level of 400 ppmv to the preindustrial maximum of 280 ppmv is most likely the culprit causing the onset of permanent Northern Hemisphere glaciations (Lunt et al., 2008). The glacial-interglacial cyclicity, linked to the waxing and waning of the Northern Hemisphere ice sheet, has been attributed to variations in solar radiation, related to Milankovitch cycles (caused by periodic variations in orbital parameters such as the tilt of the Earth's axis). During the Pleistocene the dominant periodicity of glacial–interglacial cycles changed from 41 kyr to 100 kyr (Lisiecki and Raymo, 2005). This shift from high-frequency, low-amplitude of the Late Pliocene/Early Pleistocene towards the low-frequency, high-amplitude of the Late Pleistocene is known as the Mid-Pleistocene Transition, which began 1.25 Ma ago with a gradual increase (decrease) in average ice volume (deep-water temperature), paralleled the emergence of the 100 kyr cycle, with this transition reaching completion by 700 ka when maximum glaciations became the dominant and characteristic features of the Earth's climate system of the Late Pleistocene (Clark et al., 2006).

The Pliocene and the Pleistocene tropical oceans are completely different in terms of SST, circulation, biological productivity, and upwelling states. For instance, Pliocene reconstructions of SST in the tropical and subtropical oceans show that cold surface waters were absent from the upwelling zones off the coasts of western South America (E.g. Haywood et al., 2005; Dekens et al., 2007), southwest Africa (E.g. Marlow et al., 2000; Etorneau et al., 2009) and California (E.g. Ravelo et al., 2004; Haywood et al., 2005) up to 3 Ma ago. Warmer waters also prevailed in the subtropical northeast Atlantic margin (E.g. Herbert and Shuffert, 1998), and the North Atlantic (E.g. Robinson et al., 2008; Robinson, 2009; Naafs et al., 2010), the subtropical northeast Pacific margin (E.g. Brierley et al., 2009). Most of the observed decline in the latitudinal temperature gradient during the Pliocene can be explained by increased poleward heat transport, which can be either oceanic (E.g. Dowsett et al., 1992) or atmospheric (E.g. Haywood et al., 2009a).

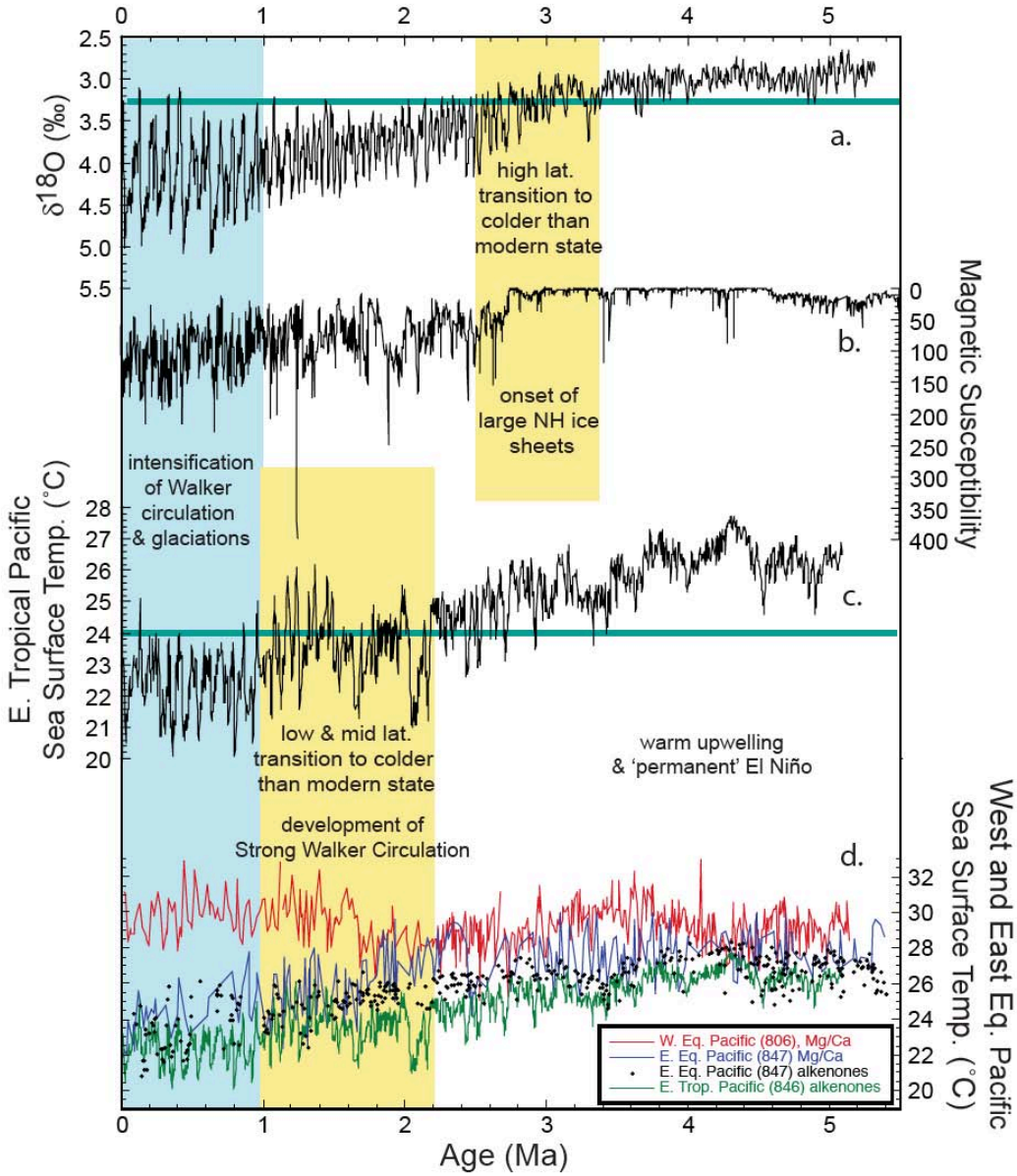

Figure 1. 3 Records of regional climate and ocean change over the last 5 million years, from Ravelo (2006). **(a)** Plio-Pleistocene composite of benthic $d^{18}O_{cal}$ record, from Lisiecki and Raymo (2005) that summarizes the growth of high-latitude ice sheets with the modern ice-volume size indicated by the green horizontal line. **(b)** The magnetic susceptibility record (Haug et al., 1999) indicates the concentration of ice-rafted debris in sediments in the North Pacific. **(c)** The alkenone-derived SST record from eastern tropical Pacific ODP Site 846 (Lawrence et al., 2006) with the modern temperature indicated by the green horizontal line. **(d)** The Mg/Ca-derived SST record from the western tropical Pacific (ODP Site 806) compared to the Mg/Ca and alkenone-derived SST records from the eastern tropical Pacific (ODP Sites 847 and 846), showing the increase in west-east temperature difference across the equatorial Pacific as climate cooled. Mg/Ca data is from Wara et al. (2005); alkenone data from Site 847 are from Dekens et al. (2007).

Most of Early to Mid-Pliocene proxy climate reconstructions of SST in the western and eastern equatorial Pacific from Mg/Ca and alkenone-based paleothermometry and $\delta^{18}O$ records suggest an El Niño-like state, characterized by a substantial reduction in the east-west SST gradient (Figure 1.3d; E.g. Cannariato and Ravelo, 1997; Ravelo et al., 2004; Wara et al., 2005; Lawrence et al., 2006; Li et al., 2011) and a strong reduction in the SST gradient from the equator to the subtropics described, which implies a vast poleward expansion of the ocean low-latitude warm pool (E.g. Brierley et al., 2009; Li et al., 2011). When compared to the present, the small east-west gradient prior to 2.7 Ma, combined with warmer subsurface temperatures (E.g. Rickaby and Halloran, 2005; Wara et al., 2005; Ravelo et al., 2006; Steph et

al., 2010), resulted in a deepening of the thermocline, a reduction of upwelling intensities in the tropical and eastern Pacific Ocean, and a dramatic modification of heat distribution and wind regimes by alteration of the pressure gradient (E.g. Fedorov et al., 2006; Ravelo et al., 2006). Additionally, meridional expansion of the warm pool provided a crucial mechanism for maintaining El Niño-like state, because cold water in the modern eastern equatorial Pacific is sourced from the subtropical subduction zones. Poleward expansion of the warm pool into the subduction regions would lead to warmer waters upwelling in the eastern equatorial Pacific, a deeper ocean thermocline, and consequently a substantial reduction of the SST gradient along the equator (E.g. Brierley et al., 2009). Furthermore, according to a simulation of the reduced meridional temperature gradient in an atmospheric general circulation model (Brierley et al., 2009), the ITCZ would widen and its precipitation intensity would decrease. Molnar and Cane (2002) compared the global effects of El Niño in the present-day climate with the differences found in paleo-records between the middle Pliocene and today's climates. They concluded that an El Niño-like state characterized the climate up to 3 Ma.

The gradual end of Pliocene warmth began about 3.6 Ma ago at both low and high latitudes, and was accompanied by an increase of the low-latitude zonal and meridional temperature gradients that forced the gradual contraction of the warm pool towards the equator (Ravelo, 2010). The increase in low-latitude zonal and meridional temperature gradients began to accelerate between 2.2 and 2.0 Ma ago, at least half a million years after the great expansion of Northern Hemisphere ice sheets, which was pronounced about 2.75 Ma ago (Etorneau et al., 2010). After that time cool water appeared at the surface in the tropical Pacific and Atlantic (Figure 1.3c, d). This altered the ocean's heat budget and circulation, allowing conditions in high latitudes to influence tropical SST by vertically shifting the thermocline, and introducing climate feedbacks: the wind-driven circulation acquired a meridional overturning component with much stronger upwelling at the equator (Philander, 2010). The long term cooling trend observed in the eastern Pacific and eastern Atlantic upwelling regions (E.g. Marlow et al., 2000; Wara et al., 2005; Lawrence et al., 2006; Dekens et al., 2007; Brierley et al., 2009; Etourneau et al., 2009) does not appear to occur in the west. Although the recent work by Herbert et al. (2010) indicate progressive cooling in glacials over the past 3.5 Ma in the tropical ocean, no obvious long term cooling since the Pliocene has been found in the western Pacific warm pool (E.g. Wara et al., 2005), so that the SST gradient along the equator in the Pacific increased as we approached the present. This difference between the eastern and western Pacific is a consequence of a long-term shoaling of the thermocline; because of its downward slope to the west, it affected SST strongly in the east but not the west (Philander, 2010). Therefore, although weakening of the El Niño-like state and intensification of the Walker circulation began during the Late Pliocene, a modern analog state started only from ~1.6 Ma, as revealed earlier from SST differences between the western and eastern tropical Pacific (Ravelo et al., 2004).

The Middle and Late Pleistocene was characterized by the shoaling of the thermocline and the development of active upwelling cells (linked to wind-cell intensification) in the equatorial Pacific Ocean and in the eastern side of ocean basins, provoking a net increase of primary productivity in these regions (E.g. Marlow et al., 2000) and thus likely an enhanced drawdown of atmospheric CO_2. During 1.6–0.9 Ma, the west–east ΔSST decreased mainly due to increasing SST during interglacial stages in the east (Li et al., 2011). The zonal ΔSST decreases may indicate a weakening Walker circulation, but whether the interglacial SST increases in the east were related to the return of an El Niño-like state is not clear. Since 0.9 Ma, after the dominant climate cycles shifted from 41 ka to 100 ka, the ΔSST between the western and eastern tropical Pacific has been fluctuating mainly between 3 and 6 °C (Li et al., 2011).

The response of the eastern tropical Pacific to Late Quaternary glacial-interglacial climate

changes has been discussed controversially. Some authors suggest that oceanographic changes in the region are regulated by high latitude climate (E.g. Pisias and Mix, 1997; Lea et al., 2000; Feldberg and Mix, 2003; Spero et al., 2003; Lea et al., 2006; Leduc et al., 2007; Pena et al., 2008). In contrast, other studies indicate that the tropical Pacific responds independently of variations in high latitude climate and might have behaved similar to the warm phase of El Niño during glacial times (E.g. Koutavas et al., 2002; Koutavas and Lynch-Stieglitz, 2003), while others consider a scenario rather similar to the cold La Niña phase (E.g. Andreasen and Ravelo, 1997; Martínez et al., 2003). Climate simulations, using models with different levels of complexity, indicate that the north-south position of the ITCZ responds to thermal forcing in the extratropics (i.e. changes in interhemispheric temperature contrast). Paleoclimate data on a variety of timescales suggest a similar behavior, with ITCZ moving away from a cooled hemisphere or toward a warmed hemisphere. Koutavas and Lynch-Stieglitz (2004) found that the marine ITCZ in the eastern Pacific is displaced southward when ice sheets at glacial maxima cooled the Northern Hemisphere. Evidence from the Cariaco Basin in the tropical Atlantic also indicates very strong coupling between tropical circulation and high-latitude climate change through the last glacial–interglacial transition (E.g. Lea et al., 2003). Modeling studies support the premise that the ITCZ is sensitive to ice cover (E.g. Chiang and Bitz, 2005) and to the Atlantic thermohaline circulation (E.g. Zhang and Delworth, 2005). In simulations with an atmospheric model coupled to a slab ocean, Broccoli et al. (2006) show that imposing antisymmetric interhemispheric heating in high latitudes induces a displacement of the ITCZ toward the warmer hemisphere.

Despite these previous studies, it remains uncertain whether an El Niño-like state existed during the Early and Late Pliocene. Rickaby and Halloran (2005) provided conflicting interpretations of the same datasets to the mean state changes to equatorial Pacific SSTs, suggesting that the SST of the western equatorial Pacific warm pool remained relatively stable and consistently warmer than the eastern equatorial Pacific, and that the Pliocene was characterized by la Niña-like conditions. On the other hand, the glacial increases in both, zonal and meridional, thermal gradients since the mid-Pliocene imply the intensification of the Walker circulation and Hadley circulation. However, as mentioned above, different opinions exist about the tropical Pacific means state over glacial-interglacial times. These uncertainties highlight the need of a better understanding of the dynamics of ocean circulation, upper ocean stratification, and atmospheric processes in the tropical Pacific.

1.5. The Plio-Pleistocene orography and its effects in atmospheric circulation and South American climate

The Andean Cordillera extends for 9,000 km along the western coast of South America, from Venezuela to the northern part of Tierra del Fuego, and the widest are 750 km in Bolivia (Figure 1.4a). It is classically subdivided in three morphostructural domains. The southern Andes extend from the islands off southern South America in the Scotia Sea at 55°S to the Gulf of Penas at 47°S. They are the lowest in average elevation at just over 1 km, and their post-Paleozoic/Early Mesozoic history is slightly older than the mountains to the north, reflecting to some extent the opening of the Atlantic Ocean along the mid-Atlantic Ridge. The opening began in the south at ca. 120 Ma ago and progressed northward until South America separated from Africa at ca. 90 Ma ago (Cordani et al., 2000). The Antarctic Plate subducting beneath the South American Plate generates the principal tectonic forces in the southern Andes, but the region is also affected by jostling at the triple junction between the Nazca, South American, and Antarctic plates, and the Scotia Plate influences it to some extent (Blisniuk et al., 2006). The central Andes are the longest segment of the mountain range and comprise 5,200 km of the 9,000- km length. It is the widest at 750 km and the highest at 3.5–4 km, including Cerro Aconcagua at 6,962 m. The central Andes extend from the Gulf of Penas

northward to around a megashear zone called the Guayaquil-Caracas at ca. 2°S near the Gulf of Guayaquil (Cordani et al., 2000). Uplift of the central Andes during the Cenozoic is directly related to the subduction of the Nazca Plate below the South American Plate (Gregory-Woodzicki, 2000). The northern Andes extend from 5°S at about the Guayaquil-Caracas Megashear at 2°S to the Oca, Romeral, and other fault systems across northern South America at the contact with the Caribbean Plate at ca. 12°N. The Andes branch in southwestern Colombia to form the Cordilleras Occidental, Central, and Oriental. The Cordillera Oriental branches again into the Serranía de Perijá and the Eastern Cordillera de Mérida in Venezuela, which two branches, enclose Lake Maracaibo (Cordani et al., 2000). The northern Andes are as complex as the central Andes, but their uplift and other features are due to the interaction of the South American, Caribbean, Cocos, and the northern portion of the Nazca Plates (Gregory-Woodzicki, 2000).

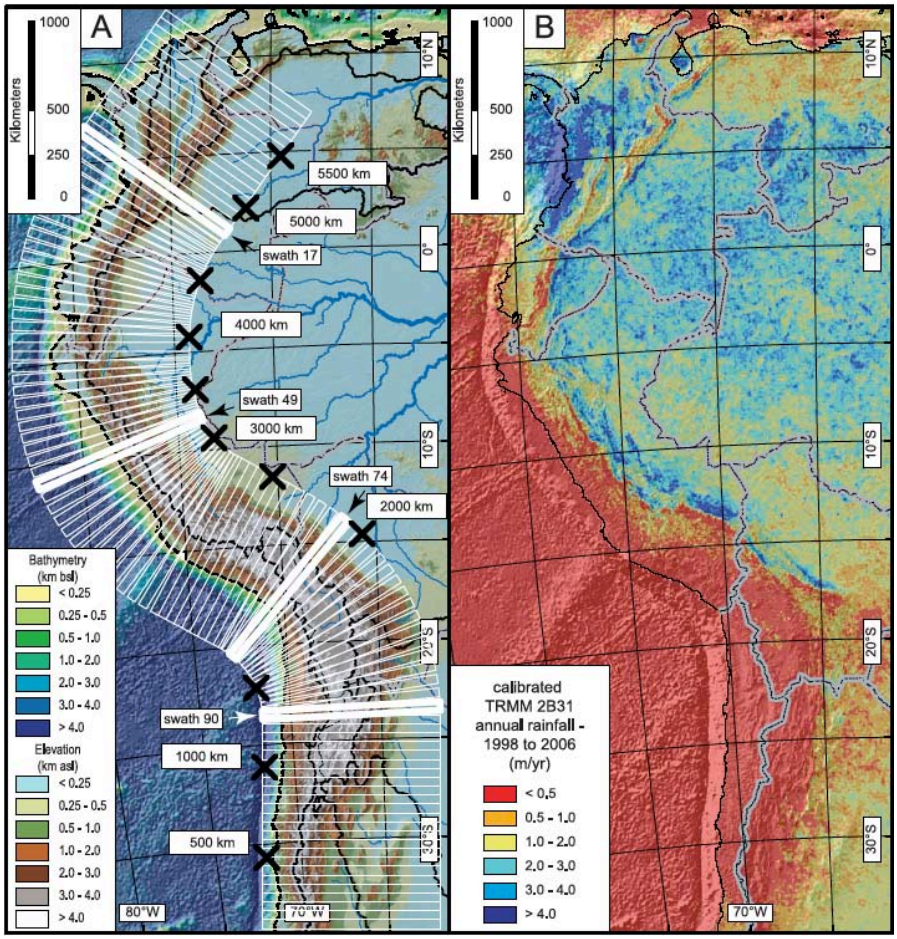

Figure 1. 4 **(a)** Color-coded topography of the Andes, from Bookhagen and Strecker (2008). White polygons mark the 115 50-km-wide and 1000-km-long swaths; bold polygons correspond to exemplary swath profiles shown in Figure 1.6. Swaths are oriented perpendicular to the orogeny and their south to north distance along the orogen is shown by large black crosses (500-km intervals). Black lines indicate major drainage divides. **(b)** Annual rainfall of the Andes averaged for the period of 9 years, from Bookhagen and Strecker (2008). Note the generally high amounts of rainfall at orographic barriers on the eastern flanks of the Andes. International borders in gray.

The uplift chronology of the Central Andes is controversial (E.g. Gregory-Wodzicki, 2000; Lamb and Davis, 2003; Ghosh et al., 2006). It is currently considered that Andean deformation and uplift began in the Western and Coastal Cordilleras ~50 Ma ago, developed later and more slowly in the Eastern Cordillera (40 to 10 Ma), and accelerated in both Cordilleras and the Altiplano around 25 to 20 My ago (E.g. Elger et al., 2005). Recent studies of the Andes indicate that their elevation remained relatively stable for long periods (tens of millions of years),

separated by rapid (1 to 4 million years) changes of 1.5 kilometers or more (Garzione et al., 2008). For instance paleotemperature estimates derived from fossil-leaf physiognomy in the northern Altiplano and Eastern Cordillera suggest that paleoelevations were <1.3 km at ~15 to 20 Ma and <2 km by ~10 Ma (E.g. Gregory-Wodzicki, 2000). Isotopic data of Garzione et al., (2008) suggests that there was at least one discrete pulse of rapid surface uplift of ~1.5 to 3.5 km (2.5 ± 1 km) between ~10 and 6 Ma and perhaps an earlier phase of surface uplift at ~25 Ma (Figure 1.5a). While the Altiplano had supposedly reached its current elevation by ~6 Ma (E.g. Garzione et al., 2008), other segments of the coastal part of the Central Andean forearc have experienced uplift also during the Pliocene (and Pleistocene) epoch(s) in the response to the eastward Nazca plate subduction under South American plate to during Pleistocene (E.g. Machare and Ortlieb, 1992; Gregory-Wodzicki, 2000; Saillard, 2008; Wipf et al., 2008).

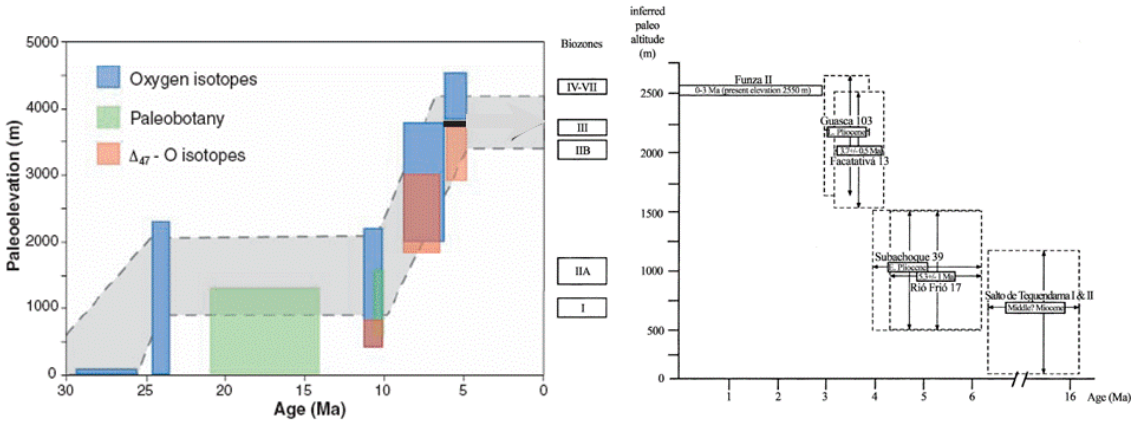

Figure 1. 5. (a) Multiple proxies of elevation versus time for the central Andean plateau over the past 30 My, from Garzione et al., (2008). Paleoelevation estimates are derived from oxygen isotopes, both Δ_{47} and oxygen isotopes, and fossil-leaf. **(b)** Main chronological, biostratigraphic, paleoenvironmental, and paleoaltitudinal properties of the five sections from exposures in the outer valleys of the basin of Bogotá, Colombia, representing the middle Miocene to late Pliocene, from Hooghiemstra et al. (2006). Elevation of past depositional environments was estimated by comparing paleofloras with present-day equivalents. Sediments were dated by fission track dating of intercalated volcanic ashes. Sections make a diagonal in this age vs. paleo-altitude diagram, indicating uplift of the Eastern Cordillera during the late Miocene and Pliocene. Vertical arrows correspond to an estimated uncertainty of ca. 3°C.

The Northern Andes have a fundamentally different tectonic history than the Central Andes in that crustal deformation was primarily associated with the collision of allochthonous terranes (Gregory-Wodzicki, 2000). In the Late Cretaceous–Paleocene, a volcanic arc that belonged to the Caribbean Cretaceous Oceanic Province collided with the South American margin from northern Peru to Colombia (Dengo and Covey, 1993). Recent studies unambiguously demonstrate that the main collision event started at 75-73 Ma (E.g. Vallejo et al., 2006). This event caused compressional deformation of the Western and Central Cordilleras and foreland deposition in the area of the Eastern Cordillera of Colombia (Gregory-Wodzicki, 2000). The second stage of accretion involved the dextral collision of the oceanic, Paleocene(?)–early Eocene, volcano-sedimentary arc sequence ~40 Ma (Spikings, 2005). Some folding and thrusting in the middle Magdalena Valley and western Eastern Cordillera occurred in the middle Eocene (Gregory-Wodzicki, 2000). By the Middle to Late Miocene (ca. 15 Ma), the northern Andes were about half their present average elevation, which is height enough so that there was substantial warping, ridging, and some tilting of the Amazon Basin eastward, and the rivers started to flow toward the Atlantic Ocean (Hoorn, 1994a, b). The Panama-Choco island arc collided with the northwest margin of the South American plate, from 12 to 6 Ma (E.g. Keigwin et al., 1982; Coates et al., 1992; Haug and Tiedemann, 1998); this event is associated with deformation in the Eastern Cordillera region. Uplift of the Eastern Cordillera to its present height occurred between 6 and 3 Ma (E.g. Clapperton, 1993; Hooghiemstra, 2006). Studies have not made quantitative estimates of uplift from this history, but in general, have

concluded that uplift of the Western and Central Cordilleras occurred mostly in the Late Cretaceous–Paleocene, and that uplift of the Eastern Cordillera mostly occurred in the Pliocene–Holocene (Figure 1.5b).

The uplift history of the central and northern Andes is of interest to both climatic and tectonic studies because provides insight into paleogeography, orogen erosion and sedimentation histories, orographic and regional climate change, and constraining geodynamic models for orogen formation. More specifically, the Andes affect global climate because they form the only barrier to atmospheric circulation in the southern hemisphere. The orogen block and deflect low-level trade winds from the equatorial Atlantic to form a northerly/northwesterly barrier jet that flows along the eastern flanks of the mountains (Virji, 1981) and transports moisture from the Amazon Basin to the subtropical regions of the continent (Vera et al., 2006). Thus, the Andes focus precipitation along the eastern flanks of the northern and central Andes due to orographic lifting and the inducement of small-scale convergence and convection (Lenters and Cook, 1995), separating sharply contrasting conditions: the humid Amazon lowlands to the west, and the generally more arid west coast of South America all the way from the subtropics to near the equator, including the Atacama Desert in northern Chile and southern Peru (Figures 1.4b and 1.6).

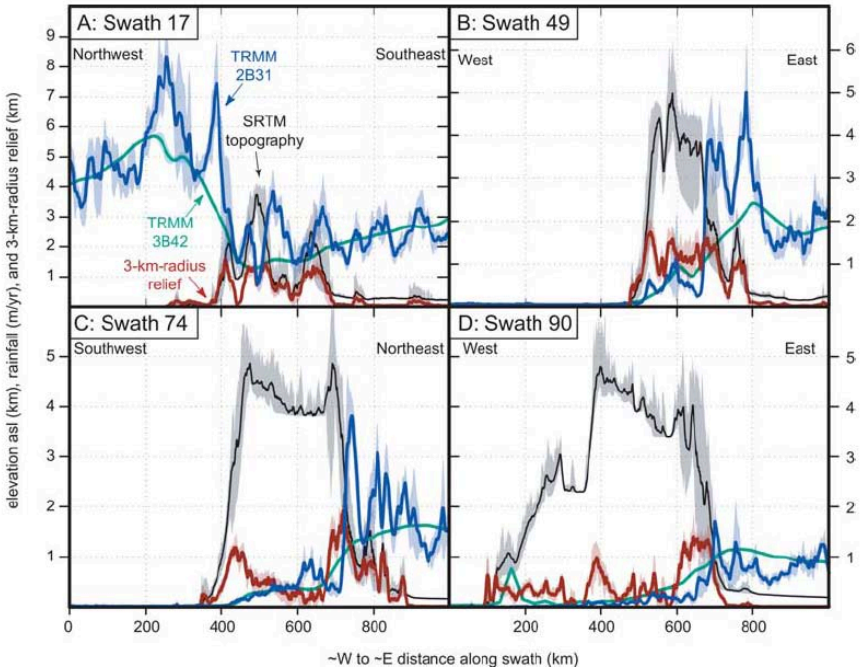

Figure 1. 6 Four sample swath profiles from the northern, central, and south-central Andes, from Bookhagen and Strecker (2008) (see Figure 1.4a for locations). Rainfall is in blue and green. Topography is in black and gray; and 3-km-radius relief is in red. Bold lines indicate mean values, and shading denotes ±2s ranges for the 50-km-wide and 1,000-km-long swaths (note: shading for topography denotes min. and max. elevation values). **(a)** Strong orographic control of rainfall on the eastern and western side of the northern Andes, as moisture is transported from both directions. **(b)– (d)** Prevailing winds are from the east or northeast (right).

Simulations altering the elevation of the orography predict that their uplift resulted in (1) a significant increase in precipitation along the eastern flanks of the Andes, (2) more arid conditions along the western flanks, and (3) no significant precipitation change over the Amazon Basin (Insel et al., 2009). Eventough Insel et al. (2009) corroborated those finding with conclusions inferred from geological observations, Garreaud et al. (2009) presents a different interpretation. The later used a simple global climate model, to study the effect of the Andean surface uplift and SST changes upon Atacama aridity. Decreasing the height of the Andes did not increase precipitation over the Atacama region, but rather decrease the precipitation over

the Central Andes and the interior of the continent. Thus, according to Garreaud et al. (2009) the Andean surface uplift had little, if any, effect on the lack of precipitation and moisture over the Atacama, regardless of the age of uplift.

Climatic responses to Andean surface uplift may extend beyond South America. For example, the presence of the Andes is enough to lower SST off the west coast of South America through evaporation, thus promoting a north-south asymmetry, deflecting the ITCZ to the north of the equator in the Pacific, which influences the strength and distribution of the Humboldt Current, coastal upwelling, and Walker circulation, with the Pacific teleconnections (E.g. Takahashi and Battisti, 2006). Blocking the warm easterly winds from South America, the Andes also help to maintain the divergence and temperature inversion and, hence, the stratocumulus cloud deck over the southeast Pacific off South America (E.g. Xu et al., 2004). The above exposed facts show how the tectonic evolution of the Andes has influenced South American climate and that modern climate is not representative of past climates when the Andes were lower. Therefore it is inferred that the surface uplift history of the Andes must be taken in account when working with paleoceanographic records of the easternmost Pacific due to the implications for the Cenozoic climatic evolution of South America.

1.6. Thesis outline and contribution to publications

In chapters 1-3 of this thesis a general introduction to the topic, the data and analysis tools used is provided. A second part of this thesis (chapters 4-8) includes manuscripts that are published in, submitted to or in preparation for international peer-reviewed journals. Finally, a third part (chapters 9) summarizes the main conclusions of the previous chapters in a synthesis of 3 million years of the background state of the tropical Pacific Ocean. The references are listed at the end of each manuscript or publication, while all other references are listed in the bibliography at the end of the thesis.

This thesis is part of the project *SE trade wind strength and dust transport (Leg 202)* funded by the German Science Foundation (DFG Ti240/17-1) within the Integrated Ocean Drilling Program (IODP)/Ocean Drilling Program (ODP). The data generated within the framework of this thesis are available in the PANGAEA database (http://www.pangaea.de).

Chapter 4: Tracking the equatorial front in the eastern equatorial Pacific Ocean by the isotopic and faunal composition of planktonic foraminifera
Daniel Rincón-Martínez, Silke Steph, Frank Lamy, Alan Mix and Ralf Tiedemann
Published in Marine Micropaleontology

The authors present a study to define the location of the equatorial front in the Pacific based on foraminifera census and stable isotope data derived from core tops scattered along the eastern tropical Pacific. The faunal population portion of the study is straightforward, and confirms the suggestions of a previous study that the ratio of *Globorotalia cultrata* to *G. cultrata* plus *Neogloboquadrina dutertrei* can be used as a way of tracking the position of the equatorial front. The isotopic approach is more complicated due to competing influences of variations in temperature, salinity, and geographically-inconsistent seasonal upwelling along the study's general north-south transect. Standard methods are used for predicting the $\delta^{18}O$ of calcite, and the oxygen isotopic difference between *Globigerinoides ruber* and *Globorotalia tumida* ($\Delta\delta^{18}O_{G.tumida\text{-}G.ruber}$) and between *Pulleniatina oliquiloculata* and *G. tumida* ($\Delta\delta^{18}O_{G.tumida\text{-}P.obliquiloculata}$) are useful paleoceanographic tools for reconstructing the latitudinal position of the eastern Pacific Equatorial Front in an area delimited by the Cocos and Carnegie ridges.

In this chapter Daniel Rincón-Martínez contributed to develop research strategy, performed laboratory work for the preparation and analysis of micropaleontological samples by Mass Spectrometer, processed and interpreted data, and produced figures. Silke Steph, Frank Lamy and Ralf Tiedemann developed research strategy. Alan Mix performed fieldtrip and provided sample set. Daniel Rincón-Martínez and Silke Steph wrote the paper. All co-authors provided editorial comments.

Chapter 5: More humid interglacials in Ecuador during the past 500 kyr linked to latitudinal shifts of the equatorial front and the Intertropical Convergence Zone in the eastern tropical Pacific.

Daniel Rincón-Martínez, Frank Lamy, Sergio Contreras, Guillaume Leduc, Edouard Bard, Cornelia Saukel, Thomas Blanz, Andreas Mackensen, and Ralf Tiedemann

Published in Paleoceanography

This study reconstructs ocean surface conditions in the equatorial eastern Pacific Ocean over the past half-million years. From a suite of marine sediment based proxies such as XRF scanning, alkenone-based SST, biomarkers and planktonic foraminifera oxygen isotopes it is inferred that precipitation along the coast of Ecuador has varied across glacial–interglacial cycles, with more aridity associated with glacial conditions. The lowest amounts of terrestrial run-off during glacial periods are accompanied with strong latitudinal and meridional SST gradients in the Pacific. The authors attribute this to more La Niña-like conditions, coupled with a northward shift of the ITCZ during glacial periods. Globally, however, the ITCZ is thought to shift southward during glacials. Strong glacial cooling in the southeast Pacific, which would locally push the ITCZ northward, may drive the contrasting movement in the equatorial eastern Pacific.

In this chapter Daniel Rincón-Martínez and Cornelia Saukel contributed to develop research strategy, performed laboratory work concerning the preparation and analysis of micropaleontological samples by Mass Spectrometer, the determination of total organic carbon (TOC), the determination of the concentration of biogenic silica, X-Ray Fluorescence (XRF) scanning and estimation of elemental concentrations by ICP-OES. Additionally Daniel Rincón-Martínez processed and interpreted data, and produced figures. Frank Lamy and Ralf Tiedemann developed research strategy, and produced age model. Sergio Contreras assisted with laboratory work for the preparation and analysis of terrigenous biomarkers (taraxerol). Thomas Blanz facilitated his laboratory at *Christian-Albrechts-Universitaet zu Kiel* and contributed with alkenone-based SST data and interpretation. Andreas Mackensen facilitated his laboratory at AWI and contributed with oxygen isotopes data and interpretation. Guillaume Leduc and Edouard Bard contributed with SST data and interpretation. Daniel Rincón-Martínez wrote the paper with major contributions from Frank Lamy, Ralf Tiedemann, Sergio Contreras and Guillaume Leduc. All co-authors provided editorial comments.

Chapter 6: **A rainy northern Atacama Desert during the last interglacial.**

Sergio Contreras, Carina B. Lange, Silvio Pantoja, Gaute Lavik, Daniel Rincón-Martínez, Marcel M. M. Kuypers

Published in Geophysical Research Letters

This study presents the response of the northern extension of the Atacama Desert and the Peruvian upwelling system to climate conditions during the last Interglacial. Using a high resolution records of molecular marine and terrestrial biomarkers preserved in Peruvian shelf sediments it is suggested that warmer and wetter conditions along the coast occurred during the last Interglacial, when global temperatures were comparable or even higher than today. The authors attribute this to a prolonged El Niño-like response of the tropical Pacific during this time interval. Globally, however, the intertropical convergence zone is thought to shift

southward during glacials. On the other hand, colder surface waters, higher export and primary productivity, and a drier climate characterized the late Holocene, more akin to the modern La Niña.

In this chapter Sergio Contreras developed research strategy, performed laboratory work concerning the preparation and analysis of biomarkers and other bulk sediment analyses. Daniel Rincón-Martínez contributed on the analysis of X-Ray Fluorescence (XRF) scanning data and built the age model from sedimentary data and benthic foraminifera oxygen isotopes. Sergio Contreras wrote the paper with contributions from Daniel Rincón-Martínez and Carina Lange. All co-authors provided editorial comments.

Chapter 7: **Late Quaternary glacial-interglacial climate variability of western South America inferred from eolian dust as preserved in marine sediments**

Cornelia Saukel, Frank Lamy, Jerry McManus, Daniel Rincón-Martinez, Jan-Berend W. Stuut, Gisela Winckler, and Ralf Tiedemann
First draft of manuscript in preparation for submission to Journal of Quaternary Science Research

This manuscript deals with dust accumulation and grain-size distributions over the tropical southeast Pacific during the Late Pleistocene. This study is based on similar methods to Chapter 5 and uses a sediment core located off southern Peru (ODP Site 1237) spanning the last 500,000 years. While grain-size distributions do not indicate any distinct changes in wind speed, dust accumulation rates oscillate on glacial cycles. This is largely attributed to changes in the source area and to meridional shifts of the atmospheric circulation system. During glacials, the South Pacific Anticyclone and the ITCZ were located further north and the Hadley Cell was intensified. It seems that while only the meridional wind component was enhanced, general wind speeds did not change, but an enhanced availability of dust in the source area and an increased gustiness provided for a 2 - 3 fold increase in dust accumulation rates at ODP Site 1237.

In this chapter Daniel Rincón-Martínez and Cornelia Saukel contributed to develop research strategy, performed laboratory work concerning the determination of total organic carbon (TOC), the determination of the concentration of biogenic silica, X-Ray Fluorescence (XRF) scanning and estimation of elemental concentrations by ICP-OES. Additionally Cornelia Saukel processed and interpreted data, and produced figures. Frank Lamy and Ralf Tiedemann developed research strategy, and produced age model. Jan-Berend W. Stuut facilitated his laboratory at MARUM and contributed with grain-size data and interpretation. Gisela Winckler facilitated his laboratory at LDEO and contributed with thorium isotopes data and interpretation of dust mass fluxes. Cornelia Saukel wrote the manuscript with contributions from Frank Lamy, Jerry McManus, and Gisela Winckler. All co-authors provided editorial comments.

Chapter 8: **Investigating the biogeochemical cycles and primary productivity changes in the eastern equatorial Pacific during the Pliocene-Pleistocene climate transition**

Johan Etorneau, Daniel Rincón-Martinez, Philippe Martinez, Frank Lamy, Thomas Blanz, Cornelia Saukel, Ralf Tiedemann and Ralph Schneider
First draft of manuscript in preparation for submission to *Paleoceanography*

Based on a multiproxy approach, this study examines different factors capable to control the overall primary productivity of the last 3 Ma in the Eastern Equatorial Pacific, a high-nutrient,

low-chlorophyll region of the ocean. The results show that increases in phytoplankton biomass since the Pliocene in the study area responded primarily to the nutrients distribution into the photic zone, and particularly to iron (Fe) fertilization. We found that nitrate - an essential nutrient for biological productivity - was likely sufficiently supplied at surface waters and has supported not limited, productivity since 3 Ma. In contrast, Fe inputs, currently limited in the modern Eastern Equatorial Pacific, have probably served as fertilizer to trigger the most productive period between 2.4 and 1.6 Ma. This was synchronous to a more vigorous cold tongue associated to a strong supply of nutrient-rich cold waters upwelled in the EEP shifting northward the EF.

In this chapter Johan Etorneau, Philippe Martinez and Daniel Rincón-Martínez contributed to develop research strategy. Johan Etorneau, Daniel Rincón-Martínez and Cornelia Saukel, performed laboratory work concerning the determination of total organic carbon (TOC), the determination of the concentration of biogenic silica and alkenones, X-Ray Fluorescence (XRF) scanning and estimation of elemental concentrations by ICP-OES. Additionally Johan Etorneau processed and interpreted data, and produced figures. Ralf Tiedemann, Frank Lamy and Ralph Schneider developed research strategy. Philippe Martinez facilitated his laboratory at EPOC Université Bordeaux 1 and contributed with nitrogen isotope data and interpretation. Thomas Blanz facilitated his laboratory at *Christian-Albrechts-Universitaet zu Kiel* and contributed with alkenone-based SST data and interpretation. Johan Etorneau wrote the paper with contributions from Daniel Rincón-Martinez, Philippe Martinez and Frank Lamy. All co-authors provided editorial comments.

CHAPTER 2

STUDY AREA: THE EASTERN TROPICAL AND SUBTROPICAL PACIFIC

2.1. The Coupled Ocean-Land-Atmosphere System in the Eastern Tropical Pacific

The eastern tropical Pacific is notable for the large asymmetry of SST about the equator. In this region SSTs are higher to the north and lower to the south throughout the seasonal cycle. As mentioned in Section 1.3, relatively cold surface waters mark the eastern equatorial cold tongue (EECT) and the eastern boundary current waters along Ecuador and Peru (Figure 2.1). The cold tongue is unusually cool for an ocean that is so close to the equator with SST at 5°S off Peru as cool as 16°C when most other tropical locations are in excess of 25°C. The cold tongue is maintained either by equatorial upwelling and advection of cold water from the Peru Current by the South Equatorial Current (Wyrtki, 1981) and by the eastward advection of cold water by the Equatorial Undercurrent as it rises to the surface near 95°W (Fiedler and Talley, 2006). The latitude of the coldest water shifts northward from about 2°S at about 85°W to the equator west of about 130°W (Figure 2.1). The eastern Pacific warm pool (>27.5°C) is centered along the coast of southwestern Mexico and Guatemala. This warm pool is the result of seasonally large net heat flux and weak wind mixing (Wang and Enfield, 2001) and is connected to the larger and slightly warmer (up to 30°C) Pacific warm pool in the western Pacific by a band of 27°C water centered along 7°N latitude (Fiedler and Talley, 2006). Salinity is low because rainfall exceeds evaporation beneath the cloudy and rainy ITCZ. Permanent SST fronts exist between the EECT and the regions to the north and south. Of particular interest for this study is the equatorial front; a shallow feature confined to the upper 100 m that separates warm Tropical Surface Waters (TSW) of the eastern Pacific warm pool, in the north, from the cool Equatorial Surface Waters (ESW) in the south, off Ecuador (Figure 2.2). The front is oriented zonally between the Galapagos Islands and 84°W, and approximately meridionally (northwest-southeast) east of 83°W (Figure 2.1). Climatological mean SST gradients across the front can be on the order of 1.7°C over a distance of 700 m, and decrease from east to west, reaching its greatest intensity in austral winter and spring (Pak and Zaneveld, 1974). Considering the seasonal variation of the Peru Current and the distance of transport, contribution by the Peru Current to the front on the west side of the Galapagos Islands seems to be secondary compared to the equatorial upwelling (Pak and Zaneveld, 1974).

Source of meridional asymmetry in the eastern Pacific are likely caused by the northwest–southeast slant of the American coastline acting in combination with positive coupled ocean–atmosphere feedback. The orientation of the American coastline means that southeasterly trade winds flow more nearly parallel to the coast in the Southern Hemisphere than do the northeast trades in the Northern Hemisphere, resulting in offshore Eckman transport and colder coastal water upwelling along the coast in the Southern Hemisphere (Philander et al., 1996). Blocked by the Andes, the zonal trade winds are weak near the South American shore and the equatorial ocean there is partly cooled by upwelling south of the equator driven by the southerly wind stress. The cross-equatorial flow pattern induced by higher SSTs on one side of the equator exhibits higher average off-equatorial trade winds on the cold side (Raymond et al., 2004). Low wind speeds occur on the warm side because it is a region of convergence between the opposing northeasterly trade winds and the southwesterly cross-equatorial flow. A stronger tendency toward evaporative cooling of the ocean therefore occurs on the cold side as a result of the stronger trade winds away from the equator, reinforcing the existing SST pattern (Raymond et al., 2004). In addition, the Peruvian coast lies beneath the descending branch of the Hadley-Walker circulation. The large static stabilities associated with cold SSTs and atmospheric subsidence result in extensive marine stratus cloud deck. Although these clouds reflect much of the incoming solar radiation, they interfere very little with the loss of energy via thermal radiation, resulting in less radiative heating of the cold water region than in the warm water area (Ma et al., 1996). The overall effect of the distribution of evaporation and radiative heating and cooling is thus reinforcement of the preexisting thermal contrast illustrated in Figure 2.2.

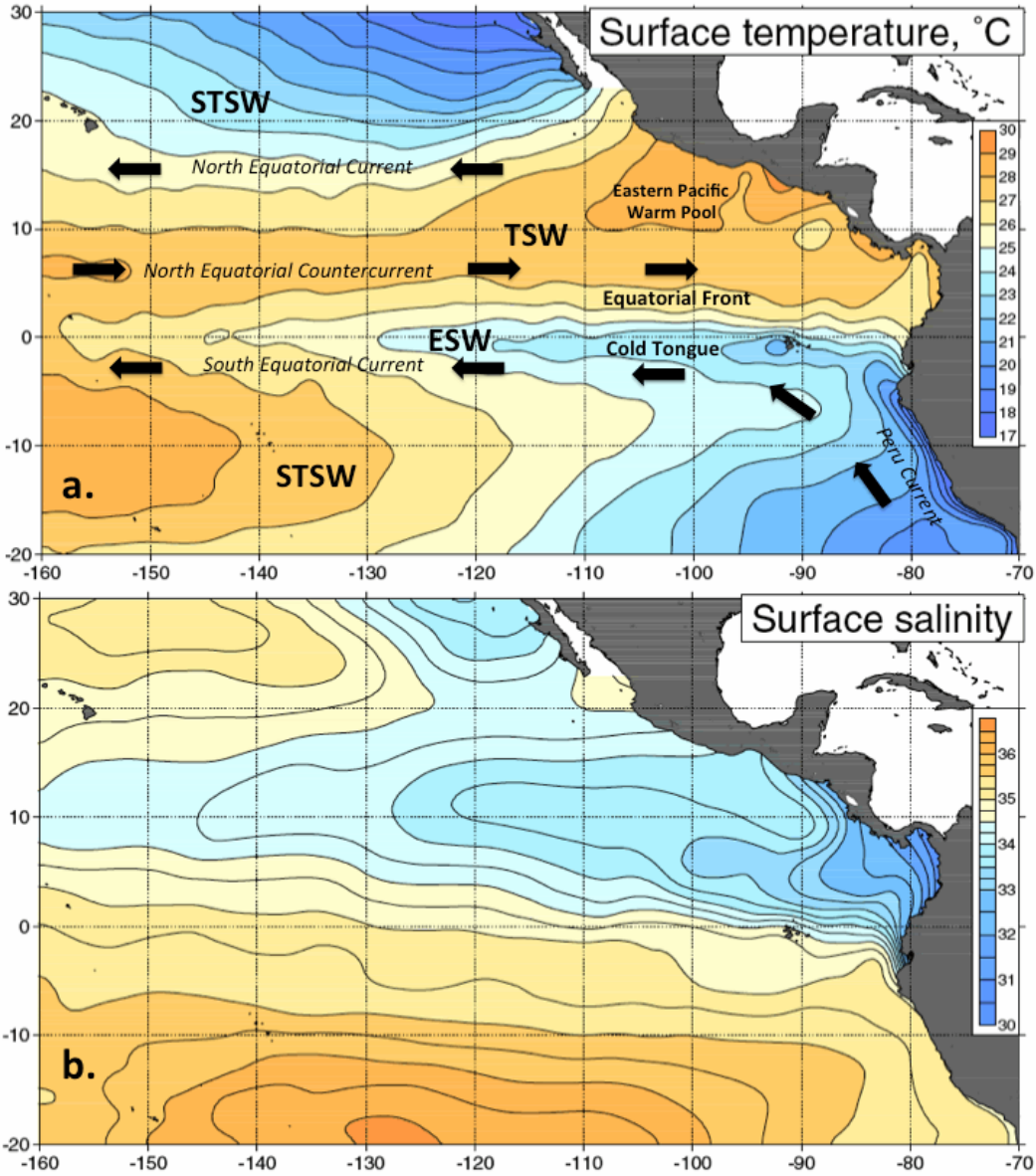

Figure 2. 1 Schematic diagram of surface water masses and currents in the eastern tropical Pacific Ocean (modified from Fiedler and Talley, 2006). **(a)** Mean surface temperature, and **(b)** mean surface salinity of the eastern tropical Pacific. The EECT extends out from the west coast of South America westward along, and south of, the equator. The eastern Pacific warm pool is centered along the coast of southwestern Mexico and Guatemala. TSW is characterized by low salinity and high temperature (S<34 p.s.u, T>25°C). ESW properties (S>34 p.s.u, T<25°C) are determined by the seasonal advection of cooler and saltier water from the Peru Current and by equatorial upwelling.

The EECT and the coastal ocean off Peru and Chile are coupled to the atmosphere through surface wind stress and heat exchange. The winds in this region are typically southeasterly. However, the strength and spatial distribution of the surface winds have shown to be closely tied to the frontal location and strength. The surface wind stress in this southeasterly cross-equatorial flow decreases by more than a factor of 4 over the cold tongue and then increases by almost the same amount to the north of the cold tongue (Chelton et al., 2001). The modulation of the surface wind field by the SST provides a potential mechanism for two-way air–sea coupling since the surface interactions are coupled to the atmospheric circulation through horizontal gradients of latent heat release in the vicinity of ITCZ convection, as well as radiative and sensible heating gradients, especially in the atmospheric boundary layer (Chelton et al., 2001). The upper ocean heat budget is strongly coupled to radiative effects of the

extensive decks of boundary layer clouds in the southeast tradewinds, off the Peru and Chilean coasts, and their extension into the equatorial zone (Raymond et al., 2004). Temperature of the EECT decreases towards the east as progressively cooler waters are upwelled from the Equatorial Undercurrent that shoals as it flows from west to east (Fiedler and Talley, 2006). The intensity and spatial extent of the EECT and associated fronts change seasonally (E.g. Mitchell and Wallace, 1992) and interannually (E.g. Deser and Wallace, 1990). During the equatorial warm season (March through June) SST colder than 25°C are confined to the upwelling region near the South American coast; the equatorial front is weak or nonexistent (Hays et al., 1989). During the cold season (July through November) the equatorial cold tongue is well developed and SST cooler than 25°C extends westward to 130°W (Figure 2.3a). The EECT seasonal amplitude is ±1–3°C, with coldest temperatures during the Southern Hemisphere winter-spring (August-September). Surface winds vary in concert with the changes in the SST distribution, meaning that southeasterly winds are strongest during the cold season (Figures 2.3a, c). During El Niño years, SST in the cold tongue is elevated throughout the year; and there is a southward penetration of warm water, and an abnormal displacement of the front towards the west while, in the east the equatorial front almost disappears (Hays et al., 1989).

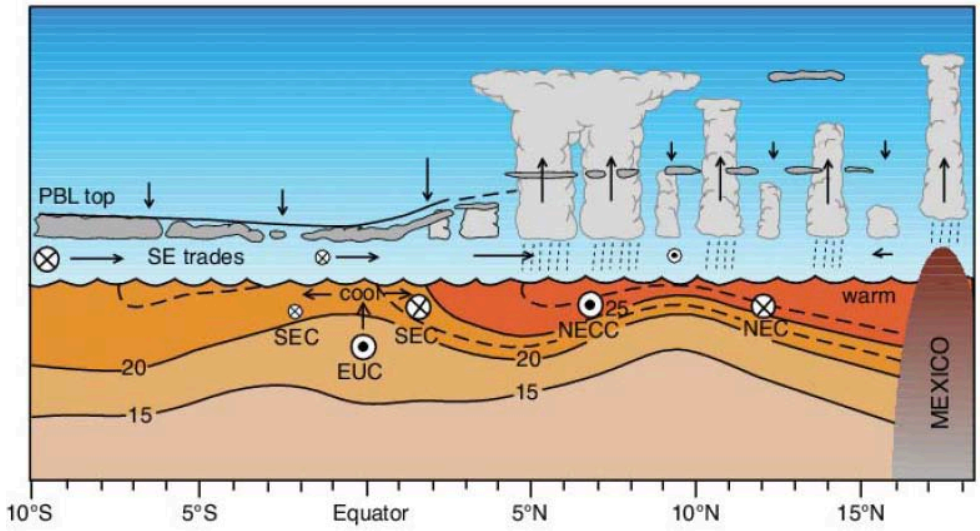

Figure 2. 2 Idealized cross-sections through the ITCZ–cold tongue complex at approx. 95°W in the east Pacific showing the atmospheric meridional circulation, atmospheric boundary layer depth, and the oceanic thermal structure, from Raymond et al., (2004). SEC=South Equatorial Current, NECC = North Equatorial Countercurrent, and the EUC = Equatorial Undercurrent. Southeasterly and northeasterly trade winds in the planetary boundary layer (PBL) converge onto the ITCZ (heavy clouds), located over the warmest SST. Encircled x's (dots) denote westward (eastward) flowing winds or currents.

The rainfall climatology of the eastern tropical Pacific is dominated by the ITCZ. The northeasterly and southeasterly tradewind belts, which occupy most of the eastern tropical and subtropical Pacific, are noted for fair weather and a large excess of evaporation over precipitation, while narrow ITCZ that separates them is marked by heavy and persistent rainfall. The annual cycle of the surface circulation is characterized by a latitude position of the wind confluence and ITCZ closest to the equator in March-April, a northward shift till June, a southward displacement in July and August, and a northernmost position in September (Figures 2.3b and c; Hastenrath, 2002).

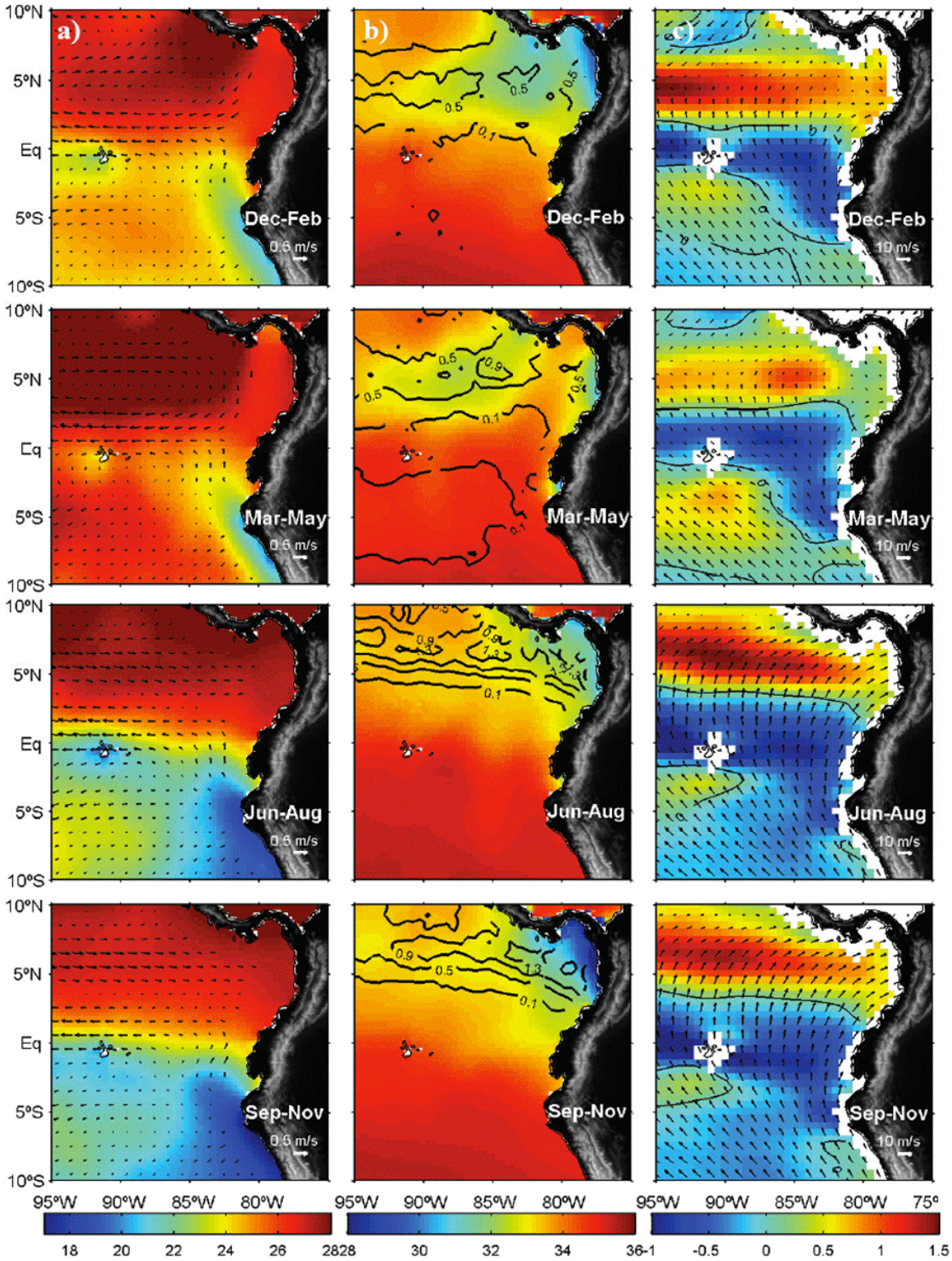

Figure 2. 3 Seasonal climatologies of **(a)** SST (°C, colors) and surface currents (m/s, vectors), **(b)** sea surface salinity (PSU, colors) and rainfall rates (mm/day, contour lines which are associated to the ITCZ) and **(c)** convergence (positive values) and divergence (negative values) of surface winds ($*10^{-5}$ s^{-1}, colors, black lines represents a value of zero) and surface winds (m/s, vectors). Taken from Garcés (2005).

In addition to the ITCZ, another convergence zone exists but in the Southern Hemisphere (SITCZ), occurring at 8°S–2°S, 130°W–90°W in the southeast Pacific (Halpern and Hung, 2001). The positions and intensities of the ITCZs are highly sensitive to the underlying sea-surface temperature distribution. For instance, only in March and April, when SSTs south of the equator approach those to the north, it is possible to observe both intertropical convergence zones, with convection north and south of the equator (Halpern and Hung, 2001). Five features

distinguish the SITCZ and ITCZ during normal conditions. (1) SITCZ is located south of the equator and ITCZ is north of the equator. (2) SITCZ occurs in March–April and ITCZ exists throughout the year. (3) SITCZ does not extend eastward to South America, and ITCZ does extend to Central America. (4) SITCZ remains poorly observed with in situ instrumentation compared to the ITCZ. (5) Numerical atmospheric general circulation model simulation of SITCZ rainfall is less accurate compared to ITCZ rainfall (Halpern and Hung, 2001). During El Niño years, when the equatorial water is warm, a southward displaced wind confluence displaces ITCZ southward across the 2°N–2°S zone where upper ocean upwelling of cold water ceased and SST rose above 27°C. However, whether the SITCZ exists during March–April of an El Niño year or is replaced by an anomalously wide ITCZ stretching from 10°S to 7°N is unknown (E.g. Halpern and Hung, 2001; Hastenrath, 2002).

2.2. Eastern Tropical Pacific biological productivity

Patterns of primary production in the world ocean reflect patterns of thermocline topography. The thermocline is that portion of the water column where temperature decreases maximally with increasing depth (Fiedler and Talley, 2006). This thermocline/productivity linkage occurs because the thermocline almost invariably coincides with the nutricline, defined as that portion of the water column where phytoplankton nutrients increase maximally with depth (Fiedler and Talley, 2006). Areas of high primary productivity occur where nutrient supply to the euphotic zone is enhanced by mixing and a shallow thermocline (Wyrtki, 1981).

The eastern equatorial Pacific contains the most productive coastal upwelling region in the world's oceans and is both a strong carbon dioxide source for the atmosphere and a biological sink for seawater pCO_2 (E.g. Tans et al., 1990; Takahashi et al., 2002). At the equator, and in the coastal waters of Peru and Chile the upwelled water is rich in dissolved CO_2 that subsequently degasses to the atmosphere. However this CO_2 release is curtailed by the photosynthetic carbon uptake of an elevated phytoplankton biomass supported by upwelled macronutrients (nitrate, phosphate and silicic acid) and micronutrients. Although seasonal variability in phytoplankton assemblages occurs in Peruvian waters, large diatoms tend to dominate the biomass in phytoplankton blooms that develop in these coastal upwelling regimes in all seasons (E.g. de Mendiola, 1981; Abrantes et al., 2007), and it has been argued that diatom-driven new production efficiently fuels the food chains leading to fish production (Smetacek, 1998). With this rich productivity, it is surprising that high-nitrate, lower than expected chlorophyll (HNLC) conditions have been reported for the Peru upwelling regime.

Both silicic acid and Fe have been hypothesized to control diatom productivity in the EEP. Past work has suggested that low concentrations of silicic acid may ultimately limit diatom growth and new production in the central and western equatorial Pacific (E.g. Ku et al., 1995; Leynaert et al., 2001). However the role of Fe as the limiting nutrient has been clearly indicated by experimental additions of Fe, which tend to result in phytoplankton blooms that primarily consist of larger diatoms (E.g. Coale et al., 1996; Landry et al., 2000). It has also been suggested that additions of Fe and Si together produce larger changes in biomass and silicic acid uptake than do adding either element alone (E.g. Coale et al., 1996), although differences in nitrate uptake when silicic acid is added alone or in combination with Fe have not been observed (E.g. Brzezinski et al., 2008).

Throughout the tropical Pacific, deficiencies in Fe can affect not only phytoplankton growth rates but also species composition. For instance, the SEC is marked by an increase in macronutrients and a decrease in Fe concentrations. The biological response shows an increase in Chlorophyll a biomass and a shift in the phytoplankton assemblage composition from a diverse community near the Galapagos Islands to one dominated in 90% by

dinoflagellates (E.g. DiTullio et al., 1995). On the other hand, the HNLC waters of the eastern equatorial Pacific, where there is a severe Fe limitation and high macronutrient concentrations, the chlorophyll concentrations are very low and phytoplankton community is quite diverse (E.g. DiTullio et al., 1995). In the western boundary of the Peru/Chile current the phytoplankton community changes abruptly from the cryptophyte-dominated assemblage in the Peru/Chile current to the haptophyte-dominated assemblage to the west without any sharp difference in macronutrients or Fe (E.g. DiTullio et al., 1995). Macronutrient concentrations on the Coastal waters of the Peruvian continental shelf are typically highest near the coast, yet chlorophyll concentrations along the coast are much lower than elsewhere across the shelf (DiTullio et al., 1995). In some coastal locations, the phytoplankton assemblage is completely dominated by diatoms, accounting for 90% of the total community chlorophyll. In other coastal regions, while diatoms still a significant portion of the phytoplankton community, cryptophytes, dinoflagellates, haptophytes, and prasinophytes are also primary members of the algal assemblage, especially near the shelf break (DiTullio et al., 1995).

Seasonal cycles are weak over much of the open-ocean eastern tropical Pacific, although the surface chlorophyll concentration in the Peru upwelling system exhibits substantial seasonality with low values in Austral winter and high values in Austral spring and summer, in phase opposition to upwelling intensity (E.g. Bakun and Nelson, 1991). The deepening of the mixed layer was shown to be mainly responsible for the decrease of surface chlorophyll in Austral winter (E.g. Calienes et al., 1985; Echevin et al., 2008). The phytoplanktonic biomass increases significantly in Austral spring and fall following periods of restratification and destratification, respectively (Echevin et al., 2008). The Peru Current system is almost as productive in Austral winter as in early summer, and the decrease in surface biomass in winter results from a dilution and light limitation effect, and that the reduced insolation during winter does not affect the amplitude and phase of the surface chlorophyll signal (Echevin et al., 2008). The thermocline deepening, produced by El Niño, results in substantial decreases in euphotic zone nutrient supply, and consequently primary production and chlorophyll by several-fold particularly in the far eastern Pacific. In coastal regions the phytoplankton community also shifts, I.e. from diatoms and larger phytoplankton to a community of picoplankton more typical of the open-ocean (cyanobacteria and prochlorophytes; E.g. Pennington et al., 2006). Warm-water species, such as rare and solitary oceanic dinoflagellates, are advected onshore and poleward into the normally productive near shore environments (E.g. Pennington et al., 2006). La Niña of 1998-1999 was one of the most dramatic in recent history, and resulted in a huge increase in primary production that contrasted with the low productivity associated with El Niño, both in the eastern tropical Pacific and globally (Pennington et al., 2006).

2.3. Geologic, geomorphologic, and climatic settings of tropical western South America

Ecuador and Peru are commonly divided into three main regions: a) the western lowlands, which are up to 200 km wide in Ecuador and called the *Región Occidental* or *Costera,* and is usually much narrower in Peru where they are simply called *Costa*; b) the Andean chain, running from north to south through both countries, with peaks of over 6,000 m, which geographically as well as climatically separate the coastal plain from the Amazonian lowlands. In Ecuador this region is called the *Región Central* or *Andina,* in Peru it is known as the *Sierra*; and c) the Amazonian lowlands, known as the *Región Oriental* or *Amazonica.* A very wet region intersected by numerous rivers, which all drain into the Amazon.

Among the objectives of this thesis is included the determination of possible sources and transport processes of terrigenous material deposited in marine sediments off South American west coast. Therefore two different continental and climatic settings such as the humid western Ecuadorian lowlands and the drier southern Peruvian Andes were chosen as potential

terrigenous sources to show the degree to which preliminary interpretations support or need to modify the currently held concepts of the process controlling the type and amount of terrigenous material deposited on the oceanic Carnegie and Nazca Ridges, respectively.

2.3.1. Geological constraints of western Ecuador

The southern Ecuador–northern Peru subduction zone extends along the western margin of South America and accommodates ~6–7 cm/year eastward convergence of the Nazca plate with the South America plate (Figures 2.4a and b; Witt and Bourgois, 2010). The Carnegie Ridge, which is part of the Nazca Plate, and the Grijalva fracture zone are currently moving east under the Ecuadorian margin (Figure 2.4a). At ~2°S, the trench axis exhibits a change in trend from N-S to the south to NNE to the north. The E-W convergence between the Nazca and South America plates becomes oblique north of ~2°S. The Ecuadorian coastal block of oceanic substratum is the southernmost leading area of the North Andes microplate, which is bounded from the Nazca Plate to the west by the Ecuador trench, and from the South American Plate to the east by a system of northeast-trending, right-lateral strike-slip faults and north trending thrust faults, known as the Guayaquil-Caracas Megashear (Figure 2.4b). The southern extremity of the Guayaquil-Caracas Megashear is commonly thought to intersect the Ecuador trench in the region of the Gulf of Guayaquil (Cantalamesa et al., 2005).

Published GPS results suggest that a large part of the northern Andes is “escaping” to the northeast relative to stable South America at a rate of 6±2 mm/year along a major right-lateral strike-slip system that extends from Ecuador to Colombia and probably to Venezuela (Egbou and Kellogg, 2010). Proposed driving mechanisms for the “escape” of the North Andes include subduction of the Caribbean plate, collision with the Panama arc, rapid oblique subduction of the Nazca plate, and the subduction of the aseismic Carnegie Ridge at the Ecuador–Colombia trench (Egbou and Kellogg, 2010). If subduction of the Carnegie Ridge is the driving mechanism for the northeastward displacement of the North Andes, then the initiation of the “escape” could indicate when the ridge arrived at the trench. The compilation of geologic estimates presented by Egbou and Kellogg (2010) suggests that the North Andean “escape” has been occurring for the last 1.8 Ma. If increased coupling, resulting from the subduction of the Carnegie Ridge beneath the South American plate, is driving the northeastward “escape” of the North Andes, the Carnegie Ridge must have reached the trench at least 1.8 Ma.

Convergence between the Pacific oceanic plates and South America has been active at least since Cretaceous time and has resulted in successive accretions of allochthonous terranes onto the previous continental margin (Jaillard et al., 1995). Repeated accretion of oceanic and arc elements during Mesozoic and Cenozoic times distinguishes them from the Central Andes south of the Huancabamba deflection, which did not experience a history of terrane accretion. West of the Guayaquil-Caracas Megashear zone, and from east to west three series of tectono-stratigraphic units, which were accreted at successive times can be identified: 1) several Palaeozoic to Cretaceous metamorphic and volcanic terranes of the Cordillera Real, which accreted during the early Cretaceous; (2) the volcanic Pallatanga Terrane, accreted during Campanian–Maastrichtian; and (3) the Paleocene–Eocene volcanic arc Macuchi Terrane and the Cretaceous Piñon Terrane (Costa), which accreted during the Eocene (Jaillard et al., 1995). The Macuchi and Pallatanga Terranes constitute the present Western Cordillera.

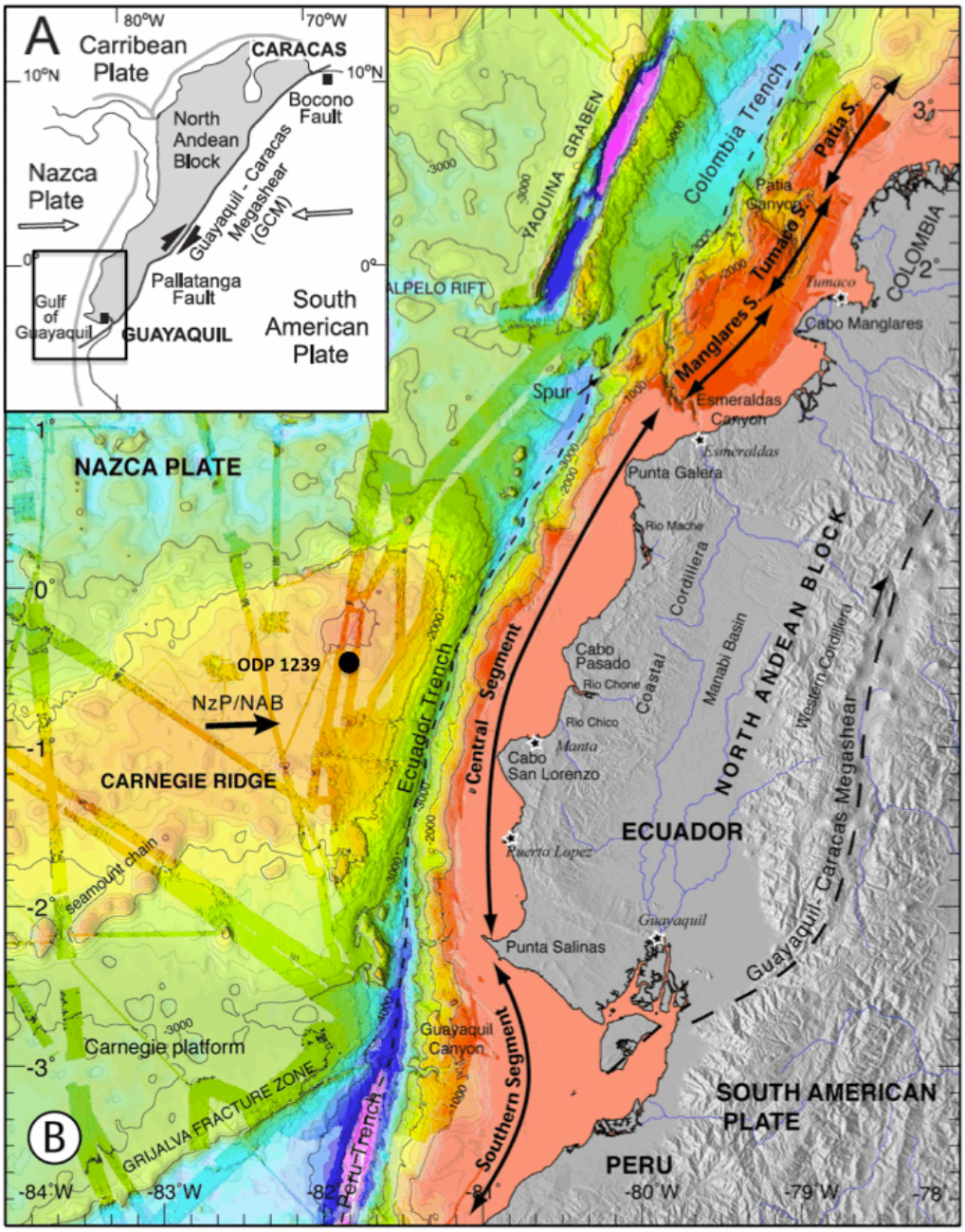

Figure 2. 4 (A) Structural sketch of the North Andean Block highlighting the area where the Carnegie ridge impinges on the Ecuador Trench, from Dumont et al. (2005). **(B)** Topography and bathymetry at 200 m intervals of the western Ecuador and Southwest Colombia, from Collot et al. (2010). Nazca(NzP)–South American Plates convergence vector is illustrated as well as the location of the Ocean Drilling Program (ODP) Site 1239.

The Coastal Cordillera (Figure 2.4b) is almost exclusively built of sandstones, clays, conglomerates and large areas of limestones. Only the Chongón-Colonche Mountains, which range from Guayaquil to near Machala, are composed of volcanic rocks. In the lowlands, the northern edge of the Gulf of Guayaquil exhibits a basement of mafic and ultramafic Cretaceous rock that crops out extensively along the E-W–trending Chongon-Colonche Sierra (Figure 2.5). This basement resulted from the accretion of oceanic terranes, although there is no consensus regarding the nature and timing age of the accretion, and ages ranging from Late Cretaceous to Eocene time (80–60 Ma; Witt and Bourgois, 2010). Paleocene to Eocene rocks occurs along the Santa Elena Peninsula and extends offshore to the south along the Santa Elena Rise (Figure 2.5), which unconformably overlies the oceanic basement. Sediments of Oligocene to Quaternary age accumulated along the Progreso Basin (Ecuador), the Gulf of Guayaquil-

Tumbes Basin, and the onshore Zorritos Basin (Peru) (Figure 2.5). The southern edge of the Zorritos basin exhibits metamorphic basement of Paleozoic age cropping out along the Amotapes Massif (northern Peru). Below the Oligocene sediment of the Zorritos Basin, Late Cretaceous to Eocene sedimentary rock unconformably overlies this basement (Witt and Bourgois, 2010). Between the Santa Elena peninsula (Ecuador) and the Amotapes Massif (northern Peru), the Gulf of Guayaquil-Tumbes Basin consists of a several-kilometer-thick accumulation of Miocene to Quaternary sediment (Witt and Bourgois, 2010).

The coastal area is characterized by four main Neogene fore arc basins (from north to South: Borbón, Manabí, Progreso, Guayaquil-Tumbes; Figure 2.5) related to dextral strike-slip displacements. The Tertiary history of the coastal margin of Ecuador is that of a fore arc basin, characterized by extensive compressive deformation and progressive uplifting of the Coastal Range, with the shallowing upward trend (Jaillard et al., 1995). Erosion began with the uplift of the Andes, leading to the deposition of continental sedimentary detritus, covering depressions and much of the lowlands. Such sandy or clay-rich deposits, conglomerates and breccias can today be found in the Loja basin and along river bottoms. On the northern Ecuador, the Borbón Basin was opened during the Late Paleocene (Evans and Whittaker, 1982), while the Progreso Basin was opened during the Miocene (Jaillard et al., 1995). The northern part of the Santa Elena Uplift and the Manabí and Progreso Basins emerged at the end of the Miocene, shifting the marine sedimentation into coastal basins sited farther west (Dumont et al., 2005). At the end of the Early Pliocene, an extensive planation surface, cutting across the older relief (Coastal Range and central Ecuadorian Cordillera) and testifying to the cessation of uplift, was created throughout Ecuador (Coltorti and Ollier, 2000). The Guayas depression, the Sechura plains in northern Peru and many coastal areas were at different times subject to marine transgressions, leading to alternating periods of oceanic and continental sedimentation. The oceanic deposits included different types of sandy, muddy and calcareous material, while the continental material was mainly alluvial in character. In summary, the Tumbesian region is covered either by volcanic rocks or by sedimentary material, providing a rather uniform nutrient-rich geological source for soil formation. The development of soils is therefore determined mainly by climate, which in the Tumbesian region shows a strong precipitation gradient. The Gulf of Guayaquil-Tumbes is the deepest Neogene fore-arc basin which main opening episode occurred during the past 1.8–1.6 Ma (Witt and Bourgois, 2010). It corresponds to pull-apart basin developed between the Guayaquil-Caracas Megashear zone and to the east, the oblique convergent Nazca-South America Plate boundary to the west (Witt et al., 2006).

2.3.2. Geography and climate of western Ecuador

The western lowlands, which are up to 200 km wide in Ecuador and called the *Región Occidental* or *Costera,* and usually much narrower in Peru where they are simply called *Costa.* North of 2°S in Ecuador the lowlands are between 100 and 200 km wide and are flanked on the western side by the Coastal Cordillera which rises to 900 m. Between these hills and the Andean cordillera lies a flat flood-plain up to 80 km wide which gently slopes from north to south and is drained by the rivers Daule, Quevedo and Babahoyo into the Gulf of Guayaquil, through the Guayas River (Figure 2.4). Several smaller rivers of which, the Esmeraldas and Santiago are the most important draining the northern part of the plain (Figure 2.4). The Gulf of Guayaquil itself, between about 2°S and 4°30'S, with its numerous inlets and islands, reaches far inland, and reduces the coastal lowlands to a narrow strip no wider than 20-30 km. Further south, from 4°30'S to 6°30'S lies another wide area of lowlands, with a hot and arid climate, forming the Sechura Desert. Only a few rivers, mainly the Chira and Piura rivers, intersect this desert and reach the sea (Best and Kessler, 1995).

Because of its geographic position and highly varied topography, the western lowlands region has a wide variety of climates. The large-scale climatic patterns, dominated by wind systems and sea currents, are modified locally by topographic factors, producing, often over very short distances, conditions ranging from deserts to tropical rainforests. Rainfall is the most variable and therefore most important climatic factor. Its general distribution is determined by the seasonal position of the ITCZ (see section 2.1). From about November to April the ITCZ reaches its southernmost position along the western South American coast at about 4°S, directly over the southern Gulf of Guayaquil region (Figure 2.6). This brings the associated cloud accumulation and abundant rainfall. During an average year of precipitation, seasonal Guayas river discharges ranges from 200 m^3/s during the dry season to 1,400m^3/s in the wet season, but rates as low as 100 m^3/s and as high as 2,400 m^3/s may occur (Twilley et al., 2001). The fact that the ITCZ does not reach further south in western lowlands region causes the rainfall to decrease sharply from north to south, giving the region its character as a climatic transition zone.

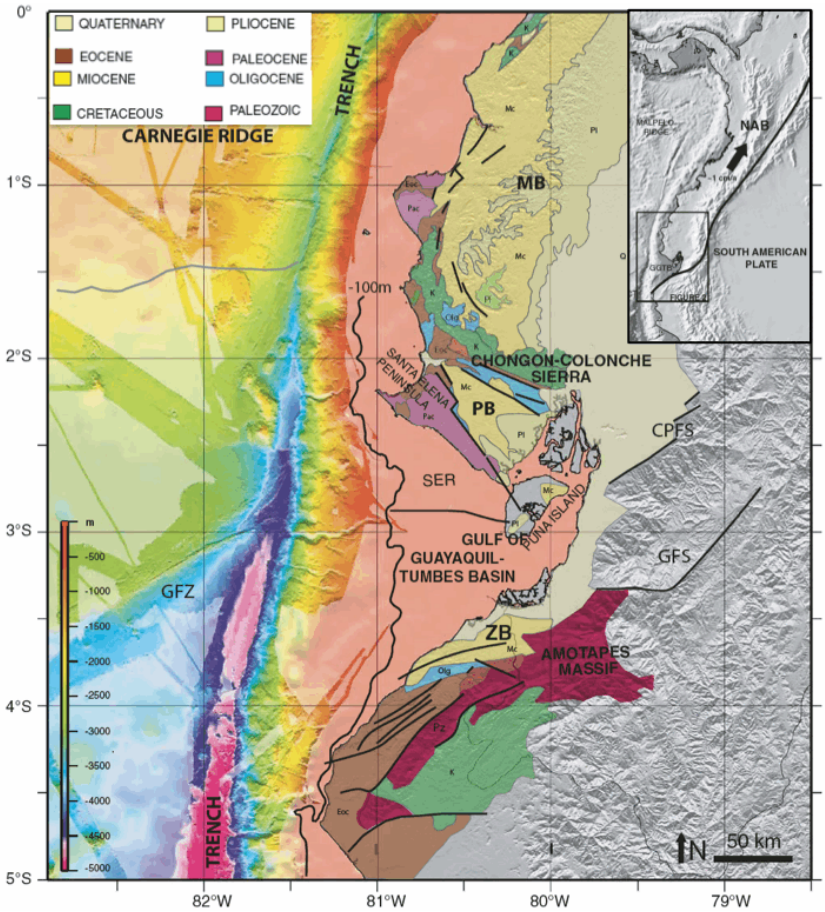

Figure 2. 5 Structural sketch of the Gulf of Guayaquil-Tumbes Basin area, northern Peru, and the central-north forearc setting of Ecuador, including the main continental features (modified from Witt and Bourgois, 2010). Bathymetry of the continental margin and trench is a compilation of data from several cruises. The black line is the –100 m bathymetric contour that grossly follows the shelf-continental margin limit. CPFS—Calacalí-Pallatanga fault system; GFS—Giron fault system; GFZ—Grijalva fracture zone; MB—Manabi Basin; PB—Progreso Basin; SER—Santa Elena Rise; ZB—Zorritos Basin.

The dominating winds in the western lowlands region are westerlies, moving inland from the Pacific Ocean (Pourrut et al., 1995a). North of about 4°S along the Ecuadorian coast, they move in over warm sea currents, bringing warm, saturated air which, upon hitting the Coastal Cordillera and Andes rises, cools clown and produces abundant orographic rainfall (Pourrut et al., 1995a). As humid air moves up along mountains, it cools down and releases rain. This leads,

on a continuous mountain slope, to an increase in precipitation with altitude. The highest precipitation levels (over 4,000 mm mean annual precipitation) are to be found along the western Andean slope in the north of the región (Pourrut et al., 1995b). Areas with over 2,000 mm reach south to 4°S on the western side of the Celica Mountains; further south precipitation decreases sharply. The Coastal Cordillera also receives more rainfall than the surrounding lowlands, but its low altitude (rarely over 900 m) prevents it from intercepting many clouds and receiving more than 1,500 mm mean annual rainfall.

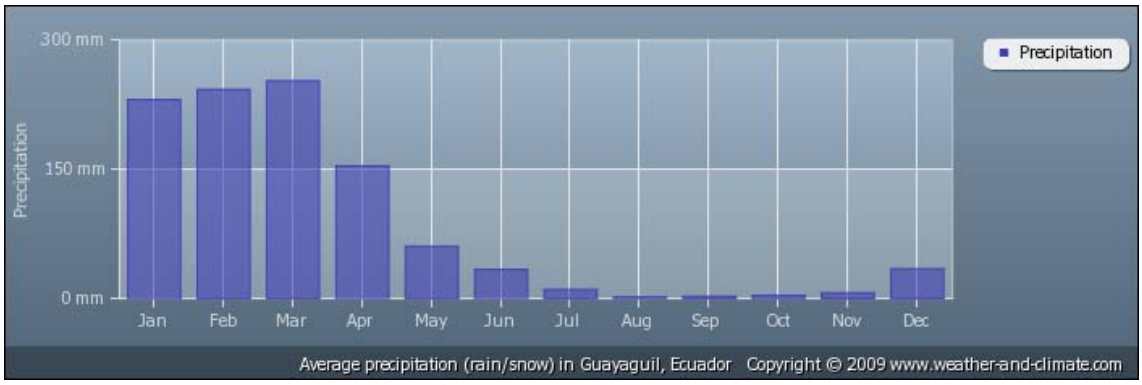

Figure 2. 6 Mean monthly precipitation (mm/month) at Guayaquil.

The western lowlands region as a whole shows a single well-marked rainy season from about December to May, with the rainiest month being March in most areas, with between 20% and 45% of the annual rainfall falling during this month (Pourrut et al., 1995a). The Gulf of Guayaquil plays an important role in the distribution of humidity in the western lowlands region. A narrow band, of about 110 km, located between Esmeraldas and the Gulf of Guayaquil is characterized by tropical megathermic and humid climatic regime. Mean annual rainfall oscillates between 1,000 and 2,000 mm, reaching higher values near the cordillera. Mean air temperatures are ~24°C and relative humidity varies between 70 and 90 % according to the season (Pourrut et al., 1995a). South of the Gulf of Guayaquil the lowlands climate is characterized by a tropical megathermic and arid to semiarid regime. Mean air temperatures are ~24°C, with maxima of 32°C and minima of 16°C (Pourrut et al., 1995a). In the immediate surroundings of the gulf, however, special conditions prevail: the large body of shallow, warm water locally increases temperatures and produces large amounts of warm, saturated air which in turn gives rise to coastal fog and, on the Andean slopes immediately east of the gulf, to markedly increased precipitation levels (Pourrut et al., 1995a).

Annual variability of the rainfall is often extreme. During El Niño events (March to April), heavy and persistent precipitation was extended over wide areas of the coastal plain of Ecuador and northern Peru (Table 2.1; Bendix, 2000a). In such years, the sea-surface temperatures are much higher than usual because a warm sea-current displaces the cold Peru Current from the north Peruvian coast and rainfall is much higher than usual (up to 10 times higher than the long-term mean). For example, at Guayaquil (mean annual rainfall 1,100 mm) and Manta (mean annual rainfall 225 mm) in the western lowlands of Ecuador, absolute extreme occurred in El Niño 1982-1983 with 4,600 mm and 1,825 mm, respectively (Pourrut and Nouvelot, 1995). A diurnal land–sea breeze system that is sometimes coupled with thermally-driven up-slope winds influences the formation and dynamics of heavy precipitation. These systems can interact with the opposite mid and upper-level trades, which transport remainders of cirrus shields from the Amazon to the coastal plain and intensify deep convection. Thermal land–sea breeze systems are only present in this area during increased SST (>27°C) due to El Niño events (E.g. Bendix, 2000b; Bendix and Bendix, 2006). On the other hand, events of extensive precipitation independent of a diurnal cycle occur mainly in the main El Niño phase (March–

April) when the Hadley circulation is increased due to a severe warming of the tropical Pacific (Hernandez and Zambrano, 2009).

Table 2.1. Correlation coefficients between the mean SST in the El Niño 1+2 region (Niño 1 is the area defined by 80°W-90°W and 5°S-10°S, Niño 2 by 80°W-90°W and 0°S-5°S) and mean monthly precipitation in several western lowland localities of Ecuador during each El Niño year, from Hernandez and Zambrano (2009). Locations are ordered from north (left) to south (right), being San Lorenzo the northernmost station, near the Ecuador-Colombia border, and Puerto Bolivar, the southernmost station, near the Ecuador-Peru border.

	San Lorenzo	Esmeraldas	Manta	La Libertad	Puna	Guayaquil	Puerto Bolivar
Niño 1982	0.70	0.84	0.61	0.52	0.78	0.82	0.76
Niño 1986	0.70	0.84	0.61	0.52	0.78	0.82	0.76
Niño 1991	0.67	0.63	0.73	0.54	0.76	0.81	0.81
Niño 1993	0.45	0.65	0.55	0.43	0.84	0.74	0.92
Niño 1994	0.32	0.51	0.73	0.58	0.90	0.72	0.74
Niño 1997	0.54	0.77	0.77	0.78	0.83	0.82	0.83
Niño 2002	0.64	0.84	0.59	0.70	0.69	0.69	0.59
Niño 2004	0.64	0.69	0.57	0.64	0.79	0.68	0.65
Niño 2006	0.46	0.91	0.93	0.40	0.38	0.59	0.48

2.3.3. Geological constraints of the Central Andes and coastal Peru

The Central Andes are a noncollisional orogen in a convergent margin setting. Here the Nazca plate subducts below the overriding South American plate between 4° and 35°S. This segment is characterized by a major change of strike of the Peru-Chile Trench, by great ruptures in the oceanic lithosphere sinking under South America and by active volcanism, in contrast to the gaps in the line of active volcanoes to the north and south. Subduction along this margin has been active since the Mesozoic, with the modern phase of mountain building beginning in the latest Oligocene (Cobbold et al., 2007). In the Central Andes of Bolivia and southern Peru compressional began at ~47 Ma in the pre-Cordillera (the Andean ranges closer to the Pacific coast (Oncken et al., 2006). Deformation propagated eastwards, reaching the Eastern Cordillera first at ~40 Ma and virtually the entire Altiplano and Eastern Cordillera at ~30 Ma, with higher shortening rates in the Bolivian Eastern Cordillera (Gregory-Wodzicki, 2000; Oncken et al., 2006). The most notable change in the subduction regime during the Cenozoic was the break-up of the Farallon Plate into the Nazca and Cocos plates at ~23.4 Ma (Cobbold et al., 2007). Uplift (~1 km) persisted into the latest Miocene (last 10 Ma) as the eastern extent of Andean crustal shortening shifted eastward into what is now the Sub-Andean fold-thrust belt. This Late Miocene relief was created in the absence of significant deformation (I.e. faulting or folding) in the area, suggesting that processes occurring in the lower crust (I.e. lower crustal flow) or upper mantle (I.e. lithospheric delamination) are responsible for the growth of the central Andean Plateau during this period (E.g. Gregory-Wodzicki, 2000; Hoke et al., 2007).

Several processes can produce or support elevated terranes in convergent tectonic settings. These include those that (1) thicken the crust, such as crustal shortening due to compression, crystal underplating, magmatic addition, and ductile flow of the lower crust; (2) thin the mantle lithosphere, such as delamination and tectonic erosion; and (3) either dynamically or physically support the crust, such as thermal anomalies due to magmatism and mantle plumes

and very rigid crust or mantle lithosphere (Gregory-Wodzicki, 2000). Oncken et al. (2006) present convincing arguments about the major role played by the velocity of the westward drift of South America along the Central and Southern Andes (15°–26°S) for determining the amount and rate of shortening, as well as their lateral variability at the leading edge of the upper plate. This primary control is modulated by factors affecting the strength balance between the upper plate lithosphere and the Nazca/South American Plate interface. It has been recognized that only after the onset of shortening, at ~30 Ma, can generalized mountain building with similar geographical extension as the present-day Andes be clearly documented, both in the Central Andes (E.g. Allmendinger et al., 1997; Oncken et al., 2006) and in the Northern Andes (E.g. Gómez et al., 2001; 2005). Allmendinger et al. (1997) proposed that the reorganization of Pacific plates at ~25 Ma may have caused generalized mountain building in the Central Andes. Babeyko et al. (2006) suggested that the velocity of the westward drift of South America was sufficiently high by ~25 Ma to trigger extensive deformation of the strong Andean lithosphere. The coastal region of south-central Peru displays raised marine terraces indicating that, unlike the central Peruvian coast, it underwent a strong uplift since the Late Pliocene. These recent vertical movements are considered to be closely related to the subduction of the aseismic Nazca Ridge (Machare and Ortlieb, 1992). It is emphasized that the strongest uplift has been occurring immediately south of the inland projection of the Nazca Ridge, and not along the ridge axis

Rocks characteristic of continental crust are exposed along the coast of southern Peru and northern Chile. The Coastal Cordillera is made up of upper Jurassic to Cretaceous tholeiitic rocks, plutonites and marine backarc strata of Mesozoic age (Pinto et al., 2007). The Central Depression is a forearc depression, at ~1,000 m elevation that lies between the Coastal Cordillera and the western mountain front and is underlain by subhorizontal Oligocene to Recent alluvial, colluvial and volcanoclastic deposits (Allmendinger et al., 1997; Pinto et al., 2007). A line of Miocene to Recent stratovolcanoes overlying older ignimbrite sheets marks the Western Cordillera, the modern magmatic front. The Altiplano surface is covered by several large salars, Quaternary fill, and, locally, Late Oligocene to Recent volcanic rocks, including immense Late Miocene to Pliocene ignimbrite centers at the southern end of the plateau. Sparse exposures of the underlying basement consist of Ordovician and Cretaceous rocks ignimbrites (Allmendinger et al., 1997; Pinto et al., 2007).

2.3.4. Geography and climate of coastal Peru and the Atacama Desert

South of 6°30’ S the Andes reach almost all the way to the coast, restricting the coastal lowlands to a narrow strip, which is often no wider than 10 km. This pattern continues, with minor exceptions, to Chile. Several physiographic provinces exist in the study area (Figure 2.7). From west to east, they are 1) Coastal Cordillera, 2) Central Depression, 3) western mountain front, 4) Western Cordillera, and 5) Altiplano. The Coastal Cordillera, less than 20 km wide, lies between the Pacific Ocean and the Central Depression and has peaks as high as 2,500 m and an average elevation of ~1,500 m that wanes toward the north, where it is less than 1,000 m at 18.5°S. Smoothed hills and shallow valleys form it. The deepest canyons of South America were cut by the Cotahuasi, Ocoña, and Colca rivers at 15°–16°S. Although their valley heads currently impinge beyond the Quaternary volcanic arc into the semi-arid Altiplano (rainfall 250–350 mm/yr), these canyons occur in a region where rainfall is <100–200 mm/yr (Thouret et al., 2007).

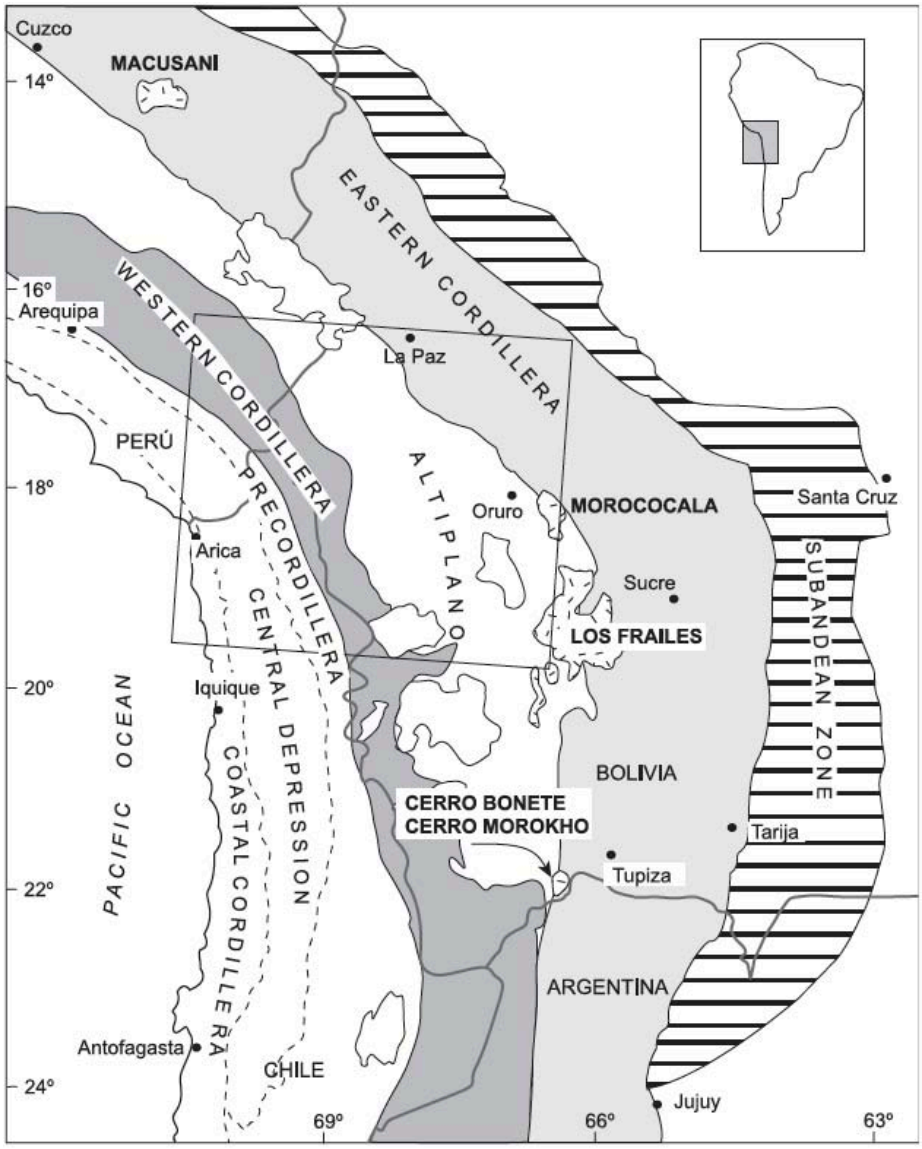

Figure 2. 7 Morphostructural units in the orocline of the Central Andes, from Pinto et al. (2004).

To the west, the Coastal Cordillera is cut by a subvertical escarpment ("Coastal Escarpment") of 1,000 m high. To the east, the altitude diminishes towards the Central Depression and the deposits filling the Central Depression overlap the basement rocks. The Central Depression extends parallel to the continental margin, bracketed between the Coastal Cordillera and the Precordillera. It corresponds to a forearc continental basin with a flat top surface at altitudes from 500 to 1,000 m in the west to 1,900 to 2,300 m in the east (Allmendinger et al., 1997; Pinto et al., 2007). The Central Depression is void of hydrologic processes, and is where the Atacama's hyper-arid conditions occur. The surface of the northern part of Central Depression has been locally deeply dissected by quebradas (canyons), in some cases up to 1.5 km deep, but typically less than 1 km (Mortimer, 1980). Their incision postdates deposition of the Late Tertiary valley-fill sediments of the Central Depression succession. Only the trunk drainages of the quebradas contain actively flowing or intermittent streams. Some tributaries are relict and contain no evidence of recent flow or even of relict fluvial sediments along their floors, and may have been shaped, at least partly, by groundwater sapping (Hoke et al., 2004). The western mountain front connects the high elevations of the Western Cordillera and Altiplano to the Central Depression. The Western Cordillera is a magmatic arc that consists of widely spaced volcanic peaks superimposed on a 4,000 to 5,500 m plateau. The Altiplano province is a

250 km wide, 3,700 m high plateau with internal drainage. The eastern limit of the plateau is marked by the high topography of the Eastern Cordillera (Allmendinger et al., 1997; Pinto et al., 2007).

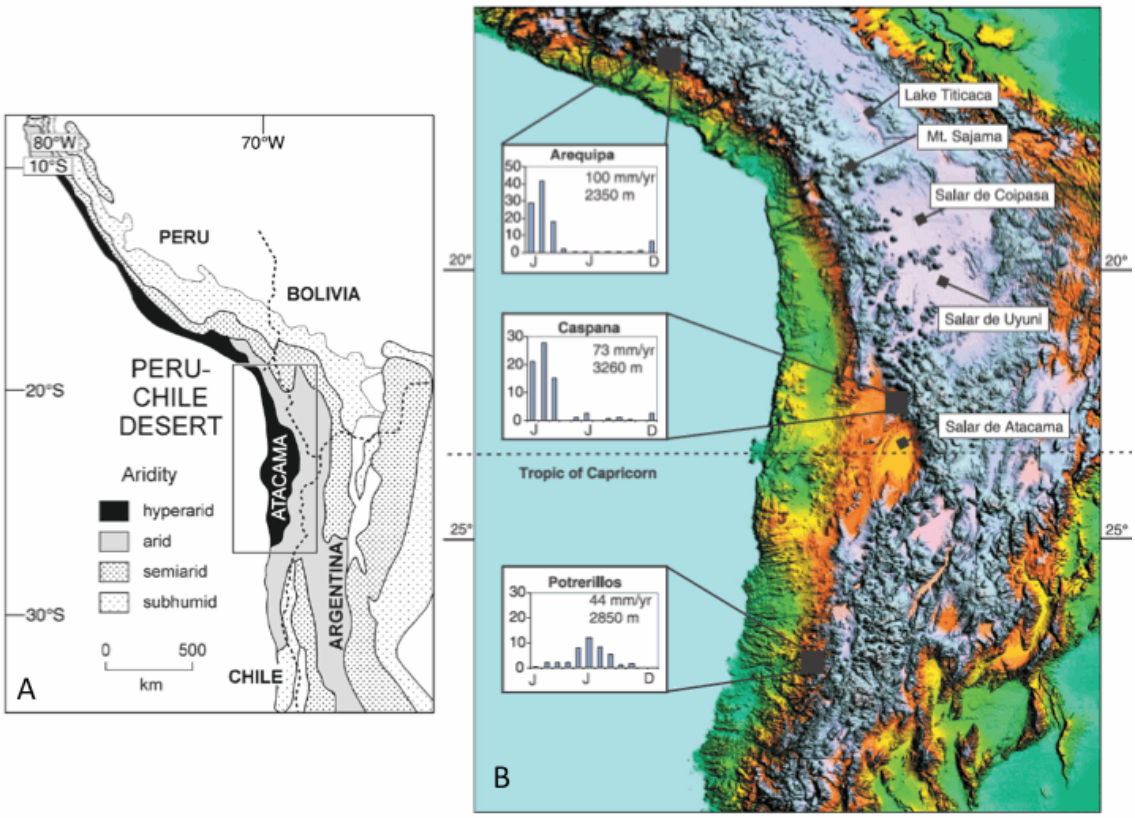

Figure 2. 8 (A) Location map showing present-day climatic zones of western South America, from Hartley and Chong (2002). **(B)** Digital Elevation Map of the subtropical Andes showing precipitation seasonality in the Atacama Desert and key sites, from Betancourt et al. (2000). Approximate elevations are >4,000 m (blue), 4,000 to 3,500 m (pink), 3,500 to 3,000 m, 3,500 to 2,500 m (brown), 2,500 to 1,000 (yellow), and, 1,000 m (green). Broad areas of pink denote the Bolivian/Peruvian Altiplano.

All parts of the study area below 3,500 m elevation are subject to the hyperarid and arid conditions of the Atacama and Peruvian Coastal Desert, which extends from the Ecuador-Peru border (3°30'S) to la Serena (30°S), Chile (Figures 2.8a, b). The Atacama Desert is one the driest locations in the world and harbors no vegetation. A primary cause for Atacama aridity is its location at the eastern boundary of the subtropical Pacific. In that region, large-scale atmospheric subsidence of the Hadley circulation significantly reduces precipitation (Houston, 2006) and maintains a surface anticyclone over the southeast Pacific that hinders the arrival of mid-latitude disturbances (Garreaud et al., 2010). The subtropical anticyclone drives equatorward winds along the coast that, in turn, foster the transport of cold waters from higher latitudes (I.e., the Peru Current), forcing upwelling of deep waters, that inhibits the moisture capacity of onshore winds creating a persistent inversion that traps any Pacific moisture below 1,000 m.a.s.l., and that also leads to the formation of a persistent deck of stratus clouds (see section 2.1). These factors result in a marked regional cooling of the lower troposphere that is compensated by enhanced subsidence along the Atacama coast (E.g. Takahashi and Battisti, 2007) further drying this area. The proximity of the Andes Cordillera has been regarded as an additional factor for the dryness of the Atacama. The effect of the Andes on continental precipitation was discussed on section 2.1. This mountain range supposedly restricts the moisture advection from the interior of the continent thus producing a rain shadow effect that is reflected in the marked east–west rainfall gradient (Houston and Hartley, 2003).

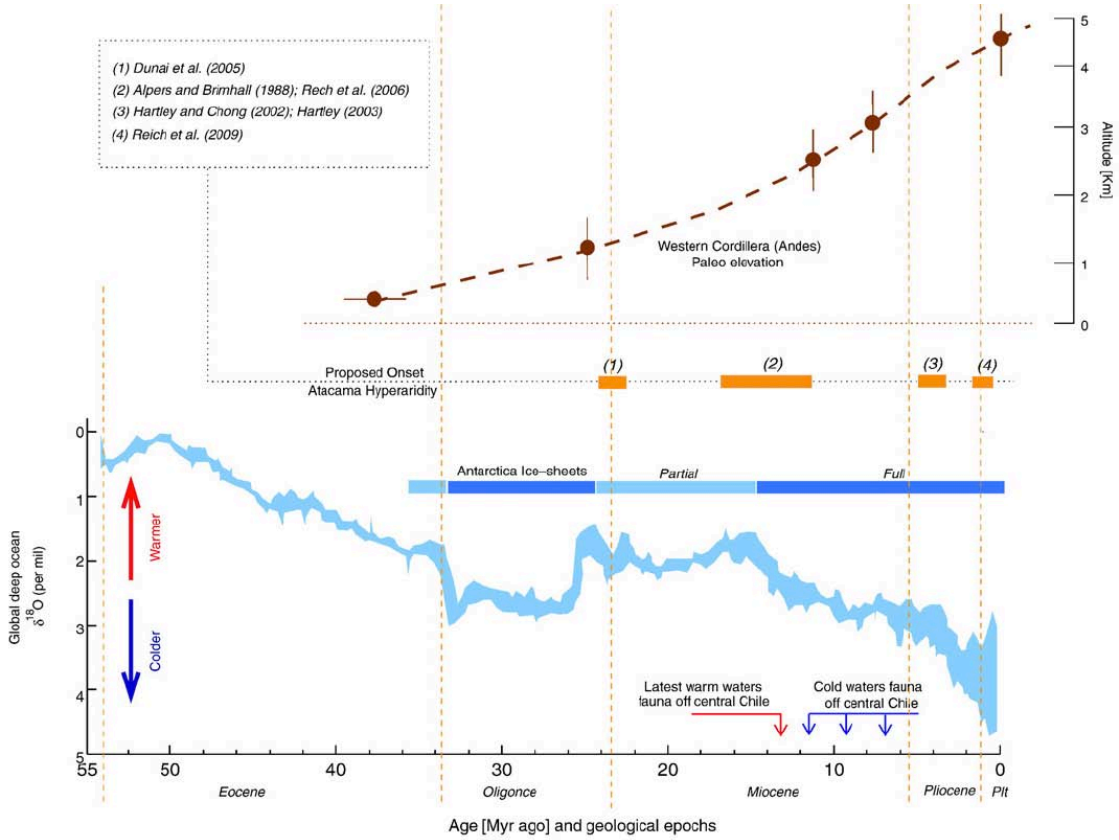

Figure 2. 9 . Schematic chronology of the Andes cordillera paleoelevation, from Garreaud et al., (2010), proposed onset of Atacama hyperaridity (different sources indicated in inset), presence of Antarctic ice sheets and global deep-sea oxygen and carbonate isotopes reflecting cooling of the deep ocean and changes in ice volumen, and some key biotic events off north-Central Chile.

In the central and northern Atacama Desert >80% of the mean annual precipitation occurs in the summer months (December–March). Absolute precipitation amounts depend on elevation and distance from the crest of the Andes, which controls rainout from spillover storms. The analysis of meteorological station data by Houston and Hartley (2003) shows that rainfall is strongly dependent on elevation in this area. At 1,000 m, in the Central Depression, rainfall is <50 mm/yr. Between 1,000–2,000 m above sea level is less than 50 mm, generally falling in Austral winter and decreasing with latitude in the coastal desert and at elevations >3,500 m, rainfall is ~150 mm/yr. The high peaks of the Western Cordillera (5,000–6,000 m) do not have station data but are believed to have annual precipitation in excess of 200 mm/yr. Temperature and precipitation vary with both latitude and elevation within the Atacama Desert. Mean annual temperatures range between 10° and 16°C (mainly varying with elevation and proximity to the coast). Marine fog, which gives rise to light drizzling rain (*garúa*) in coastal areas, is the most important source of water for native plants and biological soil crusts in the Atacama Desert, but inland incursion of this fog, as well as formation of inland radiation fogs, depends on elevation and topographic connection to the coast (E.g. Cereceda et al., 2002; Cáceres et al., 2007). Thus biological systems such as soil bacteria, hypolithic cyanobacteria, lichens and even cacti that rely on fog moisture will be more abundant along the coast.

The El Niño events affect interannual precipitation variability on the Altiplano, especially during Austral Summer (Aceituno, 1988). Precipitation during Austral Winter (JJA) shows no relationship with the extremes of the Southern Oscillation. The Eastern and Western Cordilleras, however, exhibit different levels of sensitivity to El Niño events (Garreaud, 1999; Vuille et al., 2000). High-altitude westerly wind anomalies that inhibit convection over the western edge of the Altiplano characterize El Niño years, causing sustained dry conditions by

limiting moist air advection from the eastern Cordillera across the Altiplano (Garreaud, 1999). Conversely, a southward displacement of the Bolivian High and enhanced easterly circulation that produces greater advection and increased precipitation characterized La Niña years (Vuille, 1999). In the western coastal regions of the Americas, an El Niño event is associated with increased precipitation (E.g. Quinn and Burton, 1970). This increase in precipitation enhances plant productivity in terrestrial ecosystems; this effect is especially dramatic in desert ecosystems where water is the main limiting factor to plant productivity (E.g. Holmgren et al., 2006). The La Niña years are characterized by rainfall anomalies of the opposite sign (E.g. Quinn and Burton, 1970).

The history of aridity in the core of the Atacama Desert has persisted for the past 200 Ma and is first recorded by Late Triassic–Early Jurassic (pre-Sinemurian) evaporites (Clarke, 2006). Late Jurassic evaporites occur at modern latitudes of 21°–35°S, which are close to the Quaternary distribution of 19°–27°S, indicating that there has been little latitudinal shift of South America and the climatic arid zone over this period, although the Jurassic zone was twice as wide as the Quaternary (Clarke, 2006). Consistent with the nearly fixed latitudinal position of the South American continent during the last 150 Ma (E.g. Beck et al., 2000; Clarke, 2006) it is generally accepted that stable arid/semiarid conditions (≤50 mm/year) have prevailed over the Atacama region at least since 150 Ma ago despite extreme fluctuations in climate during the Plio-Pleistocene. The main influence on desert development in northern Chile is the location within an area of anticyclonic subsidence, which is controlled by the global Hadley circulation and is not strongly related to the regional distribution of land and sea (see above). In the southern hemisphere the area of atmospheric subsidence occurs at present between 15° and 30°S, and during global hothouse conditions would have been displaced slightly polewards (Hartley et al., 2005). Global circulation model experiments for Neogene times suggest broadening of the Hadley cell with an associated prediction of reduced total precipitation over tropical areas, but no change in the location of the southern limit of the Hadley cell (Hartley et al., 2005). The rain shadow effect associated with the Andean Cordillera can be discounted as a climate-controlling mechanism in the Mesozoic and Palaeogene, as Andean uplift did not commence until ~50 Ma ago (see section 1.5). An ancestral Humboldt Current may have influenced climate, as evidence for the initiation of a cold, upwelling current off the west coast of South America dates back to latest Cretaceous to earliest Cenozoic times (E.g. Keller et al., 1997).

The onset of the current hyperarid conditions (≤5 mm/year), however, is a matter of controversy as illustrated in the time-line of Figure 2.9. The wide range of geological dates proposed (25 Ma to 1.5 Ma) for the onset of current hyperarid conditions in the Atacama partially arise from the different methods, scope (local versus regional conditions), record resolution (fine versus coarse) and location (I.e. coastal areas versus Andean foothills) of the above mentioned studies (Garreaud et al., 2010). Moreover, the geological literature is confused by an inconsistent definition of aridity, which represents the degree to which a climate lacks effective, life-promoting moisture. Long-term precipitation records allow designating a region as arid (hyperarid) when mean annual precipitation is below than 50 mm (5 mm). In contrast, paleoclimate studies can only establish the degree of aridity very indirectly upon interpretation of geological evidence (Garreaud et al., 2010).

Conceptually, both Andean uplift and southeast Pacific cooling may produce hyper-aridification of the Atacama by creating a rain shadow or increasing the atmospheric subsidence, respectively. However numerical simulations of the climate system (Garreaud et al., 2010) suggest that SST cooling off Chile/Peru since the Late Miocene and, especially, during the Pliocene/Pleistocene transition, very effectively resulted in a drying over the Atacama Desert, either gradual or stepwise, that culminated with the present day hyperarid conditions. Conversely, the Andean surface uplift had little, if any, effect on the lack of precipitation and

moisture over the Atacama, regardless of the age of uplift (Garreaud et al., 2010).

2.4. Sedimentary record off the western South American coast

The sedimentary process in the basins of coastal western South America and the adjacent Pacific deep-sea differ significantly. The continental climate south of the equatorial front is exceptionally arid, so there are no major streams entering the Pacific along the Peru and northern Chilean coasts. Recently, uplifted coastal terranes of unconsolidated sediment and ash from Andean volcanoes provide abundant detritus for the intermittent streams that do exist in the desertic coastal areas of Peru and northern Chile, while numerous rivers drain the coast and Andes of Ecuador.

2.4.1. Carnegie Ridge (Ocean Drilling Program Site 1239)

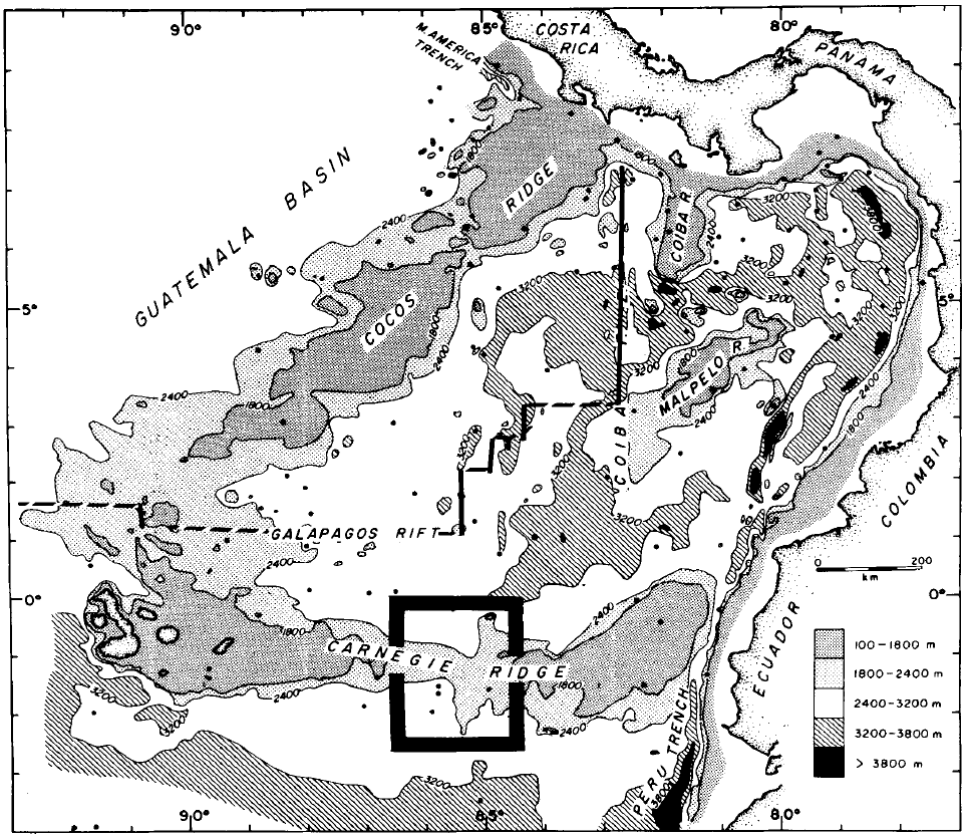

Figure 2. 10. Bathymetric map of the Panama Basin, from Malfait and Van Andel (1980). The crest is generally shallower than 2000 m. Near 86°W longitude, the Carnegie Ridge is marked by a 2300 m deep saddle. West of the saddle the ridge shoals toward the pedestal of the Galápagos Islands, eastward it rises to about 1400 m before terminating in a trough along the Ecuadorian continental margin.

The Carnegie Ridge is an east-west trending submarine ridge about 300 km wide and 1,350 km long on the ocean floor of the northern Nazca Plate (Figures 2.4b and 2.10). Its E-W trend is almost normal to the strike of the Ecuadorian Trench, along which it is being subducted beneath the South American Plate. The most ancient parts of the Carnegie Ridge were formed at around 20-22 Ma, when hotspot volcanism traces began to form (Meschede and Barckhausen, 2001). The youngest part of the Carnegie Ridge is at its western end in the Galápagos archipelago where active volcanism related to the Galápagos hotspot is observed (Meschede and Barckhausen, 2001). Based on examination of the basement uplift signal along trench-parallel transects Gutscher et al. (1999) estimated that the Carnegie Ridge has been colliding with the margin since at least 2 Ma.

The composition of surface sediments along the elongated shape of Carnegie Ridge and the surrounding basin areas is directly related to the surface productivity, crustal age, carbonate compensation depth, distance from the mainland (source of terrigenous sediment), dissolution, and bottom water flow (Pazmiño, 2005). Dilution by terrigenous material near the mainland, and eroded volcanic debris around the Galapagos Volcanic Platform are locally important to the sediment composition (Pazmiño, 2005). The Carnegie Ridge is exposed to productivity changes that affect mainly pelagic settling, with high primary productivity gradients associated with the upwelling from coastal margins and equatorial divergence, and advection of nutrients by currents (Pazmiño, 2005). The pelagic sediment contains more biogenic carbon and silica and more organic matter than neighboring sediments (Pazmiño, 2005).

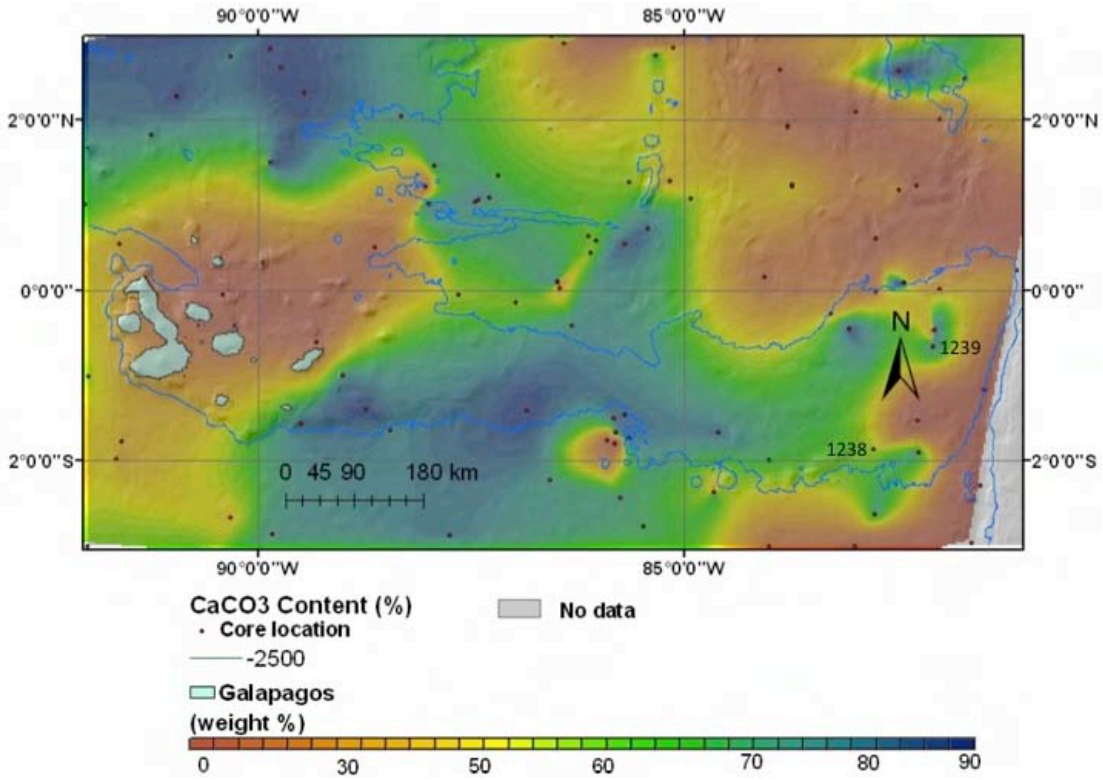

Figure 2. 11. $CaCO_3$ content distribution in bottom deposits along the Carnegie Ridge, from Pazmiño (2005). Dots show sample locations.

The patterns in the $CaCO_3$ distribution are marked by the terrigenous dilution, siliceous zones, and the differences between the climatic (productivity) zones produced by the geographical position of the equatorial front. The dominant carbonate is found in the eastern portion of the ridge (Figure 2.11), where siliceous sediment accumulation is not so important (Figure 2.12). In the hills of the eastern ridge, Ocean Drilling Program (ODP) Sites 1238 and 1239 exhibit moderate accumulation of 58% and 72%, respectively (Pazmiño, 2005). Sediment deposition on the ridge occurs above the lysocline, which is either located at 2,800 m (Thunell et al., 1982), or at 2,700 m (Lyle, 1992), therefore dissolution is not evident in the upper 2,500 m of the ridge.

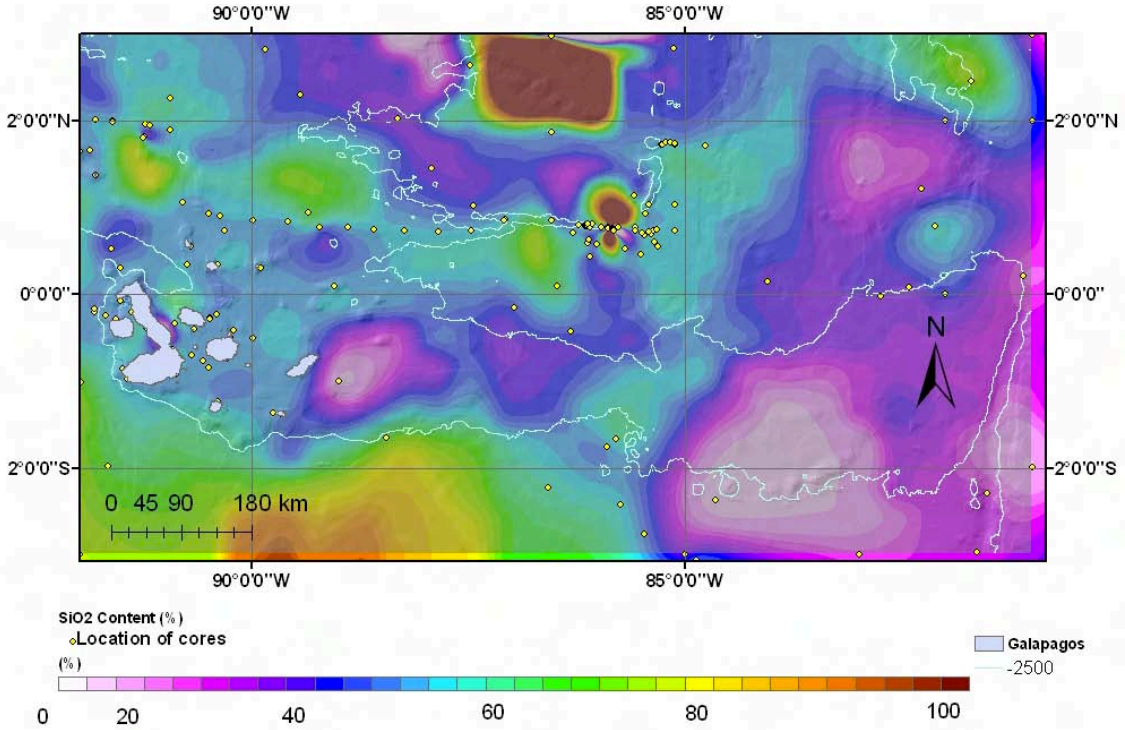

Figure 2. 12. Content of opal in surface sediments (as a percent of the sample) along the Carnegie Ridge, from Pazmiño (2005). Dots show sample locations.

The content of opal in recent sediments (Figure 2.12) in the Carnegie Ridge ranges from 13 to 80 weight percent. Three essential zones of recent silica deposition are identified: (1) the east ridge, which has the lowest values; (2) the west ridge area shows moderate values and (3) siliceous rich deposits are found in Peru Basin, where $CaCO_3$ undergoes dissolution. Opal silica located on the seafloor is composed of remains of biogenic siliceous sediments formed of the residues of diatom and radiolarian and its distribution is well correlated with the surface productivity maps (Pazmiño, 2005).

Terrigenous sediments in the area surrounding the Eastern Galapagos Islands, and the boundaries of the ridge-trench junctions at the north and south, which are mainly composed of clay from the mainland and glass volcanic from Galapagos Volcanic Platform (Pazmiño, 2005). Terrigenous sediments and basaltic ash originating from the volcanic Galapagos Islands was found around the Galapagos Volcanic Platform, and more silicic glass shards of volcanic origin are found on the east side of the Carnegie Ridge (Pazmiño, 2005). The East Ridge receives a moderate supply of terrigenous sediment from the mainland delta systems formed around river mouths located along the continental shelf. These rivers deposit most of their sediments in the Ecuadorian Trench. Sedimentary quartz distributions are linear with respect to bottom conditions, and their source is mostly continental (Pazmiño, 2005). The general distributions match the highest concentration values of quartz closer to the continent (Figure 2.13), confirming a heightened input of terrigenous sediments closer to the mainland. The main patterns of non-carbonate sediments match the flux rates of terrigenous sediment. Maximum flux rates occur near the mouths of the Guayaquil, Esmeraldas, and Magdalena rivers, and at the corners of the Carnegie Ridge-Trench Junction (Pazmiño, 2005). Sediment is distributed latitudinally, in accordance with the water masses and aeolian forces. The concentration of terrigenous material produces a dilution of the other components of the sediment system, such as planktonic skeletons, which significantly reduces concentration of $CaCO_3$ (Pazmiño, 2005).

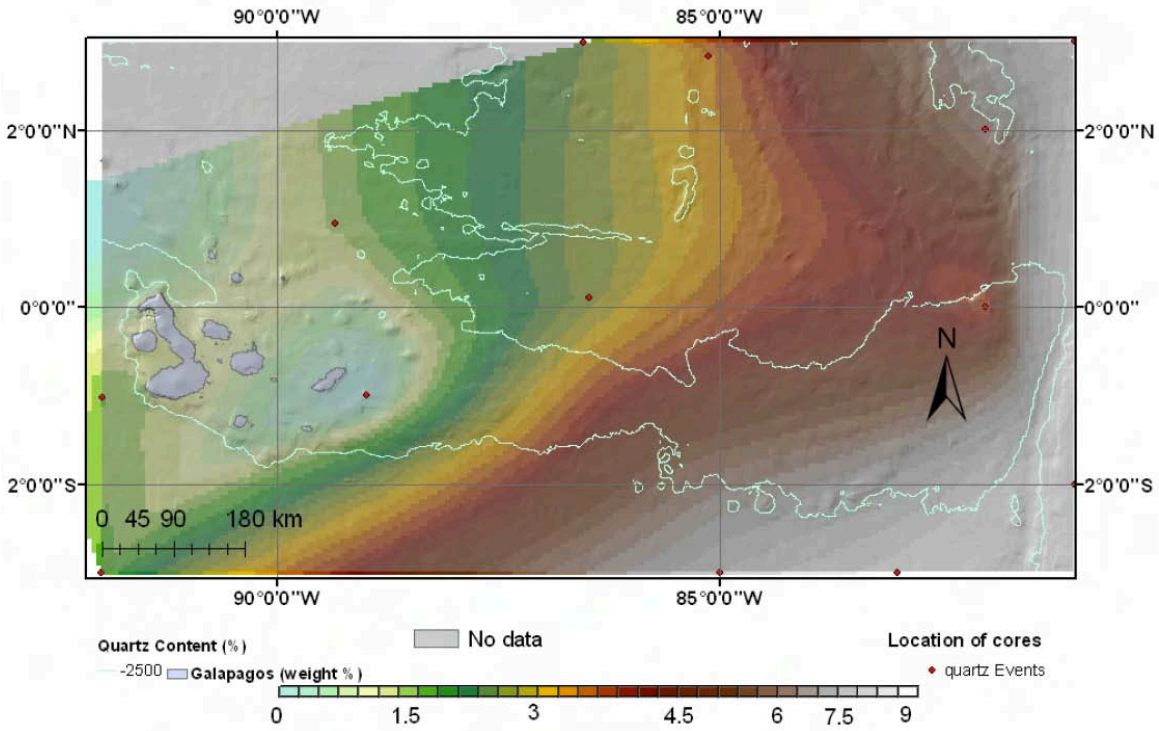

Figure 2. 13. Content of quartz in surface sediments (as a percent of the sample) along the Carnegie Ridge, from Pazmiño (2005). Dots show sample locations.

The concentrations of sand and silt on the ridge are mainly foraminifera material, the abundance is between 10 and 30%. The clay fraction is less than 10% and between 50 and 70% in the abyssal plain surrounding the ridge. Major input of clay is observed in the ridge-trench junction, between 70 and 90% (Pazmiño, 2005). Surface sediments containing concentrations of metals were limited to manganese nodules in the Carnegie Ridge (Pazmiño, 2005). The northeast ridge and surrounding areas have greater concentration of clay minerals than the rest of the ridge (Pazmiño, 2005). They are composed mainly by kaolinite and chlorite, which are mixing with feldspar lavas (Pazmiño, 2005). Smectite, clay mineral formed in the ocean as well supplied from continents, is distributed with high content in the Galapagos Platform. Oceanic debris rich in basalt is also supplied to the Galapagos Platform as a product of volcanism of the Galapagos Islands (Pazmiño, 2005).

2.4.2. Nazca Ridge (Ocean Drilling Program Site 1237)

The Nazca Ridge is a major, 250-km-wide, aseismic and volcanic bathymetric high, which reaches more than 1.5 km above the surrounding ocean floor (Figure 2.14). This ridge has swept southwards along the margin since its first collision at about 11°S some 10 Myr ago to 15°S where it presently subducts beneath the Peruvian margin (Kukowski et al., 2008).

The detrital contribution increases strongly as a function of the proximity to the South American continent. Except for the coastal upwelling region where biogenic dilution occurs, sediments from areas closer than 1,000 km are composed of greater than 80% detritus (Dymond, 1981). However the Nazca Ridge exhibits mixed characteristics, with sediments dominated by biogenic constituents produced by foraminifera and coccolithophores (Figure 2.15; Krissek et al., 1980).

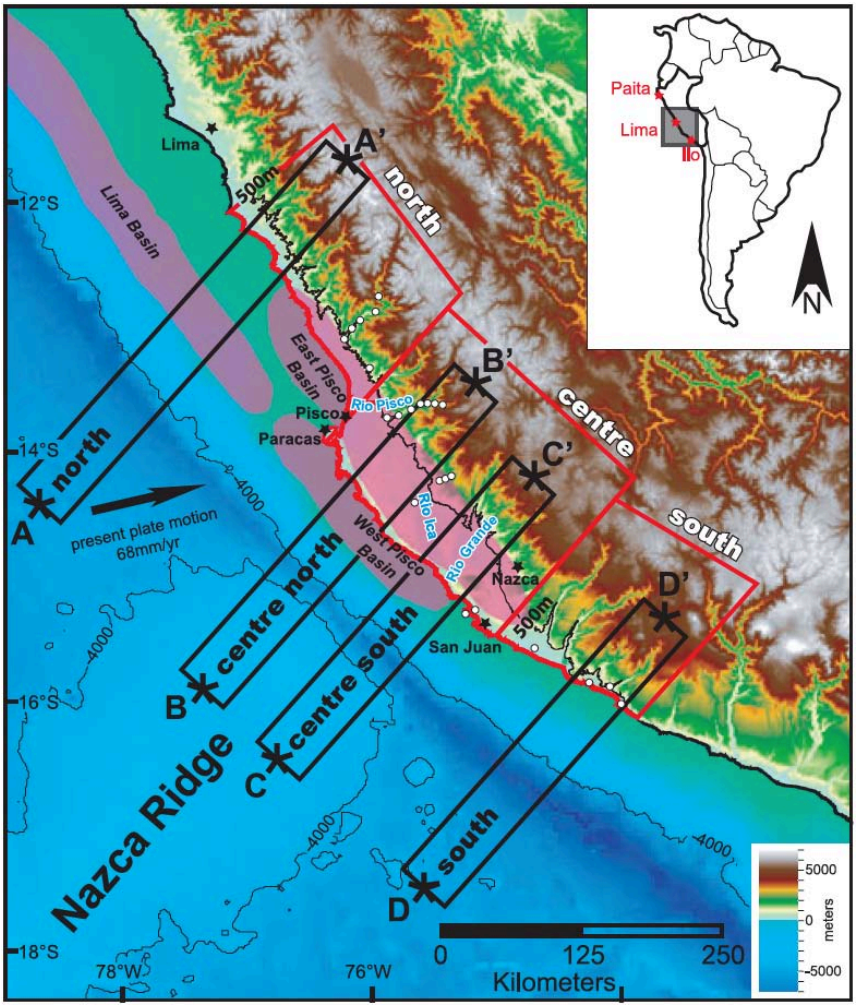

Figure 2. 14 Digital elevation model of the Peruvian coastal margin from 10° to 18°S and from 72° to 82°W, from Wipf et al. (2008). Sedimentary basins are added. In red are the areas used for river dispersal patterns. The 500 m contour line is highlighted in black.

Molina-Cruz and Price (1977) interpreted a lobe of quartz-rich sediments that trends to the northwest off central and northern Peru to be a consequence of eolian transport and sedimentation (Figure 2.16). Additionally, Scheidegger and Krissek (1982) found a striking resemblance between wind-driven surface currents of the southeast Pacific and the dispersal pattern of clay-sized and fine silt-sized material. However, on crossing to the seaward side of the Peru Trench, sedimentation rates decrease dramatically, and clay mineral assemblages change abruptly. Therefore, Scheidegger and Krissek (1982) argue that the trench is an imposing barrier to seaward near-bottom advection of suspended particulates; thereby deposition of terrigenous eolian components must be dominant seaward of the trench. According to Saukel (2010), the northern/central Peruvian coast and the Atacama/ Altiplano region further south, deliver quartz to the Eastern Pacific, highest quartz contents on the Nazca Ridge and in the southern Peru Basin a few hundred kilometers offshore point to the southern area as the stronger source.

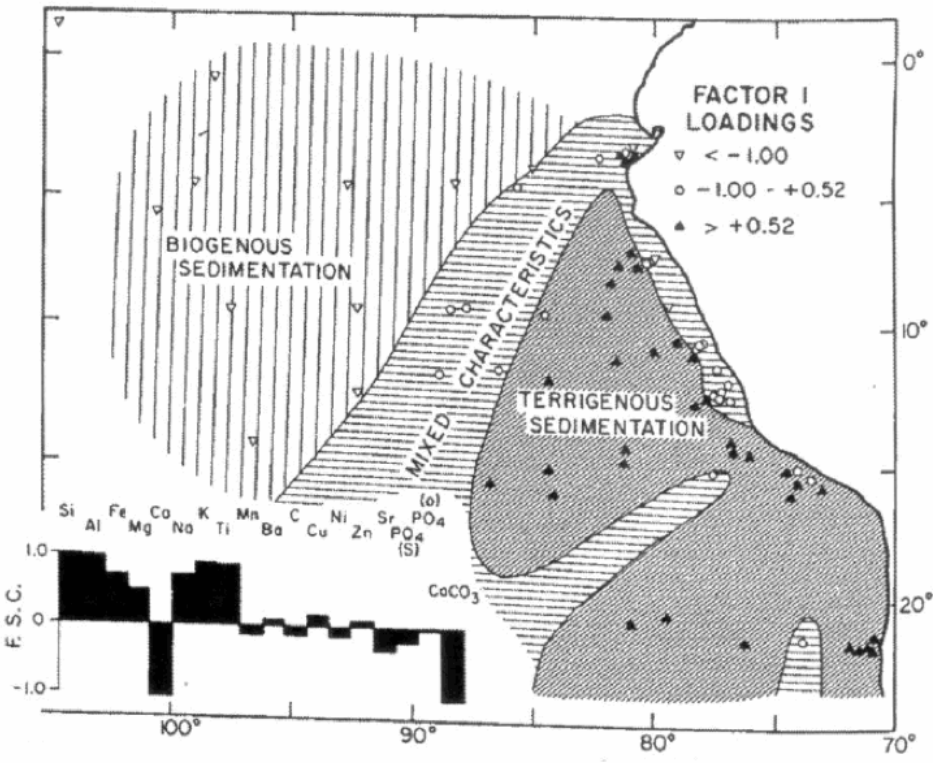

Figure 2. 15 Results of and R-mode factor analysis of chemical data on surface samples from the Peruvian coastal margin and Nazca Plate, from Krissek et al. (1980). Factor score coefficients (F.S.C) are noted for the chemical variables for each factor.

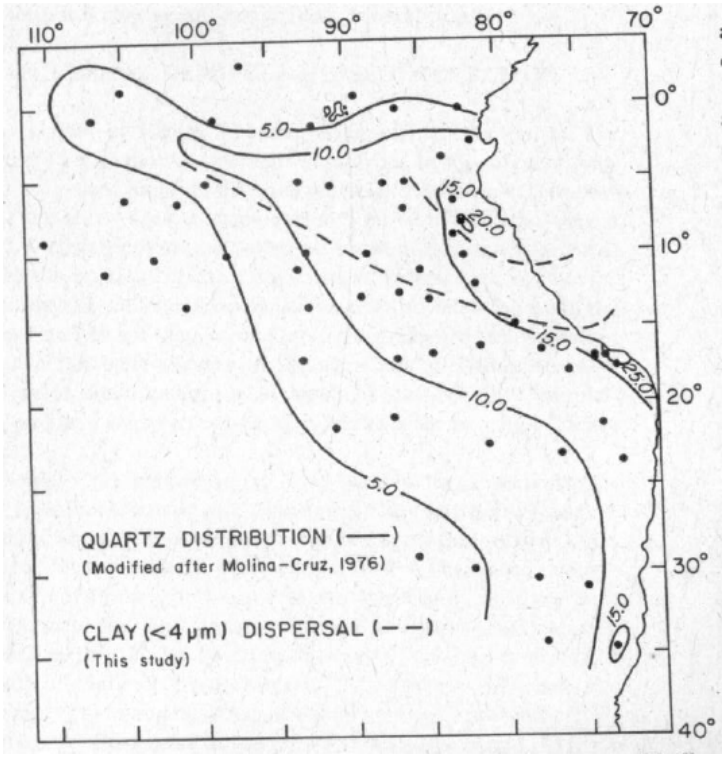

Figure 2. 16 Relationship of distribution of quartz of bulk-sediment samples, on an opal and carbonate-free basis, relative to the dispersal pattern of clay-sized sediment determined by using quartz/feldspar ratios, from Scheidegger and Krissek (1982). Quartz-rich lobe is associated with sediments derived from the quartz-rich sediment sources of central and northern Peru.

2.4.3 Peruvian Shelf (Ocean Drilling Program Site 1229)

The entire length of the Peruvian coastal region is characterized by a constant, orogen-parallel architecture and an arid climate. Off northern Peru the continental slope is extremely irregular, marked by several prominent canyons. Size and frequency of occurrence of the canyons decreases to the South (Busch and Keller, 1981). North of 19°S small basins are common on the lower and middle slope and prominent plateaus occur on the upper slope (Figure 2.14).

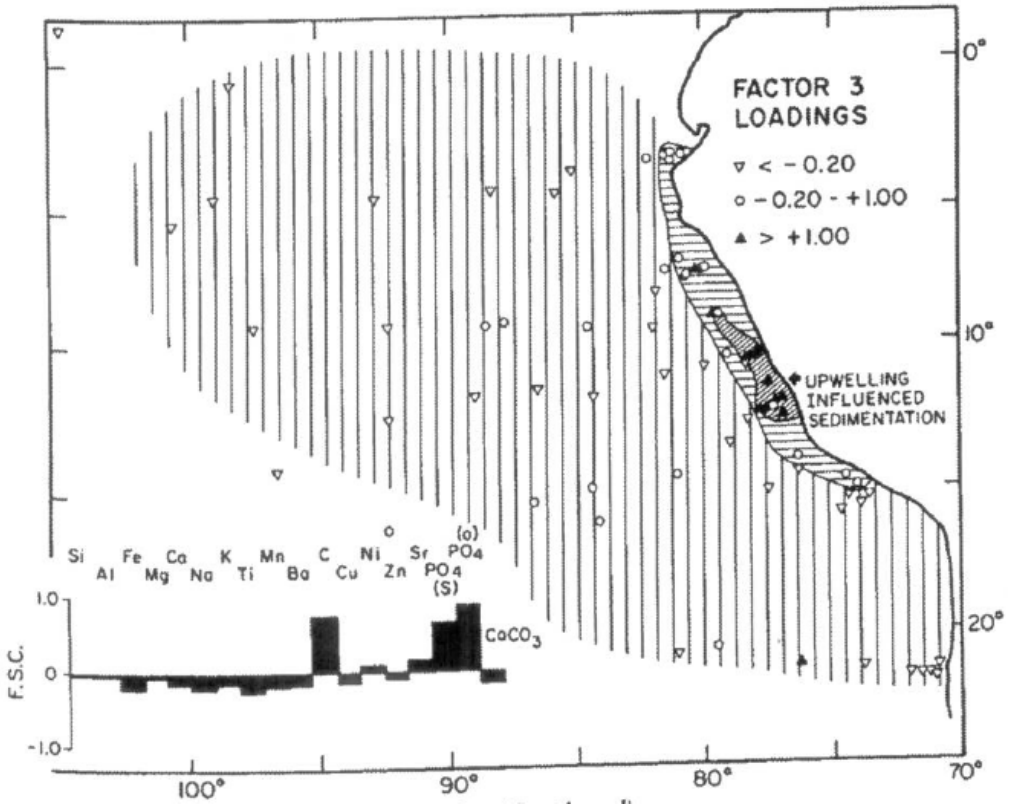

Figure 2. 17. Results of and R-mode factor analysis of chemical data on surface samples from the Peruvian coastal margin and Nazca Plate, from Krissek et al. (1980). Factor score coefficients (F.S.C) are noted for the chemical variables for each factor.

Patterns of sediment composition and distribution on the Peruvian continental margin are strongly influenced by the surface-water circulation in the eastern Pacific (E.g. Krissek et al., 1980; Scheidegger and Krissek, 1982). Coastal upwelling is a prominent feature of the circulation north of 20°S and occurs within 50 km of shore in response to the prevalent trade winds. This upwelling is accompanied by the rapid accumulation of organic matter, PO_4 (soluble), and PO_4 (organic) in the underlying sediments (Figure 2.17; Krissek et al., 1980). Typical surface sediments between the coast and the Trench are diatomaceous muds. They are green and grey as result of the near reducing conditions, and have epiclastic and pyroclastic volcanic components. These sediments are also characterized by relatively high contents of fecal pellets, glauconite, phosphorite nodules, biotite, glass and detrital grains. Submarine canyons, basins, and the trench also contain turbidite sands (Moberly et al., 1982)

Krissek et al. (1980) recognized a progressive fining of the sediments along the slope from south to north and across the slope with increasing distance from shore. Increased grain sorting accompanies the offshore decrease in grain size. Krissek et al. (1980) concluded that the textural patterns along the Peru-Chile margin reflect the influence of water depth, proximity of the continental sediment sources, altitudinal changes in terrigenous input, accelerated settling of fecal pellets and bottom transport by nepheloid layers. Offshore fining

of the sediments was interpreted to be a product of the decrease in particle size that is maintained in suspension with increasing water depth and distance from shore. Climatic variation onshore is responsible for the decrease in grain size from south to north along the margin. Northern Peru has a wetter climate, and rivers draining this area deliver finer-grained sediment to the ocean. High primary productivity in the area of intense upwelling supports large zooplankton stocks, which can incorporate fine terrigenous particles into fecal material.

CHAPTER 3

SAMPLE MATERIAL AND METHODS

3.1. Site Locations and Sample Material

Part of this study (Chapter 4) is based on a set of surface sediment samples of the eastern tropical and subtropical Pacific (10°N - 25°S, 100°W - 70°W), provided by Prof. Alan Mix (Oregon State University). While this case study on the "equatorial front track" was based on a set of surface sediment, down-core analyses were performed on ODP Sites 1239 (Chapters 5 and 8), and 1237 (Chapter 7), both retrieved during Ocean Drilling Program Leg 202; on ODP Site 1229 (Chapter 6), which was retrieved during Ocean Drilling Program Leg 201, and core MD02-2529 (Chapter 5), collected during the images VIII/MD 126 Mona Oceanographic cruise. In the following, the relevance of the core locations for reconstructing the evolution of the eastern tropical Pacific background state and the continental climate of the west coast of South America are outlined.

3.1.1. Surface Sample Material

Surface sediment samples were retrieved from water depths between 192 and 4,622 m.b.s.l, mostly on the Cocos and Carnegie ridges (Figure 3.1). They were analyzed to define the location of the equatorial front in the Pacific, based on foraminifera census and stable isotope data (see Chapter 4). The sample material was obtained by means of multi-corers, box-corers, gravity or piston corers.

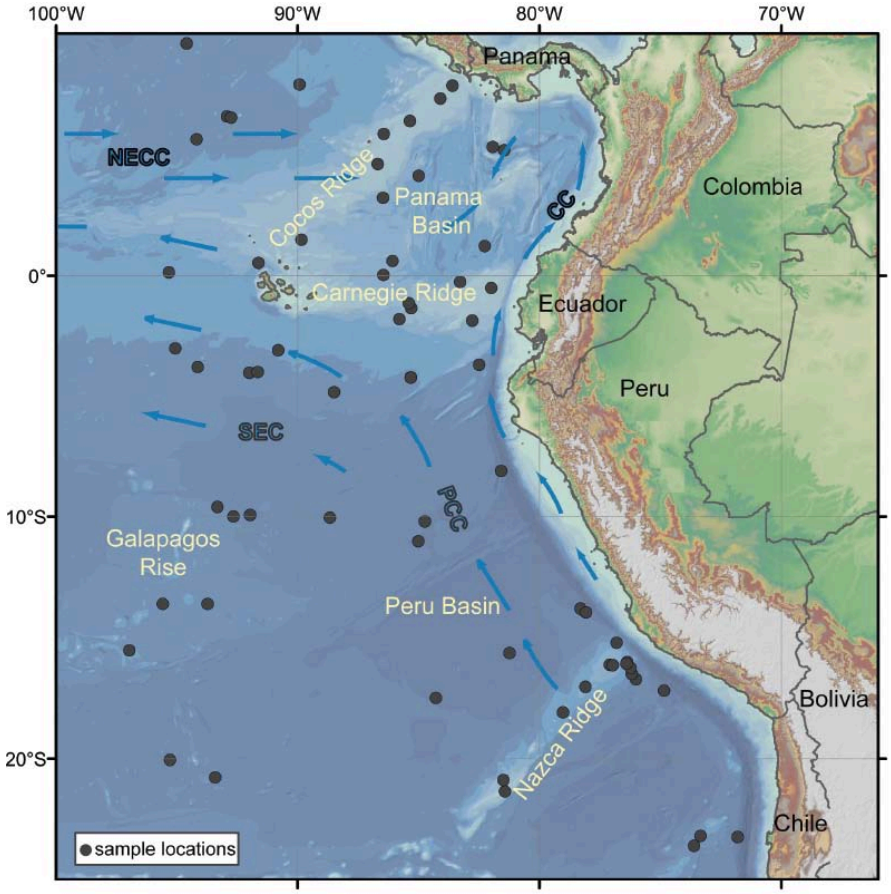

Figure 3. 1 Eastern Pacific bathymetry and location of surface samples, from Saukel (2011). Oceanographic features off Peru, Ecuador and Colombia are illustrated. CC = Coastal Current, PCC = Peru-Chile Countercurrent, PCC = Peru-Chile Current, NECC - North Equatorial Counter Current; SEC - South Equatorial Current.

3.1.2. ODP site 1239 (0.40°S, 82.41°W)

Site 1239 was drilled approximately 120 km off the coast of Ecuador, close to the eastern crest of Carnegie Ridge at a water depth of 1,414 m (Figure 2.4b; Shipboard Scientific Party, 2003a). Sedimentation rates are considerably higher on Carnegie Ridge than on Nazca Ridge, ranging from 5-18 cm/kyr (Shipboard Scientific Party, 2003a). A tectonic backtrack path on the Nazca plate moves Site 1239 about 600 km westward and slightly to the south relative to a fixed South America to a position southeast of the Galapagos hotspot about 12 Ma ago (Shipboard Scientific Party, 2003a). Today the site is located under the eastern reaches of the equatorial cool tongue, close to the equatorial front that separates cool, relatively high salinity surface waters south of the equator from the warm, low-salinity waters of Panama Basin (Shipboard Scientific Party, 2003a). Therefore, an open-ocean upwelling system occurs above Site 1239 location and sediments there consist of foraminifer and nannofossil oozes with variant amounts of clay, diatoms, and micrite. High concentrations of calcareous deposits produced in the upper waters are also reflected in closely spaced reflectors in seismic profiles from Ventura cruise, Melville Nemo3 cruise, and Sisteur Geoazur (Pazmiño, 2005). Due to its equatorial position and its proximity to the Ecuadorian coast, Site 1239 is likely to record changes in upwelling, biological production, as well as long-term changes in upper-ocean temperature, pycnocline depth, and changes in fluvial supply, related to the variability of precipitation in northwestern South America (see section 2.4.1).

Three holes were drilled at 20 m offset between each other, leading to full recovery of a 560.7 meters composite depth (mcd) sequence of Miocene (~15 Ma) to Pleistocene pelagic sediments (Shipboard Scientific Party, 2003a). The uppermost 400 mcd of the core correspond to the last 5Ma. The dominant lithology is nannofossil ooze with varying diatom and clay abundance (Shipboard Scientific Party, 2003a). Transitions between nannofossil ooze and diatom-bearing nannofossil ooze are present on a meter to decimeter scale. Foraminifer ooze is present in the upper 24.6 mcd. Minor components include radiolarians, silicoflagellates, micrite, and pyrite. Nannofossil abundance increases from the top (~20%) to ~50%–70% near 100 mcd. Farther downhole, nannofossil contents fluctuate, with average values gradually increasing downhole to values of ~80% at ~500 mcd. Below that level, nannofossils decrease again toward the base of the sequence the foraminifer and nannofossil oozes contain variable minor amounts of radiolarians, silicoflagellates, spicules, micrite, and siliciclastic components. The combined abundance of radiolarians, spicules, and silicoflagellates are quite variable throughout the sequence with pronounced minima at~85 mcd and from 250 to 290 mcd (Shipboard Scientific Party, 2003a). Clay minerals constitute ~90%–100% of the siliciclastic component with minor contributions from feldspars, amphiboles, micas, and pyroxenes. Siliciclastic content is highly variable with low mean values (~10%) throughout. In the top ~10 mcd and bottom ~50 mcd of the sequence, siliciclastic are more abundant (Shipboard Scientific Party, 2003a).

For the Late Pleistocene (approx. upper 17 mcd, 0-0.5 Ma) the age model was based on benthic oxygen isotope ($\delta^{18}O$) stratigraphy correlating high-frequency variations to the chronology of the LR04 stack (Lisiecki and Raymo, 2005). From 17 to ~211 mcd, the previous stratigraphy from (Shipboard Scientific Party, 2003a) was fine-tuned by correlating the alkenone-derived SST record of Site 1239 (0.5 to 3.2 Ma) to the SST record from the nearby and well-dated Site 846 (Etorneau et al., 2010). Between ~211 and ~400 mcd (3.2 to 5 Ma) the benthic $\delta^{18}O$ and carbon isotope ($\delta^{13}C$)-based age model of Tiedemann et al. (2007) was used. Although the latter is regarded as very preliminary and maybe not acute in orbital timescales, the age uncertainties are irrelevant for the timing of major changes in the Plio-Pleistocene eastern Pacific climatology.

3.1.3. ODP site 1237 (16.01°S, 76.37°W)

Site 1237 is located ~140 km off the southern Peruvian coast on the easternmost flank of Nazca Ridge at a water depth of 3,212 m (Figure 3.2; Shipboard Scientific Party, 2003b). Sedimentation rates at pelagic Site 1237 vary from 1-3 cm/kyr (Shipboard Scientific Party, 2003b). The tectonic backtrack path on the Nazca plate moves Site 1237 about 20° westward relative to South America over the past 42 Ma (Shipboard Scientific Party, 2003b). Today, Site 1237 is situated near the eastern edge of the northward-flowing Peru-Chile Current, a major conduit of cool-water transport from high to low latitudes. The site's position near the productive upwelling systems of Peru suggests that it may record changes in upwelling and biological production in this eastern boundary current setting. Primary productivity roughly follows SST trends along the backtrack path and implies that 30 Ma ago primary productivity would have been less than one-third of its present value at the site. Thus lower biogenic sedimentation rates and relatively minor amounts of terrigenous sediment are expected with greater age at Site 1237 (Shipboard Scientific Party, 2003b). According to Saukel (2011) Site 1237 could document past variations of deep, intermediate, and surface water masses in the subtropical South Pacific and changes of dust flux and trade-wind intensity, due to its proximity to the dust source area (coastal deserts of Peru and Chile, as well as the Atacama).

Three holes were drilled at 5-10 m offset between each other, leading to full recovery of a 360.4 meters composite depth (mcd) sequence of Oligocene (~31 Ma) to Holocene pelagic sediments. The uppermost 92 mcd of the core correspond to the last 5 Ma (Shipboard Scientific Party, 2003b). Sediments of the upper 92 mcd consist of clay minerals, nannofossils, and diatoms. Changes in the relative percentages of components in smear slide samples are often subtle yet result in different lithology classifications, such as diatom nannofossil clay, silty clayey diatom nannofossil ooze, diatom-bearing clay, and clayey diatom ooze, for almost identical lithologies. Siliciclastic content ranges from ~90% to 40%. Higher values of siliciclastics are present near the top of the hole and decrease below ~30 mcd. Siliceous microfossil percentages, including diatoms and sponge spicules, average ~15%, reaching maxima of >75% at ~5 and 40 mcd. The percentage of siliceous microfossils below 40 mcd is ~10%, whereas calcareous microfossils represent >50% of the sediment and increase to nearly 100% near the base of the interval. Calcareous and/or siliceous (silty) clays and clayey oozes are disrupted by 37 ash layers characterized by rapid sedimentation rates.

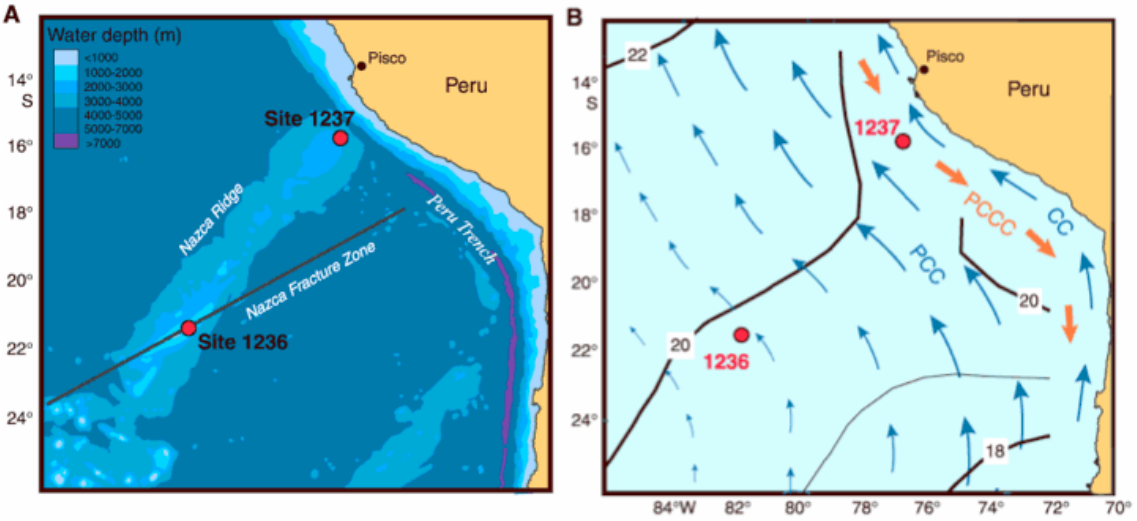

Figure 3. 2 (a) Southeast Pacific bathymetry and location of ODP Site 1237, from Shipboard Scientific Party (2003b). **(b)** Oceanographic features off Peru and northern Chile. CC = Coastal Current, PCCC = Peru-Chile Countercurrent, PCC = Peru-Chile Current. Modern mean annual SST (contours are in degrees Celsius).

The age model for Site 1237 was established by correlating high-frequency variations in gamma ray attenuation density, percent sand of the carbonate fraction, and benthic $\delta^{13}O$ to variations in Earth's orbital parameters (for details see Saukel, 2011). The excellent paleomagnetic stratigraphy at Site 1237, with all chrons and subchrons clearly defined for the past 5 Ma, led to a satisfying temporal classification of the sediment.

3.1.4. ODP site 1229 (10.58°S, 77.57°W)

Site 1229 is located on the Lima Basin (Peru shelf) in 150.5 m water depth. It is in the immediate vicinity of Leg 112 Site 681 (Figure 3.3). Sedimentation rates are on the order of 8 cm/kyr for the Jaramillo Normal event to the Holocene (Shipboard Scientific Party, 1988). This site is also located nearest the origin of coastal upwelling centers around the headlands near 11°S; its depth nearly coincides with the top of the oxygen-minimum zone (Shipboard Scientific Party, 1988). Being the most landward (and consequently the shallowest) site in the upwelling deposits of the Peruvian shelf, Site 1229 provides an expanded Quaternary record that reflects the seaward-landward shift of upwelling centers during changes in sea level (Shipboard Scientific Party, 1988). This shift may have been so dramatic in the past that the most landward part of the shelf may have been entirely removed from the influence of coastal upwelling during extremely low stands of sea level. Because this site is located nearest the coast, it might record continental climate conditions on the arid coast of Peru.

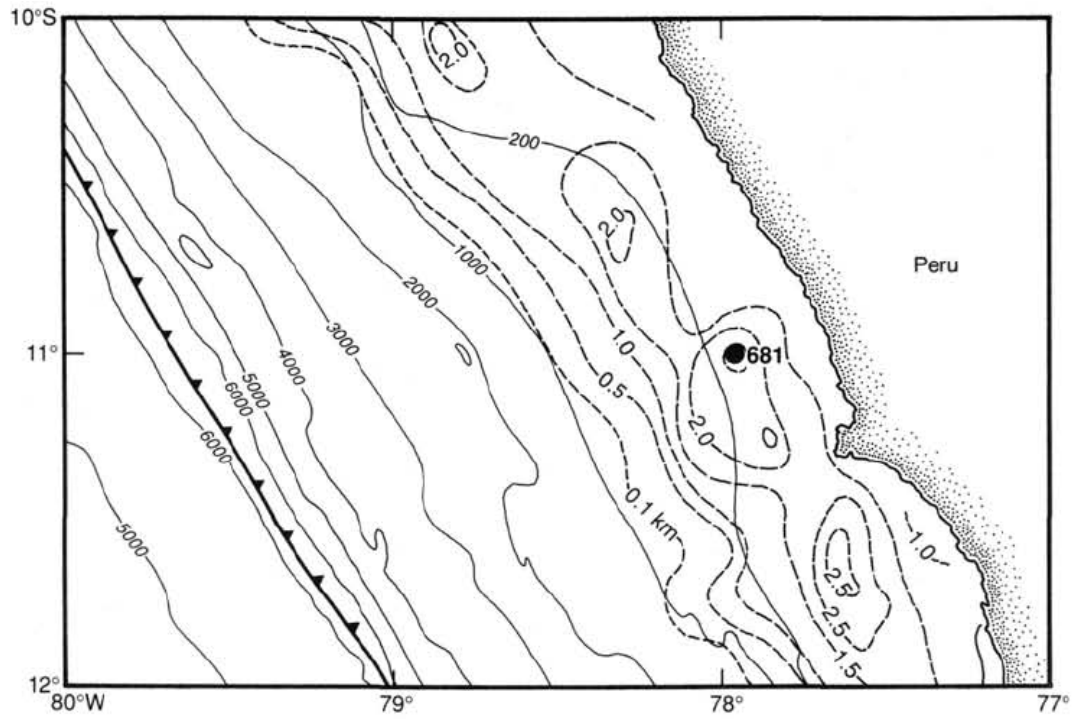

Figure 3. 3. **(a)** Bathymetry and sediment isopachs along Peru Continental Margin at 11°S, from Shipboard Scientific Party (1988). Water depths are in intervals of 1000 m, beginning at a water depth of 200 m; sediment isopachs are in increments of 0.5 km. The dashed line outlines the landward flank of an outer shelf basement high, where sediment thickness is only 0.1 km. Site 681 is situated above the depositional center of the outer shelf.

Five holes were drilled at Site 1229, with offsets of 5 to 20 m among them; Hole 1229E penetrated to 121.5 mbsf and about 80% of the sediment record was recovered (Shipboard Scientific Party, 2003c). The section to this depth consisted of repeated sequences of dark olive gray diatomaceous mud containing laminae of diatom ooze, and massive dark gray clay-rich silt. The uppermost 3 m of consist of brown, bioturbated, and poorly laminated clay-rich diatom ooze. Bioturbation is poorly developed throughout the rest of the sequence.

Authigenic dolomite becomes common below 30 mbsf. An alternation of gray homogeneous quartz- and feldspar-rich clay layers and olive-green laminated diatom-rich silty clay characterizes the lithology of the interval 40.7-96.9 mbsf, Below this interval the dominant component is diatom ooze, which is present mixed with variable amounts of sand, silt, and clay (Shipboard Scientific Party, 2003c). During glacial periods, sea levels may have dropped 100 m or even more, at which times the water depth at Site 1229 may have been only 60 m or less (Shipboard Scientific Party, 1988). The silty muds and silts poor in organic matter and rich in terrestrial components probably were deposited during these periods. Diatoms form the major microfossil component, and benthic and planktonic foraminifers are common to ~130 mbsf, while radiolarians, calcareous nannofossils, and silicoflagellates are sparse (Shipboard Scientific Party, 1988).

The stratigraphic framework was established by correlating the magnetic susceptibility from Site 1229E to Site 681B). The age model was improved between 5 and 9 mbsf by tuning an alkenone-based SST record to the one of Site TR163-19 (2.27°N; 90.95°W) (Lea et al., 2000), and for the upper Holocene section, calibrated radiocarbon (^{14}C) data were used. Radiocarbon ages were obtained from the organic carbon fraction extracted from bulk sediments samples (Skilbeck and Fink, 2006).

3.1.5. MD02-2529 (08.12°N, 84.07°W)

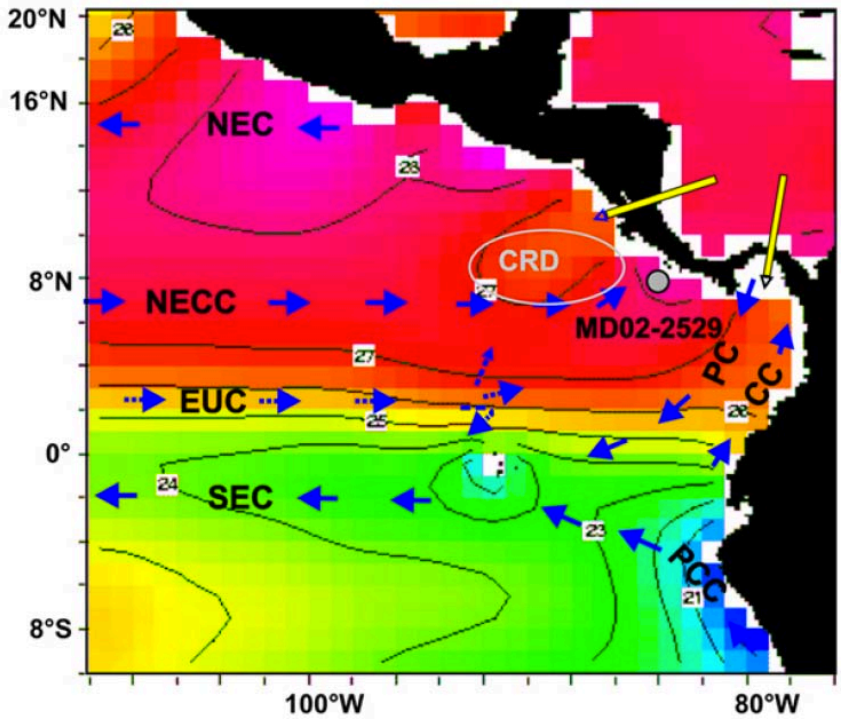

Figure 3. 4. Oceanographic setting of the eastern Pacific, from Ivanova et al. (2012). Modern sea-water temperature at 10 m water depth (in colors, red being warmer), surface circulation, summer position of the Costa Rica Dome (CRD). Currents: SEC (NEC) - South (North) Equatorial Current, NECC - North Equatorial Countercurrent, EUC - Equatorial Undercurrent, PCC – Peru Coastal Current, CC - Colombia Current, PC - Panama Current. Yellow arrows indicate the direction of local wind jets during winter in the gulfs of Panama and Papagayo.

Core MD02-2529 was collected off the Costa Rican margin in the Panama Basin at a water depth of 1619 m using a Calypso piston corer (Figure 3.4). This core recovered a total of 36.25 m of sediment (Beaufort, 2002). The dominant sediment consists of nannofossil clay to nannofossil silty clay, dark grey to dark olive grey in color. With the exception of the uppermost 3 m, the sediment is extensively bioturbated, with an increase in the degree of Bioturbation below 24 m. Shell, seed and wood fragments are present from 29.6 m to the

bottom of the core (Beaufort, 2002). At the core location, SSTs are higher than 27°C and SSS is lower than 33.2 p.s.u., throughout the year (Figure 3.4). The permanently low salinity of surface waters of the Panama Basin is maintained by the annual cycle of the ITCZ and its related surface currents (Leduc et al., 2007). Therefore the sedimentary record of this core is ideal to complete a latitudinal transect (8°N to 17°S) that will permit a better understanding of the relations between long-term SST variability in the Eastern Pacific area and the ITCZ position and the El Niño-like dynamics.

A detailed description of the stratigraphy of MD02-2529 is presented in Leduc et al. (2007) and Leduc et al. (2010). The age model for core MD02-2529 is based on calibrated radiocarbon ages for the last 40 kyr B.P, and on the benthic foraminifera $\delta^{18}O$ record correlated to the chronology of the reference stack of benthic foraminifera $\delta^{18}O$ LR04 (Lisiecki and Raymo, 2005) for the rest of the sequence.

3.2. Paleoceanographic proxies and techniques

The methodological approach used in this study will be briefly introduced in the following sections. The main part of this thesis is based on multi-proxy approaches chosen for the interpretation of terrigenous material delivered to deep-sea sediments, past localizations of the equatorial front and paleoproductivity. Methods applied to the analysis of eolian grain size and flux records (chapter 7) are not elaborated in this document since my project partner C. Saukel provides insight into them (see Saukel, 2011). Analytical methods used to produce bulk parameters, such as stable oxygen isotopes, total organic carbon (TOC), total carbon (TC), and biogenic opal will not be discussed here as the applied methods – mass spectrometry for oxygen isotopes, LECO analysis for TOC and TC and automated leaching for biogenic opal – are standard procedures in inorganic and organic geochemistry. Figure 3.5 illustrates the analyses performed on the samples of ODP sites 1237 and 1239. All samples were freeze-dried before processing). Below, each proxy is briefly explained to provide a general background for the work discussed in Chapters 4-8.

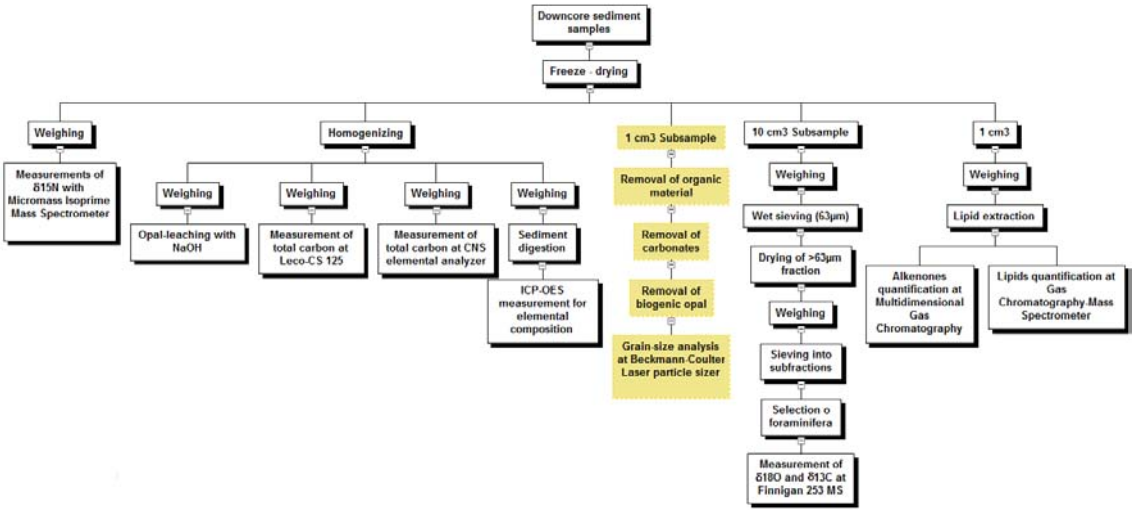

Figure 3. 5. Summary of the individual preparation steps for analyses of ODP sites 1237, 1239 and 1229 sediment samples, from Saukel (2011). Yellow column represents analyses performed exclusively on ODP Site 1237 (see Saukel, 2011 for details)

3.2.1. Stable oxygen isotopes in sea-water and foraminiferal calcite

Stable oxygen isotopes are one of the most important tools for reconstructing past climate, largely because (1) they circulate in the main components of the climate system (I.e. atmosphere, hydrosphere, cryosphere), (2) they are fractionated whenever a phase transition between or within the reservoirs occurs, (3) they show a high potential of being recorded in paleoenvironmental archives (e.g. stalagmites, marine carbonates, ice cores), and (4) the recorded composition can be routinely measured via mass spectrometry.

There are three stable isotopes of oxygen in nature: ^{16}O, ^{17}O, and ^{18}O, with relative natural abundances of 99.76%, 0.04%, and 0.20%, respectively (Rohling, 2007). Because of the higher abundances and the greater mass difference between ^{16}O and ^{18}O,research on oxygen isotopic ratios deals normally with the $^{18}O/^{16}O$ ratio (Rohling, 2007). The oxygen isotopic composition of sample ($\delta^{18}O$) is generally expressed as a departure of the $^{18}O/^{16}O$ ratio from an arbitrary standard as parts per thousand (per mil) and are calculated as:

$$\delta^{18}O = \{^{18}O/^{16}O_{\text{sample}} - {}^{18}O/^{16}O_{\text{standard}}) / {}^{18}O/^{16}O_{\text{standard}}\} \times 1000$$

A sample enriched in ^{18}O relative to the standard will show a positive δ-value (with a corresponding negative value for a sample enriched in ^{16}O relative to the standard). The oxygen isotopic composition of carbonate samples is analyzed by gas mass spectrometric determination of the mass ratios of carbon dioxide (CO_2) released during reaction of the sample with a strong acid, and is expressed with reference to a standard carbon dioxide of known composition. The standard commonly used in carbonates is referred to as Pee Dee belemnite (PDB) (a cretaceous belemnite from the Pee Dee Formation in North Carolina, USA). This standard is not available any longer; however, various international standards have been run against PDB for comparative purposes (Bassinot, 2007). Two standards are commonly used and distributed by the National Institute of Standards and Technology (NIST) in the USA, and the International Atomic Energy Agency (IAEA) in Vienna. They are NBS-18 (carbonatite) and NBS-19 (limestone).

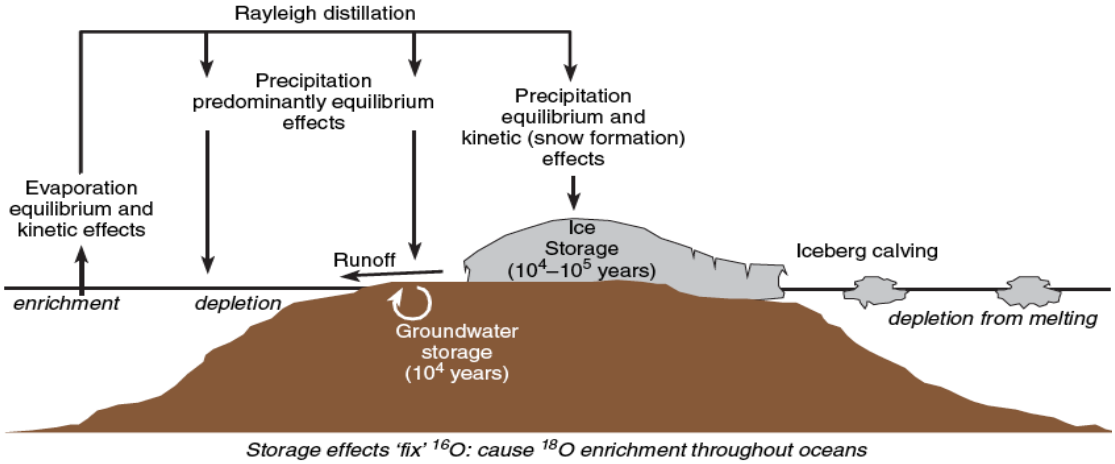

Figure 3. 6 Schematic presentations of the hydrological-cycle influences on oxygen isotope ratios, from Rohling (2007). Effects on seawater are described in italics. The 'fix' comment refers to the storage of preferentially ^{16}O-enriched precipitation in ice sheets and groundwater, which constitutes a preferential removal of ^{16}O from the oceans and thus relative ^{18}O enrichment in the oceans.

The oxygen isotope ratio of seawater is intimately linked with fractionation processes within the hydrological cycle (Figure 3.6). Schematically, this cycle comprises evaporation, atmospheric vapor transport, precipitation, and subsequent return of freshwater to the ocean (directly via precipitation and via runoff or iceberg melting). Long-term storage of freshwater

in aquifer sand especially ice sheets is also important for seawater isotope ratios. Formation and melting of seasonal sea ice imposes strong local variability. Finally, the spatial distribution of oxygen isotopes in the world ocean depends on processes of advection and mixing of water masses from different source regions with different isotopic signatures (Rohling, 2007).

Two main types of isotopic fractionation processes occur in natural environments, (1) kinetic and (2) equilibrium fractionation. Kinetic fractionation separates stable isotopes from each other by their mass and is associated with a unidirectional process (e.g. evaporation, precipitation). Because of kinetic fractionation, water evaporating from the sea surface is depleted in ^{18}O relative to ocean water, while rain precipitating from a cloud is enriched in ^{18}O relative to the cloud's moisture (Rohling, 2007). The tropical oceans are the major source of atmospheric water vapor. Poleward transport of this water results in a gradual rainout and thus in a depletion of ^{18}O in the remaining moisture (Rohling, 2007). Hence, the isotopic composition of precipitation varies strongly with latitude, altitude and sentimentality. On short time-scales (e.g. seasons), evaporation and precipitation largely control the oxygen isotopic composition of seawater ($\delta^{18}O_{sw}$), the source of oxygen for marine carbonate precipitation (Rohling, 2007). On geologic timescales water–rock interactions control the mean isotopic composition. On glacial– interglacial timescales, ^{18}O -depleted water is locked up in ice sheets leaving the ocean more enriched in ^{18}O (Rohling, 2007). Thus, during glacial periods when this high latitude precipitation is locked up in ice sheets, the ocean has more ^{18}O in it than during interglacials or, if preferred, less ^{16}O, which leaves the ocean relatively 'enriched' in ^{18}O with a corresponding more positive $\delta^{18}O_{sw}$. Regarding equilibrium fractionation, temperature-dependent fractionation occurs between two or more substances in chemical equilibrium. If $CaCO_3$ is crystallized slowly in seawater, ^{18}O is slightly concentrated in the calcium carbonate relative to that in seawater. As mentioned, this process is temperature-dependent, with the concentration effect diminishing as temperature increases.

Foraminifera, unicellular marine organisms floating in the water column (planktonic species) or living at the seafloor (benthic species), whose calcite test are one of the main components of marine carbonates that accumulate in oceanic sediments. When interpreting foraminifera calcite oxygen isotopes ($\delta^{18}O_c$) the following factors have to be taken into account: (1) the pH effect; (2) the photosynthetic activity of symbiotic algae; (3) the ontogenetic effect; (4) seasonality; (5) vertical migration; and (6) post-depositional effects. Increased pH and photosynthetic activity both result in a decrease of $\delta^{18}O_c$ values in foraminiferal shells (E.g. Spero and Lea, 1993; Spero et al., 1997). Due to an ontogenetic effect, small shells are depleted in ^{18}O compared to larger ones (E.g. Berger et al., 1978; Bemis et al., 1998). Juvenile foraminifers calcify faster and respire at higher rates. During rapid calcification a discrimination of the heavier isotope ^{18}O occurs due to kinetic fractionation. Planktonic foraminifera show a temporal (seasonal) distribution pattern, occurring usually in highest abundances during their most preferred conditions of temperature, food and light availability (E.g. Field, 2004). Such conditions may exist in a specific hydrographic regime for only a short period of the year generating species-specific fluxes to peak during different periods. Since planktonic foraminifera live dispersed in the upper water column, their $\delta^{18}O_c$ differences are a function of water column stratification and mixed-layer depth (E.g. Fairbanks et al., 1980). Some species migrate vertically up to hundreds of meters within the upper water column to complete their ontogenetic cycle. Since temperature decreases with increasing depth in the surface oceans, vertical migrations will influence equilibrium fractionation (Rohling, 2007). To minimize the influence of these kinetic effects, often grouped under the name 'vital effects', analytical strategies have been designed that focus on time series of single species (to avoid vital effect differences between species), and that use very narrow size windows from which specimens are picked for analysis (to minimize changes in the vital effects with growth). Finally,

postdepositional effects like bioturbation and calcite dissolution should also be taken into account while interpreting foraminiferal $\delta^{18}O_c$ (E.g. Broecker, 1986).

Based on equilibrium fractionation, Harold Urey first proposed that paleotemperatures could be reconstructed using the composition of oxygen isotopes in carbonate fossils. Urey and his colleagues had found that the carbonate shells of marine organisms from cold water contained a higher proportion of the heavier ^{18}O isotope than did organisms living in warmer water (Bassinot, 2007). Since then, empirical calibrations of modern planktonic foraminifer's marine organism $\delta^{18}O_c$ relative to seawater temperatures derivate equations that could be used to estimate past temperatures from fossilized biologic carbonate remains (Bassinot, 2007). Direct paleotemperature estimates exclusively based on $\delta^{18}O$ of marine carbonates are rather complex, mainly because the oxygen isotopic composition in marine carbonates varies with temperature and $\delta^{18}O_{sw}$. The latter, in turn, depends on local precipitation-evaporation balance and global continental ice volume.

In this study, we used planktonic foraminiferal $\delta^{18}O_c$ to determine regional distribution patterns and its relationship with the latitudinal position of the equatorial front – ITCZ complex, which is reflected in north to south changes in SST, surface salinity and upper ocean stratification (Chapters 4 and 5). Benthic foraminifera $\delta^{18}O_c$ were used to get a stratigraphic framework at ODP sites 1237, 1239, and core MD02-2529. As mentioned above, over glacial–interglacial cycles, global seawater oxygen isotopic excursions recorded in the foraminifera calcite reflect the waxing and waning of continental ice sheets, enriched in the light ^{16}O isotope relative to seawater.

3.2.2. Major-element concentration

Reconstruction of proxy records of chemical weathering from the deep sea sediments is usually based on elemental or mineralogical analyses using the traditional instruments such as X-ray Fluorescence (XRF) core scanning, Inductively Coupled Plasma – Optical Emission Spectroscopy (ICP-OES) and X-ray diffraction (XRD). The major-element composition of sediments can be 'unmixed' to reconstruct the relative contribution of marine particulate matter, dust- and river-born material. This can be then used as a climate indicator since dust mobilization and river discharge depend on precipitation (Calvert and Pedersen, 2007).

The principle of XRF analysis is based on excitation of electrons from the inner shells of atoms by incident X-radiation. Ejection of electrons creates vacancies, which are filled by electrons falling back from the outer shells; where by surplus energy is emitted as a pulse of secondary X-radiation. Emitted fluorescence energy and the peaks of different wavelength spectra are characteristic for atoms of specific elements, which permit estimation of their relative abundances in the sediment (E.g. Richter et al., 2006; Tjallingii, 2007). As a result of progress in XRF instrumentation, in-situ and on-line analysis of soft sediment cores by XRF core scanners has become increasing popular during the past decade. The major advantage of XRF core scanning over conventional geochemical analysis of discrete specimens is that element intensities are obtained directly at the surface of a split sediment core. In addition, the spatial resolution of XRF core-scanning devices is much higher than that of conventional destructive methods, and allows the extraction of near-continuous records of element intensities from sediment cores (E.g. Richter et al., 2006; Tjallingii, 2007). However, conversion of element intensities measured by XRF core scanners to element concentrations, essential for quantitative applications involving mass-balance and flux calculations, is perceived as problematic due to the influence of water content and grain size on the scanner sensitivity (Tjallingii, 2007). Additionally, it is important to note that XRF scans only analyze the surface of

split sediment cores, so that scans of material with a laterally heterogeneous composition may not reflect the real sediment composition. Therefore, results obtained by XRF core scanning are usually presented in the form of count rates (expressed as counts per unit time per unit area), or as ratios of counts, count rates, or intensities of elements (Richter et al., 2006; Tjallingii, 2007). Conversion of core-scanner output to quantitative measures of sediment composition with associated measures of uncertainty requires a calibration with discreet samples, covering the range of compositions downcore, which are measured using a quantitative technique on dried, homogenized samples (Weltje and Tjallingii, 2008)

Optical emission spectrometry (ICP-OES) was used to convert XRF scanner counts to element concentrations in mg/g of sediment by means of linear regression (Figure 3.7). In OES, the sample is subjected to temperatures high enough to cause not only dissociation into atoms but to cause significant amounts of collisional excitation (and ionization) of the sample atoms to take place. Once the atoms or ions are in their excited states, they can decay to lower states through thermal or radiative (emission) energy transitions. In OES, the intensity of the light emitted at specific wavelengths is measured and used to determine the concentrations of the elements of interest (Boss and Fredeen, 1997).

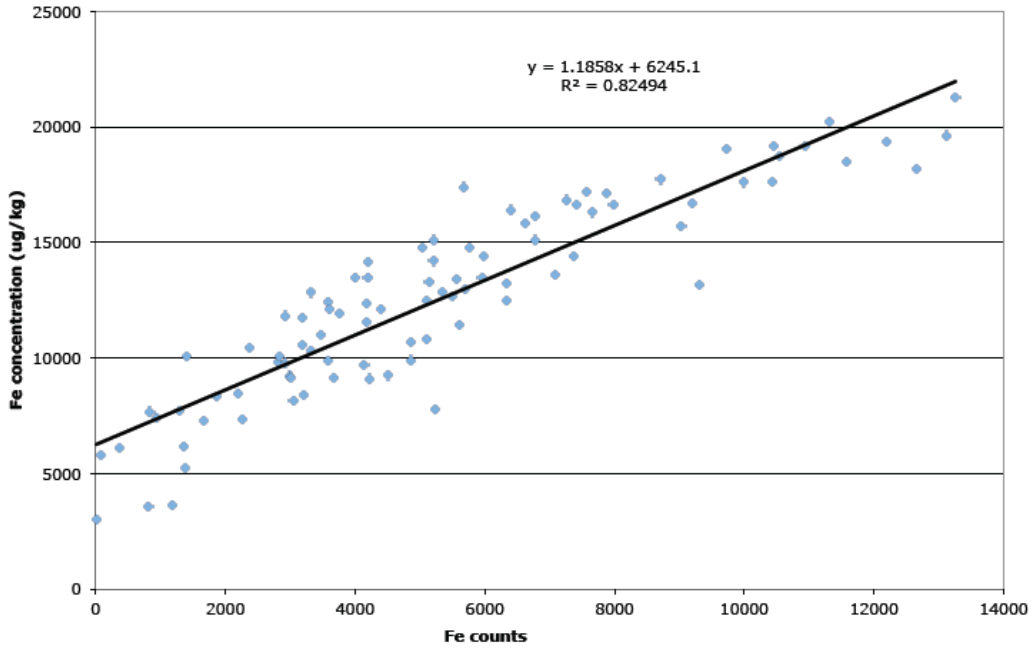

Figure 3. 7 Linear correlation of Fe counts from XRF scans and Fe contents in mg/g from ICP-OES measurements.

One of the most important advantages of OES results from the excitation properties of the high temperature sources used in OES. These thermal excitation sources can populate a large number of different energy levels for several different elements at the same time. All of the excited atoms and ions can then emit their characteristic radiation at nearly the same time. This results in the flexibility to choose from several different emission wavelengths for an element and in the ability to measure emission from several different elements concurrently. However, a disadvantage associated with this feature is that as the number of emission wavelengths increases, the probability also increases for interferences that may arise from emission lines that are too close in wavelength to be measured separately (Boss and Fredeen, 1997).

The stratigraphically complete sediment record of ODP Site 1237 corresponding to the past 5.16 Ma as well as the complete sediment record of ODP Site 1239 corresponding to the past 5

Ma were scanned with an Avaatech Core Scanner (2nd generation, XRF-CS) at the Alfred-Wegener-Institute in Bremerhaven. The scanning was performed with steps of 1-2 cm and 1-5 cm, respectively. Energy settings used were 10 and 50 kV to cover all elements of interest. ICP-OES measurements were carried out at an IRIS Intrepid spectrometer (Thermo Fisher Scientific Inc., USA) at the geochemistry laboratories of the AWI.

For this study, element intensities and element ratios indicative of dust deposition at Site 1237 and terrigenous input at Site 1239 are of special interest. These predominantly include element concentrations of iron (Fe), titanium (Ti), potassium (K), aluminum (Al) and silica (Si) (E.g. Duce and Tindale, 1991; Bareille et al., 1994). Aluminium is bound in aluminosilicate minerals, which are mostly detrital, although some Al can be derived from oceanic volcanic rocks, hydrothermal exhalations and authigenic growth. Titanium is much less abundant than Al and restricted to certain minerals like ilmenite, rutile, titano-magnetite and augite. In many open-ocean environments Ti is dominantly hosted in aluminosilicate phases, added through eolian processes, and generally immobile after deposition (E.g. Murray et al., 1993; Murray and Leinen, 1996). Titanium can also be bounded to volcanic material. Iron in pelagic and semi-pelagic sediments is mainly bound to clays, and therefore to detritic components too, and present in authigenic minerals (Wedepohl, 1971).

Calcium (Ca) and barium (Ba), on the other hand, can be useful for inferences about changes in productivity and/or preservation at the study sites. Barium in sediments is mostly present as barite, which is formed, when particulate organic matter is descending to the bottom through the water column (Dehairs et al., 1980). Barite contributes up to 90 % of the total Ba concentration into the pelagic sediment, while clastic material provides an important source of Ba closer to the continent (Gingele and Dahmke, 1994). Dymond et al. (1992) estimate that around 70 % of the produced biogenic Ba in the water column is lost to the bottom deposits by dissolution. The amount of terrigenous Ba remains comparably constant.

Each working area displays its specific geochemical composition so that different elements can be used as proxies for different mechanisms and potential sources. For instance as part of the essentially fine-grained particles transported by the river, one can include Fe particles (resultant from the weathering of continental rocks and soils), and continental derived organic matter (Martin and Meybeck, 1979). The Fe content of the sediments has been used as a simple chemical proxy for the input of land-derived materials and Fe variations are considered to be a direct measure of rainfall and river input by several authors such as Haug et al., (2001), Itambi et al., (2009) and Nizou et al., (2010). On this basis, the Fe content of the ODP Site 1239 sedimentary sequence has been assumed to be mainly river-born material, determined by continental precipitation (Chapter 5). On the other hand Fe content of the ODP Site 1237, further south, has been assumed to be mainly wind-transported (Chapter 7). Potassium (K), for example, is used as an indicator of fluvial terrigenous input off northwestern Africa (E.g. Mulitza et al., 2008) and off northwestern continental slope of the Gulf of Mexico (E.g. Kujau et al., 2010), whereas it serves as a proxy for ash layers at ODP Site 1237 in SE Pacific sediments originating from andesitic volcanism that is rich in potassium (Chapter 7).

3.2.3. Terrigenous supply

The mean state of climate is also often called upon as an erosive agent, either directly though the action of water, wind, and ice, or indirectly through climatic control of vegetation, or glacial control of sea level. Tectonic uplift is also likely to promote erosion by steepening slopes and increasing precipitation on the windward side of mountain ranges. Although local examples of high erosion driven by drainage area, slope, and precipitation can all be found in

the modern world (E.g. Montgomery et al., 2001), it remains unclear whether long-term continental erosion rates are governed primarily by tectonics or climate (E.g. Molnar and England, 1990). Hemipelagic terrigenous sedimentary components preserved in the eastern tropical Pacific at ODP Sites 1237 and 1239 offer an opportunity to assess the relative role of climate change and tectonics in long-term erosion (fluvial and eolian) of the source region in tropical South America.

Changes in the supply of terrigenous material to deep-sea sediments can be roughly estimated by determining the proportions of biogenic carbonate, total organic matter and biogenic silica (opal), since these contents in pelagic sediments are inversely related to dilution with terrigenous material (Hays and Perruzza, 1972; Tiedemann and Mix, 2007). This provides crude, first-order approximation for physical erosion integrated over the entire basin, one that clearly overestimates, as we did not account for salt, hydrothermal and volcanic sediments, and other minor constituents. The mass accumulation rates (MAR in g/cm^2 kyr) of terrigenous sediment, that are unaffected by dilution, were calculated as:

$$T_{MAR} = (100\% - \%\ CaCO_3 - \%\ \text{Biogenic opal} - \%\ TOC)*DBD*LSR$$

Where $CaCO_3$ (wt %) is the weight percentage of calcium carbonate calculated – assuming that calcite/aragonite is the main carbonate phase - from both measurements as follows:

$$CaCO_3\ (\text{wt \%}) = (\%TC-\%TOC)*\ 8.33$$

Total organic carbon (TOC, wt %) was measured with a LECO Carbon Sulfur Analyzer (LECO-CS 125). Estimation of total carbon (TC) was determined with a CNS elemental analyzer (Elementar Vario EL III). The concentration of biogenic opal in the bulk sediment was determined applying the automated leaching method according to Müller and Schneider (1993). DBD is dry bulk density in g/cm^3, calculated from shipboard gamma ray attenuation porosity evaluator (GRAPE) data, corrected for porosity variability using a grain density of 2.65 g/cm^3 (following Weber et al., 1997). LSR is the linear sedimentation rate (cm/kyr), estimated from the age model of each core.

3.2.4. Alkenones

In paleoceanography, the term 'alkenones' refers to a series of C_{37}-C_{40} straight chain methyl and ethyl ketones with one to four unsaturations and all transconfiguration in the double bonds (Grimalt and Lopez, 2007). These compounds are widespread in modern ocean sediments but occur in only a few living species of haptophyte, such as *Emiliana huxleyi* and *Gephyrocapsa oceanica* (Bijma et al., 2001). Other coccolithophorid species tested to date do not yield alkenones. In addition, alkenone production has been reported from some, but not all, species of the noncalcifying haptophyte genera Isochrysis and Chrysotila (Bijma et al., 2001). Cruises along the California margin and the equatorial Pacific suggest that noncalcifying haptophyte algae often dominate over coccolithophorid forms (E.g. Thomsen et al., 1994). The possibility therefore exists that other noncalcifying haptophyte species that synthesize long-chained alkenones may well have gone undetected (Brassell et al., 1987). As far as is known, no marine algal groups other than the haptophytes synthesize long-chained alkenones. Unfortunately, the physiological functions of alkenone biomarkers remain an enigma. Despite de high levels of alkenones found in *E. huxleyi*, the cellular locations, biochemical functions and biosynthetic pathways of these long-chain hydrocarbons remain elusive (Laws et al., 2001).

The alkenone-producing species are typically reduced in abundance or excluded in oceanic provinces that favor diatom growth (Brand, 1994). The abundance of *E. huxleyi* and *G.*

oceanica is also reduced in regions of high silicate availability, such as in many coastal zones and upwelling regions. Where nutrients such as nitrate and phosphate, or trace metals, such as iron, are low, the competitive advantage reverses to favor coccolithophores over the siliceous phytoplankton (Brand, 1991). Alkenone production occurs in the context of the annual cycle of upper water-column temperatures. Standing stocks of alkenone-producing species and their falling products display strong changes over the course of the year in all studies to date (see review by Herbert, 2001). In most cases, the time of maximum abundance of *E. huxleyi* and/or *G. oceanica*, and the maximum flux of alkenones into sediment traps, coincides with the dominant period for phytoplankton blooming. Thus, production peaks in spring months in most subtropical and mid latitude locations. Alkenone fluxes in sediment traps generally show a spring peak, indicating that surface ecological signals are exported to depth (see review by Herbert, 2001). Twice-yearly flux maxima of alkenone production were observed by Harada et al. (2001) in the central equatorial Pacific. A lack of dissolved silica may inhibit diatom growth and promote haptophyte production during the fall months in such locations. Because so few sediment trap experiments report data for much more than one year's duration; we have only a glimpse at the importance of interannual variability in the productivity of alkenone-synthesizing species. Reports do suggest strong year-to-year variations in fluxes downward flux of either coccolith/coccosphere or alkenones between years (see review by Herbert, 2001).

The alkenones are then intensively studied for the well-defined relationship between relative composition of the C_{37} di- and triunsaturated homologs and SST (Prahl and Wakeham, 1987). Alkenones have been found in sediments as old as the early Cretaceous and used to reconstruct SSTs on time-scales ranging from 10–10^6 years (Sachs et al., 2007). The temperature estimates using the C_{37} alkenones are generally based on the compilation of two indices, which are linearly correlated with SST (Brassell et al., 1986):

$$U^K_{237} = [Me37:2 – Me\ 37:4]/\ [Me37:2 + Me37:3 + Me\ 37:4]$$

And

$$U^K_{237} = [Me37:2 – Me\ 37:4]/\ [Me37:2 + Me37:3 + Me\ 37:4]$$

Where Me37: *x* denotes the concentration of the alkenone with *x* carbon–carbon double bonds (Grimalt and Lopez, 2007).

Examination of laboratory cultures of the coccolithophore *E. huxleyi* (E.g. Prahl et al., 1988) showed that the relationship between these alkenone indices and SST was linear in a range of 8–25°C (Figure 3.8a), giving rise to the following equation:

$$U^K_{37} = 0.034 \times T + 0.039\ (r^2 = 0.994,\ n = 22)$$

Many other studies have also performed calibrations between the alkenone indices and SST, using other algal cultures, examining the relationship between water-column particulates and in situ temperature measurements, or comparing core-top alkenone measurements with water-column temperatures from oceanic databases (Figure 3.8b).

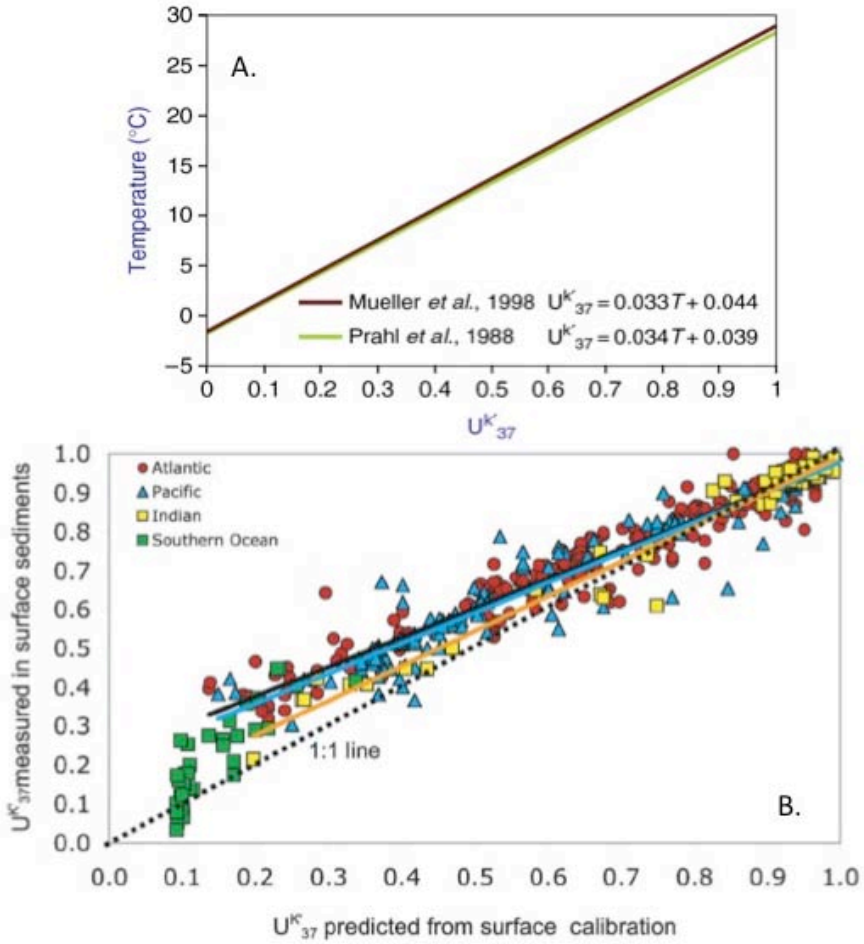

Figure 3. 8 (a) Comparison of the calibration equations of greatest general use for the estimation of SSTs from the unsaturation alkenone index (U^{K}_{37}), from Grimalt and Lopez (2007). The equation of Prahl et al. (1988) was obtained from cultures of *E. huxleyi* under controlled conditions. The equation of Mueller et al. (1998) was obtained from measurements of core tops and comparison with water-column temperatures from oceanic databases. **(b)** The U^{K}_{37} measured in surface sediments plotted against the U^{K}_{37} predicted in the sediments from the overlying annual mean SST at 0m depth, from Conte et al. (2006). The lines show linear fits to the Atlantic (black line), Pacific (blue line), and Indian (orange line) samples.

The core- top determinations based on sediments collected between 60°N and 60°S in the world oceans showed a remarkably strong linear correlation with mean annual SST (Müller et al., 1998) and the regression line can be depicted as:

$$U^{K}_{37} = 0.033 \times T + 0.044 \ (r^2 = 0.958, n = 370)$$

This is identical, within error limits, to that previously mentioned based on *E. huxleyi* cultures (Figure 3.8a). The strong agreement between these two equations has led to most studies using one of these two equations for SST estimation.

Most studies, including the core-top U^{K}_{37}-SST calibration of Müller et al. (1998), assume that U^{K}_{37} values reflect temperatures at the sea surface. However, alkenone concentrations in sediment traps indicate that the depth of maximum production varies regionally and can even change between different seasons. Alkenone-producing haptophytes show highest abundance at high and low latitudes, while thermocline production prevails at mid-latitudes (Sachs et al., 2007).

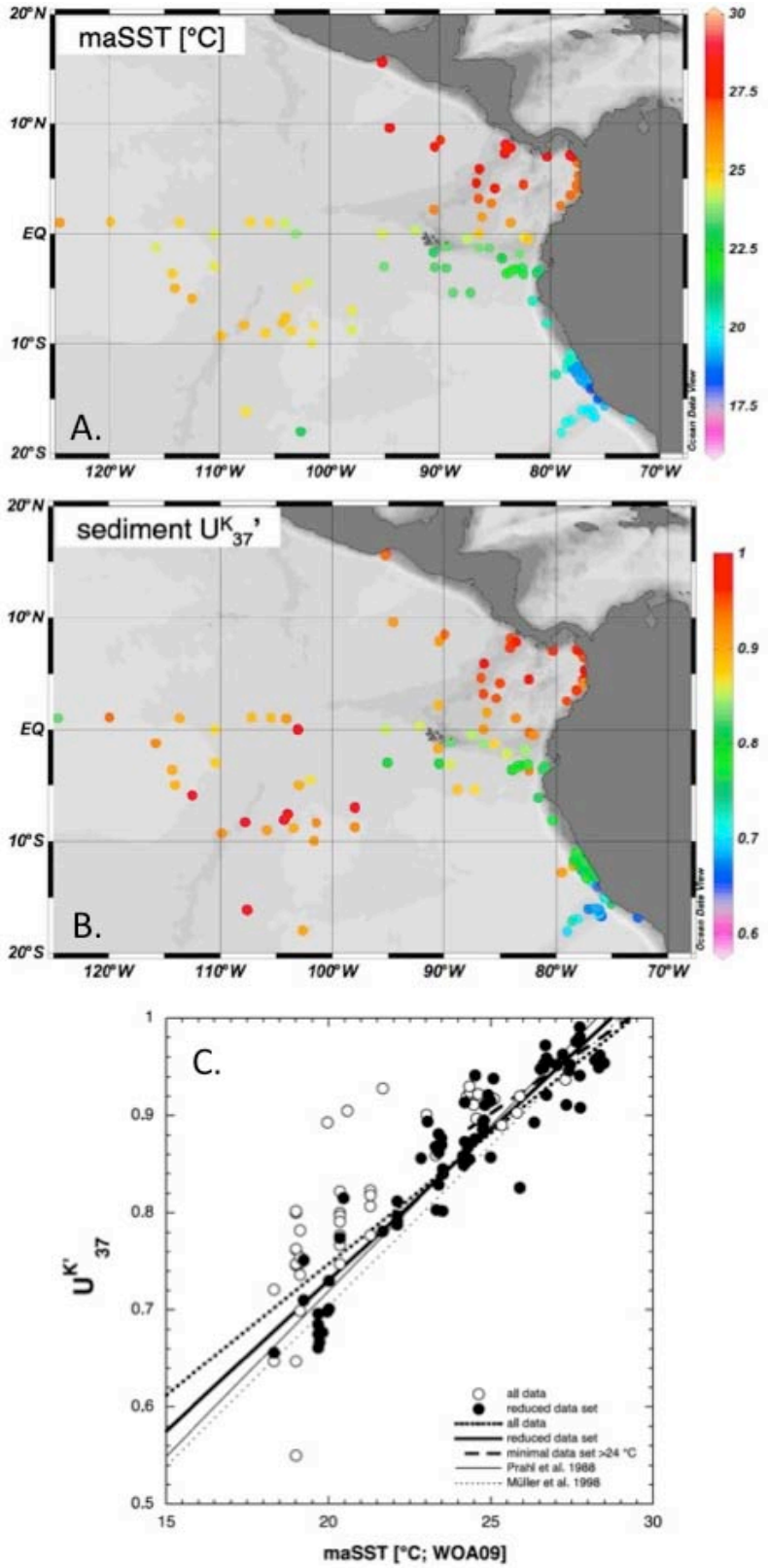

Figure 3. 9 **(a)** Mean annual SSTs (maSST) at the sampling sites, compared to **(b)** the surface sediment U^{K}_{37} in the EEP, from Kienast et al. (2012). **(c)** Scatterplot of U^{K}_{37} indices in EEP surface sediments versus maSST, from Kienast et al. (2012). Lines represent the best linear fit for the full (thick dotted line; all data points) and the reduced data sets (thick solid line, filled circles only) and the calibration equation of Prahl et al. (1988) (thin solid line) and Müller et al. (1998) (thin dashed line). The dashed thick line is the regression of the minimal data set (see text for discussion) for maSST above 24°C only. Data include U^{K}_{37} values reported previously by other investigators. Note that the dark red samples west of 95°W in Figure3.10b have a nominal U^{K}_{37} of 1 due to undetectable triunsatured alkenones.

Despite substantial alkenone loss both in the water column and in the sediment after deposition, several studies indicate stability of the U^{K}_{37}-index over geologic time and therefore no effect on paleo-SST reconstructions (Sachs et al., 2007). However, contrasting studies indicate differential removal of Me37:3, which can have implications for alkenone paleothermometry, depending on the conditions under which degradation occurred (I.e. anoxic, oxic, and denitrifying). Other environmental factors potentially affecting the unsaturation ratio of alkenones include light limitation (causing a bias toward warmer SSTs) and nutrient limitation (bias towards lower SSTs) (Sachs et al., 2007).

In the eastern equatorial Pacific, U^{K}_{37} values range from 0.550 to 0.991, with highest values generally restricted to the warm pool north of the equatorial front, and lower values in the cold tongue off Peru (Figure 3.9). According to Kienast et al. (2012), the regional regression between U^{K}_{37} and mean annual SST ($r^2 = 0.78$, $p < 0.01$) is not statistically different at the 95% confidence level from the culture-derived regression by Prahl et al. (1988) or from previous linear global calibrations by Müller et al. (1998).

The past SST at both Site 1239 (Chapters 5 and 8) and Site 1229 (Chapter 6) was reconstructed by using the $U^{k'}_{37}$.At ODP Site 1239 the alkenones were extracted at the CAU (Christian Albrecht University of Kiel) from a sample vial containing the freeze-dried and homogenized sediment (~1 g dried weighted) after addition of 1 cm layer of silica gel, 1 µg of cholestane ($C_{27}H_{48}$) and 0.5 µg of hexatriacontane ($C_{36}H_{74}$) as internal standards, and modified diatomaceous earth (Isolute HM-N, extraction grade) to increase the sample volume to 11 ml (size of the extraction cell). Each sample was extracted twice through an accelerated solvent extractor (Dionex ASE 200) for 10 min using 25 ml dichloromethane at a temperature of 75°C and pressure of 80 bar (nitrogen). After heating, the extract was flushed from the sample cell into a standard collection vial and cooled down in a freezer (-20°C). The resulting extract was concentrated to 50 µl with a rotary evaporator (bath at 300 mbar, 20-22°C). Afterward, it was transferred into glass vials and dried over nitrogen. After drying, the residues were taken up in 100 µl hexane. The resulting sample was analyzed within a double column Multidimensional gas chromatograph (MDGC), with two Agilent 6890 gas chromatograph, equipped with two independent ovens and two flame ionization detectors (FID). MDGC combines the separation efficiency of two capillary columns with different polarities, each in a separate temperature-controlled oven, arranged in series and the sensitivity of two FID for organic biomarkers. The eluate of the first column was passed either through the monitor detector or through the second column and the main detector. In the latter mode, a preselected small fraction was cut from the eluate of the first column and transferred to the second column. The usual FID chromatogram (FID 1) was recorded by the monitor detector, only interrupted during the cut time. The chromatogram recorded by the main FID (FID 2) shows only a few peaks depending on the components included in that cut. The main detector has a much higher sensitivity than the monitor detector, because of the reduced memory effect and reduced level of contamination, as it receives small selected fractions from the first column through the heart cut.

From the main detector chromatogram, the areas of the $C_{37:2}$ and $C_{37:3}$ alkenones were thus obtained. The $U^{k'}_{37}$ index is then calculated as the ratio between the different $C_{37:2}$ and $C_{37:3}$ areas. The results were thereafter compared to those obtained from in-house standard, fine-grained sediments from the Skagerrak, a strait between the southeast coast of Norway and Denmark. Skagerrak samples, previously calibrated, enable to control the stability of the MDGC and to adjust values if necessary. The C_{36} standard peak, appearing in the chromatogram sequence just before the C_{37} group, is used to precisely define the cut time, the time from which the C_{37} group signal is transferred into the second GC, as well as the

calculation of the alkenone concentration. This relatively new technique, with two running parallel GC, allows obtaining an accurate signal, even for low alkenone concentration (> 1ng/g). According to sample and internal standard replicates, the SST precision is about ± 0.3 °C.

At Site 1229 freeze-dried sediments (1-1.5 g) were ultrasonically extracted twice with methanol, dichloromethane: methanol [1:1(vol/vol)], and dichloromethane to obtain the total lipid extract. Aliquots of the total extracts were separated into non-polar and polar fractions by column chromatography after the addition of an internal standard (a mixture of 1-nonadecanol, nonadecanoic acid, 5 alfa-cholestane, and hexatriacontane). The total lipid fractions were methylated with diazomethane and silylated with N, O-bis (trimethylsilyl) trifluoroacetamide in pyridine and then analyzed at the Max Plank Institute-Bremen by GC and GC-MS (Trace GC-MS; Thermo Finnigan) for alkenone identification and quantification.

Since several authors have hypothesized that the rate of alkenone accumulation closely resembles that of the modern alkenone producers (E.g. Müller et al., 1997; Kirst et al., 1999; Weaver et al., 1999; Bolton et al., 2010; Beltran et al., 2011), we assumed that total ketones contents of samples from ODP Site 1239 can be used as an index of productivity in the overlying water column at the time of deposition. In common with other palaeoproductivity proxies, concern has been raised over the reliability of the total C_{37} alkenone method. Potential sources of aliasing include physiological effects on alkenone production (E.g. Prahl et al., 2003), alkenone degradation in the water column and sediments (E.g. Prahl et al., 1989; Hoefs et al., 1998) and the identity of fossil species responsible for their synthesis (E.g. Marlowe et al., 1990). In the eastern equatorial pacific results of Bolton et al. (2010) imply that, on orbital timescales, C_{37} alkenone accumulation in upwelling areas is representative of surface ocean export productivity, not only of the alkenone-synthesizing coccolithophores but also of the wider phytoplankton community including the siliceous diatoms.

3.2.5. Terrestrial biomarkers

Molecular fossils, 'biomarkers', have become an increasingly common tool in the reconstruction of past biological assemblages, climate and environmental conditions. Specific organic compounds (lipid biomarkers) can identify terrigenous input especially from higher plants (I.e. certain steroids, lignin or long-chain odd-carbon-numbered n-alkanes) (E.g. Hinrichs and Rullkötter, 1997; Holtvoeth et al., 2003; Schefuß et al., 2004; Boot et al., 2006). Similar to pollen, biomarkers of unambiguous terrestrial origin are also common in marine sediments and can even be dominant in coastal regions with high fluvial inputs (E.g., Amazon fan; Hinrichs and Rullkötter, 1997) or open ocean settings where aeolian terrestrial inputs are greater than pelagic ones (E.g. Pagani et al., 2000). Although higher plant biomarkers are generally not as diagnostic as pollen, some biomarker proxies for specific organisms have been proposed. For instance, lignin monomers as indicators for gymnosperm vs. angiosperm inputs (E.g. Hedges and Parker, 1976), the α- and β-amyrins and lupeol are, in general, triterpenoids derived from vascular plant detritus (E.g. Simoneit, 1986), whereas triterpenoids taraxerol and myricadiol as biomarkers predominantly from mangrove-derived organic matter (E.g. Killops and Freewin, 1994; Versteegh et al., 2004). The phytosterols in the samples, consisting mainly of the C_{29} compounds (sitosterol and stigmasterol), are derived from terrestrial and seagrass vegetation (E.g. Volkman, 1986). Despite the loss of functional groups during diagenesis the remaining hydrocarbon skeletons still bear this biological and ecological information (E.g. Brocks and Summons, 2004; Peters et al., 2004; Brocks and Pearson, 2005).

The most prosaic application of the biomarker approach is typified by the assumption that if sediment contains a high proportion of a given biomarker (e.g. the "higher plant" n-alkanes)

then it probably received a high input from a particular source organism (I.e. terrigenous "higher plants"). Such assessments are vulnerable since they take no account of the other factors, which influence the molecular composition of the sediment. Many sediments contain abundant "higher plant" n-alkanes simply because these compounds are so refractory that they are relatively enriched as other compounds degrade.

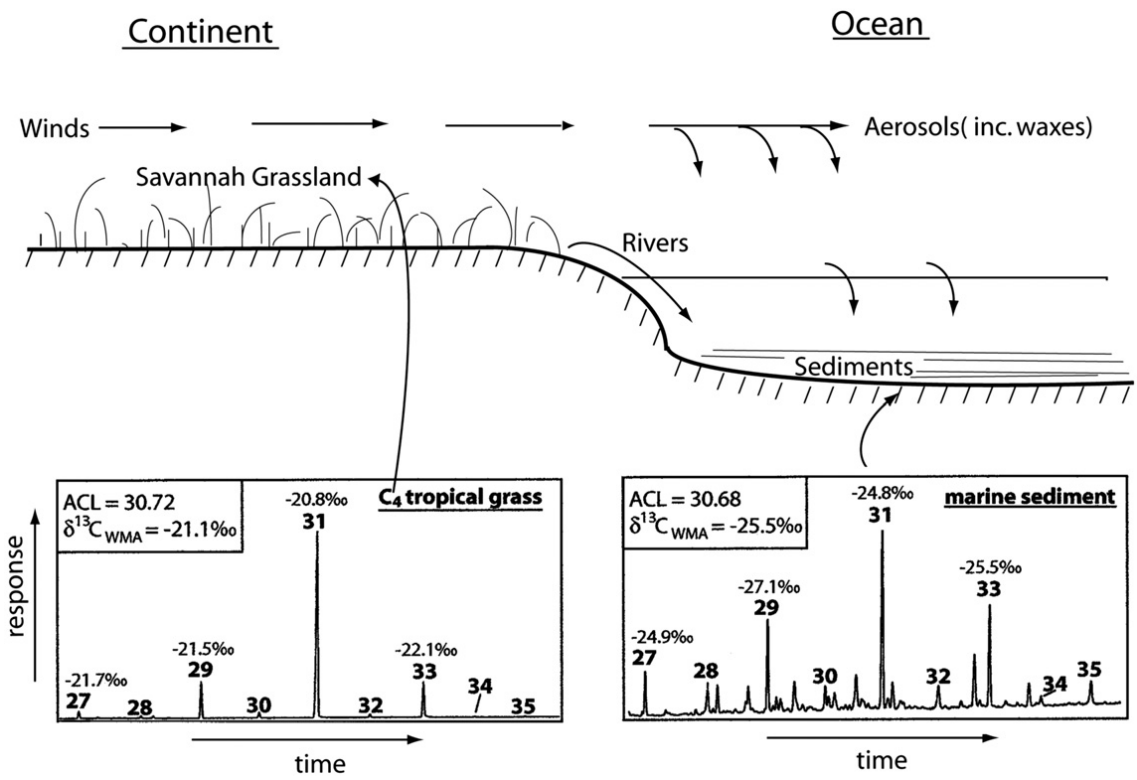

Figure 3. 10. Plant-wax lipids in ocean sediments, from Eglington and Eglington (2008). These compounds serve as proxies for continental vegetation since they reach the sediments from the continent by wind and river transport of particulates and dust and smoke aerosols. Typical GC traces are shown for the n-alkane fractions (C_{27}–C_{35}) of a C_4 tropical grass and for marine sediment from the southeast Atlantic. The $\delta^{13}C$ values (in ‰) are marked for each of the prominent odd-carbon-number homologues. The $\delta^{13}C_{WMA}$ (weighted mean average) is also shown for this carbon-number range, together with the Average Chain Length (ACL).

Long-chain n-alkyl compounds are major components of epicuticular waxes from vascular plant leaves (Eglinton and Hamilton, 1967). In marine sediments from almost anywhere on the ocean floor they come from the leaf waxes of vegetation on nearby continents and are delivered as aerosols and adsorbed on mineral particles carried by river and wind systems (Figure 3.10). These compounds are relatively resistant to degradation, which makes them suitable for use as higher plant biomarkers (Cranwell, 1981), and typically they are comprised of mixtures of long, straight-chain n-alkanes, n-alkanols, n-alkanoic acids, and wax esters. All four compound classes have been identified in recent (E.g. Rieley et al., 1991) and ancient (E.g. Bird et al., 1995) terrestrial and marine sediments, while n-alkanes, n-alkanols and n-alkanoic acids have been found in fossil plant tissues (E.g. Logan et al., 1995). N-alkanes occur in vascular plant leaf extracts, where they typically have chain-lengths ranging from C_{25} to C_{35} (Eglinton and Hamilton, 1967) and a strong predominance of odd-carbon number homologues over even-numbered ones (the most common being C_{27}, C_{29}, C_{31} and C_{33}). This characteristic odd/even carbon-number distribution is a consequence of the universal polyketide (acetate, malonate) biosynthetic pathway. The odd numbered n-alkanes are formed by the loss of a single carbon from the precursor even-numbered n-alkanoic acids (Eglington and Eglington, 2008). These relatively high molecular-weight n-alkanes are more resistant to degradation than shorter-chain homologues and other n-alkyl components, the order of stability

decreasing in the order: n-alkanes, n-alkanoic acids, n-alkanols (Cranwell, 1981). Although n-alkanes are resistant to degradation, they suffer from interference from petrogenic hydrocarbons, which have, low carbon-preference indices (Pancost and Boot, 2004). In other words, the release or formation of n-alkanes from other organic carbon pools during diagenesis or catagenesis. Catagenesis results in the typical petroleum n-alkane signature with a shift towards lower-carbon-number homologues and no predominance of odd homologues; although the precise origin of petroleum n-alkanes remains debated, it is clear that they cannot be ascribed an unambiguous higher plant source (Pancost and Boot, 2004). A related concern—even in relatively recent sediments—is that n-alkanes in sediments could derive from weathering of soil or shales. Although the input from shales, petroleum or other ancient sources is minor, the work of Pearson and Eglington (2000) reveals that caution should be exercised in developing paleovegetation records from n-alkanes in sedimentary sequences.

A variety of pentacyclic triterpenoids, typically with structures based on the ursene, oleanene or lupene hydrocarbon skeletons are common in higher plants (Pancost and Boot, 2004). Due to their ubiquity, such compounds are typically only used as general tracers of higher plant input. For example, pentacyclic triterpenoids found in marine sediments are those based on the taraxer-14-ene carbon skeleton, such as taraxerol (Pancost and Boot, 2004). Although such compounds are common in higher plants (I.e. some peat-forming plants; Pancost et al., 2002), they are particularly abundant in mangrove leaves (E.g. Wannigama et al., 1981) and seagrass blades (E.g. Gillan et al., 1984). Because taraxeroids are associated with the cuticular component of mangrove leaves, it appears that they are relatively diagenetically stable such that their abundance in marine sediments could be used as a tracer for mangrove swamps on adjacent coasts (E.g. Killops and Frewin, 1994; Versteegh et al., 2004).

Accumulation of terrestrially derived material in marine sediments is due to aeolian and/or riverine transport or to the presence of aquatic higher plant communities (Pancost and Boot, 2004). Because vascular higher plants only occur widely in a limited number of marine settings (I.e. shallow shelves and lagoons), higher plant material in sediments from most marine settings is assumed to be predominately terrestrially derived. However, the proportion of such material derived from aeolian as opposed to fluvial processes is geographically variable and probably variable over time at any given site, such that a robust understanding of higher plant organic matter transport mechanisms is essential for interpretation of past continental vegetation.

It is generally thought that in coastal sediments or sediments near the mouths of river systems, fluvial mechanisms are the dominant mode of higher plant material delivery. Rivers transport large amounts of dissolved and particulate organic carbon to the oceans (0.4 Gt per year) (Hedges et al., 1997), but much of this organic matter is sequestered in sedimentary fan systems. For example, a comparison of sediment accumulation rates with those of a variety of higher plant biomarkers, including alkanes, n-alkanols and taraxerol, reveals that almost all higher plant compounds in Amazon Fan sediments were delivered by fluvial processes (Boot et al., 2006). On the other hand, in open ocean settings, aeolian transport mechanisms are predominant and the types of higher plant biomarkers found in such settings reflect this. Lignin and cuticle-derived compounds are typically sequestered on shelf sediments with apparently only small quantities of such compounds occurring in abyssal sediments (E.g. Gough et al., 1993); conversely, leaf wax lipids can be relatively abundant in abyssal sediments and atmospheric dust. Wax particles are ablated from leaf surfaces by wind and dust action (E.g. Conte and Weber, 2002) and become airborne, or plant organic matter in soils can be lifted during dust storms. Typical terrestrial biomarkers in atmospheric dust are long-chain n-alkanes, n-alkanols and n-alkanoic acids (Simoneit, 1997).

Solvent extracts of sediment samples from Site 1239 were analyzed for the content of taraxerol as an indicator of riverine input (Chapter 5) since mangroves extend northward from the equatorial front (Ecuadorian and Colombian Pacific coasts). The Guayas River is the largest estuarine ecosystem along the Pacific coast of South America (see section 2.3.2) and together with the Esmeraldas river form river-dominated estuaries that provide optimum growth conditions to mangrove forests, with tree heights from 25 to 40 m. This region maintains low species richness usually with zones of monospecific forests (Twilley et al., 2001). Based on their higher-energy coastal setting, the conceptual model by Twilley et al. (1986) predicts that the mangrove wetlands in Ecuador are very productive and export large quantities of organic matter to the estuary (>500 g C/m^2 yr^1).

At Site 1229 solvent extracts of sediment samples were analyzed for the content of long-chain lipids such as n-alkanes and a-amyrin as terrestrial biomarkers (Chapter 6). Since the temperature effects can be ignored, and vegetation and lipid concentration changes can be attributed unequivocally to variations in seasonal precipitation over the northern extension of Atacama Desert.

3.2.6. Nitrogen isotopes

Much of the interpretation of water mass nutrient and productivity changes in paleoceanography comes from the nitrogen isotopic composition of bulk sediment. A number of studies (E.g. Altabet and Francois, 1994; Brandes and Devol, 1997; Sigman et al., 1999; Ganeshram et al., 2000; Robinson et al., 2007; Liu et al., 2008; Etourneau et al., 2009) have utilized this proxy to interpret nitrate utilization related to productivity, denitrification related to the consumption of nitrate as an alternative electron acceptor in suboxic waters, and the nature of preformed nutrient sources, which basically sets the baseline nitrogen isotopic composition (Filipelli and Flores, 2009).

Nitrogen has two stable isotopes: ^{14}N (99.6%) and ^{15}N (0.4%). Fractionation, as in the case of oxygen, is again expressed in delta notation:

$$\delta^{15}N = [(^{15}N/^{14}N)_{sample} / (^{15}N/^{14}N)_{standard} - 1]*1000$$

Where the standard is atmospheric N_2. Phytoplankton preferentially incorporates the lighter isotope, leading to $\delta^{15}N$ enrichment of the remaining dissolved NO_3^- pool. In regions where the NO_3^- supply is heavily utilized, the surface ocean isotopic enrichment can be relatively large (~10‰), and organic matter $\delta^{15}N$ increases in parallel (Marchitto, 2007). To the first order, the $\delta^{15}N$ of sedimentary organic matter may therefore be used to reconstruct past surface-ocean NO_3^-, and thus the degree of NO_3^- utilization (Altabet and Francois, 1994).

A second important influence on the $\delta^{15}N$ of dissolved NO_3^- is water-column denitrification, which represents an important loss of fixed nitrogen from the oceans. Under suboxic conditions, bacteria may use NO_3^- as an electron receptor during organic matter degradation, producing N_2O and N_2 (Marchitto, 2007). Like NO_3^- utilization, this process preferentially uses ^{14}N and results in $\delta^{15}N$ enrichment of the remaining intermediate water NO_3^- pool (Marchitto, 2007). Whereas well-oxygenated deep waters are typically, 5–6‰ in $\delta^{15}N$, denitrification may drive values above 18‰. Denitrification today occurs primarily in the intermediate-depth oxygen minimum zones of the eastern tropical North and South Pacific, and Arabian Sea (Marchitto, 2007).

The $\delta^{15}N$ signal in deep-sea sediment of the ODP Site 1239 was used to reconstruct the past NO_3^- utilization in the eastern equatorial Pacific (Chapter 8), a large area of incomplete

utilization of NO_3^- and phosphate by phytoplankton in the modern ocean. The supply of these nutrients by deep upwelling is enough to support a significantly large primary biomass than is present, but production is limited by other factors, the most important of which is probably the lack of dissolved iron and silicic acid (Si) (E.g. Brzezinski et al., 2008; Brzezinski et al., 2011). $\delta^{15}N$ and total nitrogen contents (TN, wt%) were determined on freeze-dried, ground bulk sediment. Site 1239 samples were measured with a Carlo–Erba CN analyzer 2500 interfaced directly to a Micromass-Isoprime mass spectrometer at the University Bordeaux 1 (UMR EPOC). Samples of the nearby ODP Site 1240, a Costech 4010 Elemental Analyzer with a zero blank autosampler coupled to a Thermo Delta V isotope ratio mass spectrometer at the University of Rhode Island. Sampling resolution averages one sample every 20-30 cm (~10 kyr). Precision of the isotopic analyses based on certified standards and in-house standards replicates is better than ±0.3‰. Typical precision for TN analysis is better than ±0.02%. Nitrogen isotopic values are reported in delta notation.

CHAPTER 4

TRACKING THE EQUATORIAL FRONT IN THE EASTERN EQUATORIAL PACIFIC OCEAN BY THE ISOTOPIC AND FAUNAL COMPOSITION OF PLANKTONIC FORAMINIFERA.

Daniel Rincón-Martínez[a*], Silke Steph[b], Frank Lamy[a], Alan Mix[c], and Ralf Tiedemann[a]

Published with moderate comments in Marine Micropaleontology

(Volume 79, Issues 1–2, April 2011, Pages 24-40)

a. Alfred Wegener Institute for Polar and Marine Research, Postfach 120161, 27515 Bremerhaven, Germany

b. University of Bremen, Department of Geosciences

c. Oregon State University, College of Oceanic and Atmospheric Sciences, Ocean Administration Building 104, Corvallis, Oregon 97331, USA

*Corresponding Author e-mail: (daniel.rincon.martinez@awi.de), phone: +49(471)/4831-1572; fax: +49(471)/4831-1923

Keywords: planktonic foraminifera; stable isotopes; surface sediments; equatorial front; eastern equatorial Pacific

Abstract

Core-top samples from the eastern tropical Pacific (10°N to 20°S) were used to test whether the ratio between *Globorotalia menardii cultrata* and *Neogloboquadrina dutertrei* abundance ($R_{c/d}$) and the oxygen isotope composition ($\delta^{18}O$) of planktonic foraminifera can be used as proxies for the latitudinal position of the Equatorial Front. Specifically, this study compares the $\delta^{18}O$ values of eight species of planktonic foraminifera (*Globigerinoides ruber* sensu stricto (ss) and sensu lato (sl), *Globigerinoides sacculifer*, *Globigerinoides triloba*, *Pulleniatina obliquiloculata*, *Neogloboquadrina dutertrei*, *Globorotalia menardii menardii*, *Globorotalia menardii cultrata* and *Globorotalia tumida*) with the seasonal hydrography of the region, and evaluates the application of each species or combination of species for paleoceanographic reconstructions. The results are consistent with sea surface temperature and water column stratification patterns. We found that in samples north of 1°N, the $R_{c/d}$ values tend to be higher and $\delta^{18}O$ values of *G. ruber*, *G. sacculifer*, *G. triloba*, *P. obliquiloculata*, *N. dutertrei*, and *G. menardii cultrata* tend to be lower than those from samples located south of 1°N. We suggest that the combined use of $R_{c/d}$ and the $\delta^{18}O$ difference between *G. ruber* and *G. tumida* or between *P. obliquiloculata* and *G. tumida* are the most suitable tools for reconstructing changes in the latitudinal position of the Equatorial Front and changes in the thermal stratification of the upper water column in the eastern tropical Pacific.

4.1. Introduction

One of the most prominent features in the eastern tropical Pacific (ETP) surface ocean hydrography is the meridional asymmetry in sea surface temperature (SST; Figure 4.1) separating a band of cold, high salinity Equatorial Surface Waters (ESW) in the south from warmer, fresher Tropical Surface Waters (TSW) towards the north (E.g. Wyrtki 1966; Pak and Zaneveld, 1974; Okuda et al., 1983; Fiedler and Talley, 2006). The boundary between these water masses is known as the Equatorial Front (EF). The latitudinal position of the EF is related to the intensity and spatial extent of the east Pacific cold tongue, and to the migration of a band of strong atmospheric convection and resulting rainfall, known as the Intertropical Convergence Zone (ITCZ, E.g. Pak and Zaneveld, 1974; Raymond et al., 2004; de Szoeke et al., 2007). Today, the location of the EF changes on different timescales ranging from seasonal to inter-annual, according to the annual solar radiation cycle and changes in oceanographic and atmospheric conditions in the tropical Pacific, interconnected with the El Niño-Southern Oscillation (ENSO; E.g. Wyrtki 1966; Pak and Zaneveld, 1974; Okuda et al., 1983; Fiedler and Talley, 2006). The response of the ETP to past climate changes is discussed controversially. Some authors suggest that oceanographic changes in the region are regulated by high latitude climate (E.g. Pisias and Mix, 1997; Lea et al., 2000; Feldberg and Mix, 2003; Spero et al., 2003; Lea et al., 2006; Leduc et al., 2007; Pena et al., 2008). In contrast, other studies indicate that the tropical Pacific responds independently of variations in high latitude climate and might have behaved similar to the warm phase of El Niño during glacial times (E.g. Koutavas et al., 2002; Koutavas and Lynch-Stieglitz, 2003), while others consider a scenario rather similar to the cold La Niña phase (E.g. Andreasen and Ravelo, 1997; Martínez et al., 2003). These uncertainties highlight the need of a better understanding of the dynamics of ocean circulation, upper ocean stratification, and atmospheric processes in the ETP.

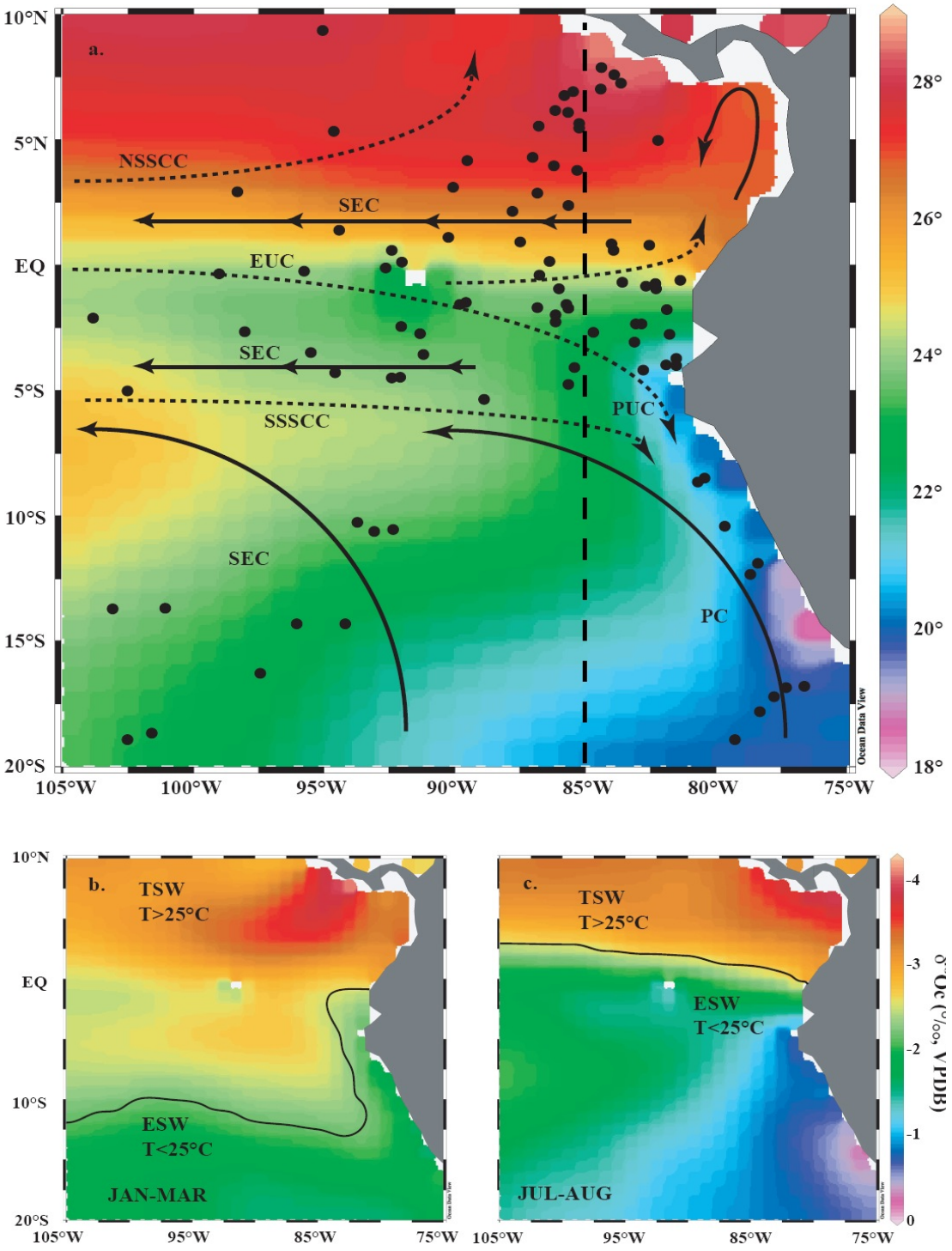

Figure 4. 1 a) Annual mean SST (°C) and schematic three-dimensional circulation in the eastern tropical Pacific, modified from Kessler (2006). It is showing the locations of the core-top samples used in this study, including those from other authors. Upper-layer geostrophic currents (black arrows) include the SEC: South Equatorial Current and PC: Peru or Humboldt Current. Subsurface currents (dashed arrows) include N/SSCC: Northern/Southern Subsurface Countercurrents; PUC: Peru-Chile Undercurrent; and EUC: Equatorial Undercurrent. Panels **(b)** and **(c)** show the seasonal (Jan-Mar and Jul-Sep, respectively) location of main surface water masses; and variability in sea-surface predicted $\delta^{18}O$ (°/₀₀) of the calcite, according to the paleo-temperature equation of Mulitza et al. (2004). Tropical Surface Waters (TSW) and Equatorial Surface Waters (ESW) were divided by the isotherm of 25°C (black line). Notice the development of a distinctive area of minimum $\delta^{18}O_c$ values (associated to warmer temperatures), located over the Cocos Ridge (axis is situated between ~0°N 90°W and ~7°N 84°W), occurs during January-March. Dashed vertical line corresponds to the transect position illustrated in Figures 4.2a and b. All graphs were generated from the World Ocean Atlas database (Conkright et al., 2002) and using Ocean Data View (R. Schlitzer, 2005; available at http://odv.awi-bremerhaven.de/)

In this study, we use the faunal and isotopic composition of planktonic foraminifera from core-top samples in order to determine which species or combination of species provides the best tool for reconstructions of N-S gradients in water temperatures or upper ocean densities in the ETP, which provide valuable information about the EF position. For this purpose, we estimated the $R_{c/d}$ and measured the oxygen isotopic values of planktonic foraminifera and compared them to annual and seasonal water column properties in an area between the west coast of South America and 105°W and between 10°N and 20°S.This study shows that the $R_{c/d}$ is a reliable tool to track the latitudinal EF position and that its application will be best in sediment cores raised to the west of 85°W. We also show that the $\delta^{18}O$ values of planktonic foraminifera calcifying in warm, fresh TSW north of the EF are relatively lower than those of planktonic foraminifera calcifying within cooler, more saline ESW south of the EF. We found that the $\delta^{18}O$ gradients between *G. ruber* ss and *G. tumida* and between *P. obliquiloculata* and *G. tumida* are reflecting the Austral summer thermal stratification between subsurface waters (20 m) subthermocline waters (100 m). We therefore suggest that $\delta^{18}O$ values of planktonic foraminifera with different habitat depths are a useful proxy for reconstructing water column hydrography and EF latitudinal position in the past.

4.2. Regional settings

4.2.1. Hydrography

The EF is a shallow feature restricted to the upper 100 m of the water column. It is located between the equator and 5°S and separates warm TSW in the north from the cool ESW in the south (Figures 4.1 and 4.2). The SST gradient across the front can be extremely strong (ΔT of 1.7°C over a distance of 700 m), and decreases from east to west (Raymond et al., 2004). Most of the year, TSW is characterized by low salinity and high temperature (S<34 p.s.u, T>25°C) as a result of seasonally strong insolation heating, weak wind mixing and an excess of rainfall over evaporation beneath the ITCZ (Figures 4.1 and 4.2). The lowest salinities are located in the Gulf of Panama associated with extreme rainfall and Andean river runoff (Benway and Mix, 2004; Amador et al., 2006; Fiedler and Talley, 2006). South of the EF, ESW properties (S>34 p.s.u, T<25°C) are determined by the seasonal advection of cooler and saltier water from the PC and by equatorial upwelling (Figures 4.1 and 4.2; E.g. Pak and Zaneveld, 1974; Fiedler and Talley, 2006). In addition, biological production across the ETP is heterogeneous and the availability of nutrients is strongly influenced by regional changes in atmospheric and oceanic circulation. North of the EF, surface waters overlying the Cocos Ridge (CR axis is situated between ~0°N 90°W and ~7°N 84°W) are oligotrophic due to low nitrate supply; whereas east and west of the CR, nutrient supply by wind-driven upwelling and near-surface mixing creates two areas of enhanced biological production: the Costa Rica Dome and the Panama Bight. The Costa Rica Dome is a permanent (year-round) feature centered at 9°N; 90°W with a diameter of 100 to 900 km, whereas enhanced biological productivity in the Panama Bight only occurs during boreal winter (December through April), driven by seasonal low-level wind jets which cross the Central American Isthmus (E.g. Okuda et al. 1983; Fiedler et al., 1991; McClain et al., 2002; Torres, 2005; Pennington et al., 2006). South of the EF, moderate productivity is supported by nutrients brought into the euphotic zone via local wind driven upwelling (E.g. Okuda et al., 1983; Fiedler et al., 1991; McClain et al., 2002; Torres, 2005; Pennington et al., 2006).

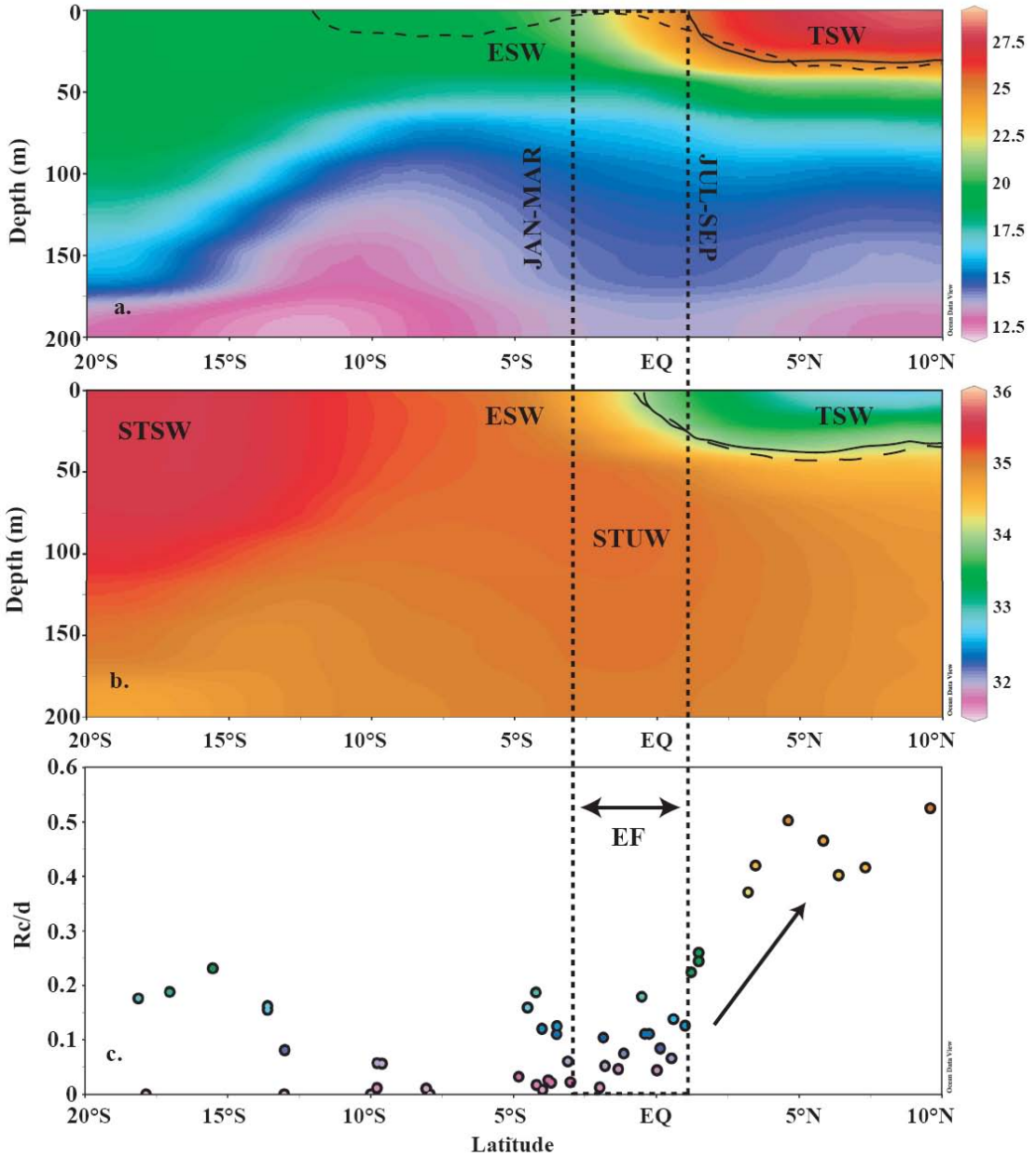

Figure 4. 2. Latitudinal transects of **(a)** annual mean temperature (°C) and **(b)** salinity (psu). Longitudinal position of transect is illustrated in Figure 4.1a by a vertical dashed line. Surface and subsurface waters masses are Tropical Surface Waters (TSW); Equatorial Surface Waters (ESW) and Subtropical Underwater (STUW). Near the top of each panel, the isotherm of 25°C was depicted for the periods January-March (dashed line) and July-September (black line), as an indication of the seasonal migration of the Equatorial Front (EF). Panel **(c)** shows the ratios between *G. cultrata* and *N. dutertrei* (Rc/d), resulting from faunal counts in core-top samples. Results are plotted in an imaginary transect built from each sample latitudinal location and show higher values towards the north of 1°N, coinciding with the distribution of TSW. The three panels present the seasonal latitudinal position of the EF, illustrated by the vertical dashed lines. Upper two graphs were generated from World Ocean Atlas database (Conkright et al., 2002) and using Ocean Data View (R. Schlitzer, 2005; available at http://odv.awi-bremerhaven.de/).http://odv.awi-bremerhaven.de/).

A zonal section along 85°W (Figure 4.2) shows that surface waters north of the EF are well stratified with a shallow and very strong thermocline. Vertical temperature gradients in this area exceed 1°C per 10 m (Wyrtki, 1964), reinforced by a strong halocline. The strong thermocline/pycnocline north of the EF corresponds to a strong nutricline, separating nutrient-poor surface waters (low PO_4, NO_3) from nutrient-enriched thermocline and sub-thermocline waters (high PO_4, NO_3). The nutrient-enriched subsurface waters are upwelled at the equator

and contribute to the formation of ESW. South of 20°S, between 150°W and 90°W, Subtropical Surface Waters (STSW, S>35 p.s.u) are subducted into the upper thermocline (~100 m), resulting in a high-salinity water mass (S~35.2 p.s.u) known as Subtropical Underwater (STUW; Fiedler and Talley, 2006).

4.2.2. Annual and inter-annual variability

From July to September (Figure 4.1c), seasonal solar heating reinforces the meridional temperature gradient across the EF, and highest SSTs occur north of the EF in a zonal band between 10° and 15°N. This SST asymmetry drives the southeasterly trade winds, cooling the tropical South Pacific by enhancing surface evaporation and equatorial and coastal upwelling off Peru and Ecuador. During this time of the year, the equatorial cold tongue is stronger and the EF is at its northernmost position and at maximum intensity, resulting in a strong N-S SST gradient (SST decreases from 25°C to 18°C in 5 degrees of latitude; 1.5°N-3.5°S at 90°W). From January to April (E.g. Figure 4.1b, only showing Jan-Mar), the southeast trades subside and SST south of the Equator increases due to reduced upwelling and less evaporative cooling. This results in an indistinct southern position of the EF and a southward migration of the ITCZ (E.g. Pak and Zaneveld, 1974; Enfield, 1974; Chelton et al., 2001; Hastenrath, 2002; Raymond et al., 2004; de Szoeke et al., 2007). Accordingly, N-S SST gradients across the EF are reduced (SST decreases from 25°C to 23°C in 3 degrees of latitude; 2°S-5°S at 90°W).

The quasi-periodic ENSO inter-annually modifies the physical and biological features in the easternmost Pacific. The El Niño warm phase is related to an abnormal presence of warm water in the normally cool eastern Pacific. During this phase, the EF becomes weaker and moves towards the southwest off South America (E.g. Pak and Zaneveld, 1974; Desser and Wallace, 1990). This is explained by variations in the flux of the SEC and EUC, which result in a deepening of the EEP thermocline as well as reduced upwelling and hence in local heating of the surface layer along the South American coast. The opposite conditions are characteristic of the cool La Niña phase when strong SE trade winds favor upwelling, resulting in sea surface cooling in the central and eastern Pacific.

4.3. Materials and methods

4.3.1.Foraminiferal sampling and analysis

We used a set of 59 core-top samples (courtesy of the Oregon State University Marine Geology Repository) located north and south of the EF in an area between the west coast of South America and 105°W and between 10°N and 20°S(Figure 4.1a, Table 4.1). The sediment samples were retrieved from water depths between 192 and 4622 m, mostly on the Cocos and Carnegie ridges. There, carbonate content is generally high and the thickness of the oxidized layer is low (Lyle, 1992). For practical purposes we assume that core-top samples represent late Holocene age. After freeze-drying, samples of 5 cc were soaked in water and washed through a 63μmsieve. The remaining coarse fraction was oven-dried and subsequently dry-sieved at 125, 250, 315, 355 and 400μm. The identification of planktonic foraminiferal species followed a conservative approach using reference assignments proposed by Parker (1962) and Bolli and Saunders (1985). *Globigerinoides ruber* ss generally corresponds to *G. ruber* specimens with spherical chambers sitting symmetrically over previous sutures with a wide, high-arched aperture over the suture; whereas *Globigerinoides ruber* sl refers to the more compact and higher trochospiral morphotypes, including of *G. pyramidalis*, *G. elongatus*, and *G. cyclostomus* (following Wang, 2000). *Globorotalia menardii cultrata* refers to thin walled, delicate *G. menardii* morphotypes, whereas *Globorotalia menardii menardii* refers to

comparatively thick walled *G. menardii* specimens, following the approach of Bolli (1970) and Knappertsbusch (2007). Most of the *G. tumida* individuals in our samples were not heavily encrusted but had the distinct *G. tumida* shape, similar to the elongate, smooth walled specimens described by Parker (1962).

Faunal analyses of 50 sub-samples were performed on the 355-400 μm size-fractions (Table 4.1). We counted >100 planktonic specimens per sample, which should be statistically sufficient for the interpretation of the relative abundance of dominant taxa (E.g. Fatela and Taborda, 2002), particularly *G. menardii cultrata* and *N. dutertrei* (right coiling). The abundance ratio between these two species has previously been used as indicator of the influence of the Panama–Costa Rica Dome and the cold tongue upwelling systems in the EEP (E.g. Martinez and Bedoya, 2001; Martinez et al., 2006). In this study, it is expressed as:

$R_{c/d}$ = abundance *G. menardii cultrata*/(abundance *G. menardii cultrata* + abundance *N. dutertrei*)

The stable isotopic composition was measured on *G. ruber* ss and sl var. white, *G. triloba*, *G. sacculifer*, *G. menardii cultrata*, *G. menardii menardii*, *G. tumida*, *P. obliquiloculata* and *N. dutertrei* (right coiling). We preferably selected specimens from the 315-400 μm size fraction range in order to minimize the fractionation-growth effect. In samples with few specimens the size range was extended to 250-400 μm (Table 4.1). The number of individuals used for each measurement varied between 10 and 20 specimens. Isotopic analyses of the tests were run at AWI (Bremerhaven) on a Finnigan MAT 251 Mass Spectrometer equipped with an automatic carbonate preparation device. Analytical precision of the laboratory based on replicate analysis of local standards is <0.08 ‰ for $\delta^{18}O$.

We additionally included previously published core-top planktonic foraminiferal $\delta^{18}O$ data from Farrell et al. (1995), Faul et al. (2000), Lea et al. (2000), Loubere et al. (2001), Koutavas and Lynch-Stieglitz, (2003), Benway et al. (2006), Martínez et al. (2006), Leduc et al. (2007), and Pena et al. (2008) to extend our dataset.

4.3.2.Calculation of the predicted $\delta^{18}O$ of calcite ($\delta^{18}O_{pc}$).

We calculated the $\delta^{18}O_{pc}$ based on modern seasonal temperature and salinity data (WOA2001; Conkright et al., 2002) from the upper 300 m of the water column in order to compare measured foraminiferal $\delta^{18}O$ with the expected $\delta^{18}O_{pc}$ variations. An Ocean Data View-based (R. Schlitzer, 2005) available at http://odv.awi-bremerhaven.de/) 3-D estimation function was used to estimate temperature and salinity for each core-top location, for further calculation $\delta^{18}O$ of seawater ($\delta^{18}O_w$) and for the prediction of $\delta^{18}O_{pc}$ at different water depths. Salinity was converted into $\delta^{18}O_w$ using the equation:

$$\delta^{18}O_w = 0.24822*S - 8.321 \ (r^2=0.90)$$

This $\delta^{18}O_w$-salinity relationship was determined using measured $\delta^{18}O_w$ data from the upper 640 m in the equatorial Pacific (178.25°W to 82°W, 23.63°S to 19.578°N) (LeGrande and Schmidt, 2006); Global Seawater Oxygen-18 Database, available at http://data.giss.nasa.gov/o18data/). The most important constraints on the use of this $\delta^{18}O$–salinity relationship are: 1) that there are no measurements of $\delta^{18}O$ of seawater in the upwelling area of Peru/Ecuador and in the cold tongue region; and 2) that the slope of the relationship may vary at seasonal timescales (e.g. due to changes in freshwater input north of the EF or intensification of upwelling south of it).

Table 4.1. Core-top location (latitude, longitude), water depths, authors of stable isotope measurements, sample depth in sediment cores, planktonic foraminiferal counts, ratios between *G. cultrata* and *N. dutertrei* (Rc/d), and oxygen stable isotopes of planktonic foraminifera. $\delta^{18}O$ values measured in this study are expressed relative to Pee Dee Belemnite (PDB) standard, based on calibrations directly to National Bureau of Standards 19.

Site	Longitude [°W]	Latitude [°N]	Water Depth [m]	Author [name, year]	Sediment depth [cm]	*N. dutertrei* counts	*G. cultrata* counts	Planktonic total	$R_{c/d}$	*G. ruber* ss $\delta^{18}O$ [‰]	*G. ruber* sl $\delta^{18}O$ [‰]	*G. trilobu* $\delta^{18}O$ [‰]	*G. sacculifer* $\delta^{18}O$ [‰]	*P. obliquiloculata* $\delta^{18}O$ [‰]	*G. cultrata* $\delta^{18}O$ [‰]	*N. dutertrei* $\delta^{18}O$ [‰]	*G. tumida* $\delta^{18}O$ [‰]	*G. menardii* $\delta^{18}O$ [‰]
VNTR01-21GC	94.603	9.588	3710	This study	1	47	52	161	0.525								-0.47	
ME0005A-41MC2	83.608	7.8557	1370	This study	1	9	1	19										
ME0005A-38MC2	84.113	7.3167	1003	This study	1	73	52	152	0.416	-2.38		-1.95	-1.49	-1.01	0.18	0.48	0.67	0.69
Y71-03-06	85.362	6.39	1945	This study	1	58	39	113	0.402	-2.51	-2.13	-1.84	-2.04	-0.81	-0.40	0.28	0.76	0.97
ME0005A-14MC2	86.449	5.8465	2045	This study	1	79	69	180	0.466	-2.95	-2.97	-1.97	-1.58	-0.35	-0.35	-0.38	0.55	0.48
Y71-03-08MG2	81.938	5.317	3888	This study	1	61	15	97										
ME0005A-15MC6	86.704	4.6137	904	This study	1	90	91	238	0.503	-2.13	-1.75	-1.51	-1.66	-0.98	-0.24	-0.31	0.45	0.12
Y69-75M2	89.693	3.475	2198	This study	3	102	74	321	0.420	-2.21	-2.13	-1.70	-1.45	-1.04	-0.56	-0.17	0.01	0.81
ME0005A-20MC8	86.486	3.2123	674	This study	1	124	73	211	0.371					-0.63	0.03	0.09	0.25	0.55
VNTR01-14GC	89.855	1.485	1033	This study	1	91	32	253	0.260	-0.93	-0.72	-0.20	-0.13	0.54	0.67	1.17	1.60	0.66
VNTR01-15GC	89.862	1.485	1033	This study	1	124	40	196	0.244									
Y71-03-010AMG2	82.277	1.217	3474	This study	0.5	125	36	244	0.224	-2.38	-2.34	-1.97	-1.64	-0.09	-0.58	0.41		
Y69-76M3	92.01	1.003	2319	This study	2	153	22	223	0.126	-1.69	-1.51	-1.36	-0.87	-0.43	-0.01	0.24	0.85	0.15
PLDS-2 ST35 33G	86.087	0.605	2708	This study	1.5	112	18	196	0.138	-2.21	-2.00	-1.66	-1.26	-0.26	-0.08	0.36	0.39	
Y69-97M1	91.632	0.53	2362	This study	1	169	12	244	0.066	-1.50	-1.42	-1.10	-1.16	-0.05	0.21	0.43	0.45	0.53
VNTR01-11GC	95.335	0.14	3345	This study	1	131	12	172	0.084									
ME0005A-21MC3	86.463	0.0215	2942	This study	1	218	10	244	0.044					-0.06	0.52	0.54	0.53	
Y71-03-11MG3	83.285	-0.252	2656	This study	1	112	14	170	0.111	-2.24	-2.03	-1.58	-1.35	-0.34	0.03	0.54		1.10
ODP1239A1-H1	82.4	-0.4	1414	This study	1	297	16	320	0.111	-1.30	-0.99	-0.96	-1.12	-0.03	0.28	0.65		0.73
ME0005A-29MC2	81.995	-0.5134	1343	This study	1	156	34	218	0.179	-1.52	-0.67	-1.10	-1.09	-0.08	0.09	0.47		1.43
Y71-03-22MG3	85.418	-1.138	2338	This study	1	99	8	281	0.075	-1.15	-1.17	-0.63	-0.74	0.12	0.34	0.75		0.72
Y71-03-20MG1	85.323	-1.335	2310	This study	1	187	9	255	0.046	-1.45	-1.02	-0.89	-0.80	-0.24	0.05	0.39	0.59	1.01
Y71-03-13MG3	85.810	-1.795	2798	This study	1	165	9	296	0.052	-0.78	-0.84	-0.52	-0.58	-0.11	0.33	0.74	0.78	1.19
ME0005A-25MC5	82.787	-1.8534	2203	This study	1	173	20	213	0.104	-1.80	-1.53	-1.13	-1.14	0.05	0.18	0.59		
Y69-86M1	91.667	-1.978	3245	This study	4	159	2	204	0.012			-1.68	-1.14	-0.23	-0.48	0.38	0.68	
Y69-104M1	81.518	-2.303	3892	This study	2	53	2	58								0.89		
VNTR01-12GC	95.07	-3.01	3535	This study	1	133	3	156	0.022	-1.56	-1.16	-1.13	-1.04	-0.22	0.20	0.53	0.99	
VNTR01-13GC	90.823	-3.092	3304	This study	1	110	7	130	0.060	-1.82	-1.49	-1.03	-1.54	-0.09	-0.10	0.50	0.66	
W7706-78	81.287	-3.483	539	This study	0.5	70	10	261	0.125									
W7706-73bag	81.483	-3.49	2116	This study	7	97	12	131	0.110						0.09	0.73		
W7706-72 bag	81.642	-3.52	3601	This study	7	82	0	96								0.63		
W7706-71GC	82.505	-3.682	1933	This study	1	139	3	146	0.021							0.73		
Y73-03-06	94.15	-3.782	3714	This study	1	114	3	122	0.026									
Y69-84M2	91.67	-3.98	3748	This study	1	128	1	131	0.008							0.70	1.05	
Y69-83M1	92.015	-4.007	3759	This study	1.5	139	19	203	0.120	-1.83	-1.62	-1.18	-1.24	-0.02	-0.02	0.57	1.00	
W7706-69	85.340	-4.2	3537	This study	1	237	4	247	0.017									
W7706-70GC	85.328	-4.215	3453	This study	1	109	25	170	0.187	-1.65	-1.05	-0.69	-0.69	0.03	0.46	0.86	1.03	1.05
VNTR01-10GC	102.015	-4.507	3405	This study	1	164	31	232	0.159			-0.61	-0.30	-0.23	0.51	0.39	0.82	1.26
W7706-68GC	88.512	-4.818	3903	This study	1	60	2	134	0.032	-0.70	-0.41	0.04	0.08	0.53	1.01	1.46	1.81	1.16
W7706-57	80.182	-7.928	192	This study	2.5	79	0	122	0.000									
W7706-58	80.405	-8.057	486	This study	3	97	1	130	0.010									
Y71-07-34MG1	93.325	-9.607	4622	This study	1	151	9	219	0.056			0.16	0.07	0.14	0.44	0.76	1.12	0.74
W7706-52	79.417	-9.767	352	This study	0.5	83	5	154	0.057									
W7706-53	79.442	-9.783	414	This study	1.5	91	1	189	0.011									
Y71-07-33MG1	92.667	-10	4093	This study	1	22	0	154	0.000							0.61	0.96	1.05
Y73-03-15MG3	100.543	-13.007	4425	This study	1.5	34	3	228	0.081			0.00	-0.01	-0.10	0.21	0.41	0.95	0.76
Y73-03-11MG2	102.575	-13.028	4555	This study	1	4	0	102	0.000							0.13	0.85	
OC170-182P	95.598	-13.612	3811	This study	1.5	82	15	224	0.155									
OC170-186P	93.737	-13.612	3784	This study	1.25	62	12	197	0.162			-0.03	-0.04	-0.02	0.25	0.41	0.75	
Y73-03-23MG1	96.97	-15.528	3656	This study	1	40	12	222	0.231									
RR9702A-66MC1	77.098	-16.127	2575	This study	1	1	0	37									0.60	
RR9702A-64MC1	78.109	-17.035	2930	This study	1	56	13	161	0.188			-0.76	-0.12	0.21	0.50	0.61	0.67	0.09
OC73-3-7MG2	101.067	-17.867	4247	This study	1	3	0	128	0.000								0.82	
RR9702A-62MC3	79.040	-18.085	2937	This study	1					-1.13	-1.58	-0.31	-0.12	0.10	0.44	0.82	0.47	0.46
OC73-3-8MG2	102.017	-18.133	4090	This study	1	14	3	138	0.176									
Y73-04-26MG3	93.417	-20.77	4394	This study	1	0	0	86	0.000									

Site	Longitude [°W]	Latitude [°N]	Water Depth [m]	Author [name, year]	Sediment depth [cm]	*N. dutertrei* counts	*G. cultrata* counts	Planktonic total	R_{sel}	*G. ruber* ss $\delta^{18}O$ [o/oo]	*G. ruber* sl $\delta^{18}O$ [o/oo]	*G. triloba* $\delta^{18}O$ [o/oo]	*G. sacculifer* $\delta^{18}O$ [o/oo]	*P. obliquiloculata* $\delta^{18}O$ [o/oo]	*G. cultrata* $\delta^{18}O$ [o/oo]	*N. dutertrei* $\delta^{18}O$ [o/oo]	*G. tumida* $\delta^{18}O$ [o/oo]	*G. menardii* $\delta^{18}O$ [o/oo]
VNTR01-20GC	94.197	5.627	3563	This study	1											1.06	0.79	0.26
ME0005A-35MC1	85.005	4.1198	3404	This study	1											0.11		
Y71-07-31MG3	91.972	-9.932	4114	This study	1											1.59	1.39	
RR9702A-76TC	76.406	-16.071	3189	This study	1											0.81	0.54	
W7706-47	78.430	-11.67	1500	This study	1.5												0.39	
RC13-113	103.300	-1.65	3195	Faul et al. 2000	0					-1.43		-0.75	-0.85	-0.25	-0.10	0.56	0.71	
RC13-138	94.000	1.8	2655	Faul et al. 2000	0					-2.42		-1.88	-1.67	-0.80	0.09	0.54	0.44	
RC23-12	83.720	1.23	3433	Faul et al. 2000	0					-2.25		-2.87	-2.21	-1.42	-0.47	0.19	0.12	
RC23-20	83.620	1	3186	Faul et al. 2000	0					-1.60		-1.67	-2.25	0.27	0.11	0.34	0.32	
RC11-238	85.820	-1.52	2573	Faul et al. 2000	0					-1.62		-1.14	-1.47	0.45	0.12	0.45	0.40	
RC9-69	82.800	-2.6	2959	Faul et al. 2000	0					-1.23		-1.07	-1.16	0.59	0.03	0.40	0.10	
VM17-44	85.100	-3.6	3358	Faul et al. 2000	0					-1.64		-1.78			-0.53	0.49	0.19	
TR163-11	85.822	6.45	1950	Martinez et al. 2006	0.5											-0.15		
ODP677B	83.737	1.202	3461	Martinez et al. 2006	0											0.36		
ODP506B	86.092	0.61	2711	Martinez et al. 2006	0											0.16		
TR163-38	81.583	-1.337	2200	Martinez et al. 2006	0.5											0.50		
TR163-33	82.568	-1.913	2230	Martinez et al. 2006	0.5											0.23		
TR163-19	90.951	-2.255	2348	Lea et al. 2000	1					-2.07						-0.02		
TR163-22	92.239	0.309	2830	Lea et al. 2000	1					-1.60								
ODP1240	86.278	0.0131	2941	Pena et al. 2008	1					-2.11						0.62		
RC-102	86.510	-1.25	2180	K & L-S 2003	0					-1.78			-1.23					
RC11-238	85.490	-1.31	2573	K & L-S 2003	0					-1.32			-1.14					
RC13-140	87.450	2.52	2246	K & L-S 2003	5					-2.71			-2.18					
V19-27	82.040	-0.28	1373	K & L-S 2003	0					-2.48			-2.16					
V19-28	84.390	-2.22	2720	K & L-S 2003	6					-1.27			-1.24					
V21-29	89.210	-1.03	712	K & L-S 2003	0								-1.57					
V21-30	89.410	-1.13	617	K & L-S 2003	0								-1.59					
V21-40	106.460	-5.31	3182	K & L-S 2003	0					-1.53			-1.19			0.31		
GS7202-56	80.422	-20.0165	3248	Loubere 2001	1											0.82		
Y71-6-12MG	77.563	-16.443	2584	Loubere 2001	1											1.14		
W7706-45	78.172	-11.266	810	Loubere 2001	1											0.25		
W7709-69	85.204	-4.12	3537	Loubere 2001	1											0.62		
W7706-73	81.290	-3.294	2116	Loubere 2001	1											0.76		
GS7202-17	97.560	-2.18	3371	Loubere 2001	1											0.56		
Y71-03-15MG2	85.692	-1.465	2660	Loubere 2001	1											0.69		
Y71-03-31GC	85.692	-0.53	2840	Loubere 2001	1											0.94		
Y69-110M1	81.093	-0.21	3083	Loubere 2001	1											0.51		
GS7202-16	98.533	0.067	3183	Loubere 2001	1											0.49		
P6702-57	87.183	1.33	2749	Loubere 2001	1											-0.28		
P6702-59	85.330	2.75	3274	Loubere 2001	1											-0.07		
GS7202-15	97.833	3.267	2986	Loubere 2001	1											0.29		
GS7202-9	89.130	4.49	3188	Loubere 2001	1											0.57		
AII54-25PC	85.897	4.27	3225	Loubere 2001	1											-0.07		
Y71-03-04MG5	84.963	5.802	2628	Loubere 2001	1											-0.12		
Y71-03-5FF5	84.938	5.92	2363	Loubere 2001	1											0.06		
Y71-03-3MG3	-85.500	7.05	2551	Loubere 2001	1											-0.02		
Y71-03-02MG3	85.152	7.172	2164	Loubere 2001	1											0.15		
ME0005A-43JC	83.365	7.51	1362	Benway et al. 2006	1					-2.46						0.15		
ODP1242	83.360	7.51	1364	Benway et al. 2006	1					-2.75						0.35		
ODP847B	95.190	0.16	3334	Farrell et al. 1995	1								-1.05					
MD02-2529	84.073	8.123	1619	Leduc et al. 2007	1					-3.00								

0.27 ‰ was subtracted from calculated $\delta^{18}O_w$ in order to convert $\delta^{18}O_w$ from the standard mean ocean water (SMOW) scale to the PDB scale (Hut, 1987). We finally calculated the $\delta^{18}O_{pc}$ profiles from the corresponding $\delta^{18}O_w$ and water temperatures by solving four different paleo-temperature equations: Shackleton (1974), Kim and O´Neil (1997), Bemis et al. (1998) and Mulitza et al. (2004). The water depth in which the measured $\delta^{18}O$ matches the $\delta^{18}O_{pc}$ is commonly assumed as the apparent calcification depth (ACD) of each species.

It has previously been shown that Shackleton´s equation provides a good prediction of the $\delta^{18}O_{pc}$: temperature relationship over most of the temperature range (8-20°C), with no significant differences (<0.8°C) from other paleotemperature equations (E.g. Kim and O´Neil, 1997). On the warm-end (20-32°C), however, Shackleton´s equation tends to be less predictive since many measured $\delta^{18}O$ values are lower than $\delta^{18}O_{pc}$ at the sea surface (E.g. Steph et al. 2009). The relationship between temperature and $\delta^{18}O_{pc}$ of Kim and O´Neil (1997) is calibrated across temperatures from 10°C to 40°C. This equation was obtained from precipitation experiments of inorganic calcite and thus does not take in account life processes like photosynthesis, the vital effect nor calcification rate. The equation provided by Mulitza et al. (2004) was developed using shallow-dwelling foraminifera pumped from the mixed layer, and produces reliable estimations of $\delta^{18}O_{pc}$ in the uppermost water column. The *Orbulina universa* equation of Bemis et al., (1998), which is also applicable to *G. ruber*, was obtained from culture experiments under high-light conditions and calibrated across a temperature range of 15-25°C.

Table 4.2. Latitudinal difference in median $\delta^{18}O_{pc}$ values for samples located north of 1°N and samples located between 1°N and 5°S. The median $\delta^{18}O_{pc}$ were calculated from several paleo-temperature equations at different waters depths and during two different seasons, which results of averaging the $\delta^{18}O_{pc}$ from 0-30 m from all four paleotemperature equations

January - March (north - south $\Delta\delta^{18}Opc$)

Water depth	Shackleton (1974)	Mulitza et al. (2004)	Kim and O´Neil (1997)	Bemis et al. (1998)	Median	Average	Stand. Dev.
0m	0.93	0.94	0.91	0.93	0.93	0.93	0.01
10m	1.02	1.04	1.00	1.03	1.03	1.02	0.01
20m	1.10	1.12	1.06	1.09	1.09	1.09	0.02
30m	1.11	1.12	1.07	1.09	1.10	1.10	0.02
50m	0.72	0.72	0.68	0.67	0.70	0.70	0.03
75m	0.28	0.28	0.26	0.26	0.27	0.27	0.01
100m	0.05	0.05	0.05	0.05	0.05	0.05	0.00
150m	0.06	0.06	0.05	0.05	0.05	0.05	0.00

July - September (north - south $\Delta\delta^{18}Opc$)

Water depth	Shackleton (1974)	Mulitza et al. (2004)	Kim and O´Neil (1997)	Bemis et al. (1998)	Median	Average	Stand. Dev.
0m	1.36	1.39	1.32	1.35	1.36	1.36	0.03
10m	1.33	1.36	1.28	1.32	1.33	1.32	0.03
20m	1.33	1.36	1.28	1.31	1.32	1.32	0.03
30m	1.27	1.29	1.22	1.23	1.25	1.25	0.03
50m	0.70	0.71	0.66	0.66	0.68	0.68	0.03
75m	0.37	0.38	0.35	0.35	0.36	0.36	0.01
100m	0.12	0.12	0.1	0.1	0.11	0.11	0.01
150m	0.03	0.02	0.03	0.02	0.03	0.03	0.01

Bemis et al. (1998) suggested that using generic equations could result in significant errors when estimating ocean temperatures from $\delta^{18}O$ due to the different fractionation of oxygen isotopes among species of planktonic foraminifera. We therefore calculated $\delta^{18}O_{pc}$ for all four equations in order to demonstrate that the relative changes in the spatial $\delta^{18}O_{pc}$ pattern across the EF show the trend (Table 4.2). In our dataset, $\delta^{18}O_{pc}$ derived from the surface water paleotemperature equation of Mulitza et al. (2004) is statistically undistinguishable from $\delta^{18}O_{pc}$

obtained by using the paleotemperature equations of Kim and O´Neil (1997) and Bemis et al. (1998) (Table 4.2). We therefore only used the paleo-temperature equations of Mulitza et al. (2004) and Shackleton (1974) for illustrating the $\delta^{18}O_{pc}$ changes in the upper water column and their association to actual measurements of $\delta^{18}O$ from shallow dwelling foraminifera and intermediate dwelling foraminifera, respectively.

In order to assess the statistical significance of regional changes in $\delta^{18}O_{pc}$ or intra- and inter-specific $\delta^{18}O$ changes we used non-parametric statistics. The Mann-Whitney (Wilcoxon) W test was used to compare medians between two samples (i.e. for comparing the isotopic composition between two species or the $\delta^{18}O_c$ between two regions: north and south of the EF). The Kruskal-Wallis ranking test was used to compare medians among several samples (i.e. for comparing the $\delta^{18}O$ values among several species). Both tests were performed using data sets (i.e. $\delta^{18}O$) from independent samples (i.e. regions, species), arranging them in a single series in ascending order, assigning a rank to them from smallest to largest, and comparing the median values of the different samples. The null hypothesis for the comparison of two independent groups assumes that the samples come from identical populations, $median_1 = median_2$. Confidence level used in both test was 95%

Table 4.3. Descriptive statistics of the $\delta^{18}O$ composition of planktonic foraminifera from samples located in the eastern equatorial Pacific. $\delta^{18}O$ values measured in this study are expressed relative to Pee Dee Belemnite (PDB) standard, based on calibrations directly to National Bureau of Standards 19.

		G. ruber ss	*G. ruber* sl	*G. triloba*	*G. sacculifer*	*P. obliquiloculata*	*G. cultrata*	*N. dutertrei*	*G. tumida*	*G. menardii*
		$\delta^{18}O$ [‰]	$\delta^{18}O$ [‰]	$\delta^{18}O$ [‰]	$\delta^{18}O$ [‰]	$\delta^{18}O$ [‰]	$\delta^{18}O$ [‰]	$\delta^{18}O$ [‰]	$\delta^{18}O$ [‰]	$\delta^{18}O$ [‰]
North of EF (north of 1°N)	Mean	-2.39	-2.01	-1.76	-1.61	-0.66	-0.13	0.19	0.47	0.57
	Standard Deviation	0.52	0.75	0.70	0.59	0.56	0.37	0.39	0.53	0.28
	Median	-2.42	-2.13	-1.88	-1.65	-0.81	-0.12	0.15	0.45	0.61
	n	13	6	9	10	10	12	25	11	8
South of EF (1°N - 5°S)	Mean	-1.59	-1.28	-0.91	-0.97	-0.01	0.18	0.58	0.74	0.84
	Standard Deviation	0.41	0.45	0.55	0.59	0.25	0.31	0.29	0.35	0.39
	Median	-1.60	-1.30	-1.03	-1.13	-0.05	0.20	0.56	0.71	0.89
	n	29	16	27	34	27	27	53	31	16
EEP	Mean	-1.84	-1.48	-1.12	-1.12	-0.19	0.09	0.46	0.67	0.75
	Standard Deviation	0.58	0.62	0.69	0.64	0.46	0.36	0.37	0.41	0.37
	Median	-1.73	-1.50	-1.12	0.09	-0.09	0.09	0.49	0.67	0.73
	n	42	22	36	44	37	39	78	42	24

4.4. Results

4.4.1.Faunal Approach

High abundances of *N. dutertrei* (>70%) occur between 5°S and the equator, while *G. menardii cultrata* represents less than 6% of the assemblage (Table 4.1). In contrast, *G. menardii cultrata* is more abundant (>21%) between the equator and 5°N, whereas the abundance of *N. dutertrei* is slightly lower (>58%). According to the W test, there is a significant difference between the median $R_{c/d}$ north and south of the front (i.e. north and south of 1°N). North of ~1°N, $R_{c/d}$ increases constantly from 0.224 up to 0.525, whereas between ~1°N and ~10°S $R_{c/d}$ values range between 0.0 and 0.187 (Figure 4.2, Supplementary Fig. 4.1). South of ~10°S, $R_{c/d}$ values of ~0.2 are only found in subtropical waters or in coastal waters off the Peru coast.

4.4.2. Predicted $\delta^{18}O$ of calcite ($\delta^{18}O_{pc}$) in the ETP

Independent of which paleo-temperature equation is applied for calculating $\delta^{18}O_{pc}$, we found a significant difference between the median values of $\delta^{18}O_{pc}$ at stations located north of 1°N and median values of $\delta^{18}O_{pc}$ at stations located between 1°N and 5°S (W test, 95% confidence level). The north-south difference in $\delta^{18}O_{pc}$ in the upper 30 m of the water column has the largest magnitude between July and September, when the EF is strongest and at its northernmost position (1.31 ± 0.04 ‰ vs. 1.03 ± 0.02 ‰; Table 4.2). Below 50 m water depth,

the July – September north-south gradient is smaller (0.68 ± 0.03 ‰) but still statistically significant (95% confidence level) down to 100 m water depth, where the N-S difference decreases to about 0.11 ± 0.01 ‰ (Table 4.2). Strong $\delta^{18}O_{pc}$ gradients within the upper water column during July-September mainly result from the marked cooling (up to 3.3°C) of ESW south of the EF, caused by the upwelling of cool thermocline waters and the advection of southern-sourced waters by the PC (see section 4.2.3). During January to March, when the EF is relatively weaker and located further south, the average difference in $\delta^{18}O_{pc}$ between northern and southern medians is smaller, but still statistically significant (95% confidence level) up to water depths of 75 m (0.27 ± 0.01 ‰). Below 75 m there is not a visible regional difference in $\delta^{18}O_{pc}$.

4.4.3.Oxygen isotopes in planktonic foraminifera tests

According to the Kruskal-Wallis test, median $\delta^{18}O$ values of the spinose species *G. ruber* ss, *G. ruber* sl, *G. triloba*, *G. sacculifer* are more negative than those of the non-spinose species *P. obliquiloculata*, *G. cultrata*, *N. dutertrei*, *G. menardii*, and *G. tumida* (Tables 4.1 and 4.3; Figures 4.3, 4.4, 4.5, and 4.6). The comparison of $\delta^{18}O$ measurements from core tops north of the EF (>1°N) and south of the EF (1°N - 5°S) also shows that $\delta^{18}O$ of the shallow-dwelling spinose species generally increases towards the south. This latitudinal difference is much smaller or even statistically insignificant in the $\delta^{18}O$ of intermediate dwelling species.

In our dataset, including the previously published data, the $\delta^{18}O$ values of *G. ruber* ss (n=42) range between -3 and -0.70 ‰ (Table 4.1; Figures 4.3, 4.5 and 4.6a). According to the W test (95% confidence), the spatial pattern of $\delta^{18}O$ *G. ruber* ss is characterized by relatively low median values (-2.42 ‰) north of the EF (>1°N), becoming more positive (-1.60 ‰) further south, between 1°N - 5°S (Table 4.3). *G. ruber* sl exhibits slightly higher $\delta^{18}O$values than *G. ruber* ss, varying between -2.97 and -0.41 ‰ (Table 4.1; Figures 4.3, 4.5 and 4.6a). The isotopic difference between sensu stricto and sensu lato morphotypes measured within the same sample is 0.22 ±0.26 ‰ (n=22). Although *G. ruber* sl is not very common (n=22), its spatial $\delta^{18}O$ pattern is very similar to the one exhibited by the sensu stricto variety (Table 4.3), displaying significant differences (W test, at 95% confidence) between the median $\delta^{18}O$ north of the EF (-2.13 ‰), and the one exhibited further south, between 1°N and 5°S (-1.17 ‰). In samples where both species were present, average $\delta^{18}O$ of *G. ruber* ss is 0.48 ± 0.33 ‰ lower than $\delta^{18}O$ of *G. triloba* (n=30); and 0.51 ± 0.37 ‰ lower than $\delta^{18}O$ of *G. sacculifer* (n=35). $\delta^{18}O$ of *G. ruber* sl is also generally lower than $\delta^{18}O$ of *G. triloba* ($\Delta^{18}O$ = 0.37 ± 0.33 ‰; n=22); and *G. sacculifer* ($\Delta^{18}O$ = 0.43 ± 0.44 ‰; n=22).

The $\delta^{18}O$ values of *G. triloba* (n=36) vary between -2.87 and 0.16 ‰, while $\delta^{18}O$ of *G. sacculifer* (n=44) ranges between -2.25 and 0.08 ‰ (Table 4.1; Figures 4.3, 4.5 and 4.6a). In samples where both species are present, their absolute $\delta^{18}O$ values are statistically undistinguishable ($\Delta^{18}O$ = 0.08 ±0.29 ‰; n=35). *G. triloba* has a median $\delta^{18}O$ value of -1.88 ‰ north of the EF (>1°N) and of -1.03 ‰ south of the EF (between 1°N and 5°S), whereas $\delta^{18}O$ *G. sacculifer* increases from -1.65 ‰ north of the EF to -1.13 ‰ south of the EF (Table 4.3). According to the W test, the median $\delta^{18}O$ values of *G. triloba* and *G. sacculifer* from core top samples located north of ~1°N are significantly more negative than the ones recorded in samples located further to the south.

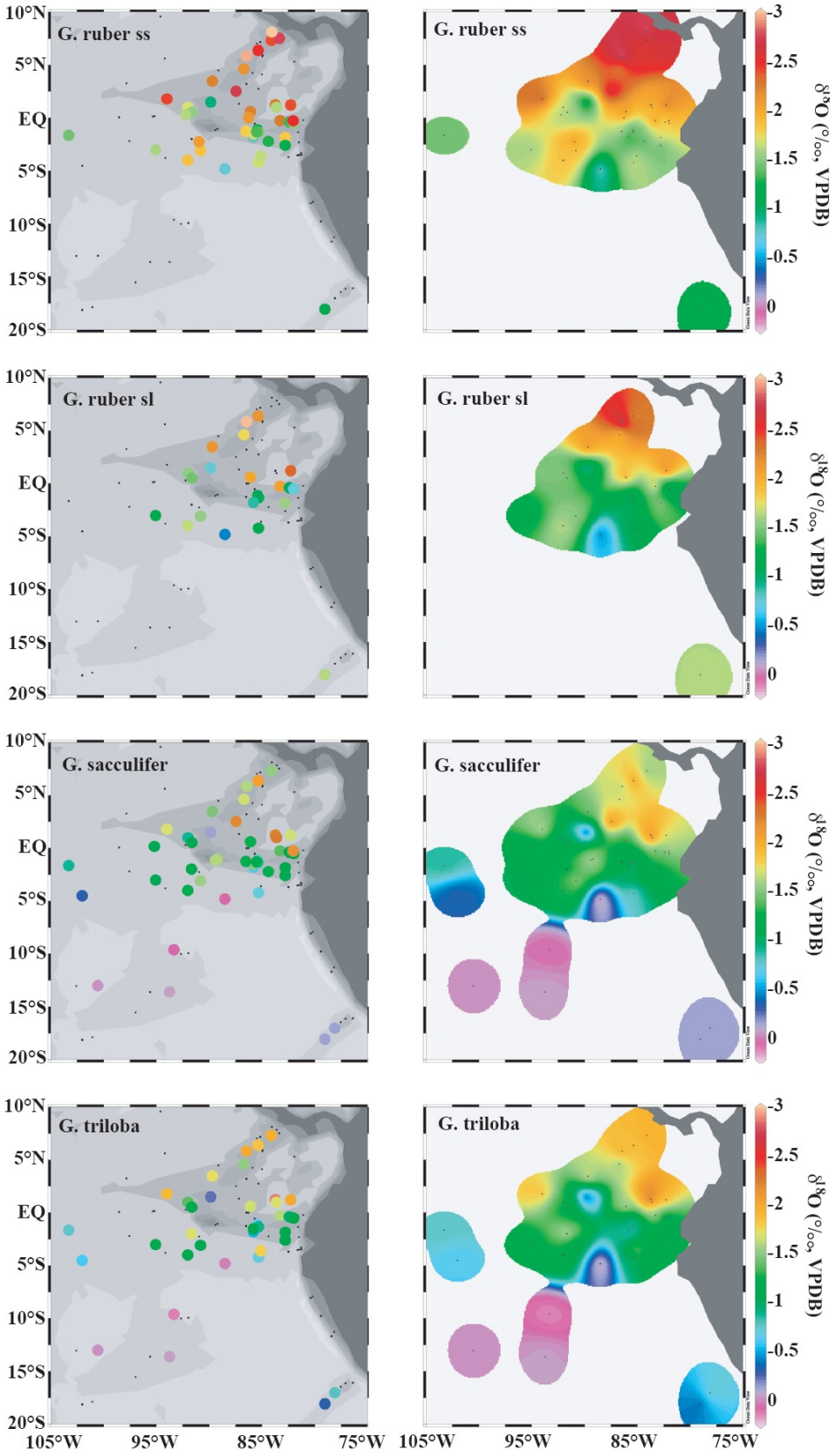

Figure 4. 3. On the left side panels, the distribution pattern of measured $\delta^{18}O$ values of the shallow-dweller planktonic foraminiferal species used in this study is plotted vs. a simplified bathymetric chart of the eastern equatorial Pacific. On the right side, $\delta^{18}O$ values interpolated. $\delta^{18}O$ values measured in this study are expressed relative to Pee Dee Belemnite (PDB) standard, based on calibrations directly to National Bureau of Standards 19. All graphs were plotted on the same $\delta^{18}O$ scale and generated using Ocean Data View (R. Schlitzer, 2005; available at http://odv.awi-bremerhaven.de/)

Among the deeper-dwelling, non-spinose planktonic foraminiferal species, *P. obliquiloculata* displays the lowest $\delta^{18}O$ values, followed by *G. menardii cultrata*, *N. dutertrei*, *G. tumida* and *G. menardii menardii* (Kruskal-Wallis test at 95% confidence). $\delta^{18}O$ of *P. obliquiloculata* ranges between -1.42 and 0.59 ‰ (n=37), being more negative (median = -0.81 ‰) north of the EF (>1°N) than towards the south (median = -0.05 ‰; see Tables 4.1 and 4.3; Figures 4.4, 4.5, 4.6b and Supplementary Fig. 4.2). When spinose species are present in the same sample, the average $\delta^{18}O$ difference between *P. obliquiloculata* and *G. triloba* amounts to 0.93 ± 0.51 ‰ (n=35), and the average $\delta^{18}O$ difference between *P. obliquiloculata* and *G. sacculifer* is 0.85 ± 0.57 ‰ (n=35). Compared to other deeper-dwelling species measured in the same sample, $\delta^{18}O$ of *P. obliquiloculata* is on average 0.29 ± 0.57 ‰ (n=37), 0.66 ± 0.36 ‰ (n=37), 0.88 ± 0.47 ‰ (n=31), and 0.98 ± 0.54 ‰ (n=21) lower than $\delta^{18}O$ of *G. menardii cultrata*, *N. dutertrei*, *G. tumida*, and *G. menardii menardii*, respectively.

The $\delta^{18}O$ of *G. menardii cultrata* (n=41) and *N. dutertrei* (n=80) varies between -0.58 and 1.01 ‰ and between -0.38 and 1.59 ‰, respectively (Table 4.1). If both species are present in the same sample, the $\delta^{18}O$ difference between them amounts to 0.39 ±0.26 ‰ (n=38). Similar to *P. obliquiloculata*, both species have slightly more negative $\delta^{18}O$ values north of the EF than further to the south (Table 4.3; Figures 4.4, 4.5 and 4.6b). The median $\delta^{18}O$ of *G. menardii cultrata* is -0.12 ‰ north of 1°N; and 0.20 ‰ between 1°N and 5°S. Median $\delta^{18}O$ of *N. dutertrei* is 0.15 ‰ north of 1°N and 0.56 ‰ between 1°N and 5°S. The average isotopic differences between *G. menardii cultrata* - *G. tumida* and *G. menardii cultrata* - *G. menardii menardii* are 0.56 ± 0.32 ‰ (n=32) and 0.57 ±0.47 ‰ (n=22), respectively. The average isotopic differences between *N. dutertrei* - *G. tumida* and *N. dutertrei* - *G. menardii menardii* are 0.19 ± 0.31 ‰ (n=39) and 0.24 ± 0.50 ‰ (n=24), respectively.

G. tumida and *G. menardii menardii* display the highest $\delta^{18}O$ values among all species analyzed in this study. $\delta^{18}O$ of *G. tumida* (n=44) and *G. menardii* (n=25) varies between -0.47 and 1.81 ‰ and 0.09 and 1.43 ‰ respectively (Table 4.1; Figures 4.4, 4.5, 4.6b and Appendix 1). When found in the same sample, the difference between the absolute $\delta^{18}O$ values of both species is 0.08 ± 0.45 ‰ (n=20). In contrast to the latitudinal $\delta^{18}O$ pattern observed in the shallow-dwelling spinose species (i.e. *G. ruber*), the median $\delta^{18}O$ values of *G. tumida* and *G. menardii menardii* from samples north of the EF (1°N) do not differ significantly from those measured in core-tops that are located further south (W test at 95% confidence; Table 4.3).

4.5. Discussion

4.5.1. Equatorial Front and $_{Rc/d}$

In our dataset, $R_{c/d}$ values are higher than 0.3 north of the EF (> 1°N), whereas Rc/d values south of the equator are generally lower than 0.3 (Figure 4.2; Appendix 1). The observed changes in $R_{c/d}$ match those reported by Martinez and Bedoya (2001), reinforcing their hypothesis that the EF can be tracked using the ratio between *G. cultrata* and *N. dutertrei*. Although both species exhibit high low susceptibility to carbonate dissolution (Berger, 1970), the application of this proxy would be best in the area delimited by the Cocos and Carnegie ridge where it has been calibrated and, because further west or south the water depth increases and accordingly the carbonate dissolution, which might have an effect on the faunal assemblages.

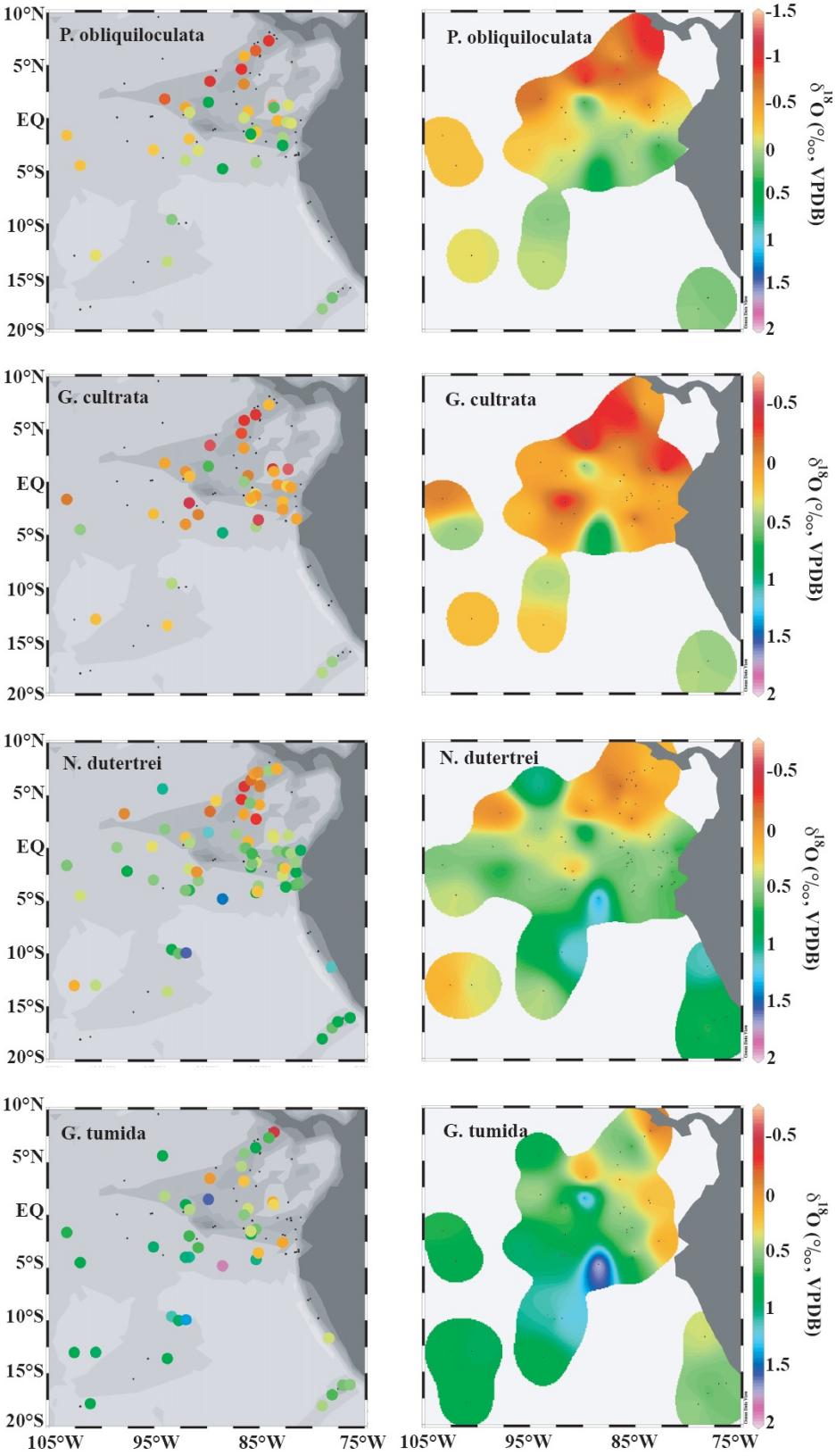

Figure 4. 4 On the left side panels, the distribution pattern of measured $\delta^{18}O$ values of the intermediate-dweller planktonic foraminiferal species used in this study is plotted vs. a simplified bathymetric chart of the eastern equatorial Pacific. On the right side, $\delta^{18}O$ values interpolated. $\delta^{18}O$ values measured in this study are expressed relative to Pee Dee Belemnite (PDB) standard, based on calibrations directly to National Bureau of Standards 19. With exception of $\delta^{18}O$ of *P. obliquiloculata*, all graphs were plotted on the same $\delta^{18}O$ scale. Visualization done using Ocean Data View (R. Schlitzer, 2005; available at http://odv.awi-bremerhaven.de/)

Since the observed variations in $R_{c/d}$ mainly result from variations in *G. cultrata* abundance (r2=85.33%), it is important to determine the factors that might be responsible for the relatively higher abundance of *G. cultrata* in the area north of the EF. According to Martínez and Bedoya (2001), the differential distribution of *G. cultrata* and *N. dutertrei* is related to different food webs rather than to differences in temperature, meaning that *G. cultrata* preys mostly on dinoflagellates and diatoms in the Panama Bight and Costa Rica Dome north of the EF, whereas *N. dutertrei* preferably feeds on diatoms and coccolithophorids within the nutrient-rich "cold tongue" region south of the EF. Yet in their as well as in our study, higher abundances of *G. cultrata* north of the EF are solely observed in samples from the CR, which apparently is neither influenced by upwelling in the Costa Rica Dome nor in the Panama Bight. Compared to the adjacent upwelling areas, surface waters over the CR are characterized by higher temperature, low salinity and a depletion of [NO_3], even during the strongest upwelling season in the Costa Rica Dome and in the Panama Bight (January-March) (Figure 4.1; E.g. Fiedler et al., 1991; Peña et al., 1994; Fiedler et al., 2002; McClain et al., 2002; Benway and Mix, 2004; Fiedler and Talley, 2006; Pennington et al., 2006).

Although we do not contradict the interpretation of Martínez and Bedoya (2001), we thus rather hypothesize that the link between *G. cultrata* abundance and EF position might be related to a preference for nutrient-poor, warm, fresh waters (E.g. Luzurriaga, 1992; Brown, 2007; Machain-Castillo et al., 2007) rather than to an specific food web. In absence of samples east (Panama Basin) and west (Costa Rica Dome) of the CR, however, it is difficult to ultimately determine the specific physical or biological parameters that control the *G. cultrata* abundance north of the EF.

4.5.2. ACD of planktonic foraminifera

Previous studies focusing on ecology, vertical distribution and isotopic composition of planktonic foraminifera, which have been carried out north of the EF in the Panama Bight (E.g. Fairbanks et al., 1982; Curry et al., 1983; Thunell et al., 1983; Thunell and Reynolds, 1984; Wefer et al., 1983; Bé et al., 1985; Loubere, 2001; Martinez and Bedoya, 2001) indicate that the ACDs derived from our isotope data are generally consistent with relative habitat depths determined by plankton tow and core top studies. These studies as well as our new data suggest that the spinose species *G. ruber*, *G. sacculifera* and *G. immatura* inhabit the uppermost water column (mixed layer), whereas *P. obliquiloculata*, *G. cultrata*, *N. dutertrei*, *G. menardii*, and *G. tumida* dwell deeper in the water column (Fairbanks et al., 1982; Bé et al., 1985; Watkins et al., 1996; Faul et al., 2000). Although we tried to investigate a possible seasonal bias of the $\delta^{18}O$ signals (Figure 4.5), we were not able to identify a seasonal preference for any of the species.

According to the ACDs derived from the Mulitza et al., (2004) paleotemperature equation, *G. ruber* is generally the shallowest-dwelling spinose species in the ETP, and seems to inhabit the upper mixed layer (0-50 m), with no difference in ACD north and south of the EF (Figure 4.5). The ACD derived from our study is comparable to the habitat depth of *G. ruber* determined by most plankton tow studies (E.g. Fairbanks et al., 1982; Curry et al., 1983; Bé et al., 1985) and is supported by the Kruskal-Wallis test (95% confidence), in which the median $\delta^{18}O$ values of *G. ruber* ss are the lowest among the spinose species followed by *G. ruber* sl, *G. triloba*, and *G. saccculifer*. The average isotopic difference between the sensu stricto and sensu lato morphotypes of *G. ruber* (0.22 ± 0.26 ‰) is small, consistent with the results of (Wang, 2000) (0.21 ± 0.21 ‰). We therefore suggest that the habitat depths of both *G. ruber* morphotypes overlap, whereas *G. ruber* sl probably calcifies slightly deeper than *G. ruber* ss.

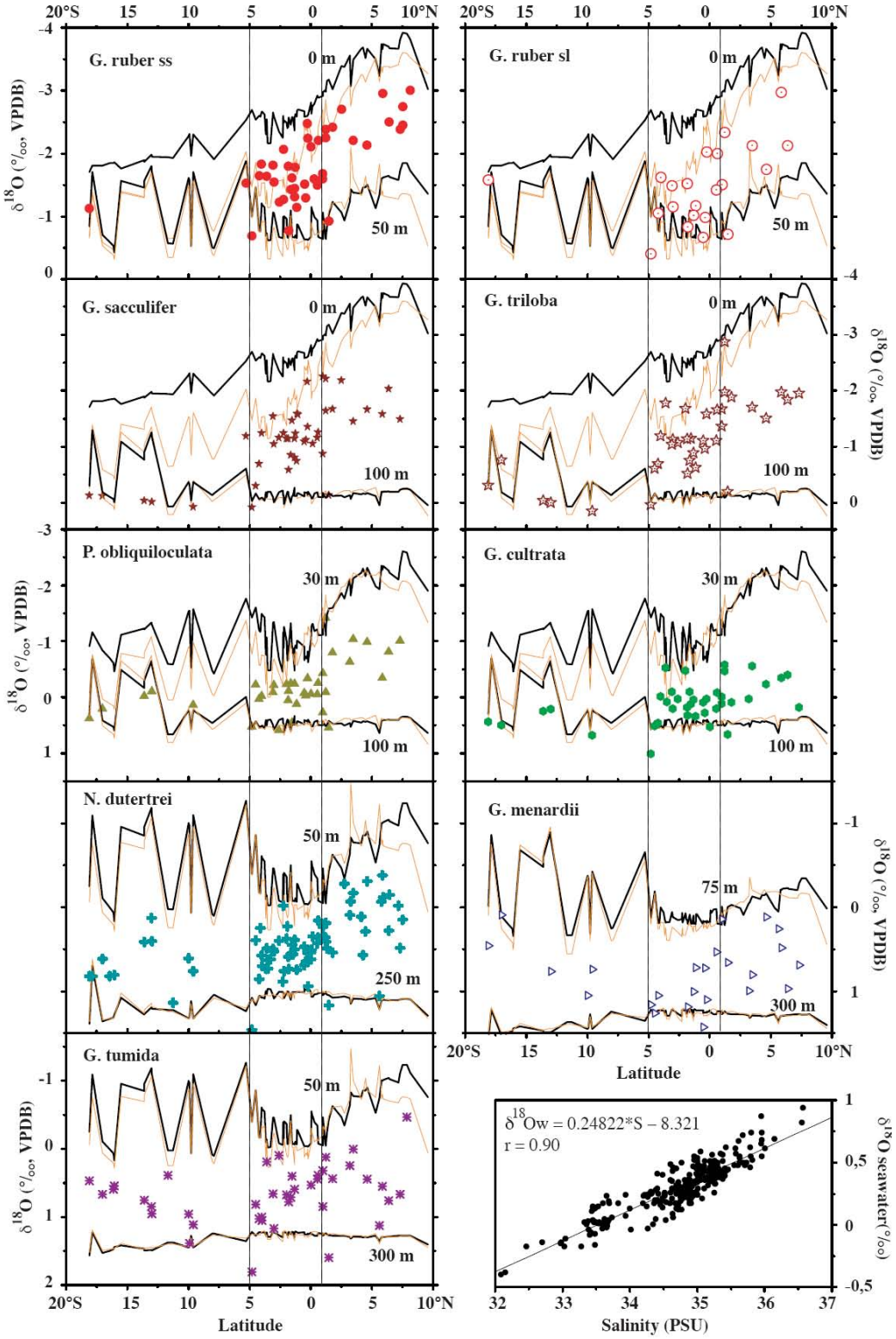

Figure 4. 5 Individual comparisons of latitudinal variations in predicted $\delta^{18}O$ of calcite ($\delta^{18}O_{pc}$) at selected depth levels and observed $\delta^{18}O$ values of each planktonic foraminiferal species used in this study. Results are plotted in an imaginary transect built from each sample latitudinal location and physical parameters extracted from World Ocean Atlas database (Conkright et al., 2002). In the case of shallow-dwellers, the predicted $\delta^{18}O_c$ in the background was calculated for January-March (black line) and July-September (orange line) using the equation of (Mulitza et al., 2004). In the case of intermediate- and deep-dwellers, the predicted $\delta^{18}O_c$ in the background was calculated for January-March (black line) and July-September (orange line) using the paleo-temperature equation of Shackleton et al. (1974). Dashed vertical lines indicate the seasonal position of the equatorial front. The lowermost right panel illustrates the relationship between $\delta^{18}Ow$ and salinity (S) used for estimation of $\delta^{18}O_w$ Oceanographic data were taken from the NOAA World Ocean Atlas (WOA2001; Conkright et al., 2002)

Our dataset suggests a wider ACD range for G. sacculifer and G. triloba: 0-100 m north of 5°S and slightly deeper south of it. Plankton tow studies previously carried out in the Panama Basin (E.g. Fairbanks et al., 1982; Curry et al., 1983), however, indicate a shallower habitat for the spinose, dinoflagellate-bearing *G. sacculifer*, either close to the surface or near the chlorophyll maximum zone between 25 and 37 m, and also suggest that *G. triloba* inhabits slightly shallower depths than other spinose species, recording signatures of the uppermost water column. This conflict between core-top and plankton-tow studies might be explained by the fact that foraminiferal shells found in the sediment are generally heavier in $\delta^{18}O$ than those collected alive in the water column (Vergnaud-Grazzini, 1976; Mulitza et al., 2004). It has also been suggested that under oceanic conditions of low salinity and warm temperature in the mixed layer (as in the Panama Basin), *G. sacculifer* continues to secrete calcite between the base of the mixed layer and up to 200 m, thereby enriching the oxygen-18 (E.g. Duplessy et al., 1981). Moreover, it is believed that this species experience gametogenic calcification, which implies that adults which undergo gametogenesis would extract additional $CaCO_3$ from deeper (cooler) waters than the epipelagic waters where the foraminifera form the bulk of their shells (E.g. Bé, 1980).

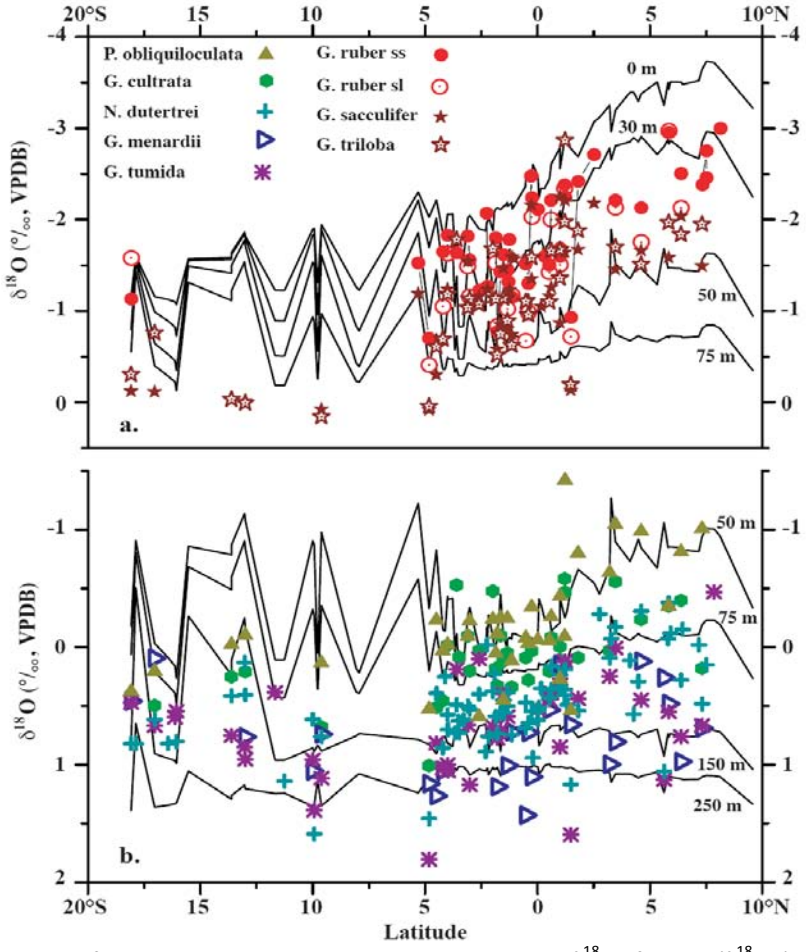

Figure 4. 6. Comparison of latitudinal variations in annual mean predicted $\delta^{18}O$ of calcite ($\delta^{18}O_{pc}$) at selected depth levels and observed $\delta^{18}O$ values of a) shallow-dweller and b) intermediate- and deep-dweller planktonic foraminiferal species used in this study (see legend inside upper panel). Results are plotted in an imaginary transect built from each sample latitudinal location and physical parameters extracted from World Ocean Atlas database (Conkright et al., 2002). In the case of shallow-dwellers, the predicted $\delta^{18}O_{pc}$ (lines) was calculated using the equation of (Mulitza et al., 2004). In the case of intermediate- and deep-dwellers, the predicted $\delta^{18}O_{pc}$ (lines) was calculated using the paleo-temperature equation of (Shackleton et al., 1974).

In our dataset, the ACD of *P. obliquiloculata* varies between 30 and 100 m (Figure 4.5). This species has a distinctive polished outer cortex, and is usually found in the upper 100 m of the water column in tropical waters, mostly related to the base of the upper thermocline (E.g. Prell and Damuth, 1978; Watkins et al., 1996; Cleroux et al., 2007). Non-spinose species as *G. menardii menardii*, *G. menardii cultrata*, and *N. dutertrei* are facultative diatom- or chrysophyte-bearing and their primary life cycle might be confined to the euphotic zone (Hemleben et al., 1989). Our dataset indicates that *G. menardii cultrata* mostly calcifies in water depths between 30 and 100 m north of 5°S, and slightly deeper further to the south. These ACD estimates match the results of Regenberg et al. (2010), who suggest habitat depths of ~ 50 to ~ 80 m for *G. menardii cultrata*, in the South China Sea. In the ETP, *N. dutertrei* seems to calcify between 50 and 250 m, with no change in ACD along the north to south transect (Figure 4.5). This is consistent with plankton-tow studies showing that 90% of its total population inhabit water depths between 0 and 200 m, with peak abundances in the middle to deep thermocline (60-150 m), associated with the deep chlorophyll maximum (E.g. Fairbanks et al., 1982; Bé et al., 1985; Watkins et al., 1996; Faul et al., 2000).

The ACD of *G. menardii menardii*, whose tests are moderately encrusted and two times heavier than those of *G. menardii cultrata* (Brown, 2007) seems to overlap with the ACD of the usually heavier encrusted *G. tumida* (50 - 300 m water depth; Figure 4.5). Even though the initial test formation of *G. menardii menardii* and *G. tumida* takes place at relatively shallow depths (close to the habitat of *G. menardii cultrata*), their bulk isotopic signature is strongly controlled by the final precipitation of the crust in deeper, cooler waters within and below the thermocline (E.g. Schweitzer and Lohmann, 1991; Brown, 2007; Regenberg et al., 2010)

4.5.3. Variations in the $\delta^{18}O$ of shallow dwelling foraminifera across the EF region

The $\delta^{18}O$ values of spinose species generally increase towards the south along with increasing mixed-layer salinity and decreasing mixed layer temperature. Similar to the latitudinal pattern of $\delta^{18}O_{pc}$ (see section 4.4.2), measured$\delta^{18}O$ values of *G. ruber* ss, *G. ruber* sl, *G. triloba* and *G. sacculifer* exhibit significant differences between the medians of samples located north of 1°N and those located between 1°N-5°S. The lowest $\delta^{18}O$ values are generally observed in samples located on the Cocos Ridge, while the highest $\delta^{18}O$ values occur over the Carnegie Ridge. The fact that the southernmost core top samples (south of 5°S) were generally collected at deeper locations (>3000 m water depth) than the northern samples (at the Cocos or Carnegie Ridge) may contribute to high $\delta^{18}O$ values and, thus deeper ACDs observed in tests of species like *G. ruber*, *G. sacculifer*, *G. triloba*. The high susceptibility to carbonate dissolution of these species (i.e. Berger, 1970) causes the selective removal of thin-walled specimens, concentrating thick-walled and terminal forms that build more of their shell in deeper and cooler waters. Therefore, the tracking of the EF, by means of the oxygen isotopic composition would be better on samples taken north of 5°S and east of 90°W, were the bathymetry is shallower than the lysocline and where the EF migration is better depicted in a narrower range.

In order to determine whether the $\delta^{18}O$ values of planktonic foraminifera are reflecting the EF signature and/or position, we compared the north-south $\delta^{18}O_{pc}$ variability with measured intra-specific $\delta^{18}O$ variability. Given that our ACD estimates suggest that *G. ruber* calcifies in the upper 50 m of the water column (see 4.5.2), one would expect that the difference in the median isotopic composition of *G. ruber* north and south of the EF reflects the difference in mixed layer $\delta^{18}O_{pc}$ across the EF. Indeed, $\Delta\delta^{18}O_{n\text{-}s}$ of *G. ruber* ss ($\Delta\delta^{18}O_{n\text{-}s}$= 0.82 ‰) and *G. ruber* sl ($\Delta\delta^{18}O_{n\text{-}s}$= 0.85 ‰) is similar to the north to south difference in $\delta^{18}O_{pc}$within the upper 50 m of the water column during January-March, no matter which paleotemperature equation is applied (0.97 ±0.17 ‰; Table 4.2). Yet it has been shown that in the Panama Basin (north of

the EF) the *G. rube* flux out of the mixed layer occurs throughout the year, with enhanced test numbers in boreal summer (Thunell and Reynolds, 1984), the $\Delta\delta^{18}O_{n\text{-}s}$ recorded by *G. ruber* is substantially smaller than the modern N-S $\delta^{18}O_{pc}$ gradient observed during boreal summer (July-September). Then, the most plausible explanation for a N-S pattern of $\delta^{18}O$ *G. ruber* reflecting Jan-Mar conditions rather than boreal summer conditions would be the high-temperature preference of *G. ruber* (Bijma et al., 1990). During Jan-Mar, the EF is relatively weak and located further south, allowing for a southward expansion of warm TSW (Figures 4.1 and 4.3), which may favor *G. ruber* reproduction. Unfortunately, no information on the seasonality of *G. ruber* is available for the region south of the Panama Bight or south of the EF.

Similar to *G ruber*, both *G. sacculifer* and *G. triloba* exhibit a significant difference in the oxygen isotopic signature north and south of the EF (Figure 4.5; Table 4.3). Compared to the variability of $\delta^{18}O_{pc}$ across the EF, *G. sacculifer* ($\Delta\delta^{18}O_{n\text{-}s}$= 0.51 ‰) either reflects N-S $\delta^{18}O_{pc}$ changes at 30-100 m water depth during boreal winter (January-March; 0.53 ±0.46 ‰; Table 4.2) or at 50-75 m water depth during boreal summer (July-September; 0.52 ±0.23 ‰); while *G. triloba*($\Delta\delta^{18}O_{n\text{-}s}$= 0.78 ‰) reflects north to south changes in $\delta^{18}O_{pc}$ in the upper 100 m during the period January-March (0.74 ±0.42 ‰). Due to the large variation in $\Delta\delta^{18}O_{pc}$, overlapping between seasons, as well as the large range of ACD estimates for these species it is difficult to determine a more precise signal for *G. sacculifer* or *G. triloba* in terms of water depth or time of the year.

4.5.4. Variations in $\delta^{18}O$ of intermediate-dwellers across the EF

P. obliquiloculata, which exhibits the lowest $\delta^{18}O$ values among the intermediate dwellers, reflects a N-S $\delta^{18}O$ pattern similar to that observed in *G. triloba* ($\Delta\delta^{18}O_{n\text{-}s}$= 0.74 ‰), thereby closely matching the magnitude of the north to south change in $\delta^{18}O_{pc}$ across the front in the upper 100 m during the period January-March (0.74 ±0.42 ‰; Tables 4.2 and 4.3). Although the $\delta^{18}O$ of *P.obliquiloculata* is generally higher than $\delta^{18}O$ of *G. triloba* (section 4.4.3) their ACDs overlap (section 4.5.2), resulting in similar N-S oxygen isotope changes across the EF. This can be explained by the fact that *P.obliquiloculata* has been reported as tropical facultative symbiotic, initially calcifying within the thermocline near the chlorophyll maximum, which in the Panama Basin occurs at relatively shallow depths, between 25-40 m (Fairbanks et al., 1982). Later in its life cycle, however, it continues to calcify in cooler waters below the surface mixed layer, where it acquires the final isotopic composition of exported tests settling to the seafloor.

The non-spinose species *G. menardii cultrata* and *N. dutertrei* record slightly smaller but still statistically significant (95% confidence level) differences in $\delta^{18}O$ north and south of the EF. These N-S $\delta^{18}O$ differences of *G. menardii cultrata* ($\Delta\delta^{18}O_{n\text{-}s}$= 0.32 ‰) and *N. dutertrei* ($\Delta\delta^{18}O_{n\text{-}s}$= 0.41 ‰) are comparable to N-S differences in $\delta^{18}O_{pc}$ in the upper 200 m of the water column, independent of seasonality (Tables 4.2 and 4.3). The $\delta^{18}O$ values of the more encrusted *G. menardii menardii* and *G. tumida*, however, display no significant N-S differences. The weak correlation of their $\delta^{18}O$ values to hydrographic changes associated with the position of the EF can be attributed to the formation of secondary calcite crusts at greater water depths, where the N-S differences in $\delta^{18}O_{pc}$ associated with the EF are not detectable (Figure 4.5).

4.5.5. Inter-specific $\delta^{18}O$ gradients

With exception of samples south of the Carnegie Ridge (5°S), where spinose species might experience increases in the $\delta^{18}O$ of their tests due to carbonate dissolution (see Sections 4.4.3,

4.5.3 and 4.5.4), our study indicates that all planktonic foraminiferal species except the deep-dwelling *G. tumida* and *G. menardii menardii* display statistically significant latitudinal differences in the oxygen isotopic composition that might be related to the EEP hydrography. This provides the opportunity to evaluate the use of $\delta^{18}O$ gradients between those species, which exhibit N-S changes in $\delta^{18}O$, and intermediate-dwelling species such as *G. tumida* or *G. menardii menardii,* which do not exhibit any latitudinal $\delta^{18}O$ change, as a tool for reconstructing the position of the EF in paleo-records by means of changes in upper ocean stratification (E.g. Mulitza et al., 1997; Lin et al., 1997; Faul et al., 2000; Lin and Hsieh, 2007; Steph et al., 2009).

Strong (weak) stratification in the upper 150 m of the water column should result in large (small) $\Delta\delta^{18}O$ between shallower-dwelling species that exhibit N-S $\delta^{18}O$ changes and the deeper-dwelling species that do not, mirroring respective changes in the surface- to subsurface temperature gradients. Although several $\delta^{18}O$ gradients between species indeed show N-S changes, our dataset indicates that only the $\delta^{18}O$ difference between *G. ruber* ss and *G. tumida* and between *P. obliquiloculata* and *G. tumida* show a statistically significant (confidence level 95%) relationship to water column thermal stratification (Figure 4.7). The N-S changes in these $\delta^{18}O$ gradients are closely reflecting the boreal summer/austral summer (Jan-Mar) temperature gradient between 20 and 100 m water depth ($\Delta T_{20\text{-}100m}$) or between 20 and 75 m water depth ($\Delta T_{20\text{-}75m}$; but with a slightly weaker correlation coefficient; see Figure 4.7). In contrast to *G. ruber* (see section 4.5.3), the lack of information on the seasonal preference of *P. obliquiloculata* in the EEP makes it hard to postulate any direct link between the $\Delta\delta^{18}O_{G.tumida\text{-}P.obliquiloculata}$ and the season during Austral summer.

In the northernmost tropical waters (north of 5°N), where a steep and shallow thermocline exists year-round, the $\delta^{18}O$ difference between the deeper dweller *G. tumida* and the shallow dweller *G. ruber* ss is larger than 3‰ (Figure 4.7a, c). Between 5°N and 5°S, $\Delta\delta^{18}O_{G.tumida\text{-}G.ruber}$ shows large variations (2.58 – 1.33‰) with more positive values north of the EF (median = 2.53‰) than between 1°N and 5°S (median = 2.09‰). At the southernmost station (18°S), $\Delta\delta^{18}O_{G.tumida\text{-}G.ruber}$ is only 1.80‰. The N-S pattern of changes in $\Delta\delta^{18}O_{G.tumida\text{-}G.ruber}$differs from that observed in the $\delta^{18}O$ of the shallow dwellers alone (see Sections 4.4.3 and 4.5.3), since the largest changes in $\Delta\delta^{18}O_{G.tumida\text{-}G.ruber}$occur 4° north of the modern EF position. The $\delta^{18}O$ difference between *G. tumida* and *P. obliquiloculata*, however, closely reflects the trend observed in the $d^{18}O$ of the shallow-dwelling spinose species (see Sections 4.4.3 and 4.5.4), with higher $\Delta\delta^{18}O_{G.tumida\text{-}P.obliquiloculata}$ north of 1°N (generally >2.86‰) and lower values further to the south.

With respect to the different ACDs (0-50 m for *G. ruber* and 30-100 m for *P. obliquiloculata*), it is surprising, however, that both $\Delta\delta^{18}O_{G.tumida\text{-}P.obliquiloculata}$and $\Delta\delta^{18}O_{G.tumida\text{-}G.ruber}$ reflect the temperature gradient between 20-100 m water depth. Assuming that *P. obliquiloculata* calcifies within the entire depth range in question, the link between $\Delta\delta^{18}O_{G.tumida\text{-}P.obliquiloculata}$ and $\Delta T_{20\text{-}100m}$ cannot simply be explained by habitat differences between *G. tumida* and *P. obliquiloculata*. Therefore, further studies are needed to establish $\Delta\delta^{18}O_{G.tumida\text{-}P.obliquiloculata}$ as a useful tool for paleo-reconstructions of the EF position.

In order to test the use of $\Delta\delta^{18}O_{G.tumida\text{-}G.ruber}$ for paleoreconstructions of the EF position, we applied it to the down-core record of core RC11-238, located on the Carnegie Ridge between the coast of South America and the Galapagos Islands (1.52°S 85.82°W, 2573m). The core location is seasonally influenced by ESW and shows high surface productivity due to divergent equatorial upwelling and the advection of cool, nutrient rich waters from the PC (data from Faul et al., 2000). Results illustrated in Appendix 1 show that during the past ~20 kyr, the

$\Delta\delta^{18}O_{G.tumida\text{-}G.ruber}$ values are generally within the range of $\Delta\delta^{18}O$ displayed in our core-top data-set (0.9 - 2.7 ‰), with maxima at 4.8 and 8 kyr BP and minima at 11.6 and 19 kyr BP. The fact that the core-top $\Delta\delta^{18}O_{G.tumida\text{-}G.ruber}$ locates the EF further north (see above) and that values at core RC11-238 are generally similar to modern $\Delta\delta^{18}O$ values south of the EF suggests that the core RC11-238 was always located underneath the path of seasonal migration of the EF. The general trend of increasing $\Delta\delta^{18}O$ values from the last glacial maximum (LGM) towards the Holocene suggests an increasing influence of TSW, from cooler SST during the LGM towards warmer SST during the Holocene, pointing to a general southward movement of the EF-ITCZ complex from the glacial towards the Holocene also supported by studies of Martinez et al. (2003) and Rincón-Martinez et al. (2010).

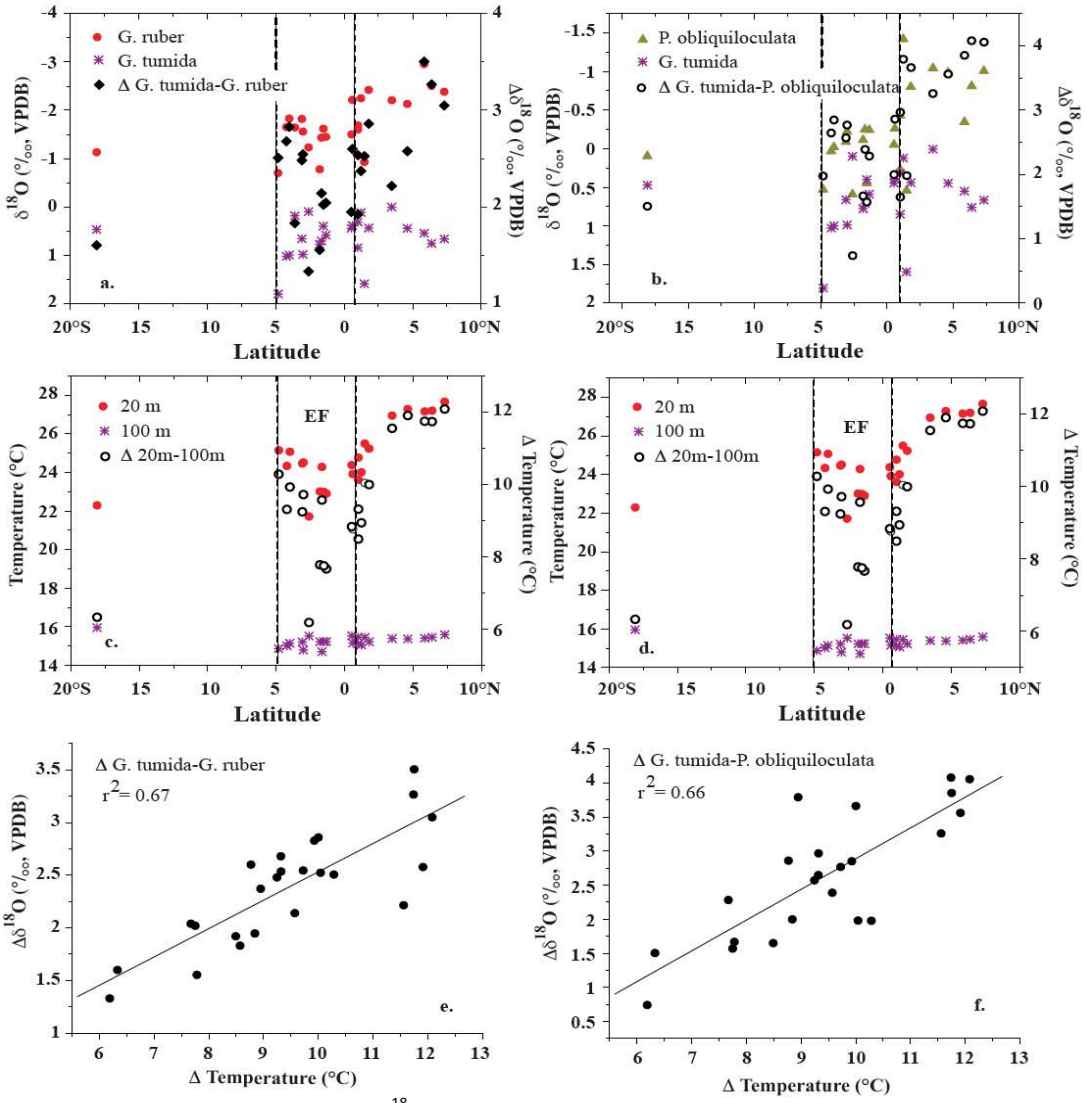

Figure 4. 7. Latitudinal variations in $\Delta\delta^{18}O$ between **a)** *G. tumida* and *G. ruber* ss and **b)** *G. tumida* and *P. obliquiloculata*. Individual $\delta^{18}O$ values for each species are also plotted (see internal legend) together with the range of seasonal migration of the Equatorial Front (vertical dashed lines). Northernmost line corresponds to the EF position during Austral summer (January-March), while the southernmost line indicates the EF position during Austral winter (July-September). In panels **c)** and **d)** the Jan-Mar latitudinal variations in temperature and ΔT are illustrated between isobars at 20 and 100 m from the same stations where $\Delta\delta^{18}O$ was calculated. Note that north of the Equatorial Front (EF), the difference between the temperature at 20 and 100 m is bigger. Lower panels show the relationship between **e)** $\Delta\delta^{18}_{G.tumida\text{-}G.ruber\ ss}$ and the Jan-Mar ΔT between isobars at 20 and 100 m and **f)** $\Delta\delta^{18}O_{G.tumida\text{-}P.\ obliquiloculata}$ and the Jan-Mar ΔT between isobars at 20 and 100 m.

4.6. Paleoceanographic implications and conclusions

We propose that the ratio between *G. menardii cultrata* and *N dutertrei* abundances ($R_{c/d}$) as well as the oxygen isotopic difference between *G. ruber* and *G. tumida* ($\Delta\delta^{18}O_{G.tumida\text{-}G.ruber}$) and between *P. oliquiloculata* and *G. tumida* ($\Delta\delta^{18}O_{G.tumida\text{-}P.obliquiloculata}$) are useful paleoceanographic tools for reconstructing the latitudinal position of the eastern Pacific Equatorial Front in an area delimited by the Cocos and Carnegie ridges. In our core top dataset, high $R_{c/d}$ values (>0.3) as well as high $\Delta\delta^{18}O_{G.tumida\text{-}G.ruber}$ values are related to warm, low salinity TSW north of the EF, whereas cool, nutrient-rich ESW south of the front are characterized by lower $R_{c/d}$ values and $\Delta\delta^{18}O_{G.tumida\text{-}G.ruber}$. We suggest that high $R_{c/d}$ north of the EF reflects an increase in the abundance of *G. menardii cultrata* in warmer and more oligotrophic TSW compared to ESW south of the EF. The isotopic data are unfortunately more difficult to interpret. Both $\Delta\delta^{18}O_{G.tumida\text{-}G.ruber}$ and $\Delta\delta^{18}O_{G.tumida\text{-}P.\ obliquiloculata}$ measured on core top samples reflect the modern $\Delta T_{20\text{-}100m}$ during Austral summer/Boreal winter (January-March). The strongest N-S changes in $\Delta\delta^{18}O_{G.tumida\text{-}G.ruber}$, however, occur 4° north of the modern EF position. In contrast, N-S changes in $\Delta\delta^{18}O_{G.tumida\text{-}P.obliquiloculata}$ match the modern EF position, but the link between $\Delta\delta^{18}O_{G.tumida\text{-}P.obliquiloculata}$ and $\Delta T_{20\text{-}100m}$ is difficult to interpret given the relatively deep habitat (30-100 m water depth) of *P. obliquiloculata*.

Although we are currently not able to explain the latitudinal difference between modern EF position and the observed changes in $\Delta\delta^{18}O_{G.tumida\text{-}G.ruber}$, the application of the $\Delta\delta^{18}O_{G.tumida\text{-}G.ruber}$ to a down-core record located south of the EF indicates nevertheless a potential value of this proxy. The down-core record of $\Delta\delta^{18}O_{G.tumida\text{-}G.ruber}$ at core RC11-238 shows a long-term increase in $\Delta\delta^{18}O$ from the last glacial to the Holocene. The long-term increase in $\Delta\delta^{18}O$ is interpreted as glacial to Holocene warming of SST, reflecting an EF-ITCZ complex migration, bringing TSW towards southern latitudes and hence increasing stratification in the upper water column. However, most absolute $\Delta\delta^{18}O_{\ G.tumida\text{-}G.ruber}$ values correspond to the expected range of values from core-top samples obtained south of 5°N, which would contradict a significant latitudinal migration of the EF over the last termination.

The main advantage of using $\delta^{18}O$ gradients between different planktonic foraminiferal species to detect past changes in water mass boundaries is that they provide local signals (I.e. frontal movements), whereas global changes in $\delta^{18}O$ are canceled out. It is thus theoretically possible to reconstruct EF movements with $\delta^{18}O$ gradients measured in only one sediment core. On the other hand, temporal changes in $\Delta\delta^{18}O$ can be biased by several critical factors, such as habitat changes, different seasonality, mixing by bioturbation, or calcite dissolution. When applying the $\Delta\delta^{18}O$ gradients determined by our core-top dataset to reconstruct paleo-migrations of the EF, it has to be assumed that: 1) all species maintain approximately the same mean ACD in different climate states; 2) seasonality of the species does not change; and 3) that the age of every specimen from the same sample is identical.

Since the core-top $\delta^{18}O$ values of shallow- and intermediate-dwelling planktonic foraminiferal species such as *G. ruber* ss, *G. ruber* sl, *G sacculifer*, *G. triloba*, *P. obliquiloculata*, *G. menardii cultrata*, and *N. dutertrei* display significant N-S changes, which can be linked to the position and structure of the modern EF, it is also possible to use $\delta^{18}O$ of single species to track past changes in the EF position. Yet because the reconstruction of latitudinal EF movements based on single species can only be achieved by mapping spatial $\delta^{18}O$ patterns, applying this tool in paleoceanographic studies requires the establishment of planktonic $\delta^{18}O$ records from several sediment cores along a latitudinal transect (E.g. Koutavas and Lynch-Stieglitz, 2003).

Acknowledgements

We thank Dr. J. I. Martínez (EAFIT University) for helpful discussions and Andreas Mackensen, Lisa Schönborn, and Günter Meyer (AWI-Bremerhaven) for their invaluable assistance with oxygen isotope measurements. Core-top samples were provided by the Marine Geology Repository at the Oregon State University. The German Science Foundation funded this project through grants Ha 2756/9-1 and TI240/17-2. We acknowledge R. Schlitzer for making available a powerful way to visualize data from World Ocean Atlas 2001 using the software package Ocean data View (http://awi-bremerhaven.de/GEO/ODV/).

Species list

Globigerinoides ruber var. white (d´Orbigny, 1839), *Globigerinoides triloba* s.l (Reuss, 1850), *Globigerinoides sacculifer* (Brady, 1877), *Globorotalia menardii cultrata* (d´Orbigny), *Globorotalia menardii menardii* (Parker, Jones and Brady, 1865), *Globorotalia tumida* (Brady, 1877), *Pulleniatina obliquiloculata* (Parker and Jones, 1865), and *Neogloboquadrina dutertrei* (d´Orbigny, 1839)

References

- Abrantes, F., Lopes, C., Mix, A., and Pisias, N. 2007. Diatoms in Southeast Pacific surface sediments reflect environmental properties. Quaternary Science Reviews 26, 155-169.
- Amador, J. A., Alfaro E. J., Lizano, O. G., and Magaña, V. O. 2006. Atmospheric forcing of the eastern tropical Pacific: A review. Progress in Oceanography 69, 101-142.
- Andreasen, D. J., and Ravelo, A. C. 1997. Tropical Pacific Ocean thermocline depth reconstructions for the last glacial maximum. Paleoceanography 12(3), 395-413.
- Andreasen, D. J., Ravelo, A. C., and Broccoli, A. J. 1997. Remote forcing at the last glacial maximum in the tropical Pacific ocean. Journal of Geophysical Research 106, 879-897.
- Archer, D., Aiken, J., Balch, W., Barber D., Dunne, J., Flament, P., Gardner, W., Garside, C., Goyet, C., Johnson, E., Kirchman, D., McPhaden, M., Newton, J., Peltzer, E., Welling, L., White, J., and Yoder, J. 1997. A meeting place of great ocean currents: Shipboard observations of a convergent front at 2°N in the Pacific. Deep-Sea Research II 44(9-19), 1827-1849.
- Bé, A. W. H. 1980. Gametogenic calcification in a spinose planktonic foraminifer, *Globigerinoides sacculifer* (Brady). Marine Micropaleontology 5, 283-310.
- Bé, A. W. H., Bishop, J. K. B., Sverdlove, M. S., and Gardner, W. D. 1985. Standing stock, vertical distribution and flux of planktonic foraminifera in the Panama Basin. Marine Micropaleontology 9, 307-333.
- Bemis, B. E., Spero, H. J., Bijma, J., and Lea, D. W. 1998. Reevaluation of the oxygen isotopic composition of planktonic foraminifera: Experimental results and revised paleotemperature equations. Paleoceanography 13,150-160.
- Benway, H. M., and Mix, A. C. 2004. Oxygen isotopes, upper-ocean salinity, and precipitation sources in the eastern tropical Pacific. Earth and Planetary Science Letters 224, 493-507.
- Benway, H. M., Mix, A. C., Haley, B. A., and Klinkhammer, G. P. 2006. Eastern Pacific Warm Pool paleosalinity and climate variability: 0-30Kyr. Paleoceanography 21, PA3008, doi: 10.1029/2005PA001208.
- Berger, W. H. 1970. Planktonic foraminifera: Selective solution and the lysocline. Marine Geology 8, 111-138.
- Berger, W. H., Bonneau, M. -C., and Parker. F. L. 1982. Foraminifera on the deep-sea floor: Lysocline and dissolution rate. Oceanologica Acta 5(2), 249-258.
- Bijma, J., Faber Jr., W. W., and Hemleben, Ch. 1990. Temperature and salinity limits for growth and survival of some planktonic foraminifers in laboratory cultures. Journal of Foraminiferal Research 20, 95–116.
- Bolli, H. M. 1970. The foraminifera of sites 23-31, Leg 4.In Bader, R. G. et al. 1970.Initial reports of the Deep Sea Drilling Project, Volume IV. Washington (U.S. Government Printing Office) pp. 577-644.
- Bouvier-Soumagnac, Y., and Duplessy, J. C. 1985. Carbon and oxygen isotopic composition of planktonic foraminifera from laboratory culture, plankton tows and recent sediment: implication for the

reconstruction of paleoclimatic conditions and of the global carbon cycle. Journal of Foraminiferal Research 15, 302–320.
- Brown, K. R. 2007. Biogeographic and morphological variation in late Pleistocene to Holocene globorotalid foraminifera. Inaugural dissertation Philosophish-Naturwissenschaftlichen Fakulät Del Universität Basel. 170 p.
- Chelton et al. 2001. Observations of Coupling between Surface Wind Stress and Sea Surface Temperature in the Eastern Tropical Pacific. Journal of Climate 14(7), 1479-1498.
- Cleroux, C., Cortijo, E., and Duplessy, J.-C. 2007. Deep-dwelling foraminifera as thermocline temperature recorders. Geochemistry, Geophysics, Geosystems 8(4). Doi:10.1029/2006GC001474.
- Conkright, M. E., Locarnini, R. A., Garcia, H. E., O'Brien, T. D., Boyer, T. P., Stephens, C., and Antonov, J. I. 2002. World Ocean Atlas 2001: Objective analyses, data statistics, and figures, CD-ROM documentation, NODC Internal Rep. 17, 17pp. Natl. Oceanogr.Data Cent., Silver Spring, Md.
- Cruz, M; Gabor, N., Mora, E., Jiménez, R., and Mair, J. 2003. The known and unknown about marine biodiversity in Ecuador (Continental and Insular). Gayana 67(2), 232-260.
- Curry, W. B., Thunell, R. C., and Honjo, S. 1983. Seasonal changes in the isotopic composition of planktonic foraminifera collected in Panama Basin sediment traps. Earth and Planetary Science Letters 64, 33-43.
- Desser, C., and Wallace, J. M. 1990. Large-scale atmospheric circulation features of warm and cold episodes in the tropical Pacific. Journal of Climate 3(11), 1254-1281.
- De Szoeke, S. P., Xie, S. -P., Piyama, T., Richards, K. J. and Small, R. J. O. 2007. What maintains the SST front north of the eastern Pacific equatorial cold tongue?. Journal of Climate 20, 2500-2514.
- Duplessy, J. C., Bé, A. W. H. and Blanc, P.L. 1981. Oxygen and carbon isotopic composition and biogeographic distribution of planktonic foraminifera in the Indian Ocean. Palaeogeography, Palaeoclimatology, Palaeoecology, 33, 9-46.
- Enfield, D. 1974. Oceanografía de la región Norte del Frente Ecuatorial: Aspectos físicos. Reunion de trabajo sobre el fenómeno conocido como "El Nino". Guayaquil, Ecuador, 4-12 Diciembre. FAO, Informe de Pesca 185, 411p.
- Fairbanks, R. G., and Wiebe, P. H. 1980. Foraminifera and chlorophyll maximum: vertical distribution, seasonal succession, and paleoceanographic significance. Science 209, 1524–1526.
- Fairbanks, R. G., Sverdlove, M., Free, R., Wiebe, P. H. and Bé, A. W. H. 1982. Vertical distribution and isotopic fractionation of living planktonic foraminifera from the Panama Basin. Nature 298, 841-844.
- Farrell, J. W., Murray, D. W., McKenna, V. S., and Ravelo, A. C. 1995. Upper ocean temperature and nutrient contrasts inferred from Pleistocene planktonic foraminifer $\delta^{18}O$ and $\delta^{13}X$ in the eastern equatorial Pacific. In Pisias, N. G., Mayer, L. A., Janecek, T. R., Palmer-Julson, A. Ad van Andel, T. H. (Eds). Proceedings of the Ocean drilling Program, Scientific Results 138, 289-311.
- Fatela, F., and Taborda, R. 2002. Confidence limits of species proportions in microfossil assemblages. Marine Micropaleontology 45(2), 169-174.
- Faul, K. L., Ravelo, C., and Delaney, M. L. 2000. Reconstructions of upwelling, productivity, and photic zone depth in the eastern equatorial Pacific Ocean using planktonic foraminiferal stable isotopes and abundances. Journal of Foraminiferal Research 30(2), 110-125.
- Feldberg, M. J., and Mix, A. C. 2003. Planktonic foraminifera, sea surface temperatures, and mechanisms of oceanic change in the Peru and south equatorial currents, 0-150 ka BP. Paleoceanography 18(1), 1016, doi: 10.1029/2001PA000740.
- Fiedler, P. C., Philbrick, V., and Chavez, F. P. 1991. Oceanic upwelling and productivity in the eastern tropical Pacific. Limnology and Oceanography 36(8), 1834-1850.
-Fiedler, P. C. 2002. The annual cycle and biological effects of the Costa Rica Dome. Deep-Sea Research I (49), 321-338.
- Fiedler, P. C., and Talley, L. D. 2006. Hydrography of the eastern tropical Pacific: A review. Progress in Oceanography 69, 143-180.
- Hastenrath, S. 2002. The Intertropical Convergence Zone of the Eastern Pacific revisited. International Journal of Climatology 22, 347-356.
- Hayes, S.P., McPhaden, M. J., and Wallace, J. M. 1989. The influence of sea-surface temperature on surface wind in the Eastern Equatorial Pacific: Weekly to monthly variability. Journal of Climate 2(12), 1500-1506.
- Hemleben, Ch., Spindler, M., and Anderson, O. R. 1989. Modern Planktonic Foraminifera. Springer-Verlag, Heidelberg, 8-32.

- Hut, G. 1987. Stable isotopes reference samples for geochemical and hydrological investigations, report to the Director General, 42 pp., Int. At. Energy Agency, Vienna.
- Johnson, G. C. and McPhaden, M. J. 1999. Interior pycnocline flow from the subtropical to the equatorial Pacific Ocean. Journal of Physical Oceanography 29, 3073-3089.
- Kim, S. T. and O´Neil, J. R. 1997. Equilibrium and nonequilibrium oxygen isotope effects in synthetic carbonates. Geochimica et Cosmochimica Acta 61(16), 3461-3475.
- Knappertsbusch, M. 2007. Morphological variability of Globorotalia menardii (planktonic foraminifera) in two DSDP cores from the Caribbean Sea and the Eastern Equatorial Pacific. Carnets de Géologie / Notebooks on geology, Brest, Article 2007/04 (CG2007_A04), 34 p., 16 figs., 2 tables, 2 pls.
- Koutavas, A., and Lynch-Stieglitz, J. 2003. Glacial-interglacial dynamics of the eastern equatorial Pacific cold tongue –Intertropical Convergence Zone system reconstructed from oxygen isotope records. Paleoceanography 18(4), 1089, doi: 10.1029/2003PA000894.
- Koutavas, A., Lynch-Stieglitz, J., Marchitto, T. M., and Sachs, J. 2002. El-Niño-like pattern in Ice Age tropical Pacific sea surface temperature. Science 297, 226-230.
- Kroopnick, P. M. 1985. The distribution of ^{13}C of $\Sigma XO2$ in the world oceans. Deep-Sea research parts A, Oceanographic research papers 32, 57-84.
- Lea, D. W., Pak, D. K., and Spero, H. J. 2000. Climate impact of late Quaternary equatorial Pacific sea surface temperature variations. Science 289, 1719-1724.
- Lea, D. W., Pak, D. K., Belanger, C. L., Spero, H. J., Hall, M. A., and Shackleton, N. J. 2006. Paleoclimate history of Galápagos surface waters over the last 135,000 yr. Quaternary Science Reviews 25, 1152-1167.
- Leduc, G., Vidal, L., Tachikawa, K., Rostek, F., Sonzogni, C., Beaufort, L. and Bard, E. 2007. Moisture transport across Central America as a positive feedback on abrupt climatic changes. Nature 445, 908-911.
- LeGrande, A. N. and Schmidt, G. A. 2006. Global gridded data set of the oxygen isotopic composition in seawater. Geophysical Research Letters 33, L12604, doi: 10.1029/2006GL026011.
- Lin, H. -L., Hsieh, H. -Y. 2007. Seasonal variations of modern planktonic foraminifera in the South China Sea. Deep-Sea Research II 54, 1634-1644.
- Lin, H. -L., Peterson, L. C., Overpeck, J. T., Tumbore, S. E. and Murray, D. W. 1997. Late Quaternary climate change from $\delta^{18}O$ records of multiple species of planktonic foraminifera: high-resolution records from the anoxic Cariaco Basin, Venezuela. Paleoceanography 12, 415–427.
- Loubere, P. 1994. Quantitative estimation of surface ocean productivity and bottom water oxygen concentration using benthic foraminifera. Paleoceanography 9(5), 723-737.
- Loubere, P. 1996. The surface ocean productivity and bottom water oxygen signals in deep water benthic foraminiferal assemblages. Marine Micropaleontology 28, 247-261.
- Loubere, P. 2000. Marine control of biological production in the eastern equatorial Pacific Ocean. Nature 406, 497-500.
- Loubere, P. 2001. Nutrient and oceanographic changes in the Eastern Equatorial Pacific from the last full Glacial to the Present. Global and Planetary Change 29, 77-98.
- Lukas, R. 1986. The termination of the Equatorial Undercurrent in the eastern Pacific. Progress in Oceanography 16, 63-90.
- Luzuriaga, M. 1998. Planktic Foraminifera of the Eastern South Pacific. Universidad de Guayaquil, Ecuador (http://ron.udec.cl/index.php?option=com_content&task=view&id=25)
- Machain-Castillo, M. L., Monreal-Gómez, M. A., Arellano-Torres, E., Merino-Ibarra, M., and González-Chávez, G. 2007. Recent planktonic foraminiferal distribution patterns and their relation to hydrographic conditions of the Gulf of Tehuantepec, Mexican Pacific. Marine Micropaleontology 66(2), 103-119.
- Martínez, I., Keigwin, L., Barrows, T.T., Yokoyama, Y., and Southon, J. 2003. La Niña-like conditions I the eastern equatorial Pacific and a stronger Choco Jet in the northern Andes during the last glaciation. Paleoceanography 18(2), 1033, doi: 10.1029/2002PA000877.
- Martinez, I., Rincón, D., Yokohama, Y., and Barrows, T. 2006. Foraminifera and coccolithophorid assemblage changes in the Panama Basin during the last deglaciation: Response to the sea-surface productivity induced by a transient climate change. Palaeogeography, Palaeoclimatology, Palaeoecology 234, 114-126.
- Martinez, J. I. and Bedoya, G. 2001. Recent planktonic foraminifera from deep-sea sediments from the Eastern Equatorial Pacific: Proxies of the equatorial front in the late Quaternary. Journal of Marine and Coastal Research 30, 151-176.

- McClain, C. R., Christian, J. R., Signorini, S. R., Lewis, M. R., Asanuma, I., Turk, D., and Doupouy-Douchement, C. 2002. Satellite ocean-color observations of the tropical Pacific Ocean. Deep-Sea Research II 49, 2533-2560.
- Molina-Cruz, A. 1977 .Radiolarian assemblages and their relationships to the oceanography of the subtropical southeastern Pacific. Marine Micropaleontology 2, 315-352.
- Molina-Cruz, A. 1984. Radiolarian as indicators of upwelling processes: the Peruvian connection. Marine Micropaleontology 9, 53-75.
- Mulitza, S., Dürkoop, A., Hale, W., Wefer, G., and Niebler, H. S. 1997. Planktonic foraminifera as recorders of past surface-water stratification. Geology 25(4), 335–338.
- Mulitza, S., Donner, B., Fischer, G., Paul, A, Pätzold, J., Rulemán, C., and Segl, M. 2004. The South Atlantic oxygen-isotope record of planktic foraminifera in: The South Atlantic in the Late Quaternary: Reconstruction of Mass Budget and Current Systems, edited by G. Fischer and G. Wefer, Springer, NY, 121-142 pp.
- Okuda, T., Trejos de Suescun, R., Valencia, M., and Rodríguez, A. 1983. Variación estacional de la posición del Frente Ecuatorial y su efecto sobre la fertilidad de las aguas superficiales ecuatorianas. Acta Oceanográfica del Pacífico INOCAR 2(1), 53-84.
- O'Neil, J. R., Clayton, R. N., and Mayeda, T. K. 1969.Oxygen isotope fractionation in divalent metal carbonates. The Journal of Chemical Physics 51, 5547-5558.
- Owen, R. W., and Zeitzschel, B. 1970. Phytplankton production: Seasonal change in the oceanic eastern tropical Pacific. Marine Biology 7, 32-36.
- Pak, H. and Zaneveld, J. R. V. 1974. Equatorial Front in the Eastern Pacific Ocean. Journal of Physical Oceanography 4, 570-578.
- Pena, L. D., Cacho, I., Ferreti, P. and Hall, M. A. 2008. El Niño-Southern Oscillation –like variability during glacial terminations and interlatitudinal teleconnections. Paleoceanography 23, PA3101, doi: 10.1029/2008PA001620.
- Peña, M. A., Lewis, M. R., and Cullen, J. J. 1994. New production in the warm waters of the tropical Pacific ocean. Journal of Geophysical Research 99(C7), 14225-14268.
- Pennington, J. T., Mahoney, K. L., Kuwahare, V. S., Kolber, D. D., Calienes, R., and Chavez, F. P. 2006. Primary production in the eastern tropical pacific: A review. Progress in Oceanography 69, 285-317.
- Peterson, M. N. A. 1966. Calcite: Rates of dissolution in a vertical profile in the Central Pacific. Science154, 1542-1544.
- Pisias, N. G., and Mix, A. C. 1997. Spatial and temporal oceanographic variability of the eastern equatorial Pacific during the late Pleistocene: Evidence from radiolarian microfossils. Paleoceanography 12(3), 381-393.
- Prell, W. L., and Damuth, J. E. 1978. The climate-related diachronous disappearance of Pulleniatina obliquiloculata in late Quaternary sediments of the Atlantic and Caribbean. Marine Micropaleontology 3, 267-277.
- Ravelo, A. C., and Fairbanks, R. G. 1992. Oxygen isotopic composition of multiple species of planktonic foraminifera: Recorders of the modern photic zone temperature gradient. Paleoceanography 7(6), 815-831.
- Ravelo, A. C., and Fairbanks, R. G. 1995.Carbon isotopic fractionation in multiple species of planktonic foraminifera from core-tops in the tropical Atlantic. Journal of Foraminiferal Research 25, 53-74.
- Raymond, D.J. et al. 2004. EPIC2001 and the coupled ocean-atmosphere system of the tropical East Pacific. American Meteorological Society 85(9), 1341-1354.
- Regenberg, M., Nielsen, S. N., Kuhnt, W., Holbourn, A., Garbe-Schönberg, D., and Andersen, N. 2010. Morphological, geochemical, and ecological differences of the extant menardiform planktonic foraminifera *Globorotalia menardii* and *Globorotalia cultrata*. Marine Micropaleontology 74, 96-107.
- Restrepo, J. D., and Kjerfve, B. 2000. Water discharge and sediment load from the western slopes of the Colombian Andes with focus on Rio San Juan. The Journal of Geology 108, 17-33.
- Rincón-Martínez; D., Lamy, F., Contreras, S., Leduc, G., Bard, E., Saukel, C., Blanz, T., Mackensen, A., and Tiedemann, R. 2010. More humid interglacials in Ecuador during the past 500 kyr linked to latitudinal shifts of the equatorial front and Intertropical Convergence Zone in the eastern equatorial Pacific. Paleoceanography 25, PA2210; doi: 10.1029/2009PA001868.
- Rodríguez-Rubio, E., Schneider, W., and Abarca del Rio, R. 2003. On the seasonal circulation within the panama Bight derived from satellite observations of wind, altimetry and sea surface temperature. Geophysical research Letters 30(7), 1410, doi: 10.1029/2002GL016794.

- Ruddimann, W. F., and Hezeen, B. C. 1967. Differential solution of planktonic foraminifera. Deep-Sea Research 14, 801-808.
- Shakleton, N. J. 1974. Attainment of isotopic equilibrium between ocean water and the benthonic foraminifera genus Uvigerina: Isotopic changes in the ocean during the last glacial in: Les méthodes quantitatives d'étude des variations du climat au cours du Pléistocène. Colloques internationaux du Centre national de la recherche scientifique 219, 203-210.
- Schweitzer, P. N., and Lohmann, G. P. 1991. Ontogeny and habitat of modern menardiiform planktonic foraminifera. Journal of Foraminiferal Research 21(4), 332-336.
- Spero, H. J., and Williams, D. F. 1988. Extracting environmental information from planktonic foraminiferal $\delta^{n}X$ data. Nature 335, 717-719.
- Spero, H. J., Bijma, J, Lea, D. W., and Bemis, B. E. 1997. Effect of seawater carbonate concentration on foraminiferal carbon and oxygen isotopes. Nature 390, 497-500.
- Spero, H. J., Mielke, K. M., Kalve, E. M., Lea, D. W. and Pak, D. K. 2003. Multispecies approach to reconstructing eastern equatorial Pacific thermocline hydrography during the past 360 kyr. Paleoceanography 18 (1), 1002, doi: 10, 1029/2002PA000814.
- Steph, S., Regenberg, M., Mulitza, S., and Nürnberg, D. in press. Stable isotopes of planktonic foraminifera from tropical Atlantic/Caribbean core-tops: Implications for reconstructing upper ocean stratification. Marine Micropaleontology.
- Takahashi, K., and Battisti, D. S. 2006. Processes controlling the mean tropical Pacific precipitation pattern: I. The Andes and the Eastern Pacific ITCZ. Journal of Climate 20(14), 3434–3451.
- Thunell, R. C., Curry, W. B., and Honjo, S. 1983. Seasonal changes in the isotopic composition of planktonic foraminifera collected in Panama Basin sediment traps. Earth and Planetary Science Letters 64, 33-43.
- Thunell, R. C. and Reynolds, L. A. 1984. Sedimentation of planktonic foraminifera: Seasonal changes in species flux in the Panama Basin. Micropaleontology 30, 243-262.
- Thunell, R. C., Keir, R. S. And Honjo, S. 1981. Calcite dissolution: An in situ study in the Panama Basin. Science 212, 659-661.
- Torres, G. 2005. Áreas de mayor productividad biológica (clorofila “a”) en el Pacifico ecuatorial (82°W-92°W) durante 1988-1999 y su relación con los eventos El Niño. Acta Oceanográfica del Pacifico 13.
- Verganud-Grazzini, C. 1976. Non-equilibrium isotopic composition of shells of planktonic foraminifera in the Mediterranean Sea. Palaeogeography, Palaeoclimatology, Palaeoecology, 20, 263-276.
- Wallace, J. M., Mitchell, T. P., and Deser, C. 1989. The influence of sea-surface temperature on surface wind in the Eastern Equatorial Pacific: Seasonal and interannual variability. Journal of Climate 2(12), 1492-1499.
- Wang, B., and Wang, Y. 1999. Dynamics of the ITCZ equatorial tongue complex and causes of the latitudinal climate asymmetry. Journal of Climate 12 (6), 1830-1847.
- Wang, L. 2000. Isotopic signals in two morphotypes of Globigerinoides ruber (white) from the South China Sea: implications for monsoon climate change during the last glacial cycle. Palaeogeography, Palaeoclimatology, Palaeoecology 161, 381–394.
- Watkins, J. M., Mix, A. C., and Wilson, J. 1996. Living planktonic foraminifera: Tracers of circulation and productivity regimes in the central equatorial Pacific. Deep-Sea Research 43(4-6), 1257-1282.
- Weber, M. E., Wiedicke, M., and Riech, V. 1995. Carbonate preservation history in the Peru Basin: Paleoceanographic implications. Paleoceanography 10(4), 775-800.
- Wefer, G., Dunbar, R. B., and Suess, E. 1983. Stable isotopes of foraminifers off Peru recording high fertility and changes in upwelling history. In: Thiede, J. and Suess, E. Coastal Upwelling Its sedimentary record. Part B: Sedimentary records of ancient coastal upwelling. Plenum Press, NY. 295-308.
- Wyrtki, K. 1964. The thermal structure of the eastern Pacific Ocean. Deutschen Hydrographischen Zeitschrift, Ergaenzungsheft A6, 84.
- Wyrtki, K. 1966. Oceanography of the eastern equatorial Pacific Ocean. Oceanography and marine Biology Annual Review.

CHAPTER 5

MORE HUMID INTERGLACIALS IN ECUADOR DURING THE PAST 500 KYR LINKED TO LATITUDINAL SHIFTS OF THE EQUATORIAL FRONT AND THE INTERTROPICAL CONVERGENCE ZONE IN THE EASTERN TROPICAL PACIFIC.

Daniel Rincón-Martínez[1*], Frank Lamy[1], Sergio Contreras[2], Guillaume Leduc[3], Eduard Bard[4], Cornelia Saukel[1], Thomas Blanz[3], Andreas Mackensen[1], and Ralf Tiedemann[1]

Published with moderate comments in *Paleoceanography*
(Paleoceanography, 25, PA2210, doi:10.1029/2009PA001868, 2010)

[1] Alfred-Wegener Institute for Polar and Marine Research, D-27568 Bremerhaven, Germany

[2] Max Planck Institute for Marine Microbiology, Celsiusstrasse 1, D-28359 Bremen, Germany

[3] Institut für Geowissenschaften, Christian Albrecht Universität, 24118 Kiel, Germany

[4] CEREGE, Aix-Marseille Université, CNRS, Collège de France, IRD, Europôle Méditerranéen de L'Arbois, BP 80, 13545 Aix en Provence

*Corresponding Author e-mail: (daniel.rincon.martinez@awi.de), phone: +49(471)/4831-1572; fax: +49(471)/4831-1923

Keywords: Eastern equatorial Pacific, terrigenous input, la Niña-like, el Niño-like, glacial, interglacial.

Abstract

Studying past changes in the eastern equatorial Pacific (EEP) ocean dynamics and their impact on precipitation on land gives us insight into how the Intertropical Convergence Zone (ITCZ) movements and the El Niño/Southern Oscillation (ENSO) modulate regional and global climate. In this study we present a multi-proxy record of terrigenous input from marine sediments collected off the Ecuadorian coast spanning the last 500 ka. In parallel we estimate sea surface temperatures (SST) derived from alkenone paleothermometry for the sediments off the Ecuadorian coast and complement them with alkenone-based SST data from the Panama Basin to the north, in order to investigate SST gradients across the Equatorial Front (EF). Near the equator, today´s river runoff today is tightly linked to SST, reaching its maximum either during the Austral summer when the ITCZ migrates southward or during El Niño events. Our multi-proxy reconstruction of riverine runoff indicates that interglacial periods experienced more humid conditions than the glacial periods. The North-South SST gradient is systematically steeper during glacial times, suggesting a mean background climatic state with a vigorous oceanic cold tongue, resembling modern La Niña conditions. This enhanced North South SST gradient would also imply a glacial northward shift of the Intertropical Convergence Zone (ITCZ) at least in vicinity of the cold tongue - a pattern that has not yet been reproduced in climate models.

5.1. Introduction

Today, the average state of the EEP is characterized by a pronounced north-to-south SST gradient, with warm and stratified waters remaining north of the equator (Eastern Pacific Warm Pool, EPWP), while a cold tongue, associated with equatorial upwelling and advection of cold waters from the Peru Current, is located south of the equator. On inter-annual to decadal timescales these conditions are significantly modified through atmosphere-ocean changes related to ENSO dynamics. During the warm (El Niño) phase of ENSO, warm waters spread eastward from the western Pacific warm pool and SSTs in the cold tongue substantially warm. Conversely, during the cold (La Niña) phase, the cold tongue strengthens and the cross-equatorial SST gradient in the EEP is substantially larger (E.g. McPhaden et al., 2006; Wang and Fiedler, 2006).

Long-term ENSO changes on millennial, orbital, or even tectonic time-scales throughout the Plio-Pleistocene and their role for global climate have been intensively discussed (E.g. Markgraf and Diaz, 2000;Cane, 2004;Fedorov et al., 2006). On glacial-interglacial timescales, some authors suggest that the average glacial state of the EEP was more similar to that occurring during modern El Niño years (E.g. Koutavas et al., 2002; Koutavas and Lynch-Stieglitz, 2003), while others consider a mean glacial state similar to the cold La Niña phase (E.g. Andreasen and Ravelo, 1997; Andreasen et al., 2001; Martínez et al., 2003). Low-latitude orbital forcing has been suggested to exert control on the mean state of ENSO as well (Clement et al., 1999; Pena et al., 2008). Other authors again link SST changes in the EEP to high-latitude climate variability in the Southern Hemisphere without invoking ENSO changes (E.g. Pisias and Mix, 1997; Lea et al., 2000; Feldberg and Mix, 2003; Spero et al., 2003; Lea et al., 2006).

Hence the scenarios drawn from these studies are diverse. Most studies focus on paleoceanographic features such as SST, paleoproductivity, or water stratification, whereas continental climate changes are rarely considered (E.g. Pahnke et al., 2007). Yet, modern atmosphere-ocean reorganizations related to ENSO strongly impact onshore precipitation, particularly in northern Peru and coastal Ecuador. During El Niño phases, unusually warm EEP waters promote convection of the overlying atmosphere, while the ITCZ and associated

precipitation anomalies shift further south than during the regular seasonal cycle (E.g. Horel and Cornejo-Garrido, 1986; Bendix, 2000; Bendix and Bendix, 2006).

Here, we present a combined analysis of proxy data that allude to paleoceanographic changes in the EEP and concomitant continental paleoclimate variations onshore during the past 500 kyr. The proxy profiles are derived from samples obtained from sediment cores off the coast of Ecuador and in the Panama Basin. A systematic pattern of changes in the terrigenous sediment input during glacial-interglacial periods can be linked to tropical rainfall changes over coastal Ecuador. These glacial-interglacial rainfall changes are paralleled by latitudinal shifts of the EF moving southward during interglacials as is indicated by higher SST, enhanced surface water stratification, higher abundances of the foraminifera species *Globorotalia cultrata* relative to *Neogloboquadrina dutertrei*, and increases in mangrove biomarker accumulation rates. A comparison of our SST record with the EPWP SST record from Site MD02-2529 covering the past ~300 kyr indicates that fluctuations in the latitudinal SST gradients during glacial-interglacial periods across the EF in the EEP played a pivotal role in past precipitation changes in the region.

5.2. Modern climatology and oceanography at study sites

Our study is based on two sites in the EEP (Figure 5.1), the first of which is Ocean Drilling Program (ODP) Site 1239 (0°40.32´S, 82°4.86´W, 1414 m water depth) located at the northern margin of the eastern Pacific cold tongue close to the EF and ~120 km off the Ecuadorian coast. The area is characterized by a thermocline shoaling and local wind-driven upwelling that supplies nutrient-rich waters from the Equatorial Undercurrent (EUC) to the surface, creating high standing stocks of phytoplankton and enhanced primary productivity rates (Lukas, 1986; Fiedler et al., 1991; Pennington et al., 2006). The second site, MD02-2529 (08°12.33'N; 84°07.32'W; 1619 m water depth), is situated close to the Costa Rica margin of the Panama Basin within the EPWP, where SST are above 27°C and sea surface salinities are below 33.2 p.s.u throughout the year (Leduc et al., 2007).

5.2.1. EEP Oceanography

A striking feature of the west coast of South America is the presence of unusually cool, and highly saline (T<25°C, S>34 p.s.u) surface waters extending westwards slightly south of the equator. This cold tongue is fed by seasonal advection of cold waters from the Peru Current (PC) and by equatorial upwelling (Pak and Zaneveld, 1974; Fiedler and Talley, 2006). The cold tongue is bounded by the EF, a narrow band located around the equator between the Peruvian coast and the Galapagos Islands (Figure 5.1). North of the EF, warm, low-salinity waters (T<25°C, S>34 p.s.u) of the Panama Basin occur due to a large net heat flux, weak wind mixing and intense rainfall beneath the ITCZ (Pak and Zaneveld, 1974; Fiedler and Talley, 2006).

The cold tongue and associated frontal zone are persistent features but their strength varies both seasonally and inter-annually. During Austral winter, solar heating reinforces the meridional SST gradient, strengthening the southeasterly trade winds and the equatorial cold tongue, and shifting the EF to its northernmost position. From January to April, SST increases south of the Equator due to the subsidence of the southeast trades, resulting in a diffused southern position of the EF (E.g. Pak and Zaneveld, 1974; Raymond et al., 2004; de Szoecke et al., 2007). The quasi-periodic El Niño/Southern Oscillation (ENSO) dominates the inter-annual variability in this region. The El Niño warm phase is related to anomalous eastward advection of warm water in the eastern Pacific cold tongue, associated with a weaker EF (E.g. Pak and Zaneveld, 1974; Kessler, 2006; McPhaden et al., 2006; Wang and Fiedler, 2006). At this time, variations in the water transports of the South Equatorial Current (SEC) and Equatorial

Undercurrent (EU) induce a deepening of the thermocline, causing positive SST anomalies (Kessler, 2006). The opposite conditions occur during the cool La Niña phase.

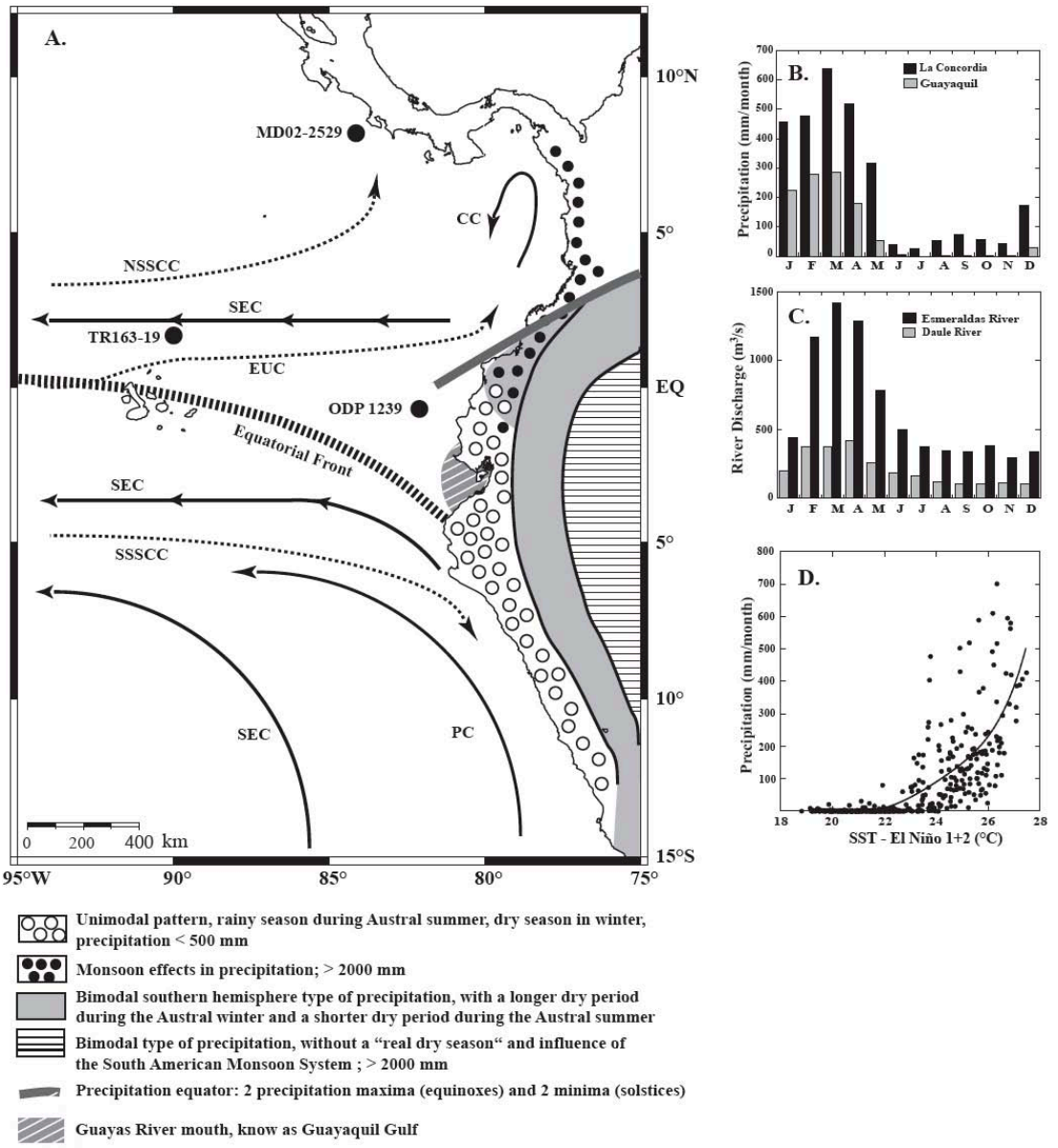

Figure 5. 1. (A) Schematic (sub)surface circulation in the Eastern equatorial Pacific (modified after Kessler, 2006). Locations of ODP Sites 1239, TR163-19, Site MD02-2529, and the Guayas and Esmeraldas river mouths; as are precipitation patterns over northern South America (modified after Bendix and Lauer, 1992). Upper-layer currents (black arrows) are the SEC: South Equatorial Current; CC: Colombia Current and PC: Peru or Humboldt Current. Subsurface currents (dashed arrows) are N/SSCC: Northern/Southern Subsurface Countercurrents; PUC: Peru-Chile Undercurrent; and EUC: Equatorial Undercurrent. **(B)** Mean monthly precipitation at Guayaquil (2.20°S, 79.90°W, 6 m.a.s.l; Guayas Basin) and La Concordia (0.1°N, 79.30°W, 300 m.a.s.l; Esmeraldas Basin) meteorological stations. **(C)** Mean monthly fluvial discharge of the Daule River (1.69°S, 79.99°W, 20 m.a.s.l; at La Capilla hydrological station), one of the main tributaries of the Guayas River, and the Esmeraldas River (0.52°N, 79.41°W, 50 m.a.s.l; at Esmeraldas hydrological station). **(D)** Polynomial fit between monthly SST at El Niño 1+2 region (0-10°South; 90°-80°West) and monthly precipitation at Guayaquil meteorological station. SST data are generated from the World Ocean Atlas database (Conkright et al., 2002), precipitation (Peterson and Russell, 1997) and river discharges from R-HydroNET (Vörösmarty et al., 1998, available at http://www.r-hydronet.sr.unh.edu/).

5.2.2. EEP atmospheric circulation

The EEP atmospheric convection and its associated continental precipitation are mostly linked

to the ITCZ and occur preferentially over the EPWP waters. This pattern is maintained most of the year by several positive feedbacks. First, the temperature asymmetry along the equator reinforces surface winds over the cold tongue, which further cools the water through evaporation and upwelling (E.g. Xie and Philander, 1994; Xie, 2004). Secondly, the combination of cold surface waters with warm, dry air aloft, results in large and persistent subtropical stratocumulus decks, which reflect much of the incoming solar radiation, and help to maintain the cool SST of the "cold tongue" (E.g. Klein and Hartmann, 1993; Raymond et al., 2004). In addition, the northwest-southeast orientation of the coastline of South America combined with the topographic barrier of the Andes constrain winds to blow along the Peruvian coastline and induce coastal upwelling there (E.g. Philander et al., 1996; Xie, 2004).

During late Austral summer, the north to south SST contrast is relaxed, the EF is weakest, and the ITCZ and associated precipitation migrate southward along the Colombian and Ecuadorian coasts (E.g. Horel and Cornejo-Garrido, 1986; Bendix and Lauer, 1992; Hastenrath, 2002; Amador et al., 2006; Poveda et al., 2006). Conversely, a northward displacement of the ITCZ occurs during late Austral winter, when the cold tongue is intensified and the advection of the Peru-Chile current is strongest (E.g. Hastenrath, 2002; Amador et al., 2006; Poveda et al., 2006; de Szoecke et al., 2007).

During an El Niño event the trade winds weaken along the equator, as atmospheric pressure rises in the western Pacific and falls in the eastern Pacific, and permit an eastward expansion of warm waters from the Central Pacific (McPhaden et al., 2006; Wang and Fiedler, 2006). This phenomenon acts to weaken the Humboldt Current and the equatorial and coastal upwelling systems. Atmospheric convection cells and the associated precipitation of the ITCZ shift to the south causing heavy rainfall over the northern Peruvian desert and coastal Ecuador (E.g. Horel and Cornejo-Garrido, 1986; Neill and Jørgensen, 1999; Hastenrath, 2002; Waylen and Poveda, 2002; Poveda et al., 2006).

5.2.3. The Guayas and Esmeraldas drainage systems, precipitation and fluvial runoff.

The Guayas and the Esmeraldas basins are the largest drainage systems in western Ecuador, both in terms of area (32,674 km^2 and 21,418 km^2, respectively) and water volume drained per area unit. Annual precipitation and river discharges in both basins, including the Coastal Mountain Range and the western slopes of the Andes at altitudes <1800 m.a.s.l, experience a uni-modal pattern, that is characterized by a rainy season from December to April. Precipitation and river runoff maxima occur in March and broadly coincide with the southernmost seasonal excursion of the ITCZ in the EEP, and with the seasonal SST maximum at ODP Site 1239 (Figures 5.1b-d). The rest of the year, precipitation is limited by the combined effects of low SST, atmospheric subsidence of dry air and reduced insolation due to persistent low-level stratus decks (E.g. Horel and Cornejo-Garrido, 1986; Bendix and Lauer, 1992).

Heavy precipitation and severe floods also affect the coastal area of Ecuador during El Niño events, with rainfall differences between normal years and El Niño events as large as 200% for Guayaquil (Guayas Basin). Extensive precipitation during El Niño years occurs during the normal rainy season, when the Hadley circulation is increased and the ITCZ displaced southwards due to the strong warming of the Niño 1+2 region (0-10°South; 90°-80°West; Figure 5.1d) (E.g. Rossel et al., 2006; Bendix and Bendix, 2006).

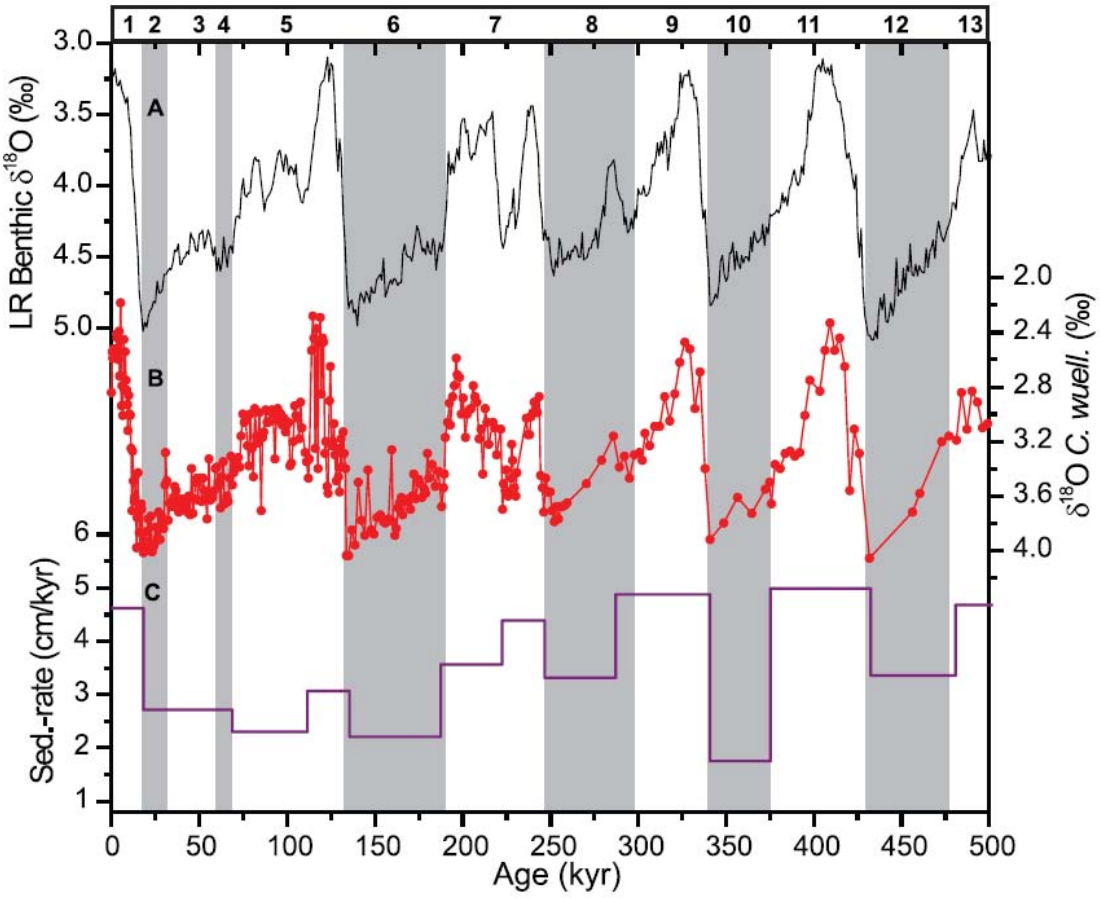

Figure 5. 2 Oxygen isotope stratigraphy for the ODP Site 1239. **(A)** Benthic oxygen isotope stack (Lisiecki and Raymo, 2005). **(B)** $\delta^{18}O$ ($^{o}/_{oo}$) record of the benthic foraminifera *Cibicidoides wuellerstorfi* from ODP Site 1239. **(C)** Linear sedimentation rates (cm/kyr) of the uppermost ~17.4 m (past ~500 kyr) from ODP Site 1239. Shading highlights glacial marine isotopic stages (MIS).

5.3. Methods

5.3.1. Stratigraphic framework (ODP Site 1239/MD02-2529)

Sampling of Site 1239 followed the meters composite depth (mcd) scale that was developed for the multiple offset cores (Shipboard Scientific Party, 2003). The age model of the uppermost ~17.4 m, representing the past ~500 kyr, is based on oxygen isotope stratigraphy. We correlated the $\delta^{18}O$ record of the benthic foraminifera *Cibicidoides wuellerstorfi* to the chronology of the LR04 stack (Lisiecki and Raymo, 2005) using the Analyseries software (Paillard et al., 1996) (Figure 5.2). Sedimentation rates range from ~2 cm/kyr to ~5 cm/kyr, with higher values occurring during interglacials (Figure 5.2). Stratigraphy at site MD02-2529 over the past three climatic cycles is based on the benthic $\delta^{18}O$ record performed on *C. wuellerstorfi*, and on a previously published chronostratigraphy for the last 90 ka (Leduc et al., 2007).

5.3.2. Paleoceanographic Proxies

5.3.2.1 Foraminifera Oxygen Isotopes

We measured the stable oxygen isotope composition of the epibenthic foraminifer *Cibicidoides wuellerstorfi*, as well as of two planktonic foraminiferal species, the surface dweller *Globigerinoides ruber* and the deep-dwelling *Globorotalia tumida*. Approximately 4 individuals of *C. wullerstorfi* and 10 individuals of each planktonic species were selected from the 315-355

µm and 355-400 µm fractions, respectively. $\delta^{18}O$ measurements were performed on a FINNIGAN 253 MS with a Kiel CARBO device at the Alfred-Wegener-Institute Bremerhaven (Germany) with an analytical reproducibility of ~0.08$^{o}/_{oo}$ for $\delta^{18}O$. The oxygen isotope composition values were calibrated using the NBS-19 (National Bureau of Standards) standard and are reported relative to the IAEA Vienna Pee Dee Belemnite (VPDB) Standard. The resolution of sampling was defined on the basis of a preliminary age model from biostratigraphy in order to obtain intervals of 1000 years or less for benthic foraminifera and of 3000 yrs for planktonic foraminifera. The $\delta^{18}O$ difference between *G. ruber* ss - *G. tumida* is used as a proxy for water column thermal stratification (Rincón-Martínez et al., 2011).

5.3.2.2 Alkenones

Alkenones are a series of long-chain (C_{37}, C_{38}, C_{39}) unsaturated methyl and ethyl ketones synthesized mainly by *Emiliania huxleyi* and some other species of the class *Prymnesiophyceae* that live in the uppermost meters of the euphotic zone. To obtain the total lipid extract, freeze-dried sediments (~1 g) from ODP Site 1239 were solvent extracted with 25 ml dichloromethane (DCM) at 75°C at a pressure of 80 bar on an accelerated solvent extractor (Dionex ASE 200) at the Christian Albrecht University of Kiel. An internal standard (cholestane [$C_{27}H_{48}$] and hexatriacontane [$C_{36}H_{74}$]) was added and used to quantify organic compounds. Aliquots (1-5 %) of the total lipid fractions were separated using a double column multidimensional gas chromatograph with two Agilent 6890 gas chromatographs for $C_{37:2}$ and $C_{37:3}$ alkenones identification and quantification. The procedure used at CEREGE (Aix-Marseille Université) to extract and quantify $C_{37:2}$ and $C_{37:3}$ alkenones from MD02-2529 is fully described in Sonzogni et al. (1997) and Pailler and Bard (2002). Alkenone-derived temperatures from MD02-2529 for the last 90 kyr have been previously published and discussed by Leduc et al. (2007). The alkenones unsaturation index ($U_{37}^{K'}$) was calculated with the peak areas of the di- and triunsaturated C_{37} methyl alkenones using the ratio $(C_{37:2})/(C_{37:2} + C_{37:3})$. To reconstruct the SST, we used the alkenones unsaturation and the global calibration derived by Müller et al. (1998):

$$UK'_{37} = <0.033 * SST> + 0.044$$

5.3.2.3 Foraminiferal assemblage ($R_{c/d}$)

The abundance ratio between *Globorotalia menardii cultrata* and *Neogloboquadrina dutertrei* (right coiling) has been used as an index for the influence of the Panama–Costa Rica Dome and the cold tongue upwelling systems, and therefore is of value for locating the EF in the EEP (E.g. Martinez and Bedoya, 2001; Martinez et al., 2006; Rincón-Martínez et al., 2011). In this study, we counted >300 specimens from the 355-400 µm size fraction, and the ratios were calculated according to Rincón-Martínez et al., (2011):

$$R_{c/d} = \text{No. specimens of G.cultrata} / (\text{No. specimens G.cultrata} + \text{N.dutertrei})$$

5.3.3. Terrigenous Sediment input

5.3.3.1 Siliciclastic content

The lithogenic record for ODP 1239 represents the residual sediment percentage obtained after subtraction of carbonate, opal and organic matter:

$$\text{Siliciclastic (wt\%)} = 100 - \%CaCO_3 - \%\text{Biogenic opal} - \%\text{TOC}$$

The determination of total organic carbon (TOC) was performed with the LECO technique (Leco Carbon-Sulfur Analyzer CS-125) and previous dissolution of the calcium carbonates by adding 1M solution of HCL to the dry sediment. Total carbon (TC) and nitrogen (TN) were measured on the same TOC samples, using a CNS elemental analyzer (Elementar Vario EL III). The carbonate content (wt %) was determined by the difference between TC and TOC:

$$CaCO_3\ (wt\%) = (\%TC - \%\ TOC) * 8.33$$

The concentration of biogenic silica (wt %) was quantified by using the automated leaching method according to Müller and Schneider (1993). Biogenic opal was extracted from dry bulk sediment by using sodium hydroxide at ~85°C for ~45 min. The leaching solution was continuously analyzed for dissolved silicon by molybdenum-blue spectrophotometry. The deMaster´s (1981) mineral correction was consequently applied.

5.3.3.2 X-Ray Fluorescence (XRF) Scanning and ICP-OES Elemental Concentrations

Elemental concentrations (unit = total elemental counts) were measured using an Avaatech^{TM} XRF Core Scanner (AWI-Bremerhaven), a non-destructive measuring technique that allows rapid semiquantitative geochemical analysis of split sediment cores (Richter et al., 2006). Sampling intervals ranged from 1 to 5 cm, resulting in a time-resolution of 200 and 400 years for the upper ~350 kyr of the XRF records and 1000 to 1500 years for the oldest part. Iron (Fe) and titanium (Ti) XRF counts were calibrated to absolute elemental concentration by using Inductively Coupled Plasma - Optical Emission Spectrometry (ICP-OES). Previous to analysis all samples were freeze-dried and 34 discrete sediment samples were digested using HF (23M), HNO_3 (15M) and HCl (12M). Measurements were carried out in a TJA-IRIS-Intrepid spectrometer at the geochemistry laboratories of the AWI and the results were used to convert XRF counts to element concentrations in mg/g of sediment by means of linear regressions (r^2=0.83 n=32 for Fe; and r^2=0.63 n=33 for Ti).

5.3.3.3 Taraxerol

Taraxerol has been reported to dominate the free and bound lipid composition inside *Rhizophora mangle* leaves and has been used to track past changes in mangrove ecosystems (E.g. Versteegh et al., 2004; Grosjean et al., 2007). Total lipid extracts (see section 3.2.2) were methylated with diazomethane and silylated with N, O-bis(trimethylsilyl) trifluoroacetamide in pyridine and then analyzed by GC-MS (Trace GC-MS; Thermo Finnigan) at the Max Planck Institute for Marine Microbiology in Bremen. The relative abundance of taraxerol was estimated by peak integration in the mass chromatograms using a characteristic m/z value of 204 (E.g. Killops and Frewin, 1994; Versteegh et al., 2004).

5.3.3.4 Mass Accumulation Rates

Linear sedimentation rates (LSR; cm kyr^{-1}) and mass accumulation rates (AR) are derived from the calculated ages of individual samples along with the high resolution corrected bulk density (HROM; g cm^{-3}) based on bore-hole logging at Site 1239 (Shipboard Scientific Party, 2003):

$$AR_{component} = \text{Concentration component} * LSR * HROM;$$

where AR is in ng cm^{-2} kyr^{-1}for the Taraxerol, mg cm^{-2} kyr^{-1} for iron, titanium; and g cm^{-2} kyr^{-1} for the bulk siliciclastic fraction.

5.4. Results and discussion

5.4.1. Terrigenous Sediment Supply to the ODP Site 1239

Terrigenous sedimentation supply at Site 1239 (Figure 5.3) is reconstructed from three independent proxy data sets: (1) AR of siliciclastic material, (2) high-resolution XRF core scanning (Fe, Ti), and (3) lipid biomarker taraxerol, indicative of the supply of plant debris from mangroves at the Ecuadorian coast.

The terrigenous records at Site 1239 exhibit a consistent glacial/interglacial pattern over the past 500 kyr (Figures 5.3 and 5.4f). Sediments are predominantly terrigenous during interglacials, with siliciclastic contents generally above 50% and reaching maximum values of up to 80% during marine isotope stage seven (MIS 7) (Figure 5.3b). Glacial siliciclastic contents are substantially lower, within the range of 20 to 40% with lowest values during MIS 2 and MIS 12. As siliciclastic contents may be substantially affected by productivity changes and carbonate dissolution, we calculated siliciclastic AR (Figure 5.3c) as a more reliable proxy for terrigenous supply changes. In line with higher sedimentation rates during interglacials (Figure 5.2c), the siliciclastic AR record reveals pronounced interglacial maxima with values 3 to 5 times higher than that found during glacials. Highest ARs are found in MIS 7 and MIS 11, whereas MIS 5 values are relatively low, and minimum ARs occur in MIS 10. Similar results are recorded in Fe and Ti AR records (Figures 5.3d-g). The strong similarity between the Fe and Ti records suggests that diagenetic alteration potentially affecting Fe has not been a critical factor at Site 1239. Moreover, when log ratios of Fe and Ti over calcium (Ca) are computed to account for dilution by carbonates and non-linearities between XRF counts and elemental concentrations (Weltje and Tjallingii, 2008), the first-order sign of changes in terrigenous supply on glacial-interglacial timescales remains unchanged (data not shown). Low AR of terrigenous components during MIS 5 indicates variable glacial/interglacial amplitudes in terrigenous supply to Site 1239. However, total siliciclastic, Fe, and Ti contents during MIS 5 are similar to other interglacials (Figures 5.3b, d, f) and the low siliciclastic AR during MIS 5 are solely the result of low sedimentation rate.

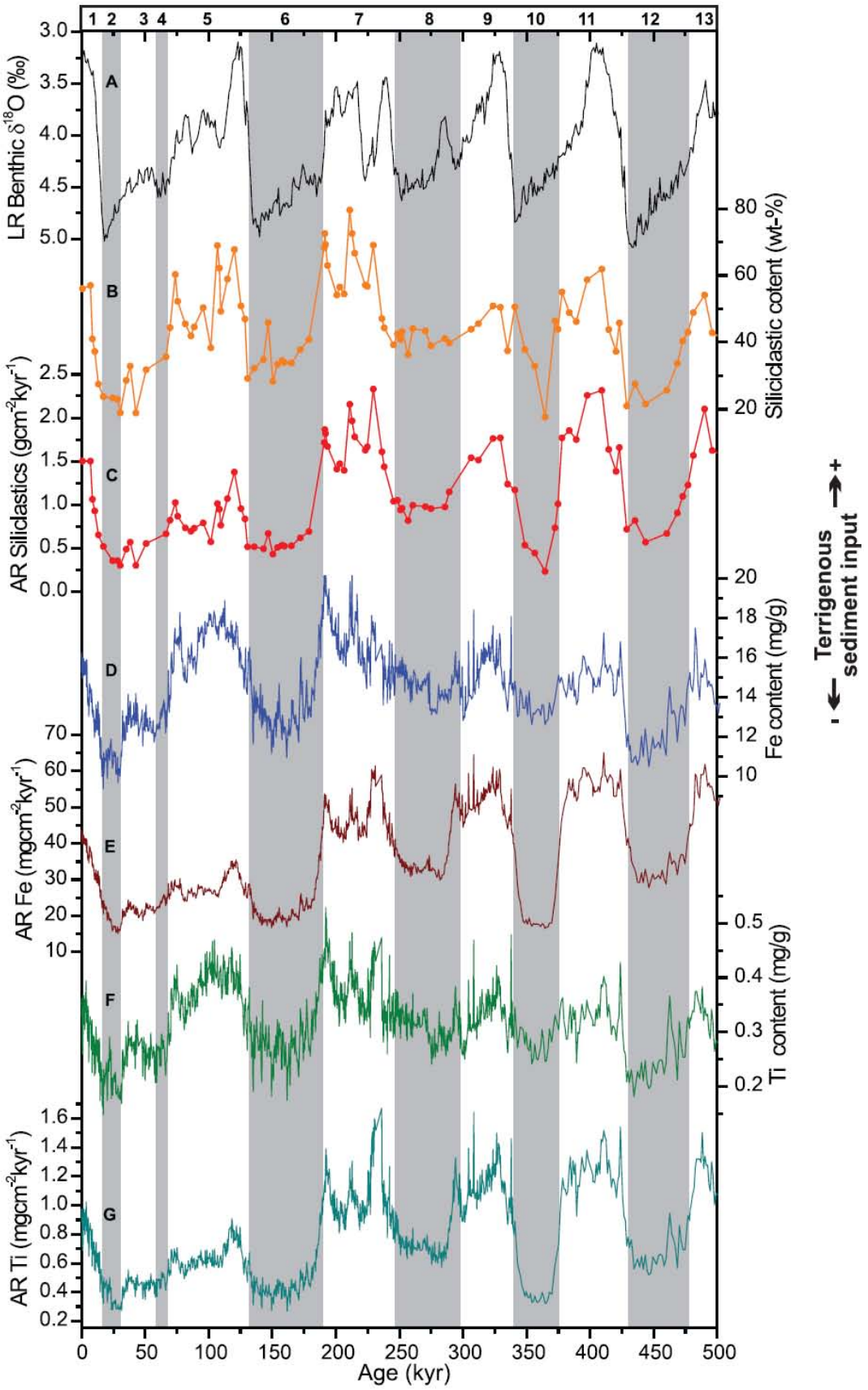

Figure 5. 3. Records of changes in terrigenous sediment input to ODP Site 1239 over the last 500 kyr. **(A)** Benthic oxygen isotope stacks (Lisiecki and Raymo, 2005) for stratigraphic reference. **(B)** Content (wt %) and **(C)** accumulation rates (AR, g/cm^2 kyr) of siliciclastics. **(D)** Iron contents (mg/g). **(F)** Titanium contents (mg/g). **(E)** Iron AR (mg/cm^2 kyr). **(G)** Titanium AR (mg/cm^2 kyr).

Glacial-interglacial siliciclastic AR variations at Site 1239 are unlikely due to post-depositional processes such as horizontal focusing or winnowing. According to Lyle et al. (1995) sediment focusing preferentially increases from elevated regions to the deeper parts of the basins and in the Panama and Peru Basins the bulk sediment burial match surface water patterns. Moreover, the observed glacial-interglacial pattern in local sediment supply to ODP Site 1239 demonstrates that continental rainfall rather than glacio-eustatic sea level variations were the main factor controlling the basin-ward terrestrial transport off Ecuador. For example, during glacial times, when the global sea-level was at low-stand, one would expect an ocean-ward migration of fluvial depo-centers and widespread fluvial incision of the subaerially exposed continental shelf producing increased siliciclastic AR at ODP Site 1239. In contrast, our records show higher concentrations and AR of terrigenous material during interglacials that over-compensated any potential sea-level influence on fluvial sediment supply.

High terrigenous ARs during interglacial also contradict the concept that, in the equatorial Pacific, transport of terrigenous material was increased during glacial periods (Anderson et al., 2006; McGee et al., 2007; Winckler et al., 2008). We attribute the contrasting results to the fact that far from shore, the terrigenous component of deep-sea sediments consists of eolian dust, and that these fluxes were generally greater during glacial periods than during interglacials (Mahowald et al., 1999; Kohfeld and Harrison, 2001). Hence, the rather near-shore location of Site 1239 suggests that fluvial input from the Guayas and/or Esmeraldas drainage systems were increased during interglacial periods relative to glacial periods.

Our third proxy for terrigenous input is taraxerol AR, which was used as a proxy for sedimentation of mangrove leaf remains (*Rhizophora*) that were washed offshore by riverine runoff (Versteegh et al., 2004; Grosjean et al., 2007). The *Rhizophora* genus is the dominant mangrove along the Colombian and Ecuadorian coast and its distribution is associated with the presence of warm waters and humid coastal conditions north of the EF (E.g. Heusser and Shackleton, 1994; Neill, 1999). Compared to glacials, taraxerol ARs are higher during the Holocene and MIS 5 and reach extremely high values during MIS 7 (Figure 5.4f). These higher interglacial ARs are consistent with our interpretation of predominantly fluvial terrigenous input induced by enhanced tropical rainfall. However, the supply of mangrove material may also be affected by sea-level changes. For instance, in the nearby Angola Bight, Kim et al. (2005) showed that high taraxerol contents during Terminations I and II were controlled by global sea-level rise resulting in strong shelf erosion supplying pre-existing deposits of mangrove material. Additional support for deglacial sea-level control on EEP mangrove input into marine sediments comes from pollen analyses (E.g. Heusser and Shackleton, 1994; Gonzalez et al., 2006) and Mn/Ca of planktonic foraminifera (E.g. Klinkhammer et al., 2009), which display maxima in mangrove pollen and dissolved terrestrial input to coastal surface waters during the last deglaciation. Our record shows early maxima in taraxerol AR during Terminations I, II, and particularly III (Figure 5.4f), while taraxerol levels remain high during the whole interglacial periods. Hence we suggest that increased taraxerol sedimentary fluxes during interglacials are driven to some extent by increased riverine runoff.

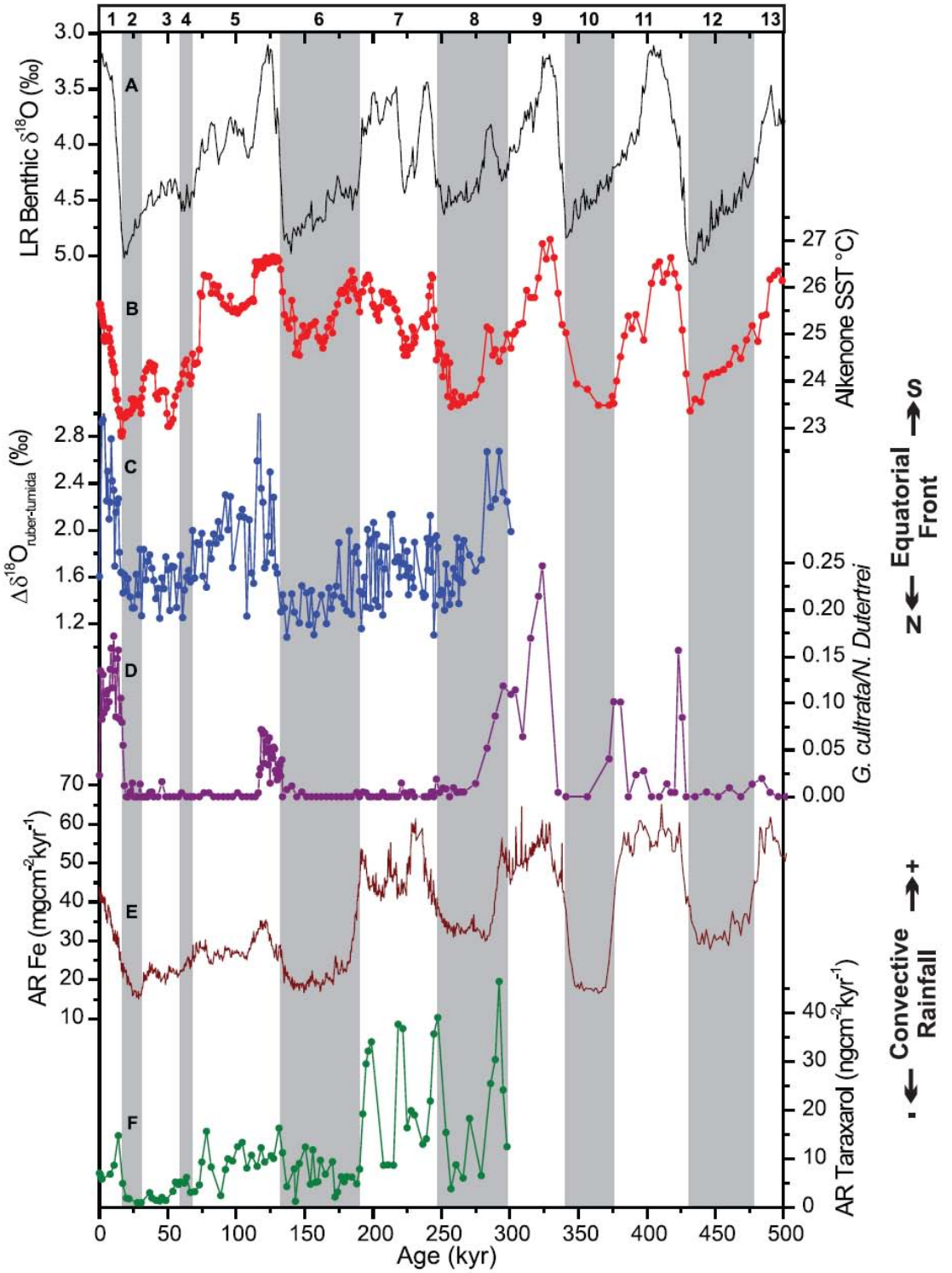

Figure 5. 4. EEP paleoceanographic changes as reconstructed at ODP Site 1239. **(A)** Benthic oxygen isotope stack (Lisiecki and Raymo, 2005) for stratigraphic reference. **(B)** Alkenone sea surface temperature (SST) record. **(C)** $\Delta\delta^{18}O$ between *Globorotalia tumida* and *Globigerinoides ruber*. High values are indicative of strongly stratified waters north of the equatorial front. **(D)** Abundance ratio ($R_{c/d}$) between planktonic foraminifera *Globorotalia cultrata* and *Neogloboquadrina dutertrei*. High values are indicative of warm waters north of the equatorial front. **(E)** Iron AR (mg/cm^2 kyr). **(F)** Taraxerol AR (ng/cm^2 kyr). High values are interpreted as enhanced fluvial runoff as a result of increased continental rainfall.

5.4.2. SST, EF latitudinal position and their relationship to continental precipitation

Global compilations of SST estimations from modern sediments indicate that alkenones unsaturation, $U_{37}^{K'}$, is almost linearly related to annual mean SST from 0-10 m water depth (E.g. Müller et al., 1998; Conte et al., 2006; Prahl et al., 2006). $U_{37}^{K'}$ Sensitivity to temperature has been assessed in laboratory cultures (Prahl and Wakeham, 1987), and second-order mechanisms such as salinity, and alkenones synthesized by thermocline-dwelling coccolithophorids or diagenetic alterations are known to play a minor role on the alkenone-SST signal (see review by Conte et al., 2006). It is unclear, however, why alkenones that are produced during an often discrete and short period of the annual cycle, are representative of annual mean SST (E.g. Prahl et al., 2000).

Alkenone-derived SST at Site 1239 reveals pronounced glacial/interglacial cycles, with temperatures ranging from ~22.8°C during MIS 2 to ~27°C during MIS 9 (Figure 5.4b). We find SST amplitudes of up to 3.5°C for the oldest glacial-interglacial cycles (MIS 8-13), ~2.5°C for the MIS 8-7 transition, only ~2°C for Termination II (MIS 6-5), and again higher amplitudes of ~3°C for Termination I (MIS 2-1). The magnitude of the deglacial SST increase during Termination I is consistent with previous studies conducted in the eastern tropical Pacific that used Mg/Ca ratios and faunal assemblages (E.g. Lea et al., 2000; Pena et al., 2008; MARGO Project, 2009). Glacial-interglacial SST amplitudes in other $U_{37}^{K'}$ estimations from the region are, however, somewhat lower (~1 to ~2°C) (Horikaga et al., 2006; Pahnke et al., 2007;Koutavas and Sachs, 2008; Dubois et al., in press). SST at Site MD02-2529 range from minima of ~25°C during MIS 2 and 8 to maxima of ~28°C during the Holocene (Figure 5.5b). Glacial-interglacial SST amplitudes are generally smaller than at Site 1239, on the order of 2°C for Termination I (MIS 2-1) and III (MIS 8-7) and less than 1°C for Termination II (MIS 6-5).

Comparison of the global benthic $\delta^{18}O$ record (LR04-stack) with the Site 1239 SST estimates reveals several interesting features: (1) an early warming is recorded prior to Terminations I, III and IV, (2) SSTs during MIS 6 are warmer than those recorded during the other glacial periods, (3) an abrupt cooling occurs during early MIS 3 and is followed by a warming of the same magnitude at the end of MIS 3, and (4) SST estimates recorded during the Holocene reveal ~1°C lower SST by ~1°C when compared to other interglacial periods (Figure 5.4b). The early warming during the glacial Terminations is also observed in other tropical records (review by Schneider et al., 1999) and has been suggested to be linked with low-latitude insolation forcing. Elevated glacial SSTs during MIS 6 are also found at Site MD02-2529 (Figure 5.5b), in the eastern Pacific cold tongue (E.g. Calvo et al., 2001) and in many other Indian and Atlantic equatorial records (review by Schneider et al., 1999). In contrast, EEP $\delta^{18}O$ and Mg/Ca records of planktonic foraminifera suggest a colder MIS 6 in comparison with alkenone-based SSTs, with a cooling of similar magnitude to those found on the preceding and following glacial periods (E.g. Lea et al., 2000; Pena et al., 2008).

Given the importance of tropical SST patterns in determining present-day Ecuadorian rainfall formation and associated fluvial discharges (E.g. Rossel et al., 1996; Bendix and Bendix, 2006) (Figures 5.1b-d), past SST changes offshore Ecuador likely impacted the terrigenous material fluxes at ODP Site 1239. Based on this modern SST-rainfall correlation (Figure 5.1d), the range of glacial-interglacial SSTs plausibly resulted in substantial precipitation changes in coastal Ecuador (I.e. more than doubling of rainfall for the glacial-interglacial increase from 23.5°C to 26.5°C). Thus, we infer that higher accumulation of lithogenic sediments at Site 1239 generally reflects higher fluvial input and a wetter Ecuadorian coast, most likely coupled to warmer SSTs in combination with southward shifts of the EF-ITCZ system as observed today during austral

summer or during El Niño years. Lower lithogenic accumulations during glacial periods indicate decreased fluvial input and arid conditions on the continent.

Further support for EF-ITCZ southward excursions during interglacials comes from the $\delta^{18}O$ gradient between planktonic foraminifera living at different depths (hereafter referred to as $\Delta\delta^{18}O$) (Figure 5.4c) and the $R_{c/d}$ index (Figure 5.4d). Planktonic foraminifera $\Delta\delta^{18}O$ is indicative of water column stratification in the EEP (E.g. Rincón-Martínez et al., 2011). High interglacial $\Delta\delta^{18}O_{\text{G.ruber-G.tumida}}$ values (Figure 5.4c) indicate stratified waters north of the EF, where a strong thermal gradient occurs in the upper 100 m. Low glacial $\Delta\delta^{18}O_{\text{G.ruber-G.tumida}}$ values reflect intensified upwelling linked to a stronger Peru Current and a northward location of the EF-ITCZ complex. With exception of MIS 7, glacial-interglacial patterns are also evident in the $R_{c/d}$ record (Figure 5.4d) that exhibits higher values during interglacials, indicating southward shifts of the EF-ITCZ. Low and minimum $R_{c/d}$ values recorded during MIS 5 and 7, respectively are attributed to potential changes on ecologic factors such as food web or nutrient supply, that might also exert control on the abundance of *G. cultrata* (E.g. Martinez and Bedoya, 2001; Martinez et al., 2006; Rincón-Martínez et al., 2011).

Glacial-interglacial relation of enhanced fluvial input patterns and thus tropical precipitation of coastal Ecuador to warmer offshore SSTs appears to be a robust feature. But low siliciclastic AR during MIS 5 (Figures 5.4b) and low $\Delta\delta^{18}O_{\text{G.ruber-G.tumida}}$ and $R_{c/d}$ values during MIS 7 beg the question of whether there is a consistent signature of rainfall response to the SST forcing. The specific mechanism behind the disproportion in the magnitude of lithogenic supply among interglacials is unknown. Differences in atmospheric CO_2 concentrations, astronomical forcing and glacial ice-volume (see Tzedakis et al., 2009) plausibly fostered variations in moisture advection to the ITCZ and to the continent hence stimulating variations in precipitation, vegetation cover and fluvial suspended loads that are reflected in the variable magnitude between the different interglacials of terrestrial input to the EEP.

5.4.3. Changes of equatorial Pacific mean states during the last 300,000 years

Tropical Pacific SST patterns translate into trans- and cross-equatorial pressure gradients that control the position and intensities of atmospheric convection over the Pacific Ocean. We apply this concept and investigate past changes in zonal and meridional SST gradients (Figures 5.5c and e) as indication of changes in the large-scale tropical atmospheric circulation, notably the Walker and Hadley cells. The zonal SST gradient was estimated using published *Globigerinoides ruber* Mg/Ca measured at ODP Site 806B from the Ontong Java Plateau (0°19.1'N; 159°21.7'E; 2520 m water depth) (Medina-Elizalde and Lea, 2005), and at Site TR163-19 (2°15'S; 90°57'W; 2348 m water depth) just north of the EEP cold tongue (Lea et al., 2000). The meridional gradient was calculated using alkenone-derived SST from ODP Site 1239 and Site MD02-2529 (this study). Here we use the terms "El Niño-like" and "La Niña-like" to describe mean changes in the zonal and meridional SST gradients across the equatorial Pacific, either in the form of decreased (El Niño) or increased (La Niña) gradients without specifically implying changes in frequency or amplitude of ENSO variability.

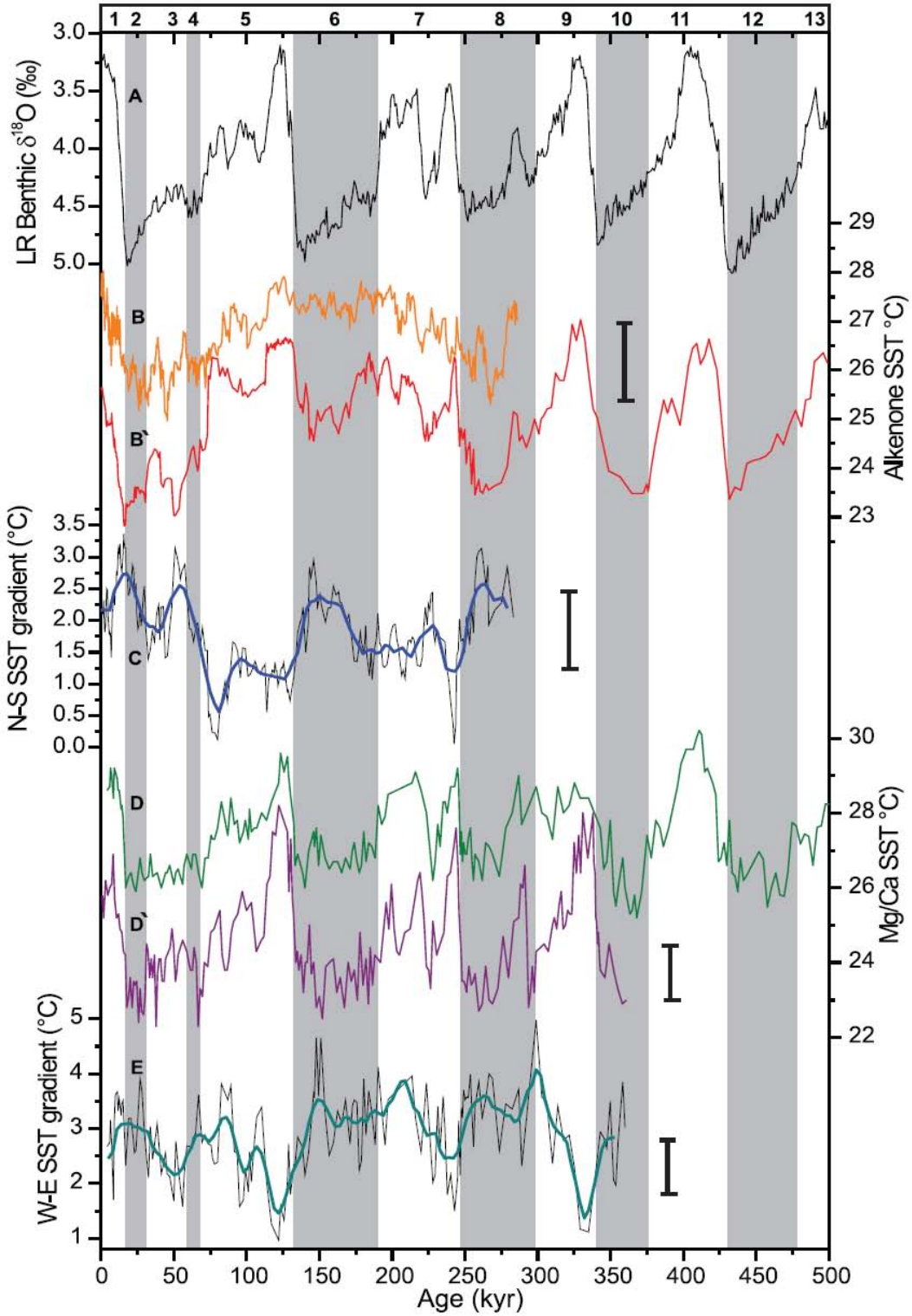

Figure 5. 5. Comparison of eastern and western equatorial Pacific SST records. **(A)** Benthic oxygen isotope stack (Lisiecki and Raymo, 2005) for stratigraphic reference. **(B)** Alkenone-derived SST records from the two eastern equatorial Pacific sites. MD02-2529 (top line; this study) data are used as representing the eastern Pacific warm pool; ODP Site 1239 data (bottom line; this study) are used as representing the northernmost reach of the cold tongue. **(C)** SST gradient between the northern Site MD02-2529 (08°12.33'N) and the southern Site 1239 (0°40.32´S). Increased SST difference between the equator and the eastern Pacific warm pool, represent La Niña-like mean conditions. **(D)** Mg/Ca SST record from ODP Site 806B (0°19.1'N; 159°21.7'E; top line), in the western Pacific warm pool (Medina-Elizalde and Lea, 2005), and Site TR163-19 (2°15'S; 90°57'W; bottom line), from north of the EEP cold tongue (Lea et al., 2000). **(E)** SST gradient between the eastern and western tropical Pacific sites. Reduced west-to-east SST gradients represent El Niño-like mean conditions.

Previous studies comparing SST derived from alkenones and Mg/Ca in the EEP have reported contrasting results. For example, on millennial-scale alkenones and Mg/Ca SST changes that have punctuated the last deglaciation are known to be out of phase (E.g. Mix, 2006; Koutavas and Sachs, 2008). Other studies based on compilations of Holocene SST data have revealed divergent SST trends over the last 10 ka, with warming vs. cooling recorded by alkenone- vs. Mg/Ca-based SST, respectively (E.g. Leduc et al., submitted; Sachs, 2008). These dissimilarities suggest that coccolithophorids and foraminifera do not record the same paleoceanographic features. For this reason we avoided using different proxies when we compiled the zonal and meridional SST gradients across the equatorial Pacific, and assume that these gradients best represent past changes in the equatorial SST mean state. Reported error bars in alkenone and Mg/Ca temperature estimates are of ± 1.5°C and ± 0.6°C, respectively (E.g. Müller et al. 1998; Lea et al., 2000).

The zonal SST gradient shows a distinct glacial-interglacial pattern, with minima during the interglacials and maxima during glacials (Figure 5.5e). For instance, during MIS 5e, MIS 7e and MIS 9e the west-east SST gradient was ~1.5°C, while for MIS 2 and MIS 8 it was ~3°C and ~3.5°C, respectively. This suggests a weakened Walker circulation (El Niño-like conditions) during interglacials and intensified Walker circulation (La Niña-like conditions) during glacial periods. Such scenario is consistent with reduced upwelling activity or intensity, an anomalous warming in the easternmost Pacific, an EF-ITCZ southward migration and heavy rainfall on the Guayas and Esmeraldas basins during interglacials (Figure 5.3) (E.g. Horel and Cornejo-Garrido, 1986; Hastenrath, 2002; Rossel et al., 1996; Bendix and Bendix, 2006).

Systematic glacial-interglacial patterns are also recorded in the meridional SST gradient record (Figures 5.5b and c). Low meridional SST gradients occur during MIS 5 (0.8 to 1.4°C) and MIS 7 (1.4 to 1.8°C), while MIS 2, 4, 6, and 8 were characterized by a steeper SST gradient (2.2 to 2.6°C). Today, the annual mean position of the eastern Pacific ITCZ is located in the vicinity of 10°N and remains north of the equator due to a strong cross-equatorial SST gradient. During El Niño years, mainly during the months of March and April, the meridional gradient is weakened, leading to extensive precipitation over coastal Ecuador linked to an equator-ward shift of the meridional position of the ITCZ. Taken together, the co-occurrence of weaker meridional and zonal SST gradients suggest an El Niño-like state during interglacial periods contrasting with La Niña-like conditions recorded during glacial periods. This result is consistent with reconstructions of the ENSO suggesting reduced ENSO activity during the last glacial maximum (LGM) (E.g. Leduc et al., 2009). Sea surface temperature reconstructions from the southeastern Pacific margin suggest that remote advection of cold waters from high latitudes is a valid mechanism for explaining the observed glacial La Niña-like state (E.g. Kaiser et al., 2005).

The zonal SST gradient is particularly well expressed during peak interglacials (i.e. MIS 5e, MIS 7e, and MIS 9e), while it does not show much change between late interglacials and glacials. In contrast, the meridional SST gradient clearly mimics glacial-interglacial patterns. One explanation for the disparate pattern of zonal and meridional SST gradients is that zonal the SST gradient was estimated from *G. ruber* Mg/Ca measurements, while the meridional SST gradient was calculated from alkenone ratios. The signal offset between both SST gradients might reflect contrasting sensitivities to different seasonal/inter-annual variations or depth distribution of proxy carriers (i.e. Mix, 2006; Leduc et al., submitted), rather than disentanglement of the Hadley and Walker circulations. Alternatively, possible long-term modifications of the tropical Pacific mean state, such as migration of the main centers of deep convection, could explain the divergent patterns of SST gradients, plausibly in conjunction with non-conventional El Niño namely the El Niño-modoki or Pseudo El Niño (E.g. Yeh et al., 2009). During such anomalous conditions, the maximum SST anomaly persists in the central Pacific,

sandwiched between anomalous cooling in the east and west, hence modifying the atmospheric circulation and resulting in distinctly different global impacts than conventional El Niño conditions.

5.4.4. Comparison to previous paleoceanographic and paleoclimatic studies from the EEP and adjacent South America continent

Our findings contradict the common view that, during glacial times, the location of tropical rainfall zones experienced a southward displacement globally. Modeling studies simulate a southward displacement of the marine ITCZ in response to changes in continental ice volume at high latitudes (E.g. Yin and Battisti, 2001; Chiang et al., 2003; Chiang and Bitz, 2005; Broccoli et al., 2006). However, today's climatology and variability of the eastern tropical Pacific SST have proven difficult to reproduce, even with current state-of-the-art coupled ocean–atmosphere general circulation models (E.g. Mechoso et al., 1995; Wang et al., 2005; Wittenberg et al., 2006). For instance, in simulations of the seasonal cycle, the modeled ITCZ tends to move across the equator following the seasonal movement of the sun rather than remaining in the Northern Hemisphere as is suggested by monthly monitoring (I.e. http://trmm.gsfc.nasa.gov/). Moreover, in the current models, the ITCZ persists too long at a southern position compared to observations, causing a double ITCZ in the annual mean. Therefore, numerical models appear to overestimate the control of Northern Hemisphere ice sheets on the ITCZ and do not adequately implement low latitude air-sea interactions.

Our results also challenge previous suggestions that a glacial relaxation of the SST asymmetry across the equator and a southward displacement of the marine ITCZ in the eastern Pacific were likely reflecting an El Niño-like pattern (E.g. Koutavas et al., 2002; Koutavas and Lynch-Stieglitz, 2003). Alternatively, the LGM reduction in the meridional $\delta^{18}O$ gradient reconstructed by Koutavas and Lynch-Stieglitz (2003) can be interpreted in terms of a northward migration of the EF-ITCZ system because their records are located primarily on the seasonal path of the EF-ITCZ system. Thus, a glacial northward shift of the EF would cause weaker meridional $\delta^{18}O$ gradients, due to minimum changes in SST and salinity within the cold tongue. Other eastern Pacific alkenone-SST reconstructions (E.g. Calvo et al., 2001; Liu and Herbert, 2004; Horikawa et al., 2006; Pahnke et al., 2007; Koutavas et al., 2008; Dubois et al., in press), together with previous SST estimates based on marine microfossils (E.g. Pisias and Mix, 1997; Feldberg and Mix, 2003; Martínez et al., 2003), support this view by demonstrating that sites located south of the EF experienced stronger cooling during the LGM and stronger warming during the last deglaciation compared to sites located north of the EF.

Paleoclimate records from South America indicate southward ITCZ displacements during northern hemisphere ice sheet expansions (E.g. Amazon basin: Wang et al., 2004; Jacob et al., 2007; Bolivian Altiplano: Baker et al., 2001; Venezuela: Rull, 1996; Ice cores: Thompson et al., 1998; Bradley et al., 2003; Glaciers: Heine, 2000). This is in opposition to what is indicated by our marine data. The divergent behavior of the ITCZ in the continent plausibly relates to differences in heat flux patterns over the relatively dry continent as compared to the ocean where meridional temperature gradients were more prominent. This results in latitudinal ITCZ migrations over the continent that are much larger over the Amazon Basin and the Altiplano, while at the same time the ITCZ position over the EEP is defined by the geometry of the cold tongue-EF complex and the Subtropical gyre circulation (E.g. Horel et al., 1989; Poveda et al., 2006; Garreaud et al., 2009).

5.5. Summary and Conclusions

We find prominent glacial-interglacial changes of fluvial sediment input that reflects more humid conditions along the Ecuadorian coast during interglacials. A warmer interglacial EEP cold tongue and a southward shift of the EF-ITCZ system likely control these humid interglacial conditions. Conversely, reduced fluvial input during glacials suggests more arid conditions coinciding with larger tropical Pacific SST gradients and a more northward location of the EF-ITCZ system. Despite this general tight coupling of rainfall changes in Ecuador to offshore oceanographic conditions, there are distinct differences between the individual interglacials, plausibly reflecting offsets in precipitation as well as duration and variability of interglacial climates of the past 500,000 years. Numerical modeling is required to test the sensitivity of past interglacial conditions and notably, the distribution and intensity of tropical rainfall to variable atmospheric CO_2 concentrations, glacial ice-volume, and orbital forcing.

Zonal SST gradients in the eastern Pacific are reduced throughout interglacials and enhanced during glacials. With regards to long-term changes in the mean climate state, our data suggest a predominance of El Niño-like conditions off Ecuador during interglacials, while glacial conditions seem to more closely mimic La Niña-like conditions.

Contrary to climate models our data indicate a northern EF-ITCZ position during glacials in the EEP. This was plausibly favored by the facts that: 1) the cross-equatorial SST asymmetry was enhanced with stronger cooling south of the EF, which would drive the southeasterly trade winds across the equator, displacing the ITCZ to a northerly position (E.g. Calvo et al., 2001; Liu and Herbert, 2004; Horikawa et al., 2006; Dekens et al., 2007; Pahnke et al., 2007; Koutavas et al., 2008; Dubois et al., in press); 2) the southeast-to-northwest tilted coastal geometry has not changed during the last 500 kyr, promoting coastal upwelling predominantly active south of the equator; and 3) the influence of the Andes and the South Pacific subtropical anticyclone on the regional atmospheric circulation remained reasonably stable during the entire time span hence keeping cool the ocean surface through evaporation and suppressing deep convection in the Southern Hemisphere (E.g. Takahashi and Battisti, 2007).

The glacial-interglacial latitudinal shifts of the EF-ITCZ system suggested by our data may be restricted to the EEP and the coastal area of northwest South America. Glacial cooling is particularly pronounced in the Southeast Pacific (E.g. Kaiser et al., 2005), which suggests a possibility that ITCZ migration in the region may be controlled by the northward advection of cold waters with the Humboldt Current system. Conversely, in the Central and Western Pacific, the magnitude of the cross-equatorial pressure gradient diminishes because the broad western Pacific warm pool dominates the SST pattern, leading to a potentially wider latitudinal range for ITCZ migrations during glacial times. Over the South American continent, away from the coast, the Andes and Amazon Basin impact atmospheric circulation patterns, allowing larger southward migrations of the ITCZ during glacial periods.

Acknowledgements

At AWI, Reza Ahi assisted with TOC, opal and CNS analyses and Lisa Schönborn provided invaluable assistance with oxygen isotopic measurement. Funding was provided through the German Science Foundation (grants Ha 2756/9-1 and TI240/17-2). DRM and SC acknowledge Marcel Kuypers for his interest and support of this project and Gail Lee Arnold for her editorial comments. The authors further thank Frauke Rostek (CEREGE) who generated a considerable amount of alkenones data for Site MD02-2529 and Silvia Koch, for her assistance at the biomarker laboratory at the CAU-IfG. This research used samples provided by the Integrated

Ocean Drilling Program/Ocean Drilling Program (IODP/ODP) and the IMAGES program. Editorial comments by Rainer Zahn and critical reviews by George Philander and two anonymous reviewers substantially improved this manuscript.

References

- Amador, J. A., Alfaro, E. J., Lizano, O. G., and Magaña, V. O. 2006. Atmospheric forcing of the eastern tropical Pacific. Progress in Oceanography 69, 101-142, doi:10.1016/j.pocean.2006.03.007.
- Anderson, R. F., Fleisher, M. Q., and Lao, Y. 2006. Glacial-interglacial variability in the delivery of dust to the central equatorial Pacific Ocean. Earth and Planetary Science Letters 242, 406-414, doi:10.1016/j.epsl.2005.11.061.
- Andreasen, D. J., and Ravelo, A. C. 1997. Tropical Pacific ocean thermocline depth reconstructions for the last glacial maximum. Paleoceanography 12(3), 395-413.
- Andreasen, D. J., Ravelo, A. C., and Broccoli, A. J. 2001. Remote forcing at the last glacial maximum in the tropical Pacific ocean. Journal of Geophysical Research 106, 879-897.
- Baker, P. A., Seltzer, G. O., Fritz, S. C., Dunbar, R. B., Grove, M. J., Tapia, P. M., Cross, S. L., Rowe, H. D., and Broda, J. P. 2001. The history of South American tropical precipitation for the past 25,000 years. Science 291, 640-643.
- Bendix, A., and Bendix, J. 2006. Heavy rainfall episodes in Ecuador during El Niño events and associated regional atmospheric circulation and SST patterns. Advances in Geosciences 6, 43-49.
- Bendix, J. 2000. Precipitation dynamics in Ecuador and northern Peru during the 1991/92 El Niño: a remote sensing perspective. International Journal of Remote Sensing 21(3), 533-548.
- Bendix, J. and Lauer, W. 1992. Die Niederschlagsjahreszeiten in Ecuador und ihre Klimatdynamische interpretation. Erdkunde 46, 118-134.
- Bradley, R. S., Vuille, M., Hardy, D., and Thompson, L. G. 2003. Low latitude ice cores record Pacific sea surface temperatures. Geophysical Research Letters 30(4), 1174, doi:10.1029/2002GL016546.
- Broccoli, A. J., Dahl, K. A., and Stouffer, R. J. 2006. Response of the ITCZ to Northern Hemisphere cooling. Geophysical Research Letters 33, L01702, doi:10.1029/2005GL024546.
- Calvo, E., Pelejero, C., Herguera, J. C., Palanques, A., and Grimalt, J. O. 2001. Insolation dependence of the southeastern Subtropical Pacific sea surface temperature over the last 400 kyr. Geophysical Research Letters 28(12), 2481-2484.
- Cane, M. A. 2004. The evolution of El Niño, past and future. Earth and Planetary Science Letters 230(3-4), 227-240.
- Chiang J. C. H., Biasutti, M., Battisti, D. S. 2003. Sensitivity of the Atlantic Intertropical Convergence Zone to Last Glacial Maximum boundary conditions. Paleoceanography 18(4), 1094, doi:10.1029/2003PA000916.
- Chiang, J. C. H., and Bitz, C. M. 2005. Influence of high latitude ice cover on the marine Intertropical Convergence Zone. Climate Dynamics 25, 477-496, doi: 10.1007/s00382-005-0040-5.
- Clement, A. C., Seager, R., and Cane, M. A. 1999. Orbital controls on the El Niño/Southern Oscillation and the tropical climate. Paleoceanography 14(4), 441-456.
- Conkright, M. E., Locarnini, R. A., Garcia, H. E., O'Brien, T. D., Boyer, T. P., Stephens, C., and Antonov, J. I. 2002. World Ocean Atlas 2001: Objective analyses, data statistics, and figures, CD-ROM documentation, NODC Internal Rep., 17, 0-17.
- Conte, M. H., Sicre, M-. A., Rühlemann, C., Weber, J. C., Schulte, S., Schulz-Bull, D., and Blanz, T. 2006. Global temperature calibration of the alkenone unsaturation index (U) in surface waters and comparison with surface sediments. Geochemistry, Geophysics, Geosystems 7(2), doi:10.1029/2005GC001054.
- Dekens, P. S., Ravelo, A. C., McCarthy, M. D. 2007. Warm upwelling regions in the Pliocene warm period. Paleoceanography 22, PA3211, doi:10.1029/2006PA001394.
- deMaster, D. J. 1981. Measuring biogenic silica in marine sediments and suspended matter, In: Marine Particles: Analysis and Characterization, edited by Hurd, D. C. and Spenser, D. W., pp. 363–368, Geophysics Monography Ser., 63, AGU, Washington, D. C.
- de Szoeke, S. P., Xie, S.-P., Piyama, T., Richards, K. J., and Small, R. J. O. 2007. What maintains the SST front north of the eastern Pacific equatorial cold tongue?. Journal of Climate 20, 2500-2514.
- Dubois, N., Kienast, M., Normandeau, C., and Herbert, T. D. in press. The east equatorial Pacific cold tongue during the last glacial maximum as seen from alkenone paleothermometry. Paleoceanography doi:10.1029/2009PA001781.

- Fedorov, A. V., Dekens, P. S., McCarthy, M., Ravelo, A. C., deMenocal, P. B., Barreiro, M., Pacanowski, R. C., and Philander, S. G. 2006. The Pliocene Paradox (Mechanisms for a permanent El Niño). Science 312, 1485-1489, doi:10.1126/science.1122666.
- Feldberg, M. J., and Mix, A. C. 2003. Planktonic foraminifera , sea surface temperatures, and mechanisms of oceanic change in the Peru and south equatorial currents, 0-150 ka BP. Paleoceanography 18(1), 1016, doi:10.1029/2001PA000740.
- Fiedler, P. C., and Talley, L. D. 2006. Hydrography of the eastern tropical Pacific: A review. Progress in Oceanography 69, 143-180, doi:10.1016/l.pocean.2006.03.008.
- Garreaud, R. D., Vuille, M., Compagnucci, R., and Marengo, J. 2009. Present-day South American climate. Palaeogeography, Palaeoclimatology, Palaeoecology 281, 180–195, doi:10.1016/j.palaeo.2007.10.032.
- González, C., Urrego, L. E., and Martínez, J. I. 2006. Late Quaternary vegetation and climate change in the Panama Basin: Palynological evidence from marine cores ODP 677B and TR 163-38. Palaeogeography, Palaeoclimatology, Palaeoecology 234, 62-80, doi:10.1016/j.palaeo.2005.10.019.
- Grosjean, E., Logan, G. A., Rollet, N., Ryan, G.J., and Glenn, K. 2007. Geochemistry of shallow tropical marine sediments from the Arafura Sea, Australia. Organic Geochemistry 38, 1953-1971, doi:10.1016/j.orggeochem.2007.06.017.
- Hastenrath, S. 2002. The Intertropical Convergence Zone of the eastern Pacific revisited. International Journal of Climatology 22, 347-356, doi:10.1002/joc.739.
- Heine, K. 2000. Tropical South America during the Last glacial maximum: evidence from glacial, periglacial and fluvial records. Quaternary International 72, 7-21.
- Heusser, L. E., and Shackleton, N. J. 1994. Tropical climatic variation on the Pacific slopes of the Ecuadorian Andes based on a 25,000 year pollen record from deep-sea sediment core Tri163-31B. Quaternary Research 42, 222-225.
- Horel, J. D., and Cornejo-Garrido, A. G. 1986. Convection along the coast of Northern Peru during 1983: Spatial and temporal variations of clouds and rainfall. Monthly Weather Review 114(11), 2091-2105.
- Horel, J. D., Hahmann, A. N., and Geisler, J. E. 1989. An investigation of the annual cycle of convective activity over the tropical Americas. Journal of Climate 2(11), 1388-1403.
- Horikaga, K., Minagawa, M., Murayama, M., Kato, Y., and Asahi, H. 2006. Spatial and temporal sea-surface temperatures in the eastern equatorial Pacific over the past 150 kyr. Geophysical Research Letters 33, L13605, doi:10.1029/2006GL025948.
- Jacob, J., Huang, Y., Disnar, J.-R., Sifeddine, A., Boussafir, M., Spadano, A. L., and Turcq, B. 2007. Paleohydrological changes during the last deglaciation in northern Brazil. Quaternary Science Reviews 26, 1004-1015.
- Kaiser, J., Lamy, F., Hebbeln, D. 2005. A 70-kyr sea surface temperature record off southern Chile (Ocean Drilling Program Site 1233). Paleoceanography 20, PA4009, doi:10.1029/2005PA001146.
- Kessler, W. S. 2006. The circulation of the eastern tropical Pacific: A review. Progress in Oceanography 69, 181-217, doi:10.1016/j.pocean.2006.03.009.
- Killops, S. D., and Frewin, N. L. 1994. Triterpenoid diagenesis and cuticular preservation. Organic Geochemistry 21(2), 1193-1209.
- Kim, J-H., Dupont, L., Behling, H., and Verteegh, G. J. M. 2005. Impacts of rapid sea-level rise on mangrove deposit erosion: application of taraxerol and Rhizophora records. Journal of Quaternary Science 20(3), 221-225, doi:10.1002/jqs.904.
- Klein, S. A., and Hartmann, D. L. 1993. The seasonal cycle of low stratiform clouds. Journal of Climate 6(8), 1587-1606, doi: 10.1175/1520-0442(1993)006<1587:TSCOLS>2.0.CO;2.
- Klinkhammer, G. P., Mix, A. C., and Haley, B. A. .2009. Increased dissolved terrestrial input to the coastal ocean during the last deglaciation. Geochemistry, Geophysics, Geosystems 10(3), doi:10.1029/2008GC002219.
- Kohfeld, K. E., and Harrison, S. P. 2001. DIRTMAP: the geological record of dust. Earth-Science Reviews 54, 81-114.
- Koutavas, A. and Lynch-Stieglitz, J. 2003. Glacial-interglacial dynamics of the eastern equatorial Pacific cold tongue –Intertropical Convergence Zone system reconstructed from oxygen isotope records. Paleoceanography 18(4), 1089, doi:10.1029/2003PA000894.
- Koutavas, A., Lynch-Stieglitz, J., Marchitto, T. M., and Sachs, J. 2002. El-Niño-like pattern in Ice Age tropical Pacific sea surface temperature. Science 297, no. 5579, 226-230, doi: 10.1126/science.1072376.
- Koutavas A., and Sachs, J. P. 2008. Northern timing of deglaciation in the eastern equatorial Pacific from alkenone paleothermometry. Paleoceanography 23, PA4205, doi:10.1029/2008PA001593.

- Lea, D. W., Pak, D. K., and Spero, H. J. 2000. Climate impact of late Quaternary equatorial Pacific sea surface temperature variations. Science 289, 1719-1724.
- Lea, D. W., Pak, D. K., Belanger, C. L., Spero, H. J., Hall, M. A., and Shackleton, N. J. 2006. Paleoclimate history of Galápagos surface waters over the last 135,000 yr. Quaternary Science Reviews 25, 1152-1167, doi:10.1016/S0277-3791(01)00081-6.
- Leduc, G., Vidal, L., Tachikawa, K., Rostek, F., Sonzogni, C., Beaufort, L., and Bard, E. 2007. Moisture transport across Central America as a positive feedback on abrupt climatic changes. Nature 445, 908-911, doi:10.1038/nature05578.
- Leduc, G., Vidal, L., Cartapanis, O., Bard, E. (2009), Modes of eastern equatorial Pacific thermocline variability: Implications for ENSO dynamics over the last glacial period, Paleoceanography, 24, PA3202, doi:10.1029/2008PA001701.
- Leduc, G., Schneider, R., Kim, J- H., and Lohmann, G. (submitted), Holocene and Eemian sea surface temperature trends as revealed by alkenone and Mg/Ca paleothermometry, Quaternary Science Reviews.
- Lisiecki, L. E., and Raymo, M. E. (2005), A Pliocene-Pleistocene stack of 57 globally distributed benthic $\delta^{18}O$ records, Paleoceanography, 20, PA1003, doi:10.1029/2004PA001071.
- Liu, Z., and Herbert, T. D. (2004), High-latitude influence on the eastern equatorial Pacific climate in the early Pleistocene epoch, Nature, 427, 720-723, doi:10.1038/nature02338.
- Lukas, R. (1986), The termination of the equatorial undercurrent in the eastern Pacific, Progress in Oceanography, 16(2), 63-90, doi: 10.1016/0079-6611(86)90007-8.
- Lyle, M., Mitchell, N., Pisias, N., Mix, A., Martínez, J.I., and Paytan, A. (2005), Do geochemical estimates of sediment focusing pass the sediment test in the equatorial Pacific?, Paleoceanography, 20, PA1005, doi:10.1029/2004PA001019.
- Mahowald, N., Kohfeld, K., Hansson, M., Balkanski, Y., Harrison, S. P., Prentice, I. C., Schulz, M., and Rodhe, H. (1999), Dust sources and deposition during the last glacial maximum and current climate: A comparison of model results with paleodata from ice cores and marine sediments, Journal of Geophysical Research, 104(D13), 115895-15916.
- MARGO Project Members (2009), Constraints on the magnitude and patterns of ocean cooling at the Last Glacial Maximum, Nature Geoscience, 2, 127-138, doi:10.1038/NGEO411.
- Markgraf, V., and Diaz, H. F. (2000), The past ENSO record: A synthesis, in El Niño and the Southern Oscillation Multiscale variability and global and regional impacts, edited by Diaz, H. F., and Markgraf V., pp. 465-488, Cambridge University Press, New York.
- Martinez, J. I., and Bedoya, G. (2001), Recent planktonic foraminifera from deep-sea sediments from the Eastern Equatorial Pacific: Proxies of the equatorial front in the late Quaternary, Journal of Marine and Coastal Research, 30, 151-176.
- Martínez, I., Keigwin, L., Barrows, T. T., Yokoyama, Y., and Southon, J. (2003), La Niña-like conditions I the eastern equatorial Pacific and a stronger Choco Jet in the northern Andes during the last glaciation. Paleoceanography, 18(2), 1033, doi:10.1029/2002PA000877.
- McGee, D., Marcantonio, F., and Lynch-Stieglitz, J. (2007), Deglacial changes in dust flux in the eastern equatorial Pacific, Earth and Planetary Science Letters, 257, 215-230, doi:10.1016/j.epsl.2007.02.033.
- McPhaden, M. J., Zebiak, S. E., and Glantz, M. H. (2006), ENSO as an integrating concept in earth science, Science, 314, 1740-1745, doi:10.1126/science.1132588.
- Mechoso C. R., and coauthors (1995), The seasonal cycle over the tropical Pacific in coupled ocean–atmosphere general circulation models, Monthly Weather Review, 123, 2825–2838.
- Medina-Elizalde, M., and Lea, D. W. (2005), The Mid-Pleistocene transition in the tropical Pacific, Science, 310, 1009-1012, doi:10.1126/science.1115933.
- Mix, A. C. (2006), Running hot and cold in the eastern equatorial Pacific, Quaternary Science Reviews, 25, 1147-1149, doi:10.1016/j.quascirev.2006.03.008.
- Müller, P. J., Kirst, G., Ruhland, G., von Storch, I., and Rosell-Melé, A. (1998), Calibration of the alkenone paleotemperature index $U^{K'}_{37}$ based on core-tops from the eastern South Atlantic and the global ocean (60°N-60°N), Geochimica et Cosmochimica Acta, 62(10), 1757-1772.
- Müller, P. J., and Schneider, R. (1993), An automated leaching method for the determination of opal in sediments and particulate matter, Deep-Sea Research I, 40(3), 425-444.
- Neill, D. A. (1999), Vegetation, in Catalogue of the vascular plants of Ecuador, edited by P. M. Jørgensen and S. León-Yánez, pp. 8–13, Monographs in Systematic Botany from the Missouri Botanical Garden, 75, St. Louis, Missouri.

-Neill, D. A., and Jørgensen, P. M. (1999), Climates, in Catalogue of the vascular plants of Ecuador, edited by Jørgensen, P. M., and León-Yánez, S., 13–25pp., Monographs in Systematic Botany from the Missouri Botanical Garden, 75, St. Louis, Missouri.
-Pahnke, K., Sachs, J. P., Keigwin, L., Timmermann, A., and Xie, S-P. (2007), Eastern tropical Pacific hydrologic changes during the past 27,000 years from D/H ratios in alkenones, Paleoceanography, 22, PA4214, doi:10.1029/2007PA001468.
-Pailler, D., and Bard, E. (2002), High frequency paleoceanographic changes during the past 140 000 yr recorded by the organic matter in sediments of the Iberian Margin, Palaeogeography, Palaeoclimatology, Palaeoecology, 181, 431-452.
-Pak, H., and Zaneveld, J. R. V. (1974), Equatorial Front in the Eastern Pacific Ocean, Journal of Physical Oceanography, 4(4), 570-578, doi:10.1175/1520-0485(1974)004<0570:EFITEP>2.0.CO;2.
-Pena L. D., Cacho, I., Ferretti, P., and Hall, M. A. (2008), El Niño–Southern Oscillation–like variability during glacial terminations and interlatitudinal teleconnections, Paleoceanography, 23, PA3101, doi:10.1029/2008PA001620.
-Pennington, J. T., Mahoney, K- L., Kuwahare, V. S., Kolber, D. D., Calienes, R., and Chavez, F. P. (2006), Primary production in the eastern tropical pacific: A review. Progress in Oceanography, 69(2-4), 285-317, doi: 10.1016/j.pocean.2006.03.012.
-Peterson, T. C., and Russell, S. V. (1997), An overview of the Global Historical Climatology Network temperature data base, Bulletin of the American Meteorological Society, 78, 2837-2849.
-Philander, S. G. H., Gu, D., Halpern, D., Lambert, G., Lau, N. C., Li, T., and Pacanowski, R. C. (1996), Why the ITCZ is mostly north of the equator. Journal of Climate, 9(12), 2958-2972, doi: 10.1175/1520-0442(1996)009<2958:WTIIMN>2.0.CO;2.
-Pisias, N. G., and Mix, A. (1997), Spatial and temporal oceanographic variability of the eastern equatorial Pacific during the late Pleistocene: Evidence from radiolaria microfossils, Paleoceanography, 12(3), 381-393.
-Poveda, G., Waylen, P. R., and Pulwarty, R. S. (2006), Annual and inter-annual variability of the present climate in northern South America and southern Mesoamerica, Palaeogeography, Palaeoclimatology, Palaeoecology, 234, 3-27, doi:10.1016/j.palaeo.2005.10.031.
-Prahl, F. G., and Wakeham, S. G. (1987), Calibration of unsaturation patterns in long-chain ketone compositions for paleotemperature assessment, Nature, 330, 367-369.
-Prahl, F. G., Herbert, T., Brassell, S. C., Ohkouchi, N., Pagani, M., Repeta, D., Rosell-Melé, A., and Sikes, E. (2000), Status of alkenone paleothermometer calibration: Report from Working Group 3, Geochemistry, Geophysics, Geosystems, 1(11), doi:10.1029/2000GC000058.
-Prahl, F. G., Mix, A. C., and Sparrow, M. A. (2006), Alkenone paleothermometry: Biological lessons from marine sediment records off western South America, Geochimica et Cosmochimica Acta, 70, 101-117, doi:10.1016/j.gca.2005.08.023.
-Raymond, D. J., Esbensen, S. K., Paulson, C., Gregg, M., Bretherton, C. S., Petersen, W. A., Cifelli, R., Shay, L. K., Ohlmann, C., and Zudeima, P. (2004), EPIC2001 and the coupled ocean-atmosphere system of the tropical east Pacific, Bulletin of the American Meteorological Society, 85(9), 1341-1354, doi:10.1175/BAMS-85-9-1341.
-Richter, T. O., van der Gaast, S., Koster, B., Vaars, A., Gieles, R., de Stigter, H. C., de Haas, H., and van Weering, T. C. E. (2006), The Avaatech XRF Core Scanner: technical description and applications to NE Atlantic sediments, in New Techniques in Sediment Core Analysis, edited by Rothwell, R. G., pp. 39-50, Geological society of London Special Publication, 267, The Geological Society of London.
-Rincón-Martínez, D., Steph, S., Lamy, F., Mix, A., and Tiedemann, R. (2011), Tracking the equatorial front in the eastern equatorial Pacific Ocean by the isotopic and faunal composition of planktonic foraminifera, Marine Micropaleontology, 79 (1–2), 24-40.
-Rossel, F., Cadier, E., and Gómez, G. (1996), Las inundaciones en la zona costera Ecuatoriana: Causas; obras de protección existentes y previstas, Bulletin de l´Institut Français d´Études Andines, 25(3), 399-420.
-Rull, V. (1996), Late Pleistocene and Holocene climates of Venezuela, Quaternary International, 31, 85-94.
-Sachs, J. P. (2008), Divergent Trends in Holocene SSTs Derived from Alkenones and Mg/Ca in the Equatorial Pacific, Fall Meeting of the American Geophysical Union, San Francisco, CA, December 15-19, 2008.
-Sachs, J. P., Schneider, R., Freeman, K. H., Ganssen, G., McManus, J. F., and Oppo, D. W. (2000), Alkenones as paleoceanographic proxies, Geochemistry, Geophysics, Geosystems, 1, 2000GC000059.

-Schneider, R., Müller, P. J., and Acheson, R. (1999), Atlantic alkenone sea surface temperature records, in Reconstructing Ocean History: A window into the Future, edited by I. Abrantes, and A. C. Mix, pp. 33-55, Plenum Publishers, New York.
-Shipboard Scientific Party (2003), Site 1239, in Proceedings of the Ocean Drilling Program 202: Southeast Pacific Paleoceanographic Transects, edited by A. C. Mix, R. Tiedemann, P. Blum et al., pp. 1–93, College Station, TX (Ocean Drilling Program), doi:10.2973/odp.proc.ir.201.110.2003.
-Sonzogni, C., Bard, E., Rostek, F., Dollfus, D., Rosell-Melé, A., and Eglington, G. (1997), Temperature and salinity effects on alkenone ratios measured in surface sediments from the Indian Ocean, Quaternary Research, 47, 344-355.
-Spero, H. J., Mielke, K. M., Kalve, E. M., Lea, D. W., and Pak, D. K. (2003), Multispecies approach to reconstructing eastern equatorial Pacific thermocline hydrography during the past 360 kyr, Paleoceanography, 18(1), 1002, doi:10,1029/2002PA000814.
-Takahashi, K., and Battisti, D. S. (2007), Processes controlling the mean tropical Pacific precipitation pattern: I. The Andes and the eastern Pacific ITCZ, Journal of Climate, 20(14), 3434-3451, doi:10.1175/JCLI4198.1.
-Thompson, L. G., Davis, M. E., Mosley-Thompson, E., Sowers, T. A., Henderson, K. A., Zagorodnov, V. S., Lin, P.-N., Mikhalenko, V. N., Campen, R. K., Bolzan, J. F., Cole-Dai, J., and Francou, B. (1998), A 25,000-year tropical climate history from Bolivian ice cores, Science, 282, 1858–1864.
-Tzedakis, P. C., Raynaud, D., McManus, J. F., Berger, A., Brovkin, V., and Kiefer, T. (2009), Interglacial diversity, Nature Geoscience, 2, 751-755, doi:10.1038/NGEO660.
-Versteegh, G. J. M., Schefuß, E., Dupont L., Marret, F., Sinninghe Damsté, J. S., and Jansen, J. H. F. (2004), Taraxerol and Rhizophora pollen as proxies for tracking past mangrove ecosystems, Geochimica et Cosmochimica Acta, 68(3), 41-422, doi:10.1016/S0016-7037(03)00456-3.
-Wang, C., and Fiedler, P. C. (2006), ENSO variability and the eastern tropical Pacific: A review, Progress in Oceanography, 69, 239-266, doi:10.1016./j.pocean.2006.03.004.
-Wang, X., Auler, A. S., Edwards, R. L., Cheng, H., Cristalli, P., Smart, P. L., Richards, D. A., and Shen, C.-C. (2004), Wet periods in northeastern Brazil over the past 210 kyr linked to distant climate anomalies, Nature, 432, 740-743, doi:10.1038/nature03067.
-Wang W., Saha, S., Pan, H.-L., Nadiga, S., and White, G. (2005), Simulation of ENSO in the new NCEP coupled forecast system model (CFS03), Monthly Weather Review, 133, 1574–1593.
-Waylen, P., and Poveda, G. (2002), El Niño-Southern Oscillation and aspects of western South American hydro-climatology, Hydrological Progress, 16, 1247-1260, doi:10.1002/hyp.1060.
-Weltje, G.-J., and Tjallingii, R. (2008), Calibration of XRF core scanning for quantitative geochemical logging of sediment cores: Theory and application, Earth Planet. Sci. Lett., 274, 423-438.
-Winckler, G., Anderson, R. F., Fleisher, M. Q., McGee, D., and Mahowald, N. (2008), Covariant glacial/interglacial dust fluxes in the equatorial Pacific and Antarctica, Science, 320(5872), 93-96, doi:10.1126/science.1150595.
-Wittenberg A. T., Rosati, A., Lau, N.-C., and Ploshay, J. J. (2006), GFDL's CM2 global coupled climate models. Part III: Tropical Pacific climate and ENSO, Journal of Climate, 19, 698–722.
-Xie, S.-P (2004), The shape of continents, air-sea interaction, and the rising branch of the Hadley circulation, in The Hadley circulation: Present, Past and Future, edited by Díaz, H. R. and Bradley, R. S., pp. 121-152, Kluwer Academic.
-Xie, S.-P., and Philander, S. G. H. (1994), A coupled ocean-atmosphere model of relevance to the ITCZ in the eastern Pacific, Tellus, 46A, 340-350.
-Yeh, S- W., Kug, J- S., Dewitte, B., Kwon, M- H., Kirtman, B. P., and Jin, F- F. (2009), El Niño in a changing climate, Nature, 461, 511-515, doi:10.1038/nature08316.
-Yin, J. H., and Battisti, D. A. (2001), The importance of tropical sea surface temperature patterns in simulations of las glacial maximum climate, Journal of Climate, 14, 565-581.

CHAPTER 6

A RAINY NORTHERN ATACAMA DESERT DURING THE LAST INTERGLACIAL.

Sergio Contreras[1], Silvio Pantoja[2], Carina B. Lange[2], Gaute Lavik[1], Daniel Rincón-Martínez[3] and Marcel M.M. Kuypers[1]

Published with moderate comments in *Geophysical Research Letters*
**(Geophysical Research Letters, Vol. 37, L23612, 5 PP., 2010
doi:10.1029/2010GL045728)**

[1]Max Planck Institute for Marine Microbiology, Celsiusstr. 1, D-28359 Bremen, Germany.

[2]Department of Oceanography & Center for Oceanographic Research in the eastern South Pacific (FONDAP-COPAS Center), University of Concepción, P.O. Box 160-C, Concepción, Chile

[3]Alfred Wegener Institute for Polar Marine Research, Am Handelshafen 12, D-27570 Bremerhaven, Germany.

Corresponding author: Max Planck Institute for Marine Microbiology, Celciusstrasse 1, 13 D-28359 Bremen, Germany; phone: +49 421 2028 630; fax: +49 421 2028 690; email: scontrer@mpi-bremen.de

Keywords: Atacama Desert, Peru, Last Interglacial, El Niño-like response, Molecular Fossils.

Abstract

The response of the northern extension of the Atacama Desert and the Peruvian upwelling system to climate conditions during the Last Interglacial (LIG; ~125 kyr ago) was tracked using molecular fossils of marine and terrestrial organisms preserved in Peruvian shelf sediments. High resolution records of ODP Site 1229 (past 145 kyr) indicated that warmer and wetter conditions (rainfall and river runoff) along the coast occurred during the LIG, when global temperatures were comparable or even higher than today. A ~3°C warming of surface waters, enhanced water column stratification, rainfall and river runoff were associated with low primary productivity and a ~1.5°C decrease in the temperature gradient across the Equatorial Pacific (I.e. weak Walker circulation), suggesting a prolonged El Niño-like response of the tropical Pacific during the LIG. In contrast, the late Holocene (LH; last 3 kyr) was characterized by colder surface waters, higher export and primary productivity, and a drier climate.

6.1. Introduction

The west coast of South America is characterized by a narrow arid and continuous belt that is virtually devoid of vegetation and extends over more than 3.000 km from northern Peru (5°S) to northern Chile (30°S) (Rundel et al., 1991). The hyperarid core (annual precipitation < 3mm yr^{-1}) known as the Atacama Desert, is located between 15°S and 30°S. Permanent cold coastal conditions prevent precipitation by developing and enhancing atmospheric stability in the coastal region as a result of the strong atmospheric subsidence of the Subtropical Pacific Anticyclone (SPA) that drives upwelling forced by southeasterly trade winds channelled along the Andes, and the northward-flowing cold Humboldt Current (E.g. Hartley et al., 2005; Rech et al., 2006).

At present, the southeasterly trade winds are part of the east-west atmospheric circulation (Walker cell). The strength of the trade winds and Walker circulation are mostly controlled by the equatorial sea surface temperature (SST) gradient between the cold surface waters of the eastern Pacific and the western Equatorial Pacific warm pool. During modern-day El Niño (EN) events, when warm waters spread across the Pacific and along the Peruvian shelf and SST is particularly high, trade winds and upwelling weaken, atmospheric stability breaks, and positive rainfall anomalies occur along the northern extension of the Atacama Desert (E.g. Philander, 1990). Such rainfall episodes (E.g. 1982-1983 and 1997-1998) substantially stimulate a profuse growth of vegetation in a normally barren landscape, and increase river discharge (E.g. Holmgren et al., 2006).

Ice core and marine proxy records of the last 800 kyr indicate that the LIG (~125 kyr ago) was characterized by temperatures as warm as or even warmer than at present. Whether the LIG represents a likely scenario for the future, given current global warming, is uncertain. Nevertheless, potential climate and oceanographic responses to a rising in global temperatures may be evaluated by comparison to the LIG (Kukla et al., 2002).

We used molecular fossils (I.e. biomarkers) of marine and terrestrial organisms preserved in organic rich shelf sediments of the highly productive Peruvian coastal upwelling region (Ocean Drilling Program [ODP] Site 1229; 10.98°S, 77.95°W; Figure 6.1) to reconstruct environmental changes during the LIG and compare them to the LH. Our study provides evidence of enhanced rainfall over the northern extension of the Atacama Desert during the LIG associated with a warming of coastal waters and a reduction of zonal SST gradients in the Equatorial Pacific, contrary to the LH which appears to be a dry period linked to enhanced upwelling.

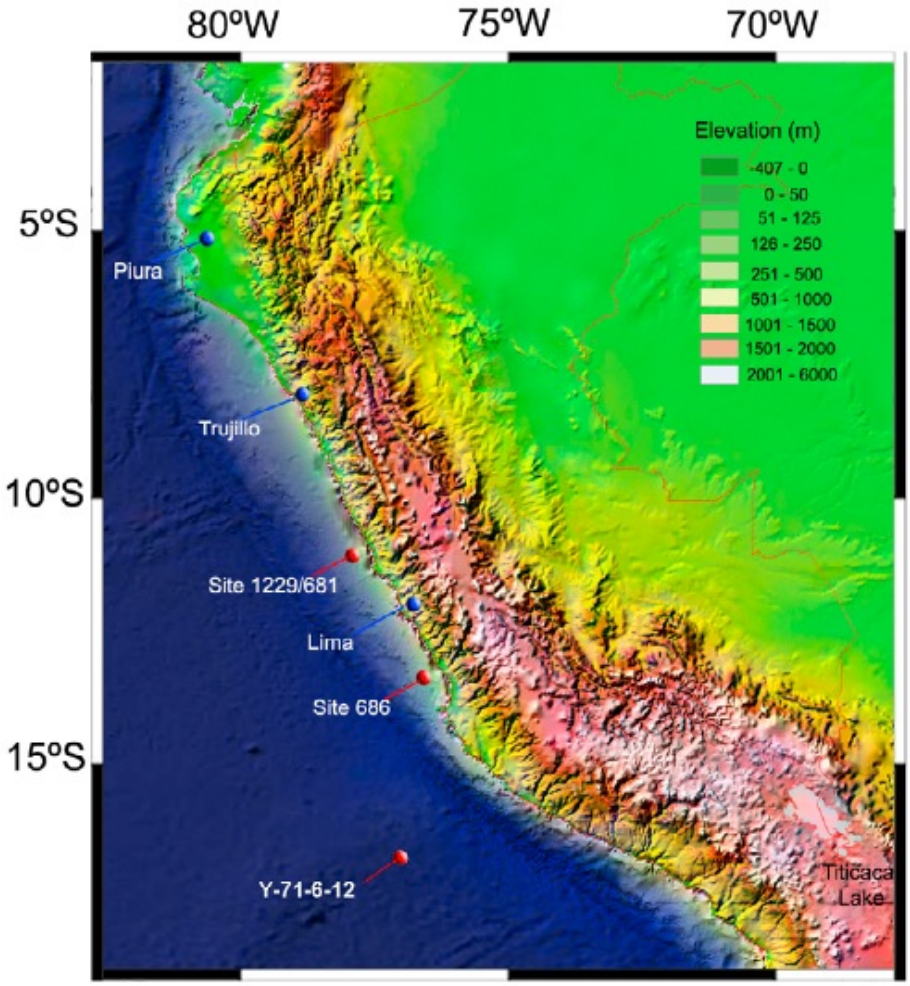

Figure 6. 1 Map showing the location of ODP Site 1229 (re-drilling of Site 681) and South American topography. The location of Site 686 (13.48ºS; 76.89ºW [446m]), where Brodie and Kemp (1994) found evidence for enhanced river input during the last interglacial (LIG), is also indicated. Site Y71-6-12 (16.44ºS; 77.56ºW; [2734m] [Loubere et al., 2003a]) mentioned in the text is also included.

6.2. Data and Methods

We studied the upper 12 meters (past 145 ka) of ODP Site 1229 (151m water depth), a revisit of ODP Site 681. Total organic carbon (TOC) was determined with a Carlo Erba NA-1500 elemental analyzer. Lipids were analyzed and quantified by GC and GC-MS (Trace GC-MS; Thermo Finnigan). Diatoms from discrete sediment samples were identified and counted on permanent microscope slides. Methodological details can be found in the Appendix 2.

Our stratigraphic framework was established by correlating the magnetic susceptibility record from Site 1229E with Site 681B (Appendix 2). The scarce abundance and patchy down core distribution of benthic foraminifera limited the establishment of an age model based on foraminiferal oxygen isotope stratigraphy. Thus, we adopted the published age model of Site 681 (Schrader, 1992) based on the occurrence of unique diatom assemblages and oxygen isotope correlations. The age model (Appendix 2) was refined by radiocarbon dating of the bulk organic fraction of the upper Holocene section (Skilbeck and Fink, 2006). Tuning of our alkenone-based SST record to the one of Site TR163-19 (2.27°N; 90.95°W; Lea et al., 2006) supports the allocation of the LIG (Appendix 2). Given the limitations of the sedimentary record at Site 1229, our discussion focuses only on a comparison of the LIG to the LH, two time intervals separated by more than 100,000 years, and for which we have a reliable age control (Appendix 2).

6.3. Results and Discussion

The record contains a well-preserved LH section (upper 2.3 m) consisting of clay-rich diatomaceous ooze with some depositional unconformities around 2.5 m and 3.5 m (Shipboard Scientific Party, 2003; Site 1229). These unconformities are common on the Peruvian continental shelf around the last glacial/Holocene transition and have been attributed to variations in sea level and upwelling strength (Skilbeck and Fink, 2006; Makou et al., 2010). The LIG is characterized by low sedimentation rates (on average 10 cm kyr^{-1}); while elevated sedimentation rates (70–100 cm kyr^{-1}) were found at the LH (Skilbeck and Fink, 2006). These apparent elevated sedimentation rates are most probably related to enhanced sediment focusing (I.e. syndepositional sediment redistribution by bottom currents) due to increased upwelling strength in the area during the LH (see discussion Appendix 2).

We used the alkenone unsaturation index to reconstruct past SST (Prahl et al., 1988). The transition from MIS 6 to 5 was associated with a ~3°C warming reaching a maximum of 24.5°C during the LIG with SSTs ~2°C warmer than the LH values (Figure 6.2a). A sharp cooling marked the end of the LIG. The mean SST value of the LH of 21.8°C is closer to the modern-day summer average SST value of 23°C than to the winter average value of 18°C (http://podaac.jpl.nasa.gov/). Warm conditions along the eastern tropical Pacific have been previously reported for the LIG (E.g. Lea et al., 2006), and a 2°C warming from MIS 6 to MIS 5 was recorded farther south of our study area, at ~17°S (E.g. Prahl et al., 2006).

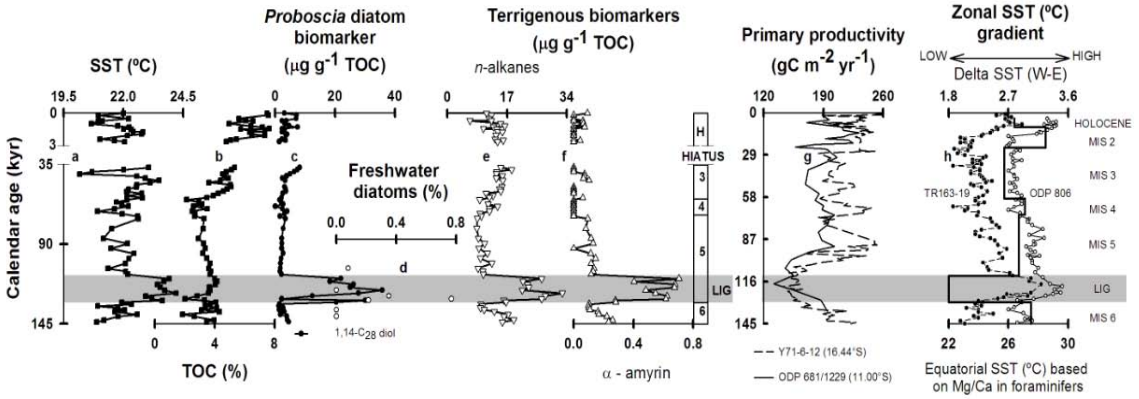

Figure 6. 2 Downcore records of geochemical data from Ocean Drilling Program (ODP) Site 1229E (this study) compared to primary productivity estimates reported for the Peruvian upwelling system and the zonal SST gradient across the equatorial Pacific for the past 145 kyr. **(a)** Reconstructed sea-surface temperature (SST ºC) based on the alkenone unsaturation index, showing ~3°C warming during last interglacial (LIG). **(b)** Percent total organic carbon (TOC). **(c)** Concentration of 1,14 C_{28} alkyl diol, a biomarker for Proboscia diatoms (Sinninghe Damsté et al., 2003); increments in the Proboscia biomarker abundance indicates more stratified water column conditions during the LIG. (**d-f**) Proxies of continental input attributed to rainfall/river runoff; note that they were enhanced during the LIG. Relative abundance of freshwater diatoms **(d)**, sum of C_{25} to C_{35} n-alkanes concentrations mainly derived from leaf waxes **(e)**, and concentrations of α-amyrin derived from angiosperms **(f)**. **(g)** Paleo-estimates of primary productivity (gC m^{-2} yr^{-1}) based on marine diatoms from ODP Site 681 (11°S; same location as ODP Site 1229) (Schrader, 1992), and benthic foraminifer assemblage distributions from core Y71-6-12 (Loubere et al., 2003a). Both records show the lowest primary productivity of the past 145 kyr during the LIG. **(h)** SST reconstructed by Lea et al., (2000) based on Mg/Ca data of planktic foraminifera in the western (Site 806B; 0.32º N 159.37º E [2520m]) and eastern (Site TR163-19; 2.27º N 90.95º W [2348m]) equatorial Pacific over the past 145 kyr. Superimposed is the zonal SST gradient across the equatorial Pacific (solid line) inferred from the difference in SST (Delta SST W-E) between the western and eastern equatorial Pacific. Delta SST was calculated by removing the colder eastern SST from the warmer western SST averages for MIS 6, MIS 5e (LIG), MIS 5 (excluding LIG), MIS 4, MIS 3, and MIS 2. The reduced thermal gradient across the equatorial Pacific can be interpreted as reduced trade winds and weakened Walker circulation during the LIG. Age boundaries were adopted from Martinson et al., (1987). Even and odd numbers on the central panel denote warm interglacial (3 and 5) and glacial (4 and 6) marine isotope stages (MIS) and H indicates late Holocene ([LH] last 3 kyrs). The grey bar across the figure refers to the LIG. All molecular fossil concentrations (µg g^{-1}) were normalized by TOC (µg g^{-1} TOC).

The presence of warm surface waters along the Peruvian coast increases stability in the water column, enhances stratification, and thus, reduces nutrient supply, primary productivity, and ultimately TOC flux to the sediment (Chavez et al., 1999). Overall TOC content varied from 2 to 8% (Figure 6.2b) with lower TOC values (~3.5 %) during MIS 5 than in the LH (>5 %, albeit high variability). These results were interpreted as higher LH export productivity (TOC flux) than during the LIG. Because differential extents of carbon preservation, or sediment focusing may affect TOC contents at Site 1229, we also compare the TOC record with published paleo-productivity estimates based on marine planktonic diatoms and benthic foraminifer assemblages (Figure 6.2g) (Schrader, 1992; Loubere et al., 2003a). These diatom and foraminifer records reveal that the nutrient supply to the eastern Pacific and subsequent primary productivity was substantially diminished during the LIG (Figure 6.2g).

Potential changes in the species composition of the marine plankton were tracked using specific molecular fossils (Appendix 2). High abundances of the lipids 1, 14 C_{28} alkyl diol and 12-hydroxy methyl alkanoates, biomarkers of Proboscia diatoms (Sinninghe Damsté et al., 2003), indicate that Proboscia diatoms were a major constituent of the community during the LIG interval (Figure 6.2c). Both lipid biomarkers (diols) have been originally proposed as indicators for high-nutrient conditions in the monsoonal upwelling of the Arabian Sea. In the highly productive Peru and northern Chile upwelling systems, the diatom genus Chaetoceros (considered an upwelling indicator) dominates the phytoplankton community while Proboscia diatoms increase in abundance during post-upwelling, when the water column is more stratified (Tarazona et al., 2003; Herrera and Escribano, 2006). Thus, we propose that high abundance of Proboscia biomarkers and the high correlation ($r = 0.61$; $n = 49$) with SSTs (Appendix 2) is indicative of enhanced water column stratification over the Peruvian shelf during the LIG (Appendix 2).

Although caution is advised when interpreting the TOC normalized biomarker abundances (see further discussion in Appendix 2) due to the elevated TOC values and sedimentation rates over the LH, non-normalized Proboscia biomarker abundances does not show the same trend and at no other time reach the high levels of the LIG (Appendix 2). Late Holocene accumulation rates of Proboscia biomarkers (e.g. 1,14 C_{28} alkyl diol) were similar to LIG accumulation rates when considering the 10 times higher sedimentation rates and elevated TOC during LH compared with LIG (Appendix 2). We attribute the high LH accumulation mostly to the elevated sedimentation associated to syndepositional sediment redistribution due to enhanced upwelling strength and export productivity instead of higher water column stratification as is the case for the LIG. Our interpretation is in accordance with López-Otálvaro et al. (2008) who used calcareous nannofossil assemblages at ODP Site 1240 (Panama Basin), and suggested a deepening of the nutri-thermocline and a collapse of the upwelling system of the eastern Pacific during the MIS 5e and typically intense eutrophic conditions during the Holocene.

A sudden occurrence of freshwater diatoms (Figure 6.2d) at the LIG onset, and a major rise in terrestrial plant biomarker abundance during the LIG suggest freshwater input by river runoff at Site 1229 (Figures 6.2e, f, and Appendix 2). The total lipid fractions of the shelf sediments contain long-chain (C_{25} to C_{35}) n-alkanes and n-alcohols that are largely derived from leaf waxes of terrestrial plants (Eglinton and Hamilton, 1967), as well as α-amyrin and taraxerol, which are biomarkers for terrestrial angiosperms (Killops and Frewin, 1994). The n-alkanes and n-alcohols can be introduced into the marine environment by both eolian and fluvial input, while α-amyrin and taraxerol are mainly transported by rivers and further redistributed by bottom currents (Volkman et al., 1987). We ascribe the enhanced abundance of terrestrial n-alkanes (Figure 6.2e), n-alcohols (Appendix 2), α-amyrin (Figure 6.2f), and taraxerol (Appendix 2) to riverine transport of terrestrial organic matter to Site 1229 as a direct consequence of

increased rainfall over the northern extension of Atacama Desert during the LIG. These findings are in good agreement with the deposition of coarse and silt-rich sub-millimetre laminae at ODP Site 686 (Peru margin at 13.5ºS, Figure 6.1), whose occurrence was attributed to enhanced river runoff during MIS 5e (Brodie and Kemp, 1994).

In contrast to the LIG setting, the LH is characterized by a lower α-amyrin average accumulation rate (11 μg m^{-2} kyr^{-1} compared to 25 μg m^{-2} kyr^{-1} in the LIG), a higher average accumulation rate of n-alkanes (9955 μg m^{-2} kyr^{-1} versus 1134 μg m^{-2} kyr^{-1} during the LIG), and the absence of taraxerol (Appendix 2). These results, together with colder LH SSTs, imply long-term influence of cold coastal upwelling and drier conditions on land (Figure 6.2). Non-normalized terrestrial biomarker abundances (Appendix 2) also support the interpretation of wetter conditions and higher fluvial input during the LIG versus drier conditions for the LH, especially in view of the absence of taraxerol in LH sediments. We suggest a prevailing eolian source for terrigenous biomarkers during the LH and a primarily fluvial source during the LIG (further discussion in Appendix 2).

Data of Lea et al. (2000) were used to reconstruct the Pacific equatorial west-east thermal gradient during the past 145 kyr, subtracting the colder eastern SST from the warmer western SST (Figure 6.2h). In the modern climate system, this thermal gradient is closely linked to the strength of the trade winds and the Walker circulation (Philander, 1990). Interestingly, the lowest thermal gradient (~1.8°C) corresponds to the LIG. We consider this as indicative of strongly reduced trade winds (weakened Walker circulation), and as a long-term EN-like setting during the LIG. Conversely, the Holocene was characterized by a higher thermal equatorial gradient (Figure 6.2h) suggestive of stronger trade winds affecting ocean temperature and productivity. This is consistent with Loubere et al. (2003b) who suggested the enhancement of trade winds, cooling of surface and thermocline waters, and increased nutrient supply and productivity for the LH when compared with the middle Holocene. Recently, a high resolution sedimentary record at nearby ODP Site 1228 (Makou et al., 2010) revealed strengthened upwelling and productivity with concomitant increases in the predominance of both warm (EN) and cold (LN) phases of the EN Southern Oscillation (SO) during the LH.

Additional support of a long-term EN-like response of the tropical Pacific during the LIG comes from continental climate records (i.e. inland Colombia and the South American Altiplano), which exhibit prolonged dry conditions during modern-day EN years (E.g. Garreaud and Aceituno, 2001; Poveda et al., 2006). Warm and dry conditions in Colombia during the LIG were inferred from a pollen record of Lake Fuquene, Eastern Cordillera of Colombia (van der Hammen and Hooghiemstra, 2003). Studies from Salar Uyuni, Lake Titicaca, and the Huiñaimarca sub-basin also revealed that the most extreme dry event over the last 150 kyr occurred during the LIG (i.e., 130 to 120 kyr) (E.g. Hanselman et al., 2005; Gosling et al., 2008). Moreover, charcoal deposits in north-eastern Australia indicated drought periods around the LIG (Kershaw et al., 2003); enhanced droughts are also typical features of modern-day EN events in Australia (Philander, 1990).

Although there are several indications that "short-term" (i.e. inter-annual to decadal-scale) ENSO variability apparently increased in the LH compared to the middle and early Holocene (i.e. Sandweiss et al., 2001; Tudhope et al., 2001), the long-term pattern seems to behave different. From a "climate-continuum-point-of-view" periods recognized as interglacials are warmer and very similar at glacial-interglacial timescales, especially when compared to the colder glacial periods (i.e. Rincón-Martinez et al., 2010). This apparent similarity is a definition based on the global mean temperature of the earth. However, regionally we might expect considerable differences between interglacials. As shown here, we found two different

regional oceanographic settings in the eastern Pacific resembling a long-term El Niño and La Niña during the LIG and the LH, respectively.

6.4. Conclusions

We provide evidence of increased rainfall and river runoff over the northern extension of the Atacama Desert (Peru) during the LIG. The warm surface waters, enhanced water column stratification, lower primary productivity and wetter conditions of the LIG were probably associated with a long-term response (EN-like) of the tropical Pacific mean state. In contrast, cold coastal upwelling, higher export and primary productivity together with drier conditions on land suggest a different ocean-atmosphere dynamics for the last 3 kyr. Similar oceanographic and climate responses to present day conditions seem to be the result of short-term (centennial-scale) changes in ENSO activity driven by tropical insolation. The more EN-like tropical Pacific conditions of the LIG may not only have contributed to the globally warmer climate during this time interval but may also serve as an analogue for the consequences of ongoing and future global warming.

Acknowledgements

We thank B. B. Jørgensen, G. Leduc, F. Lamy, G. Collins, M. Mohtadi and T. Ferdelman for discussions; the Ocean Drilling Program for providing samples; C.G. Skilbeck and D. Fink for providing ^{14}C data; G. Klockgether, D. Franzke, G. L. Sanchez, and A. Avila for technical support; and A. Montecinos and J. Garcés for suggestions and discussions on an earlier version of the manuscript. The comments and suggestions of two anonymous reviewers are greatly acknowledged. This research was funded by the FONDAP-COPAS Center (Project No. 15010007), and the Max Planck Society. S.C. was funded by CONICYT and DAAD scholarships.

References

- Brodie, I., and Kemp, A. E. S. 1994. Variations in biogenic and detrital fluxes and formation of laminae in late Quaternary sediments from the Peruvian coastal upwelling zone. Marine Geology 116, 385-398.
- Chavez, F. P., et al. 1999. Biological and chemical response of the Equatorial Pacific Ocean to the 1997-98 El Niño. Science 286, 2126-2131.
- Eglinton, G., and Hamilton, R. J. 1967. Leaf epicuticular waxes. Science 156, 1322-1335.
- Garreaud, R., and Aceituno, P. 2001. Interannual rainfall variability over the South American Altiplano. Journal of Climate, 14, 2779-2789.
- Gosling, W. D., Bush, M. B., Hanselman, J. A., and Chepstow-Lusty, A. 2008. Glacial-interglacial changes in moisture balance and the impact on vegetation in the southern hemisphere tropical Andes (Bolivia/Peru). Palaeogeography, Palaeoclimatology, Palaeoecology 259(1), 35-50, doi:10.1016/j.palaeo.2007.02.050.
- Hanselman, J., Gosling, W. D., and Paduano, G. M. 2005. Contrasting pollen histories of MIS 5e and the Holocene from Lake Titicaca (Bolivia/Peru). Journal of Quaternary Science 20(7-8), 663-670, doi:10.1002/jqs.979.
- Hartley, A J., Chong, G., Houston, J., and Mather, A. E. 2005. 150 million years of climatic stability: evidence from the Atacama Desert, northern Chile. Journal of Geological Society London 162, 421-424, doi:10.1144/0016-764904-071.
- Herrera, L., and Escribano, R. 2006. Factors structuring the phytoplankton community in the upwelling site off El Loa River in northern Chile. Journal of Marine Systems 61 (1-2), 13-38, doi:10.1016/j.jmarsys.2005.11.010.
- Holmgren, M., et al. 2006. Extreme climatic events shape arid and semiarid ecosystems. Frontiers of Ecology and the Enviroment 4, 87–95.
- Kershaw, A. P., van der Kaars, S., and Moss, P. T. 2003. Late Quaternary Milankovitch-scale climatic change and variability and its impact on monsoonal Australia. Marine Geology 201, 81-95.

- Killops, S. D., and Frewin, N. L. 1994. Triterpenoid diagenesis and cuticular preservation. Organic Geochemestry 21(12), 1193-1209.
- Kukla, G .J., et al. 2002. Last interglacial climates. Quaternary Research 58, 2-13, doi:10.1006/qres.2001.2316
- Lea, D. W., Pak, D. K., and Spero, H. J. 2000. Climate impact of late Quaternary equatorial Pacific sea surface temperature variations. Science 289, 1719-1724.
- Lea, D. W., Pak, D. K., Belanger, C. L., Spero, H. J., Hall, M. A., and Shackleton, N. J. 2006. Paleoclimate history of Galápagos surface waters over the last 135,000 yr. Quaternary Science Reviews 25 (11-12), 1152-1163, doi:10.1016/j.quascirev.2005.11.010.
- López-Otálvaro, G. -E., Flores, J. -A., Sierro, F. J., and Cacho, I. 2008. Variations in coccolithophorid production in the Eastern Equatorial Pacific at ODP Site 1240 over the last seven glacial–interglacial cycles. Marine Micropaleontology 69, 52–69.
- Loubere, P., Fariduddin, M. and Murray, R. W. 2003a. Patterns of export production in the eastern equatorial Pacific over the past 130,000 years. Paleoceanography 18, 1028-1048.
- Loubere, P., Richaud, M., Liu, Z., and Mekik, F. 2003b. Oceanic conditions in the eastern equatorial Pacific during the onset of ENSO in the Holocene. Quaternary Research 60, 142:148.
- Makou, M. C, Englinton, T. I., Oppo, D. W., and Hughen, K. A. 2010. Postglacial changes in El Niño and La Niña behavior. Geology 38(1), doi: 10.1130/G30366.1.
- Martinson, D. G., Pisias, N. G., Hays, D. J., Imbrie, J., Moore, T. C., and Shackleton, N. J. 1987. Age, dating and the orbital theory of the ice ages: Development of a high resolution 0-300 000-year chronostratigraphy, Quaternary Research, 27(1), 1-29.
- Philander, S. G. H. 1990. El Niño, La Niña and the Southern Oscillation, 293 pp., Academic Press, San Diego, CA.
- Poveda, G., Waylen, P. R., and Pulwarty, R. S. 2006. Annual and inter-annual variability of the present climate in northern South America and southern Mesoamerica. Palaeogeography, Palaeoclimatology, Palaeoecology 234(1), 3-27, doi:10.1016/j.palaeo.2005.10.031.
- Prahl, F., Muehlhausen, L., and Zahnle, D. 1988. Further evaluation of long-chain alkenones as indicators of paleoceanographic conditions. Geochimica et Cosmochimica Acta 52, 2303-2310.
- Prahl, F. G., Mix, A. C., and Sparrow, M. A. 2006. Alkenone paleothermometry: Biological lessons from marine sediment records off western South America. Geochimica et Cosmochimica Acta 70, 101-117, doi:10.1016/j.gca.2005.08.023.
- Rech, J. A., Currie, B. S., Michalski, G., and Cowan, A. M. 2006. Neogene climate change and uplift in the Atacama Desert, Chile. Geology 34(9), 761-764, doi:10.1130/G22444.1.
- Rincón-Martinez et al. 2010. More humid interglacials in Ecuador during the past 500 kyr linked to latitudinal shifts of the equatorial front and the Intertropical Convergence Zone in the eastern tropical Pacific. Paleoceanography 25, doi: 10.1029/2009PA001868.
- Rundel, P. W., Dillon, M. O., Palma, B., Mooney, H. A., Gulmon, S. L., and Ehleringer, J. R. 1991. The phytogeography and ecology of the coastal Atacama and Peruvian deserts, Aliso 13, 1-49.
- Sandweiss, D. H., et al. 2001. Variation in Holocene El Niño frequencies: Climate records and cultural consequences in ancient Peru. Geology 29, 603-606.
- Schrader, H. 1992. Peruvian coastal primary palaeo-productivity during the last 200000 years, in Upwelling Systems: Evolution since the Early Miocene, edited by Summerhayes, C.P., Prell, W.L., and Emeis, K.C., 391-410pp., The Geological Society, London.
- Shipboard Scientific Party. 2003. Site 1229, in D'Hondt, S.L., Jørgensen, B.B., Miller, D.J., et al., Proc. ODP, Init. Repts., 201: College Station, TX (Ocean Drilling Program), 1–78. doi:10.2973/odp.proc.ir.201.110.2003
- Sinninghe Damsté, J. S., et al. 2003. A diatomaceous origin for long-chain diols and mid-chain hydroxy methyl alkanoates widely occurring in Quaternary marine sediments: Indicators for high-nutrient conditions. Geochimica et Cosmochimica Acta 67, 1339-1348.
- Skilbeck, C. G., and Fink, D. 2006. Data report: radiocarbon dating and sedimentation rates for Holocene–upper Pleistocene sediments, eastern equatorial Pacific and Peru continental margin, In Jørgensen, B.B., D'Hondt, S.L., and Miller, D.J. (Eds.), Proc. ODP, Sci. Results, 201: College Station, TX (Ocean Drilling Program), 1–15. doi:10.2973/odp.proc.sr.201.108.2006
- Tarazona, J., Gutiérrez, D., Paredes, C., and Indacochea, A. 2003. Overview and challenges of marine biodiversity research in Peru. Gayana 67, 206-231.
- Tudhope, A. W., et al. 2001. Variability in the El Niño Southern Oscillation Through a Glacial-Interglacial Cycle. Science 291, 1511-1517.

- Van der Hammen, T., and Hooghiemstra, H. 2003. Interglacial-glacial Fuquene-3 pollen record from Colombia: an Eemian to Holocene climate record. Global Planetary Change 36, 181-199.
- Volkman, J. K., Farrington, J. W., and Gagosian, R. B. 1987. Marine and terrigenous lipids in coastal sediments from the Peru upwelling region at 15°S: Sterols and triterpene alcohols. Organic Geochemestry 11(6), 463-477.
- Wyrtki, K. 1975. El Niño-The Dynamic Response of the Equatorial Pacific Ocean to Atmospheric Forcing. Journal of Physics Oceanography 5, 572-584.

CHAPTER 7

LATE QUATERNARY GLACIAL-INTERGLACIAL CLIMATE VARIABILITY OF WESTERN SOUTH AMERICA INFERRED FROM EOLIAN DUST AS PRESERVED IN MARINE SEDIMENTS

Cornelia Saukel[a*], Frank Lamy[a], Jerry McManus[b,c], Daniel Rincón Martinez[a], Jan-Berend W. Stuut[d,e], Gisela Winckler[b,c], Ralf Tiedemann[a]

[a]Alfred-Wegener-Institute for Polar and Marine Research (AWI), Postfach 12 01 61, 27568 Bremerhaven, Germany (Frank.Lamy@awi.de; Ralf.Tiedemann@awi.de)

[b]Lamont-Doherty Earth Observatory of Columbia University, Palisades, New York, USA (jmcmanus@ldeo.columbia.edu; winckler@ldeo.columbia.edu)

[c]Department of Earth and Environmental Sciences, Columbia University, New York, NY, USA

[d]NIOZ – Royal Netherlands Institute for Sea Research, P.O. Box 59, 1790 AB Den Burg, The Netherlands (Jan-Berend.Stuut@nioz.nl)

[e] Marum - Center for Marine Environmental Sciences, Leobener Straße, 28359 Bremen, Germany

*Corresponding Author: Cornelia Saukel, tel: +49(0)471-4831-2120, fax: +49(0)471-4831-1923, e-mail: cornelia.saukel@awi.de

Abstract

The investigation of ocean-atmosphere linkages in the southeastern tropical Pacific allows inferences about continental climate variability in western South America. While previous studies mostly concentrated on paleoceanographic features, we focus our work on reconstructing changes in eolian transport and trade-wind strength. Measurements of independent dust proxies at Ocean Drilling Program (ODP) Site 1237 off the coast of southern Peru reveal higher supply of eolian dust during glacials than during interglacials of the past 500 ka. These results are in accordance with dust flux data from the eastern equatorial Pacific at 110°W (ODP Site 849). While glacial dust fluxes are twice as high as during interglacials at Site 1237, grain-size characteristics do not vary on glacial-interglacial time scales, but remain rather constant, indicating no distinct changes in mean wind speed or direction. From these results we infer changes in continental aridity and southeast trade-wind vigor during the late Pleistocene. A change in the extent of the dust source regions (the Atacama Desert in northern Chile and the coastal deserts of Peru) due to a varying vegetation cover and a meridional shift of the atmospheric circulation system of the Southeast Pacific as well as enhanced gustiness are the driving forces for the glacial-interglacial variability of dust input during the past 500 ka. Our results necessitate a re-interpretation of previous dust studies of the equatorial east Pacific that originally suggested increased terrigenous supply during interglacials to be of eolian origin. While findings from the equatorial East Pacific reveal enhanced fluvial input from northwestern-most South America during wetter interglacials, our data suggest increased eolian-derived terrigenous supply during drier glacials from the arid areas south of 3°S.

7.1 Introduction

The variability of western South American climate history is tightly connected to changes in the atmosphere-ocean circulation system of the southeastern Pacific (Markgraf et al., 2000; Cane, 2005), which in turn is largely dependent on the regional topography of the Andean mountain range. The regional climate is further linked to a number of interacting factors including (1) the latitudinal sea surface temperature (SST) gradient in the South Pacific along the west coast of South America, (2) the moisture balance, controlled by SSTs and evaporation in the South Pacific, (3) the El Niño - Southern Oscillation (ENSO) variability, (4) the latitudinal position of the Intertropical Convergence Zone (ITCZ), and (5) the intensity and direction of the Southeast (SE) trade winds.

The large-scale atmospheric circulation in the tropical Pacific consists of two deep overturning circulation cells, the Hadley (meridional) cell, the near-surface component of which is represented by the trade winds, and the Walker (zonal) cell, which is associated with the East-West oceanographic asymmetry. Surface winds, which control upwelling, the tilt of the thermocline, and thus the formation of the cold tongue in the Eastern Pacific, depend on changes in the Walker and Hadley cells (Reiter, 1979; Pierrehumbert, 2000). The resulting connection between surface winds and sea surface temperatures is the key to comprehending the behavior of the ocean-atmosphere coupled system.

South American climate reconstructions have been based on diverse but - compared to other continents – relatively sparse paleoclimate marine and continental records. Those studies partially reveal contradicting results concerning the relation of the five factors mentioned above on glacial-interglacial timescales. For example, some authors conclude that drier conditions in northern and central South America during glacials can be attributed to a stronger meridional SST gradient and a more northern position of the ITCZ (E.g. Martinez et al., 2003; Rincón-Martínez et al., 2010), resembling a La Niña setting. Other studies suppose a southward displacement of the ITCZ (E.g. Rea et al., 1986; Broccoli et al., 2006), implying

wetter conditions with weakened SE trade winds during glacials (Boven and Rea, 1998) and a more El Niño-like situation (Koutavas et al., 2002; Koutavas and Lynch-Stieglitz, 2003).

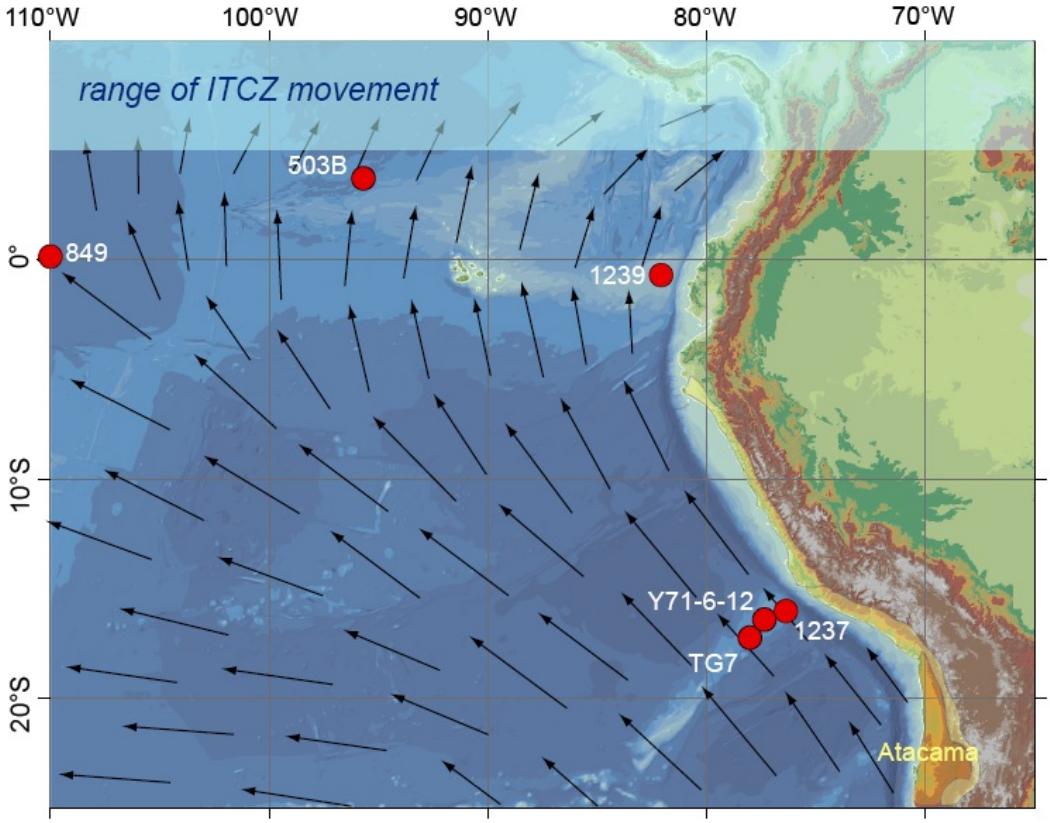

Figure 7. 1 Study area. Red dots show core locations discussed in the text, black arrows indicate the direction of the dominant wind field. The light blue bar represents the meridional range of the seasonal ITCZ movement. The orange and yellow shadings represent the (hyper-) arid core and the (semi-) arid parts of the Atacama Desert and Peru coastal deserts, respectively.

In this respect, winds and their transport of dust play a key role in the understanding of glacial-interglacial changes in the southeast Pacific and the adjacent continent as the atmospheric circulation system responds to and modulates the effects of continental and oceanographic changes. While larger (smaller) mean grain sizes can be an indication of increased (decreased) wind speeds (E.g. Sarnthein et al., 1981; Janecek and Rea, 1985), the abundance of eolian-derived deep-sea sediments also allows inferences about changes in the environmental and climatic conditions of the dust source area (E.g. Clemens, 1998). Mineral dust preserved in marine sediments is thus a useful proxy to reconstruct both climate-related changes of the atmospheric circulation pattern as well as periods of continental aridity vs. humidity (E.g. Kohfeld and Harrison, 2001; Stuut et al., 2002; Maher et al., 2010).

While the paradigm of greater dust fluxes during glacials compared to interglacials on a global scale has been widely accepted (E.g. Mahowald et al., 1999; Kohfeld and Harrison, 2001; Bauer and Ganopolski, 2010), this inference and its implications have been more controversial in the equatorial (South)-East Pacific. Rea et al. (1986; 1994) and Olivarez et al. (1991) found higher dust fluxes during interglacials in the eastern equatorial Pacific (DSDP 503B at 4°N, 95.6°W, Figure 7.1) implying dry interglacial periods with enhanced atmospheric circulation and wet glacial periods accompanied by weaker atmospheric circulation in central and northern South America. Analogous to these findings, Rea (1994) interpreted higher siliciclastic input at site Y71-6-12 (16.26°S, 77°23°W; close to our core site) just before and during glacials as increased hemipelagic input and thus wetter climate conditions. Chuey et al. (1987) on the other hand,

found enhanced eolian mass accumulation rates during glacials in the central equatorial Pacific (RC11-210 at 1.82°N, 140°W) between 800 ka and 300 ka before present and inferred drier conditions in the source areas of northwestern South America, but no significant change in wind intensities as seen in grain-size variability. Anderson et al. (2006) investigated a transect of sediment cores across the equator at the same longitude, revealing maximum dust fluxes also during glacials of the past 300 ka. Winckler et al. (2008) found an increase in dust flux by a factor of 2.5 during glacials compared to interglacials since 500 ka ago consistently throughout the equatorial Pacific, corroborating the global view of greater dust flux during cold stages.

Here we present new proxy data from Ocean Drilling Program (ODP) site 1237 drilled on the easternmost flank of Nazca Ridge, 140 km offshore (16.11°S, 76.37°W; 3212m water depth), covering the past 500 ka. Its position below the path of eolian transport from the Atacama Desert and close to the arid coasts of Peru, but west of the deep-sea trench provides an excellent opportunity to reconstruct eolian input due to its undisturbed and complete sediment record (Mix et al., 2003). Our data represent the only continuous dust record from the southeast Pacific south of 5°S covering the last 500 ka. The approach of using multiple proxies including grain-size distributions, Th-isotopes, and the geochemical composition of the sediment allows us to differentiate between changes in wind intensities and climatic changes in the source areas (E.g. Rea et al., 1985; Olivarez et al., 1991). We compare our record to previously published dust flux data from the equatorial Pacific (Winckler et al., 2008) and to a multiproxy climate reconstruction at ODP Site 1239 located on Carnegie Ridge off Ecuador, constraining latitudinal shifts of the ITCZ on glacial-interglacial timescales (Rincón-Martínez et al., 2010).

7.2 Materials and Methods

The age model of site 1237 is based on a benthic $\delta^{18}O$ record tied to the chronology of the LR04 isotope stratigraphy of Lisiecki and Raymo (2005), applying the Analyseries software (Paillard, 1996). Ba-counts of the XRF-scans were used for fine-tuning the age model (Appendix 3). The lack of sample material between 3.3 – 7.4 mcd (80 – 240 ka) at Site 1237 was compensated for by using samples from pre-site survey core RRV9702A-69PC (16.01°S, 76.33°W). The latter was aligned to ODP Site 1237 using magnetic susceptibility data from both cores (Appendix 3).

The siliciclastic content of ODP Site 1237 sediments represents the percentage of bulk sediment after subtracting measured percentages of biogenic opal, carbonate, and organic matter (TOC). The biogenic opal content (wt %) was determined with an automated leaching method, following procedures outlined in Müller and Schneider (1993). TOC and total carbon contents were analyzed with the LECO technique and a CNS elemental analyzer, respectively, before calculating $CaCO_3$ contents, following standard methods (E.g. Rincón-Martínez et al., 2010). The chemical composition of the sediment was analyzed applying X-ray fluorescence scanning (XRF) (Aavatech 2nd generation XRF Scanner at the Alfred-Wegener-Institute, Bremerhaven (AWI)) and Inductively Coupled Plasma – Optical Emission Spectrometry (ICP-OES in the Geochemistry Department at AWI). We scanned the split sediment cores in 1 cm intervals corresponding to a time-resolution of 300 – 800 years. Iron XRF counts were calibrated to absolute concentrations determined by ICP-OES on 35 samples (cf. Rincón-Martínez et al., 2010).

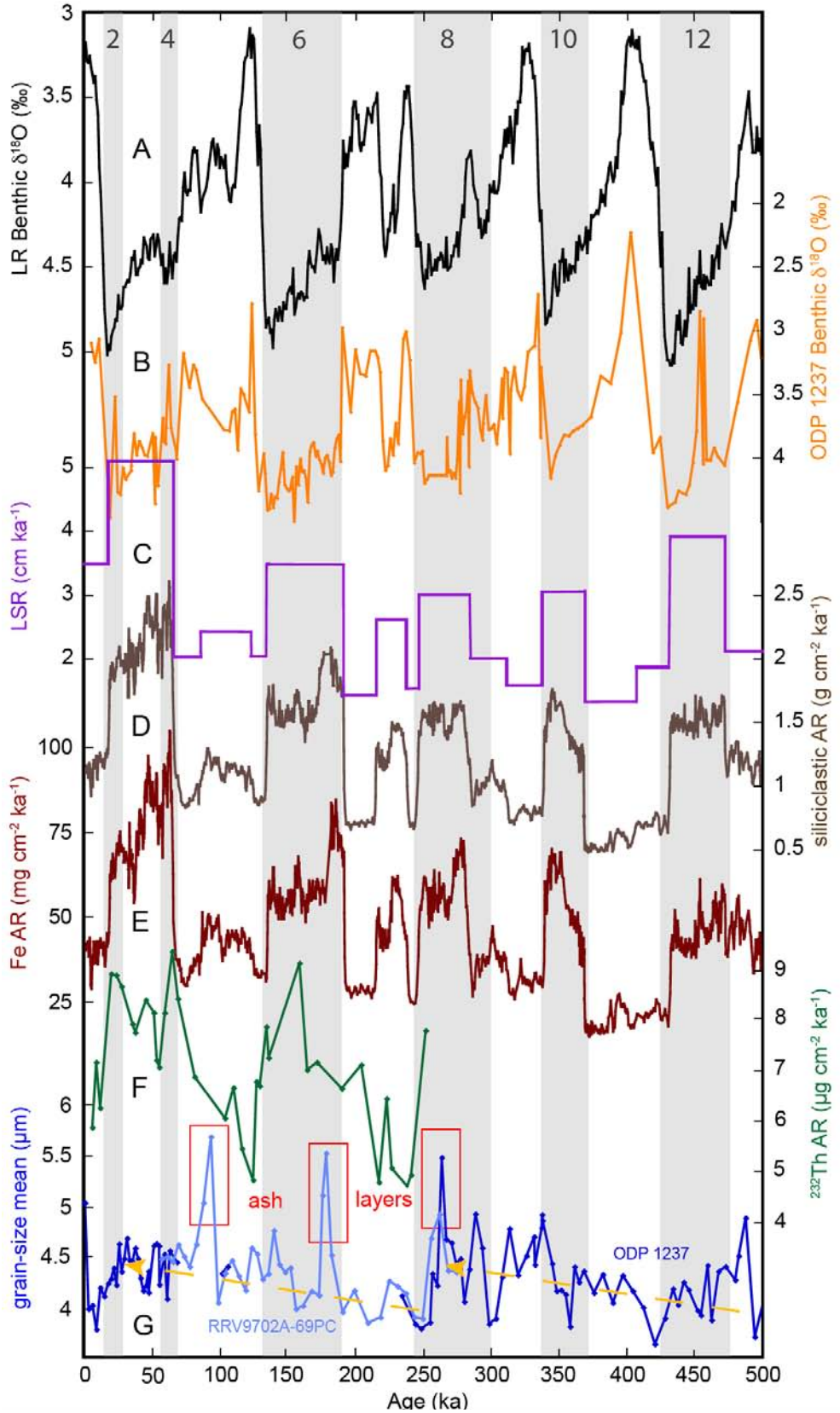

Figure 7. 2 Records of eolian-derived sediment input to ODP site 1237 over the last 500 ka. **(A)** Benthic oxygen isotope stack (Lisiecki and Raymo, 2005), **(B)** Benthic oxygen isotope record of ODP site 1237, **(C)** Linear sedimentation rates (LSR, cm ka^{-1}), **(D)** siliciclastic accumulation rates (AR, g cm^{-2} ka^{-1}), **(E)** Iron accumulation rates (Fe AR, mg cm^{-2} ka^{-1}), **(F)** ^{232}Thorium flux (µg cm^{-2} ka^{-1}), **(G)** Mean grain size of siliciclastic sediment fraction (µm).

Linear sedimentation rates (LSR, in cm ka^{-1}) were derived from the age model and multiplied by the dry bulk density (DBD in g cm^{-3}) obtained from borehole logging data at site 1237 (Mix et al., 2003) to calculate accumulation rates (MAR, in g $cm^{-2}ka^{-1}$) of individual sediment components.

The fine fractions (<63µm) of a total of 35 samples were analyzed for thorium and uranium isotopes by isotope dilution Inductively Coupled Plasma Mass Spectrometry. Fluxes were calculated using the ^{230}Th profiling method (e.g., Bacon 1984, Francois et al., 2004) to compare to the AR derived from the age model.

Dust mass fluxes were calculated from common thorium (^{232}Th) according to Winckler et al. (2008), ^{232}Th being a trace element enriched in continental crust (E.g. McGee et al., 2007). Additional measurements of 4 bulk sediment samples were conducted to test the influence of grain-size separation on Th-isotope concentrations (cf. Kretschmer et al., 2010; McGee et al., 2010; Appendix).

We measured the grain-size distribution of the terrigenous siliciclastic sediment fraction with a Beckman-Coulter Laser Particle Sizer. To isolate the terrigenous sediment fraction, we followed the methods of Stuut et al. (2007) for the removal of other, mainly biogenic constituents.

7.3 Results

LSRs largely determine accumulation rates of the individual sediment components at our site (Figures 7.2c-e). Ca-contents are higher during glacials, while siliciclastic contents are higher during interglacials (see Appendix) to avoid dilution effects; we calculated accumulation rates (ARs) as the better proxy. This resulted in siliciclastic and iron (Fe) ARs that are increased by factors of 2-3 during glacials compared to interglacials (Figures 7.2d, e and Appendix). Glacial stages 4 and 6 start out with highest accumulation rates of the terrigenous siliciclastic fraction. There seems to be a general decreasing trend throughout MIS 3. In order to have an age-model independent measure of dust accumulation rates, we determined the ^{232}Th- and Fe-fluxes to the ocean floor by applying the ^{230}Th-normalization method (E.g. Bacon, 1979; Francois et al., 2004). Age-model dependent ARs are usually limited in temporal resolution and integrated over time intervals between age control points, assuming a constant accumulation rate over each interval, which, however, cannot be ascertained (Francois et al., 2004; Loubere et al., 2004). In contrast, the ^{230}Th-normalization method gives accumulation rates for discrete points in time. Even though absolute values of ^{230}Th-normalized Fe-fluxes reach only 35 - 65% of the values obtained by age-model dependent AR calculations (Figure 7.2f), results also suggest a twofold-increased input of siliciclastic material during glacials compared to interglacials and corroborate the general trend as seen in the age-model dependent MARs. Loubere et al. (2004) also found very variable calcite accumulation rates for sediments from the equatorial East Pacific comparing the different MAR-approaches, where one explanation could be sediment redistribution leading to focusing during glacials. Focusing factors at ODP Site 1237 average approximately 2 (not shown) and vary within a few tens of percent throughout the time interval in consideration. Sediment focusing could explain the observed 35 - 65 % difference in the accumulation of bulk and constituent sediments at the study site obtained by the two methods. The combined results, however, provide a robust basis for paleoclimate interpretations, since the general trend and the amplitudes of the terrigenous input obtained by the two independent methods compare very well (Figure 7.3d).

In contrast to the variability in siliciclastic input, grain-size means (Figure 7.2g) do not vary on orbital or glacial-interglacial time-scales but remain rather constant between 3.7 and 5µm,

except of 3 outlying peaks >5.5µm, representing sediment core sections contaminated by volcanic ash. However, grain-size means do increase on a longer timescale, from 500 ka to 260 ka, when they drop to <4µm, only to slightly increase again from ~250 ka until ~30 ka, before another drop below 4µm at ~9 ka.

7.4 Discussion

7.4.1 Changes in dust flux on glacial-interglacial cycles

The data set presented in Figure 7.2 is the first record obtained from below the major dust-transporting wind field in the southeast Pacific close enough to the source area to record changes in dust supply and wind intensity (Figure 7.1). Silt-sized material deposited in areas within a few hundred kilometers offshore is considered more reliable in recording these changes than the clay-sized fraction (E.g. Sarnthein et al., 1981; Tiedemann et al., 1989), which is the only fraction documented at the core locations of previous studies further offshore. The disadvantage of a study site as close to the coast as ODP Site 1237 is the hemipelagic sediment component one would usually expect, and which would contaminate the eolian input signal (E.g. Weltje and Prins, 2003; Weltje and Prins, 2007). However, we can rule out a hemipelagic component in the sediments of ODP cores 1237 as the site is located offshore, an area where no major, but only seasonal rivers drain into the Pacific. Furthermore, the South American deep-sea trench represents a barrier catching the fluvial material from the minor, ephemeral rivers of southern Peru, making winds the most probable transport agent of the terrigenous fraction (E.g. Krissek et al., 1980; Saukel et al., 2011).

Changes in MARs of dust provide a comprehensive picture of changes in the intensity of the dust cycle, including source, transport and deposition (Kohfeld and Tegen, 2007). Two different methods of calculating accumulation rates consistently show a 2-3-time increase of siliclastic material during glacials compared to interglacials at our site. Fe MARs calculated from LSRs and DBD show the same trend and amplitude of our ^{232}Th-dust record (Figures 7.2e, f). Our records generally support the idea of dustier glacials compared to interglacials, in agreement with different modeling results for the last glacial maximum (LGM, E.g. Mahowald et al., 1999; Lunt and Valdes, 2002; Werner et al., 2002) and, in particular, support earlier results from the equatorial east Pacific (E.g. Winckler et al., 2008).

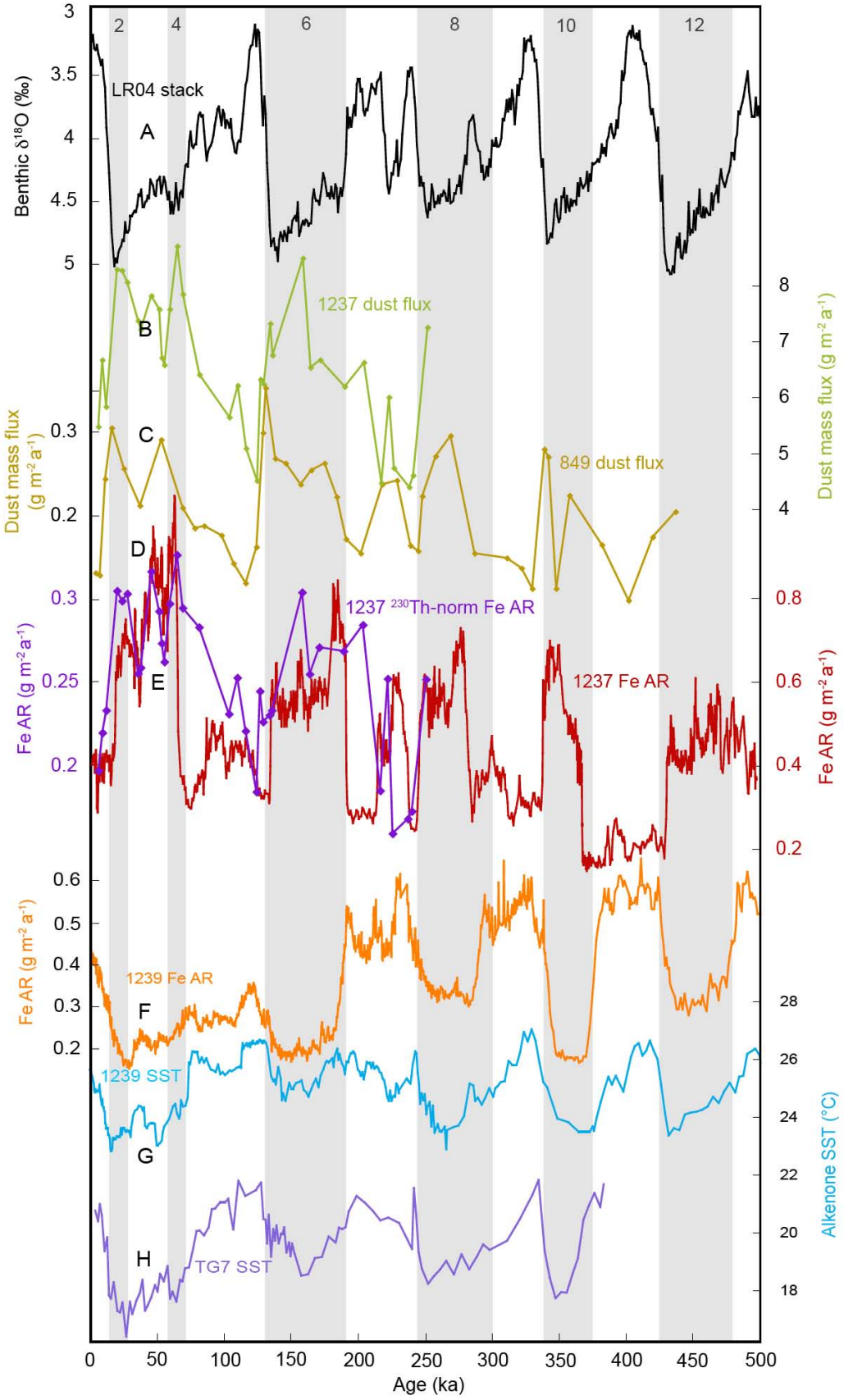

Figure 7. 3 Comparison of eolian flux records in relation to SST records. **(A)** Benthic oxygen isotope stack (Lisiecki and Raymo, 2005), **(B)** Dust flux of ODP Site 1237 (g m^{-2} a^{-1}) **(C)** Dust flux of ODP site 849 (g m^{-2} a^{-1}), B and C are calculated by dividing by the average ^{232}Th concentration of upper continental crust, **(D)** Iron accumulation rates (Fe AR, mg cm^{-2} ka^{-1}) of ODP Site 1237, **(E)** ^{230}Th-normalized iron flux at ODP Site 1237, **(F)** Iron accumulation rates (Fe AR, mg cm^{-2} ka^{-1}) of ODP Site 1239 (Rincón-Martínez et al., 2010), **(G)** Alkenone sea surface temperatures (SST, °C)

heavily influenced by the equatorial front, ODP Site 1239 (Rincón-Martínez et al., 2010), **(H)** Alkenone sea surface temperatures (SST, °C) off southern Peru, TG7 (Calvo et al., 2001). High values of dust fluxes are positively correlated with cool SSTs of the cold tongue and global ice volume, while enhanced fluvial input is accompanied by warmer SSTs.

The dust flux trends of ODP Site 1237 and Site 849 (Winckler et al., 2008), which is situated downwind from our core location (Figure 7.1), fit very well in the location of their minima and maxima (Figures 7.3b,c), even though they were measured in differing temporal resolution. The study sites are fed by the same dust source: the Atacama Desert of northern Chile and the coastal deserts of southern Peru. Dust fluxes at Site 1237 are 30 times those measured at Site 849, which can be explained by the proximal position of core 1237 relative to the distal core 849. Given the large distance between the cores, the coherence of the dust flux records between the two sites is surprisingly good, supporting the hypothesis of a common source and supporting our assumption that hemipelagic sedimentation plays a minor role at site 1237, if at all. Since the hemipelagic contribution to the terrigenous sediment component is negligible at our study site, the derived proxy record allows a re-interpretation of previously published data. We propose the signal found by Rea (1994) for site Y71-6-12 (close to our site) not to record hemipelagic deposition as suggested by the author, but to record continental dust from the arid and semi-arid regions of western South America with maximal supply just before (related to their age model) and during glacials.

Several scientists proposed higher dust fluxes in the tropical east Pacific during interglacials instead of during glacials. Rea et al. (1986) and Olivarez et al. (1991) interpreted their results to represent more arid conditions during the warm stages in northwestern South America. Our results clearly oppose this hypothesis. According to Rincón-Martínez et al. (2010), terrigenous input during interglacials at ODP Site 1239 (Figures 7.1 and 7.3) was increased due to enhanced precipitation that fed fluvial runoff in northwestern South America. We propose to alternatively interpret the higher terrigenous input at site 503B (4.05°N, 95.63°W, Figure 7.1) during interglacials (Rea et al., 1986; Rea, 1994) as a consequence of wet deposition below the ITCZ, which is then shifted to a more southern location, rather than as increased dust supply due to more arid conditions on land as proposed by Rea et al. (1986) and Rea (1994). According to Hovan (1995) and McGee et al. (2007) wet deposition below the ITCZ increases the accumulation rate of dust in comparison to core locations north or south of the tropical rainbelt. This dependency would explain the increased deposition of dust at site 503B during interglacials. In contrast, higher terrigenous input at core location V19-29 (3.58°S, 83.93°W) during glacials (Rea, 1994), in our opinion, represents enhanced dust supply from the coastal deserts and the Atacama Desert because of the study site's position south of the Equatorial Front and south of the area influenced by wet deposition. Furthermore, it is too far west to receive any fluvial material originating from the Gulf of Guayaquil that is transported with ocean surface currents in a northward direction.

7.5 Climate variability of western South America inferred from continental dust during the past 500 Ka

7.5.1 Continental aridity

Dust flux is often used as a proxy for climate change in terms of aridity and the extent of vegetation cover (E.g. Clemens, 1998). Changes in the source areas in terms of vegetation cover are also the most important factor for the increased dust supply during the LGM according to modeling studies by Mahowald et al. (1999; 2006) and Dan Lunt (University of Bristol, personal communication). Latorre et al. (2002) suggest dry conditions on the margin of the Atacama Desert during the LGM from the analysis of rodent midden. Our data support the

idea of enlarged semi-arid areas surrounding the Atacama Desert during all glacials due to decreased precipitation and vegetation cover on the western slopes of the central Andes in Peru and Chile as well as the coastal areas of Peru. If glacials can be interpreted as analogous to persistent La Niña-like conditions (E.g. Andreasen and Ravelo, 1997; Andreasen et al., 2001; Martinez et al., 2003), which prevail in austral winter, arid conditions predominated in the Atacama Desert and its eastern bordering areas due to reduced moisture transport from the south (E.g. Houston, 2006). Less precipitation then lead to a reduced vegetation cover and thus a larger potential dust entrainment area on the western Andean slopes. Glacial sea-level low-stands additionally exposed the comparably narrow but noteworthy shelf areas on the west coast of South America, also contributing to an extension of the source areas. At the same time, wetter conditions in the generally arid to semi-arid Altiplano lead to a higher dust production there and at its eastern rim. Bobst et al. (2001) reconstructed relatively wet periods in the Salar de Atacama from 75.7 to 60.5 ka, and from 53.4 to 15.3 ka, with the most humid phase from 26.7 to 60.7 ka. Those phases correspond to peaks in the ^{230}Th-normalized dust flux record from ODP Site 1237 (Figure 7.3).

However, the extension of the desert in an eastern direction is limited by the Andean mountain range and is insufficient to explain a two- to threefold increase in dust flux due to the limitation in area. A spatial extension of the desert is more likely conceivable in a north-southern direction, towards southern Ecuador and central Chile. This latitudinal extension, however, cannot be recorded at a single core site.

7.5.2 Wind intensities and direction

In order to investigate whether enhanced wind speeds during glacials were responsible for the increased dust supply, we additionally analyzed the grain-size distributions of the land-derived sediment fraction. Because of increased meridional SST gradients that would imply stronger winds during the cold stages (Figures 7.3f, h) one would expect the dust grain-size distributions to record changes in wind intensities (E.g. Lindzen and Nigam, 1987) in terms of coarser grain-size means during glacials and finer means during interglacials, as found off west Africa by Sarnthein et al. (1981). However, we don't recognize this relationship for the SE Pacific in our data (Figure 7.2g). By comparing our dust flux data to SSTs of Site TG7 (Calvo, 2001) and ODP Site 1239 (Rincón-Martínez et al., 2010), we can distinguish a clear co-occurrence of cooler (warmer) SSTs of the cold tongue and increased (decreased) dust accumulation rates (Figures 7.3b, f-h). Meridional SST gradients within the cold tongue (ODP Site 1239 – TG7) change in a glacial-interglacial pacing, the gradient being 4 - 5°C during interglacials and 6 - 7°C during glacials (Figures 7.3b, f-h). While dust mass flux depicts considerable changes on glacial-interglacial time scales (Figures 7.2d, e, f), grain-size means suggest only minor changes in mean wind intensities on longer time scales during the past 500 ka. Evidence of slight increases in wind velocity is recognized between 500 and 250 ka and also between 250 to 21 ka (Figure 7.2g), when grain-size means suddenly decrease. According to Kohfeld and Tegen (2007), higher surface wind speeds in source areas can cause enhanced dislocation of smaller as well as larger particles compared with particle sizes dislocated at lower wind speeds. In other words, the mean/mode can remain unchanged while there is a change in intensity of the entraining winds. We thus cannot exclude an increase in wind speeds during glacials, but simply don't see it recorded at our core location.

The modeled transport of mass and energy within the winter hemisphere Hadley cell intensifies as the ITCZ is moved meridionally (E.g. Lindzen and Hou, 1988), either due to changes in insolation or due to the variability inherent to the atmosphere-ocean system, I.e. tropical SSTs. A longitude-independent Hadley circulation is typical for the Pacific because of its wide ocean basin reducing longitudinal variation of the atmospheric circulation

(Pierrehumbert, 2000). Analogous to the southern hemisphere (SH) winter, evidence for a glacial northward shift of the atmospheric circulation system in the southeast Pacific comes from several different studies of the southern Westerlies (E.g. Stuut and Lamy, 2004; Kaiser et al., 2005; Toggweiler, 2009), as well as the ITCZ (E.g. Martin et al., 1997; Rincón-Martinez et al., 2010). Wind intensities comprise both the meridional (*v*) and zonal (*u*) wind components. Reiter (1979) suggested an extratropical trigger event to activate a self-enforcing feedback between the meridional trade-wind components *v*, the Hadley cell intensity, and precipitation. As the subtropical anticyclone moves further to the north, it weakens but allows $v_{Southern\ Hemisphere\ (SH)}$ to increase in the east Pacific, extending into the northern hemisphere, without necessarily influencing the behavior of the zonal wind component u_{SH} (Reiter, 1979). Because of the southern Peruvian coast bending in a northwestern direction, the Andes constrict the airflow on the eastern flank of the anticyclone and accelerate it (Hay, 1996). In this respect, our dust flux data support the idea of MARs reflecting changes in wind intensities. As the meridional component (v_{SH}) is enhanced, the capacity (dust load) of the southeast trade winds is increased, without necessarily changing the grain-size spectrum of the dust load. It remains questionable if the outlined mechanisms together with the limited extensions of the desert areas are sufficient to increase the supply in dust during the glacials by a factor of 2-3.

Additional enhanced gustiness during the cold stages (E.g. McGee et al., 2010) seems to be the most reasonable explanation for this increase, if we consider all our proxies and atmospheric circulation evidence taken together. McGee et al. (2010) found that enhanced gustiness in dust source areas appeared contemporaneous to greater meridional temperature gradients during glacial periods (as shown above), while mean wind speeds did not change considerably. More frequent dust outbreaks over enlarged source areas during cold periods then explain the amplitudes in dust supply to the ocean during the past 500 ka. Given that generally greater wind speeds are reflected by coarser grain-size distributions, it is obvious why we do not see coarser grain-size distributions during glacials, because possible wind speed changes in single events would not be revealed by grain-size distributions of samples comprising sedimentation of several hundreds of years.

7.6. Summary and Conclusions

The results of this study demonstrate that western South America, south of the Gulf of Guayaquil, was more arid during glacials and more humid during interglacials of the past 500 ka, corroborating the general idea of globally dustier glacials vs. more humid interglacials. Our findings seem to contradict earlier studies of South American continental climate presenting a wetter Altiplano during glacials (E.g. Thompson et al., 1998). However, these contrasting observations can be reconciled by considering that this situation corresponds to a typical La Niña-like austral winter season (Houston, 2006), when moisture transport from Atlantic sources to the eastern Andes is increased (cf. Garreaud et al., 2003) while it is reduced from the Pacific sources, resulting in much drier arid areas on the western slopes during the cold stages. During glacials, dust source areas around the Atacama were enlarged, the atmospheric circulation system including the ITCZ of the southeast Pacific was located further to the north, and the meridional wind component and accordingly the Hadley cell were intensified. This led to an increased capacity, I.e. dust load, of the southeast trade winds.

The southeast trade wind system intensified only slightly and slowly between 500 and 250 ka and again between 250 ka and the LGM, but without glacial-interglacial cyclicity. This is in contrast to findings in an analogous study area off the southwestern coast of Africa (Namibia) from Stuut et al. (2002), who recognized stronger southeast trade winds during glacials compared to interglacials.

The fact that grain sizes do not reveal increases in wind speed, the limited extension of the source areas, and the non-changing wind direction due to the Andean mountain range strongly argues for enhanced gustiness during the glacials as another important mechanism for the 2-3 fold increase in dust accumulation rates at ODP Site 1237.

Future regional modeling and investigations of SST gradients along the South American west coast and of the dust entraining processes in the source area will further elucidate our hypotheses.

Acknowledgements

We thank Alan Mix for providing sample material from core RRV9702A-69PC. We thank Roseanne Schwartz (LDEO), Ingrid Stimac and Ilsetraut Stölting (AWI) for technical support in the laboratory and Marty Fleisher (LDEO) for ICP-MS analyses; Sven Kretschmer for helpful discussion and comments. This study was supported by the Deutsche Forschungsgemeinschaft (DFG).

References

-Anderson, R.F., Fleisher, M.Q., and Lao, Y., (2006), Glacial-interglacial variability in the delivery of dust to the central equatorial Pacific Ocean. Earth and Planetary Science Letters, 242, 406, doi:10.1016/j.epsl.2005.11.061.

-Andreasen, D.J., Ravelo, A.C., and Broccoli, A.J., (2001), Remote forcing at the last glacial maximum in the tropical Pacific ocean. Journal of Geophysical Research, 106, 879-897, doi:10.1029/1999JC000087.

-Andreasen, D.J., and Ravelo, A.C.,(1997), Tropical Pacific ocean thermocline depth reconstructions for the last glacial maximum. Paleoceanography, 12 (3), 395-413, doi:10.1029/97PA00822.

-Bacon, M.P., (1984), Glacial to interglacial changes in carbonate and clay sedimentation in the Atlantic Ocean estimated from ^{230}Th measurements, Chemical Geology, 2,97–111.

-Bauer, E., and Ganopolski, A. (2010), Aeolian dust modeling over the past four glacial cycles with CLIMBER-2, Global and Planetary Change, v.74, p.49-60, doi:10.1016/j.gloplacha.2010.07.009.

-Bobst, A.L., Lowenstein, T.K., Jordan, T.E., Godfrey, L.V., Ku, T.-L., and Luo, S., (2001), a 106 ka paleoclimate record from drill core of the Salar de Atacama, northern Chile: Palaeogeography, Paleoclimatology, Palaeoecology, 173, 21-42.

-Boven, K.L., and Rea, D.K., 1998, Partitioning of eolian and hemipelagic sediment in eastern Equatorial Pacific core TR 163-31B and the late Quaternary paleoclimate of the Northern Andes. Journal of Sedimentary Research, 68, 850-855.

-Broccoli, A.J., Dahl, K.A., and Stouffer, R.J., (2006), Response of the ITCZ to Northern Hemisphere cooling, Geophysical Research Letters, 33, L01702, doi:10.1029/2005GL024546.

-Calvo, E., Pelejero, C., Herguera, J.C., Palanques, A., and Grimalt, J.O., 2001, Insolation dependence of the southeastern subtropical Pacific sea surface temperature over the last 400 kyrs, Geophysical Research Letters, 28, 2481 p., doi:10.1029/2000GL012024.

-Cane, M.A., (2005), The evolution of El Niño, past and future, Earth and Planetary Science Letters, 230, 227 p., doi:10.1016/j.epsl.2004.12.003.

-Chuey, J.M., Rea, D.K., and Pisias, N.G., (1987), Late Pleistocene paleoclimatology of the central equatorial Pacific: A quantitative record of eolian and carbonate deposition. Quaternary Research, 28, 323 p., doi:10.1016/0033-5894(87)90001-9.

-Clemens, S.C., (1998), Dust response to seasonal atmospheric forcing: Proxy evaluation and calibration. Paleoceanography, 13, no.5, 471-490, doi:10.1029/98PA02131.

-Francois, R., Frank, M., Rutgers van der Loeff, M.M., and Bacon, M.P., (2004), ^{230}Th normalization: An essential tool for interpreting sedimentary fluxes during the late Quaternary, Paleoceanography, 19, p. PA1018, doi:10.1029/2003PA000939.

-Garreaud, R., Vuille, M., Clement, A.C., (2003), The climate of the Altiplano: observed current conditions and mechanisms of past changes, Palaeogeography, Palaeoclimatology, Palaeoecology, 194, 5 p., doi:10.1016/S0031-0182(03)00269-4.

-Hay, W.W., (1996), Tectonics and climate. Geologische Rundschau, 85, 409-437.
-Hovan, S. A., (1995), Late Neogene atmospheric circulation intensity and climatic history recorded by eolian deposition in the eastern equatorial Pacific, Proc. ODP, Scientific Results, 138: College Station, TX (Ocean Drilling Program), 615-625.
-Houston, J., (2006), Variability of precipitation in the Atacama Desert: its causes and hydrological impact, International Journal of Climatology, 26, 2181 p., 1097-0088, doi: 10.1002/joc.1359.
-Janecek, T.R., Rea, D.K., (1985), Quaternary fluctuations in the northern hemisphere trade winds and westerlies, Quaternary Research, 24, 150-163.
-Kaiser, J., Lamy, F., and Hebbeln, D., (2005), A 70-kyr sea surface temperature record off southern Chile (Ocean Drilling Program Site 1233), Paleoceanography, 20, PA4009.0883-8305, doi:10.1029/2005PA001146.
-Kohfeld, K.E., and Harrison, S.P., (2001), DIRTMAP: the geological record of dust, Earth-Science Reviews, 54, 81 p., doi:10.1016/S0012-8252(01)00042-3.
-Kohfeld, K.E., and Tegen, I., (2007), Record of Mineral Aerosols and Their Role in the Earth System. In: H.D. Holland and K. Turekian (eds.), Treatise on geochemistry, Elsevier.
-Koutavas, A., and Lynch-Stieglitz, J., (2003), Glacial-interglacial dynamics of the eastern equatorial Pacific cold tongue-Intertropical Convergence Zone system reconstructed from oxygen isotope records, Paleoceanography, 18, 1089 p., doi:10.1029/2003PA000894.
-Koutavas, A., Lynch-Stieglitz, J., Marchitto, T.M., Jr., and Sachs, J.P., (2002), El Nino-Like Pattern in Ice Age Tropical Pacific Sea Surface Temperature, Science, 297, 226-230. doi:10.1126/science.1072376.
-Kretschmer, S., Geibert, W., Rutgers van der Loeff, M.M., and Mollenhauer, G., (2010), Grain size effects on $^{230}Th_{xs}$ inventories in opal-rich and carbonate-rich marine sediments, Earth and Planetary Science Letters, 294, 131 p., doi:10.1016/j.epsl.2010.03.021.
-Latorre, C., Betancourt, J.L., Rylander, K.A., Quade, J., (2002), Vegetation invasions into absolute desert: A 45000 yr rodent midden record from the Calama – Salar de Atacama basins, northern Chile (lat 22° - 24°S), Geological Society of America Bulletin, 114, 349 p., doi:10.1130/0016-7606.
-Lawrence, K.T., Liu, Z., and Herbert, T.D., (2006), Evolution of the Eastern Tropical Pacific Through Plio-Pleistocene Glaciation, Science, 312, 79-83. doi:10.1126/science.1120395.
-Lindzen, R.S., and Nigam, S., (1987), On the Role of Sea Surface Temperature Gradients in Forcing Low-Level Winds and Convergence in the Tropics, Journal of Atmospheric Sciences, 44 (17), 2418-2436.
-Lindzen, R.S., and Hou, A.V., (1988), Hadley Circulations for Zonally Averaged Heating Centered off the Equator, Journal of the Atmospheric Sciences, 45, 2416 p., doi:10.1175/1520-0469.
-Loubere, P., Mekik, F., Francois, R., Pichat, S., (2004), Export fluxes of calcite in the eastern equatorial Pacific from the Last Glacial Maximum to present, Paleoceanography, 19,PA2018, doi:10-1029/2003PA000986.
-Lisiecki, L.E., and Raymo, M.E., (2005), A Pliocene-Pleistocene stack of 57 globally distributed benthic $\delta^{18}O$ records, Paleoceanography, 20, PA1003, doi:10.1029/2004PA001071.
-Lunt, D.J, and Valdes, P.J., (2002), Dust deposition and provenance at the Last Glacial Maximum and present day, Geophysical Research Letters, 29, 2085 p.,doi:10.1029/2002GL015656.
-Maher, B.A., Prospero, J.M., Mackie, D., Gaiero, D., Hesse, P.P., and Balkanski, Y., (2010), Global connections between aeolian dust, climate and ocean biogeochemistry at the present day and at the last glacial maximum, Earth-Science Reviews, 99, 61 p., doi:10.1016/j.earscirev.2009.12.001.
-Mahowald, N.M., Muhs, D.R., Levis, S., Rasch, P.J., Yoshioka, M., Zender, C.S., and Luo, C., (2006), Change in atmospheric mineral aerosols in response to climate: Last glacial period, preindustrial, modern, and doubled carbon dioxide climates, Journal of Geophysical Research, 111, D10202.0148-0227, doi:10.1029/2005JD006653.
-Mahowald, N., Kohfeld, K., Hansson, M., Balkanski, Y., Harrison, S.P., Prentice, I.C., Schulz, M., and Rodhe, H., (1999), Dust sources and deposition during the last glacial maximum and current climate: A comparison of model results with paleodata from ice cores and marine sediments, Journal of Geophysical Research, 104, 15895 p., doi:10.1029/1999JD900084.
-Markgraf, V., Baumgartner, T.R., Bradbury, J.P., Diaz, H.F., B. Dunbar, R., Luckman, B.H., Seltzer, G.O., Swetnam, T.W., and Villalba, R., (2000), Paleoclimate reconstruction along the Pole-Equator-Pole transect of the Americas (PEP 1), Quaternary Science Reviews, 19, 125 p., doi:10.1016/S0277-3791(99)00058-X.
-Martin, L., Bertaux, J., CorrËge, T., Ledru, M.-P., Mourguiart, P., Sifeddine, A., SoubiËs, F., Wirrmann, D., Suguio, K., and Turcq, B., (1997), Astronomical Forcing of Contrasting Rainfall Changes in Tropical South

America between 12,400 and 8800 cal yr B.P, Quaternary Research, 47, 117 p., doi:10.1006/qres.1996.1866.
-Martinez, I., Keigwin, L., Barrows, T.T., Yokoyama, Y., Southon, J., (2003), La Niña-like conditions in the eastern equatorial Pacific and a stronger Choco jet in the northern Andes during the last glaciations, Paleocenaography, 18 (2), 1033p., doi:10.1029/2002PA000877.
-McGee, D., Marcantonio, F., and Lynch-Stieglitz, J., (2007), Deglacial changes in dust flux in the eastern equatorial Pacific, Earth and Planetary Science Letters, 257, 215p.,0012-821X, doi: 10.1016/j.epsl.2007.02.033.
-McGee, D., Broecker, W.S., Winckler, G., (2010), Gustiness: The driver of glacial dustiness?, Quaternary Science Reviews, 29, 2340-2350, doi:10.1016/j.quascirev.2010.06.009.
-Mix, A.C., Tiedemann, R., Blum, P. (eds.), (2003), Proc. ODP, Initial Reports Leg 202: College Station, TX, Ocean Drilling Program, 1-107, doi:10.2973/odp.proc.ir.202.2003.
-Müller, P.J., and Schneider, R., (1993), An automated leaching method for the determination of opal in sediments and particulate matter: Deep Sea Research Part I, Oceanographic Research Papers, 40, 425 p., doi:10.1016/0967-0637(93)90140-X.
-Olivarez, A.M., Owen, R.M., and Rea, D.K., (1991), Geochemistry of eolian dust in Pacific pelagic sediments: Implications for paleoclimatic interpretations, Geochimica et Cosmochimica Acta, 55, 2147 p., doi:10.1016/0016-7037(91)90093-K.
-Paillard, D., (1996), Macintosh Program performs time-series analysis, Eos Trans.
-Pierrehumbert, R.T., (2000), Climate change and the tropical Pacific, The sleeping dragon wakes: PNAS, 97, 1355-1358.
-Rea, D.K., (1994), The paleoclimatic record provided by eolian deposition in the deep sea, The geologic history of wind: Review of Geophysics, 32, 159p., doi:10.1029/93RG03257.
-Rea, D.K., Chambers, L.W., Chuey, J.M., Janecek, T.R., Leinen, M., and Pisias, N.G., (1986), A 420,000-year record of cyclicity in oceanic and atmospheric processes from the eastern equatorial Pacific, Paleoceanography, 1, 577p., doi:10.1029/PA001i004p00577.
-Rea, D.K., Leinen, M., and Janecek, T.R., (1985), Geologic Approach to the Long-Term History of Atmospheric Circulation, Science, 227, 721-725. doi:10.1126/science.227.4688.721.
-Reiter, E.R., (1979), Trade-Wind Variability, Southern Oscillation, and Quasi-Biennial Oscillation, Archiv für Meteorologie, Geophysik und Bioklimatologie, 28, 113p.
-Rincón-Martinez, D., Lamy, F., Contreras, S., Leduc, G., Bard, E., Saukel, C., Blanz, T., Mackensen, A., and Tiedemann, R., (2010), More humid interglacials in Ecuador during the past 500 kyr linked to latitudinal shifts of the equatorial front and the Intertropical Convergence Zone in the eastern tropical Pacific, Paleoceanography, 25, PA2210. doi:10.1029/2009PA001868.
-Sarnthein, M., Tetzlaff, G., Koopmann, B., Wolter, K., and Pflaumann, U., (1981), Glacial and interglacial wind regimes over the eastern subtropical Atlantic and North-West Africa, Nature, 293, 193p. doi:10.1038/293193a0.
-Saukel, C., Lamy, F., Stuut, J.-B., Tiedemann, R., Vogt, C., (2011), Distribution and provenance of wind-blown SE Pacific surface sediments, Marine Geology,280, 130-142, doi:10.1016/j.margeo.2010.12.006.
-Stuut, J. B.W., Prins, M.A., Schneider, R.R., Weltje, G.J., Jansen, J.H.F., and Postma, G., (2002), A 300-kyr record of aridity and wind strength in southwestern Africa, inferences from grain-size distributions of sediments on Walvis Ridge, SE Atlantic: Marine Geology, 180, 221.0025-3227, doi:10.1016/S0025-3227(01)00215-8.
-Stuut, J. B.W., and Lamy, F., (2004), Climate variability at the southern boundaries of the Namib (southwestern Africa) and Atacama (northern Chile) coastal deserts during the last 120,000 yr, Quaternary Research, 62, 301.0033-5894, doi: 10.1016/j.yqres.2004.08.001.
-Stuut, J. B.W., Kasten, S., Lamy, F., and Hebbeln, D., (2007), Sources and modes of terrigenous sediment input to the Chilean continental slope, Quaternary International, 161, 67p., doi:10.1016/j.quaint.2006.10.041.
-Tiedemann, R., Sarnthein, M., Stein, R., (1989), Climatic changes in the western Sahara: Aeolo-marine sediment record of the last 8 million years (Sites 657-661), Proceedings ODP, Scientific results, 108, 241p.
-Thompson, L.G., Davis, M.E., Mosley-Thompson, E., Sowers, T.A., Henderson, K.A., Zagorodnov, V.S., Lin, P.N., Mikhalenko, V.N., Campen, R.K., Bolzan, J.F., Cole-Dai, J., and Francou, B., (1998), A 25,000-Year Tropical Climate History from Bolivian Ice Cores, Science, 282, 1858p. 10.1126/science.282.5395.1858.

-Toggweiler, J.R., (2009), CLIMATE CHANGE: Shifting Westerlies, Science, 323, 1434-1435, doi: 10.1126/science.1169823.
-Werner, M., Tegen, I., Harrison, S.P., Kohfeld, K.E., Prentice, I.C., Balkanski, Y., Rodhe, H., and Roelandt, C., (2002), Seasonal and interannual variability of the mineral dust cycle under present and glacial climate conditions, Journal of Geophysical Research, 107, 4744p. doi:10.1029/2002JD002365.
-Weltje, G.J., and Prins, M.A., (2007), Muddled or mixed? Inferring palaeoclimate from size distributions of deep-sea clastics, Sedimentary Geology, 162, 39.0037-0738, doi: 10.1016/S0037-0738(03)00235-5.
-Weltje, G.J., and Prins, M.A., (2003), Genetically meaningful decomposition of grain-size distributions, Sedimentary Geology, 202, 409.0037-0738, doi: 10.1016/j.sedgeo.2007.03.007.
-Winckler, G., Anderson, R.F., Fleisher, M.Q., McGee, D., and Mahowald, N., (2008), Covariant Glacial-Interglacial Dust Fluxes in the Equatorial Pacific and Antarctica, Science, 320, 93p., doi:10.1126/science.1150595.

CHAPTER 8

INVESTIGATING THE BIOGEOCHEMICAL CYCLES AND PRIMARY PRODUCTIVITY CHANGES IN THE EASTERN EQUATORIAL PACIFIC DURING THE PLIOCENE-PLEISTOCENE CLIMATE TRANSITION

Johan Etourneau[a,b*], Daniel Rincón Martinez[c], Philippe Martinez[d], Frank Lamy[c], Thomas Blanz[a], Cornelia Saukel[c], Ralf Tiedemann[c] and Ralph Schneider[a]

[a]Institut für Geowissenschaften Universität Kiel, Ludewig-Meyn-Str. 10, D-24118 Kiel, Germany (je@gpi.uni-kiel.de; schneider@gpi.uni-kiel.de; tbl@gpi.uni-kiel.de)

[b]LOCEAN, CNRS/UPMC/IRD/MNHN – UMR7159, 4 Place Jussieu, 75252 Paris, France (johan.etourneau@locean-ipsl.upmc.fr)

[c]Alfred-Wegener-Institute for Polar and Marine Research (AWI), Postfach 12 01 61, 27568 Bremerhaven, Germany (Frank.Lamy@awi.de; Ralf.Tiedemann@awi.de)

[d]UMR 5805 EPOC – OASU Site de Talence Université Bordeaux 1, Avenue des Facultés 33405, Talence Cedex, France (p.martinez@epoc.u-bordeaux1.fr)

*Corresponding Author: Johan Etourneau, e-mail: je@gpi.uni-kiel.de; johan.etourneau@locean-ipsl.upmc.fr

Abstract

Over the last 3 million years (Ma), the climate switched from a Pliocene warm period to a Pleistocene glacial world. This major climate transition was accompanied by a global reorganization of the oceanic and atmospheric circulations impacting on both biogeochemical cycles and primary productivity. Investigating changes in nutrient cycling and biological production in upwelling areas is of paramount interest as it may affect in turn global climate. Here, we compare two new high resolution records of downcore nitrogen isotopes ($\delta^{15}N$) along with primary productivity and sea surface temperature proxies at two strategically located Ocean Drilling Program (ODP) Sites 1239 and 1240 of the Eastern Equatorial Pacific (EEP). Our results clearly show that variations in nutrient cycling in the EEP are the result of complex mechanisms including local, regional and global processes. At the million-year timescale, the two EEP $\delta^{15}N$ records synchronously shifted at 2 Ma probably due to the intensification of denitrification along the eastern South American margins in response to changes in the Southern Ocean circulation, the development of the polar frontal system and the resulting reduced oxygenation of water masses, later resurfacing in the EEP and the South American denitrifying zones. After removing denitrification effects, we found that overall the $\delta^{15}N$ in the EEP experienced similar values over the last 3 Ma, relatively low since the Pliocene with a minimum during the productivity maximum period and the coolest temperature around 2 Ma. This implies that nitrate - an essential nutrient for biological productivity - was likely sufficiently supplied in the EEP surface waters as today to have supported high productivity levels since ~3 Ma. In comparison, iron (Fe) measurements revealed a close relationship with productivity changes. We suggest that Fe inputs from South America have probably regulated phytoplankton activity in the EEP and likely served as fertilizer to trigger the most productive periods since the Pliocene. Variation in Fe content was probably controlled by changes in cold tongue intensity, position of the equatorial front and Intertropical convergence zone modifying the precipitation conditions and continental erosion.

8.1 Introduction

The warm Pliocene epoch (5-3 Ma ago) is often cited as a good analogue for the near future climate because of its striking resemblance with the predictions of the 'Intergovernmental Panel on Climate Change' (IPCC) for the next decades. The Pliocene oceanic surface temperatures were 3-4°C warmer than today (E.g. Ravelo et al., 2004), sea level was about 5-40 meters higher (E.g. Dwyer and Chandler, 2009), atmospheric CO_2 concentrations were similar or slightly higher (~330-415 ± 50 ppmv) (E.g. Pagani et al., 2010; Seki et al., 2010; Tripati et al., 2009), and ice-sheets were mostly restricted to Antarctica (Raymo et al., 2006). However, from 3-2.8 Ma ago, the Earth's climate underwent a major transition from a warm and relative stable state towards cooler conditions marked by large amplitude glacial/interglacial cycles and widespread ice-sheets in the northern hemisphere. The causes and consequences of this global climate shift are still uncertain and numerous hypotheses have been proposed. They include the interaction of several mechanisms tied to oceanic and atmospheric circulations (E.g. Etourneau et al., 2010; Wara et al., 2005), tectonic (E.g. Karas et al., 2009), greenhouse gases (E.g. Tripati et al., 2009; Pagani et al., 2010; Seki et al., 2010), earth's orbital changes (E.g. Lisiecki and Raymo, 2005), biological activity and biogeochemical processes (E.g. Liu et al., 2008). One of the leading hypotheses explaining the global Plio-Pleistocene climate cooling refers to greenhouse gas forcing. According to some recent proxy based studies, a pronounced decrease in atmospheric CO_2 is recorded synchronously to the late Pliocene/early Pleistocene cooling (E.g. Tripati et al., 2009; Pagani et al., 2010; Seki et al., 2010). These recent results would explain model outputs indicating that a large decrease in CO_2 over the Plio-Pleistocene transition was probably the main cause of prominent ice sheet

extension in the high latitudes, especially over Greenland (Lunt et al., 2009). However, the reasons explaining this global CO_2 shift remains unclear.

In this context, exploring the biogeochemical cycles and productivity changes in upwelling regions, where 80% of the modern marine productivity is concentrated, becomes of primary importance. This holds particularly true for the Eastern Equatorial Pacific (EEP) upwelling system where the new EEP production is estimated to account for 18% of the global new production (Chavez and Toggweiler, 1995). Today, the EEP is known as a 'high-nutrient low-chlorophyll' (HNLC) region (Thomas, 1972). Micro-nutrients like nitrate (NO_3) are not fully utilized in the EEP photic zone because diatoms and other primary producers are limited by certain micro-nutrients such as iron (Fe) and silicic acid ($Si(OH_4)$) (Brzezinski et al., 2011). Over the past, variations in EEP productivity, nutrient cycling and hydrological conditions have been longstanding investigated, especially for the last climatic cycles (E.g. Farrell et al., 1995; Pichevin et al., 2009; Robinson et al., 2009), but remains poorly known at a million-year timescale despite drastic climatic changes underwent in this region since the Pliocene. It has been recently demonstrated that the Plio-Pleistocene climate transition was accompanied in the equatorial Pacific by a switch from an El Niño-like to La Niña-like climatic pattern tied to changes of climate conditions in Polar Regions (E.g. Wara et al., 2005; Brierley et al., 2009; Etourneau et al., 2010). This transition likely corresponded to significant changes in terms of wind circulation, precipitation and upwelling intensity, impacting on the primary productivity in the EEP.

Only few studies paralleled EEP biological production and SST changes through the Plio-Pleistocene climate transition (E.g. Cortese et al., 2004; Lawrence et al., 2006; Dekens et al., 2007). They all witnessed a period of greatly enhanced productivity in this region between 3 and 1.8 Ma, mainly attributed to the upwelling of cold nutrient-rich waters (E.g. Dekens et al., 2007) derived from water masses arising from the Southern Ocean and North Pacific (E.g. Cortese et al., 2004; Lawrence et al., 2006). This high-to-low latitude nutrient exchange would have controlled the biological production. Owing to the development of the oceanic frontal zone in the polar oceans 2 Ma ago, the nutrient leakage would have ceased and limited the regional phytoplankton production (E.g. Liu et al., 2008). However, in these recent investigations, nutrient cycling, the main factor controlling EEP primary productivity, has been poorly investigated. Here, we aim to fill this gap by reconstructing the evolution of the primary productivity, biogeochemical cycles and oceanic conditions from two new ODP (Ocean Drilling Program) sites, both situated in the equatorial upwelling system, in order to disentangle the different processes regulating the EEP system since 3.2 Ma.

8.2 The bulk sedimentary $\delta^{15}N$

To reconstruct the nutrient cycling in the EEP over the last 3.2 Ma, we used the $\delta^{15}N$ signal in deep-sea sediment. This proxy basically records the degree of fixed nitrogen (mostly nitrates, NO_3^-) utilization by the phytoplankton, which corresponds to the fraction of bioavailable N taken by the primary producers during the photosynthesis. The lighter nitrogen isotope (^{14}N) is preferentially incorporated into phytoplankton, thus leaving the ambient seawater enriched in the heavier isotope (^{15}N). The degree of depletion determines the magnitude of isotopic signature, following Rayleigh fractionation kinetics. However, the $\delta^{15}N$ of organic matter buried in the sediment can also be influenced by the isotopic character of the regional N pool, which is mainly controlled by two bacterial processes: fixation of atmospheric N_2 and denitrification of dissolved nitrate.

N fixation is the main source of bioavailable N in the modern ocean. This process involves N_2-fixing microorganisms (*Bacteria*, *Archea* and *Cyanobacteria*) (Karl et al., 2002), which under warm and stratified water conditions, convert the atmospheric N_2 in fixed N. This fixed N can also be consumed by some nitrifying bacteria converting it into nitrite (NO_2^-) and nitrate (NO_3^-) as nitrification processes. The N fixation hardly discriminates ^{15}N versus ^{14}N, resulting in similar $\delta^{15}N$ values of the organic matter buried in the sediment and those found in the atmosphere (~0 ‰) (Brandes and Devol, 2002).

In contrast to N fixation, the denitrification process, the main N loss in the global ocean, occurs under suboxic water column conditions (<2-5 µM O_2) (Codispoti et al., 2005) and corresponds to bacteria-mediated reduction reaction that convert nitrates (NO_3^-) to nitrite (NO_2^-) to nitrous oxide (N_2O), and to nitrogen gas (N_2). Changes in water column denitrification could be driven by the interplay between variations in local productivity, leading to a change in remineralization rates and oxygen drawdown, and changes in ocean circulation and ocean temperature, resulting in variations of the physical supply of dissolved oxygen. While several studies emphasize the importance of variations in biological productivity (E.g. Altabet et al., 1995; Altabet et al., 2002; Ganeshram et al., 2002), others highlight the role of variable oxygen supply due to changes in upper ocean ventilation (E.g. Behl and Kennett, 1996; Galbraith et al., 2004). Contrary to N fixation and nitrate uptake, the denitrification leads to isotopically heavier residual nitrate, and consequently to typical heavy sedimentary $\delta^{15}N$ values (from 5 to 30 ‰). This is because denitrification occurs within a broad isotopic fractionation producing isotopically light N_2 and N_2O that are mainly lost to the atmosphere (E.g. Cline and Kaplan, 1975; Liu and Kaplan, 1989).

8.3 Oceanographic settings and biogeochemistry

The EEP surface waters are mainly influenced by three ocean currents: the South Equatorial Current (SEC), the North Equatorial Countercurrent (NECC), and the Equatorial Undercurrent (EUC) (Figure 8.1). The SEC is an upper-layer geostrophic current that flows westward and is mainly the continuation of the Peru-Chile, or Humboldt, Current (PCC) (Kessler et al., 2005). The latter comprises the coastal upwelling system off Peru where subsurface waters of the Gunther Undercurrent (GUC) upwell. The GUC corresponds to the lower branch of the EUC. The EUC circulate either into the GUC or seasonally upwells along the equator where convergent trade winds force the thermocline to shoal. The waters feeding the EUC have a minor northern hemisphere source and a more dominant (50-70%) southern hemisphere source (Rodgers et al., 2003; Dugdale et al., 2004). The southern hemisphere contribution is mainly derived from Subantarctic Mode Waters (SAMW) and Antarctic Intermediate Waters (AAIW) formed in the subtropical and subantarctic convergence zones, respectively.

In the modern EEP, the convergent trade winds from both northern and southern hemispheres cause divergent upwelling along the equator, which is accompanied by the rising of cold water from below the thermocline to the surface (Kessler, 2006). The shallow thermocline in the EEP mainly results from the zonal gradients in sea level pressure and SST across the equatorial Pacific, which strengthen the trade winds, and hence the upwelling in the EEP. In contrast, the thermocline in the western equatorial Pacific (WEP) is deep and warm waters from above the thermocline upwells when trade wind strengthen. The east-to-west SST asymmetry between the warm WEP and the cold EEP leads to a zonal atmospheric circulation pattern, referred to as Walker circulation (Cane, 1986). The Walker circulation is further strengthened as far as the EEP cooling and the west-to-east SST gradient increase. In addition to the equatorial upwelling, the cooling of EEP surface water can be further accentuated by the upwelling off Peru. Seasonally controlled by strong offshore trade winds, themselves governed by the meridional

atmospheric circulation, or Hadley circulation, the coastal Peru upwelling participate in a strongly developed cold tongue, spreading off the Peruvian margin and extending towards 110°W, and therefore to an enhanced Walker circulation. Inversely, when both equatorial and coastal upwelling in the eastern tropical Pacific (EEP and Peru) weaken, the EEP surface water warms, the zonal SST gradient along the equatorial Pacific decreases and the Walker circulation weaken.

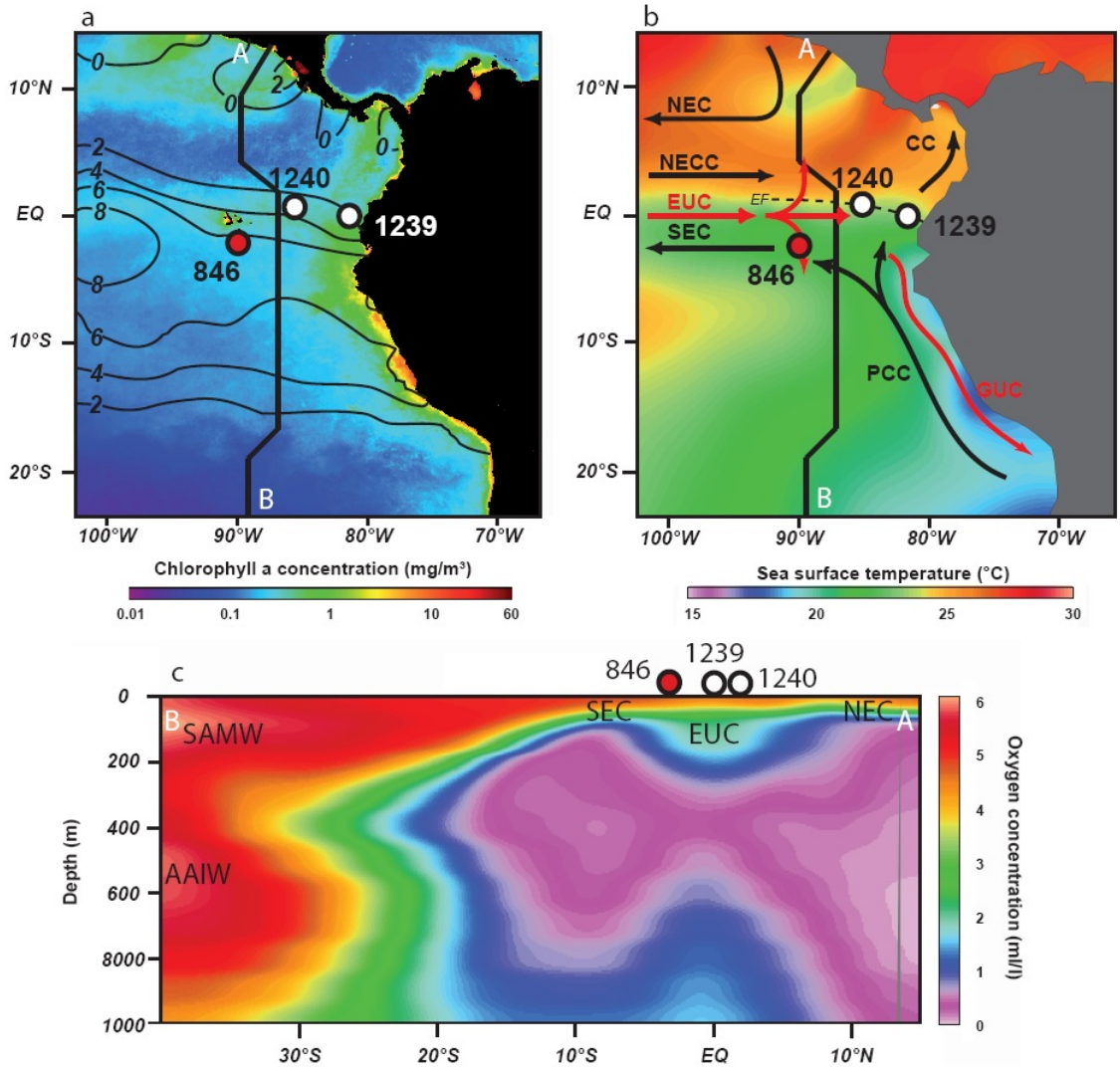

Figure 8. 1 (a) Productivity and nutrient distribution in the surface waters of the modern EEP. Colors represent the mean annual chlorophyll *a* concentration (primary productivity) and contour lines define the mean annual nitrate concentration at 10 m water depth. **(b)** Surface and subsurface oceanic currents in the EEP. Colored is the mean annual sea surface temperature (SST). **(c)** Nitrate concentration in the water column (0-1000 water depth) along a cross-equatorial A-B transects. In white circles are shown the location of our two study Sites 1239 and 1240, and in red circle, close-by reference Site 846.

When the upwelling is intense and the thermocline shallower, the biological production in the EEP increases because of the associated high supply of nutrient-rich waters transported by the EUC (Chai et al., 1996). However, the open ocean EEP upwelling region is known to be a HLNC area (Thomas, 1972) due to Fe and Si limitation (E.g. Murray et al., 1994; Dugdale et al., 1995; Coates et al., 1996; Brzezinski et al., 2011). High Fe inputs from terrestrial (fluvial and aeolian) sources mainly fertilizes surface waters along the South American coastline, but remains relatively weak in open ocean upwelling areas. In the central and the western portion of the EEP waters, Fe is mainly carried to the euphotic zone as dissolved fraction mainly through the EUC and in lesser extent through the PCC (E.g. Murray et al., 1994; Ziegler et al., 2008; Schroth

et al., 2009; Kaupp et al., 2011). Comparatively, the Si supplying the EEP surface waters is also carried by the EUC, but, contrary to the dissolved Fe fraction which originated in the western Pacific, where the EUC forms, silica sources come from both the northern and southern high latitudes (Southern Ocean and North Pacific) (Dugdale et al., 2002b). Because of the relative low Fe and Si concentrations in the upwelled EUC waters, the phytoplankton growth, especially diatoms, remains overall limited (Pennington et al., 2006).

Added to the EUC, the equatorward surface currents (I.e. PCC) can also transport nutrients to the EEP region as they origin in the coastal upwelling regions off the South American margin. However, the coastline of western South America, particularly along the Peruvian and Chilean margins as well as along the Central America margins and in less extent in the Panama Basin, is characterized by active zones of denitrification in the eastern Pacific (E.g. Farrell et al., 1995; Martinez et al., 2006). This is illustrated by extremely low oxygen concentrations observed at 200 m water depth in these areas (Figure 8.1). Along the western Central and South American coasts, strong upwelling seasonally strengthens, and nutrient-rich waters reach the surface. Stimulated by strong Fe supply, mainly from aeolian inputs, phytoplankton blooms utilize most of the nutrient contained in the upwelled waters, including Si. However, these upwelled waters rising in these regions originate from poorly oxygenated intermediate waters from both northern and southern high latitudes. The high biological production therefore consumes most of the oxygen during strong upwelling seasons, beyond the critical threshold (<5-10µM) required for promoting denitrification. As a result, the sedimentary $\delta^{15}N$ signal recording the denitrification process in the oxygen minimum zone (OMZ) along the Peru-Chile coasts for instance can attain extremely high values up to 14 ‰ (E.g. Farrell et al., 1995; Hebbeln et al., 2000a; Martinez et al., 2006).

Unlike the eastern Pacific coasts, the convergence of strong trade winds in the EEP sufficiently ventilates and oxygenates surface waters to confer at the EEP a non-denitrification zone character. Moderated denitrifying areas in the EEP are today restricted north of equator where the cold tongue and the equatorial upwelling do not spread because of the equatorial front (EF) presence separates cooler (<23°C) and relatively high-salinity surface waters south of the equator from warmer (>25°C) and low-salinity waters of the Panama Basin (Strub et al., 1998). However, changes in source and distribution of nutrients are locally tied to varying position of the EF and ITCZ, which control the isotopic signature of the nutrient and the resulting bulk $\delta^{15}N$ in the EEP. While nitrate-depleted waters and high isotopic values from the eastern tropical North Pacific can influence only the EEP surface waters by latitudinal migration of the EF, those from the eastern tropical south Pacific (ETSP)-OMZ can in contrast control it through surface advection of equatorward and westward currents. It has been recently evidenced that the isotopic signature of the $\delta^{15}N$ in the EEP was overprinted by the high $\delta^{15}N$ values produced in the Peru denitrifying zone (Robinson et al., 2009). Only a subtraction of the denitrification signal enables to record nutrient demand by local productivity depending on the upwelling activity and nutrient supply.

8.4 MATERIALS AND METHODS

In order to reconstruct the Plio-Pleistocene changes in surface oceanic circulation, nutrient cycling and primary production in the EEP, the ODP Sites 1239 (0°40.32'S, 82°4.86'W, 1414 m water depth) and 1240 (0°1.31'N, 86°27.76'W, 2921 m water depth) were selected and compared to the previously studied Site 846 (Lawrence et al., 2006) (Figure 8.1). The latter is situated south of the Galapagos Islands, while Site 1239 is located 120 km off the Ecuadorian coast and Site 1240 at the midway between continental Ecuador and the Galapagos Islands (Figure 8.1). Today, the surface waters above Sites 1239 and 1240 are mostly influenced by the variations of the EF latitudinal position, and over the last ~4 Ma their paleoposition has

changed negligibly with respect to these oceanographic settings (E.g. Gripp and Gordon, 1990; Pisias et al., 1995; Mix et al., 2003).

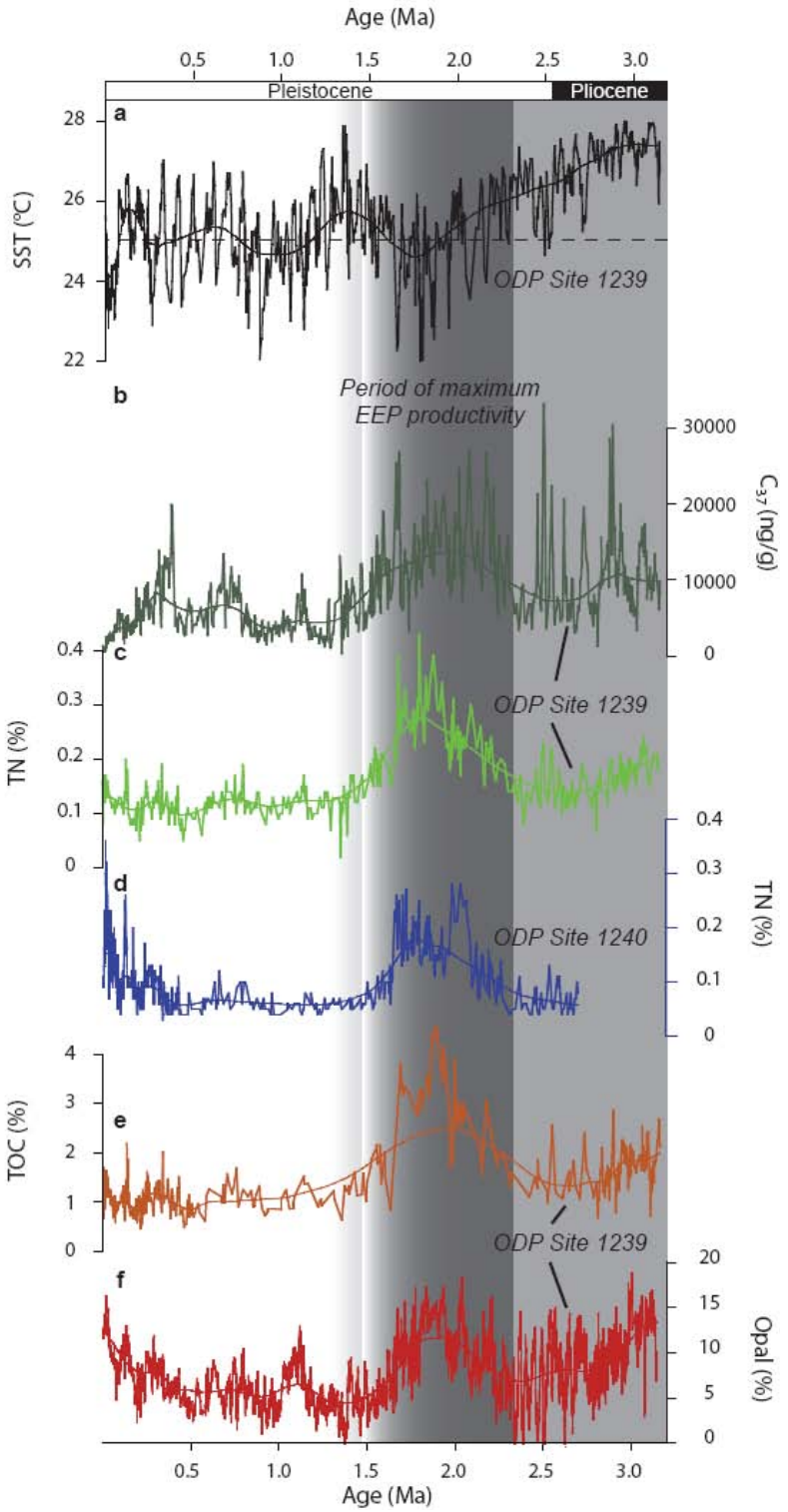

Figure 8. 2 Paleorecords in the EEP. **(a)** Site 1239 alkenone-derived SST (°C). **(b)** Site 1239 C_{37} concentration (ng/g). **(c)** and **(d)**, TN contents (%) at Site 1239 (light green curve) and 1240 (brown curve), respectively. **(e)** Site 1239 TOC content (%). **(f)** Site 1239 biogenic opal content (%). **(g)** Site 1239 sedimentation rate (SR). The period of maximum productivity has been shaded in dark grey, while the time interval of relatively high primary production has been shades in light grey.

8.4.1 Age model

Stratigraphy at the EEP Site 1239 between ~3.2 and 0.5 Ma has been published elsewhere (Etourneau et al., 2010). It is based on the correlation of the alkenone-SSTs with those measured at the nearby and well-dated Site 846 (Lawrence et al., 2006). In addition, the age model for two intervals, ~3.2-2.7 and ~0.5-0.0 Ma, is based on $\delta^{18}O$ and $\delta^{13}C$ measured on benthic foraminifera (Rincon-Martinez et al., 2010; Steph et al., 2009) and tuned to the LR04 $\delta^{18}O$ benthic stack (Lisiecki and Raymo, 2005). The stratigraphy at Site 1240 is constrained by ^{14}C dating from planktonic foraminifera for the last 40 kyr (Robinson et al., 2009) and tuned with oxygen isotopes with the LR04 $\delta^{18}O$, paleomagnetic and biostratigraphic stratigraphies for older ages (Mix et al., 2003).

8.4.2 Bulk $\delta^{15}N$ and productivity-related proxies

$\delta^{15}N$ and total nitrogen contents (TN, wt%) were determined on freeze-dried, ground bulk sediment. Site 1239 samples were measured with a Carlo–Erba CN analyzer 2500 interfaced directly to a Micromass-Isoprime mass spectrometer at the University Bordeaux 1 (UMR EPOC), while samples from Site 1240, were analyzed in a Costech 4010 Elemental Analyzer with a zero blank autosampler coupled to a Thermo Delta V isotope ratio mass spectrometer, at the University of Rhode Island. Sampling resolution averages one sample every 20-30 cm (~10 ka). Precision of the isotopic analyses based on certified standards and in-house standards replicates is better than ±0.3‰. Typical precision for TN analysis is better than ± 0.02%. Nitrogen isotopic values are reported in delta notation where:

$$\delta^{15}N = [^{15}N/^{14}N\text{sample}/^{15}N/^{14}N\text{standard})\text{-}1)]*1000 \text{ (the used standard is atmospheric } N_2\text{composition)}$$

Some discrete samples were also selected all along the record and measured for their total organic carbon (TOC, wt%) contents at both the University Bordeaux 1 and Alfred Wegener Institute - Bremerhaven, using a LECO C-S 125 analyzer after treatment of the sediment with HCL to remove $CaCO_3$. The precision for TOC is better than ± 0.5%.

The alkenone concentration (C_{37}, ng/g) can be used as a proxy for alkenone producer's abundance, as previously demonstrated (E.g. Müller et al., 1997; Mix et al., 2000). It was determined at the same time than the $U^{k'}_{37}$ published by Rincon-Martinez et al. (2010) and Etourneau et al. (2010) with a precision of about ±0.05 units. Alkenones were extracted from freeze-dried and homogenized sediment samples (~1 g dry weight for each sample) using an accelerated solvent extractor (Dionex ASE 200) at a resolution of ~0.4-1.0 ka for the last 0.5 Ma, and of ~2-4 ka between 3.2 and 0.5 Ma. The resulting extract was then concentrated with a rotary evaporator and analyzed within a double column Multidimensional gas chromatograph (MDGC) with two Agilent 6890 gas chromatograph at the University of Kiel.

The content of biogenic opal (BSi, wt%) for the last 0.5 Ma was determined at Alfred Wegener Institute Bremerhaven using an automated extraction method and wet chemical leaching as described in Müller and Schneider (1993). The precision of measurements applying this method is considered to be better than ± 4% (Müller and Schneider, 1993). For the interval between ~3.2 and 0.5 Ma, BSI content was estimated from the equation:

$$BSI\ (wt\ \%) = 103.8 - 63.22 * HROM$$

Where HROM is the high-resolution corrected bulk density. Correlation coefficient was r^2=0.8 (n=73).

8.4.3 XRF core scanning

X-Ray Fluorescence (XRF) core scanning is a non-destructive procedure that determines the chemical composition of measured sediments as element intensities in counts per second (cps), which are proportional to chemical proportions (Richter et al., 2006). XRF measurements of Fe intensities were carried out only at Site 1239 by using the Alfred Wegener Institute's Avaatech X-ray (XRF) core scanner at ~15 cm resolution (~3-7 ka), with generator settings of 10 kV. Fe data obtained by this method strikingly evolved in parallel to those performed by geochemical analyses characterizing the elemental Fe concentration contained within the sediment (Rincon-Martinez et al., 2010). The high resolution absolute Fe content record was then obtained by converting Fe measured by XRF with those measured by Inductively Coupled Plasma-Optical Emission Spectrometry (ICP-OES) by means of linear regressions (r^2 = 0.83). The latter method is based on freeze-dried samples digested using HF (23 *M*), HNO_3 (15 *M*), and HCL (12 *M*).

8.5 Results

8.5.1 Variation in paleoproductivity

C_{37} and BSi contents experienced relatively high values between 3 and 2 Ma, a maximum around 2 Ma and lower values afterwards. TN and TOC at both Sites 1239 and 1240 share overall the same pattern since the late Pliocene: decreasing values from 3 to 2.4 Ma, followed by an increasing trend towards a maximum achieved between 2.4 and 1.5 Ma, then, low values, similar to that around 2.5 Ma (Figures 8.2a-d). Between 2.4 and 1.5 Ma, during the productivity maximum, alkenone and BSi concentrations at Site 1239 reached values up to 20 mg/g and 20% respectively, and TOC and TN contents, up to 4% and 0.4% during the same time interval.

8.5.2 Variation in bulk $\delta^{15}N$

The most prominent feature of our Plio-Pleistocene bulk sedimentary $\delta^{15}N$ records at the EEP Sites 1239 and 1240 is the shift towards higher values recorded since 2 Ma (Figure 8.3a) concomitant to the productivity maximum decline. Prior to 2 Ma, during the late Pliocene/early Pleistocene EEP cooling, the $\delta^{15}N$ values were globally low and oscillated from 1 to 3‰ at Site 1239 and from 1 to 6‰ at Site 1240, between cold and warm phases with no specific changes with the onset of significant NHG at 3-2.7 Ma. Between 2 and 1.5 Ma, the $\delta^{15}N$ values increased at both sites ~2‰ on average with greater amplitude at Site 1240. Afterwards, from 1.5 Ma, the bulk $\delta^{15}N$ varied around a mean of ~5.0‰, and attained ~6‰ at Site 1239 and ~8‰ at Site 1240 during the warmest periods and ~2‰ during the coolest ones.

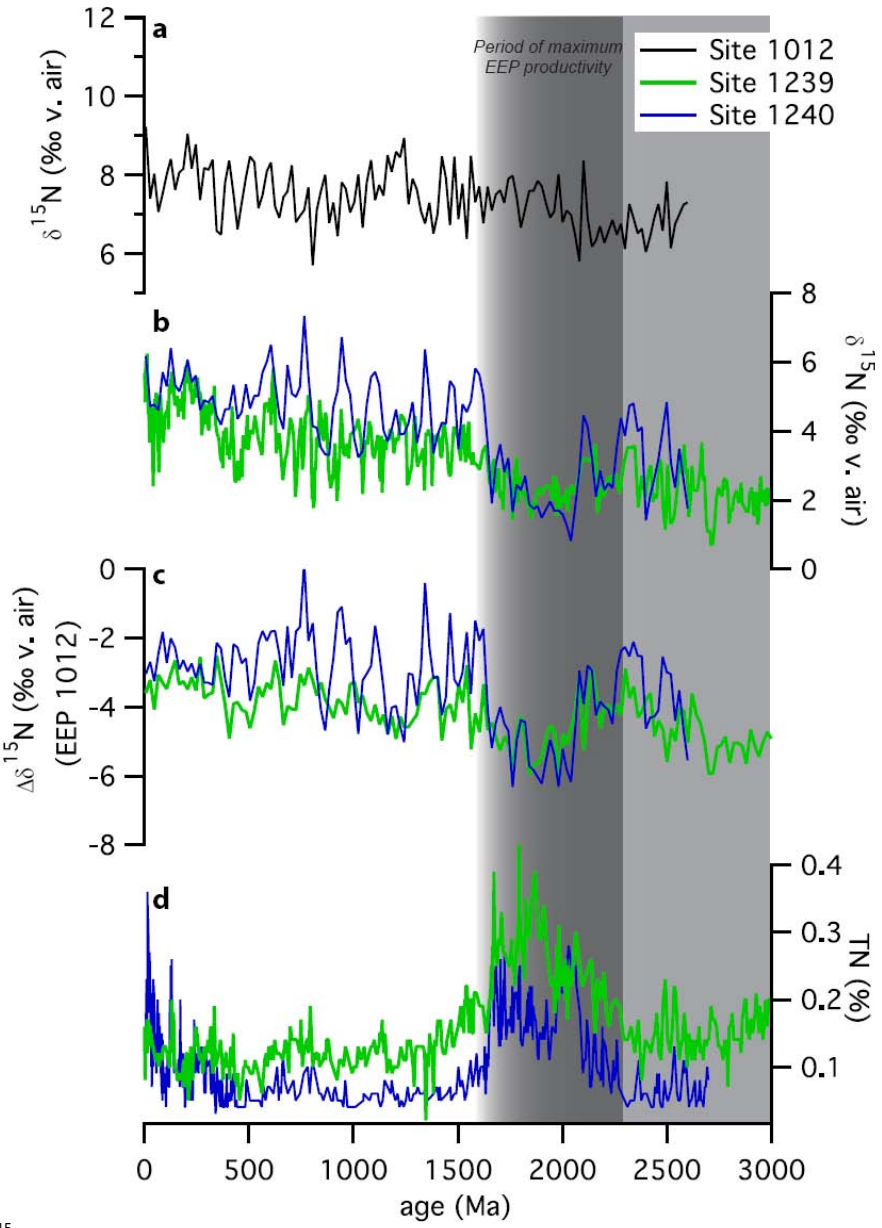

Figure 8. 3 $\delta^{15}N$ records at **(a)** Site 1012 in the California OMZ, and **(b)** Sites 1239 (green) and 1240 (blue). In **(c)** is represented the $\Delta\delta^{15}N$ between Sites 1012 and 1239 (green) and Sites 1012 and 1240 (blue). **(d)** TN content at the EEP Sites 1239 (green) and 1240 (blue).

8.5.3 Variations in Fe content

The Fe content at Site 1239 exhibited variations similar to that of the productivity-related markers, especially with TN and TOC with a slight decline from 3.0 to 2.4 Ma, a net increase where values reached up to 2% between 2.5 and 1.8 Ma (Fig.8.4), before declining until 0.8 Ma where it remained relatively stable until 0.5 Ma, prior to increasing over the last 0.5 Ma. The amplitudes changed as well, the Pleistocene corresponding to larger amplitudes variations than during the late Pliocene. Since the Pliocene, Fe varied in phase with warm and cold cycles with the highest values during the warmest periods and vice versa, the lowest during the coldest intervals.

8.6 DISCUSSION

8.6.1 Plio-Pleistocene changes in EEP primary productivity

C_{37} is commonly used as an indicator of past changes in alkenone producers (some specific coccolithophorids), while biogenic opal content (BSi) is representative of silica producers, mainly composed in this area of diatoms, and TN and TOC represent the overall phytoplankton production. The use of several proxies for reconstructing past productivity explain the slight differences observed between the records. For instance, the high variable values recorded by BSI and C_{37} concentrations during the late Pliocene/early Pleistocene cooling was not represented in the TN and TOC records which can be explained by the fact that the latters are not specific to certain species but recorded general variations. However, the biological production overall experienced large changes over the last 3 Ma with a maximum reached around 2 Ma as illustrated in all the paleoproductivity records. This profile, not unique to Sites 1239 and 1240, was also reported elsewhere in the EEP such as in the center of the cold tongue (E.g. Cortese et al., 2004; Lawrence et al., 2006; Dekens et al., 2007), thus suggesting a regional response of the biological production to a common forcing.

To explain the biological production variations over the last 3 Ma, the most conclusive assumptions associated changes in primary productivity to high latitude climatic and oceanic forcing. A shift of BSI production from North Pacific and Southern Ocean to low latitudes upwelling regions was attributed to a transfer of unused nutrient in the polar oceans due to their rapid stratification caused by the global cooling and ice sheet extension (E.g. Cortese et al., 2004). In contrast, the productivity decline ~2 Ma ago in the tropics and subtropics was attributed to the development of the polar frontal system in the Southern Ocean (E.g. Liu et al., 2008; Etourneau et al., 2009) which would have limited, as negative feedback, the nutrient leakage to eastern boundary currents and open ocean upwelling zones. This close relationship between EEP and Polar Regions was supported by spectral analyses (E.g. Lawrence et al., 2006; Bolton et al., 2010). However, these assumptions based on productivity and SST-related proxies do not explain the productivity maximum period occurring around 2 Ma, at the end of the late Pliocene/early Pleistocene cooling, and the weak biological production during the cooling interval or since the mid-Pleistocene. Moreover, it has been recently shown that the wind-driven upwelling activity in the Pacific likely strengthened from 2 Ma due to the intensification of the tropical/subtropical atmospheric circulation (Etourneau et al., 2010). In our records, the intensification of the upwelling coincided with a decline in local productivity which is unexpected when considering that stronger upwelling should correspond to more nutrient supply to the surface and thereby should support high – no low – local primary productivity.

8.6.2 The long-term δ^{15}N trend

The bulk δ^{15}N, used here as a recorder of nutrient cycling, revealed low values between ~3.2 and 2 Ma (around 2‰) with a minimum centered between 2.2 and 1.8 Ma, shifting towards heavier values at both EEP sites with large amplitudes changes. In contrast to the late Pliocene/early Pleistocene cooling when low isotopic values occurred during the high productive interval, the mid-to-late Pleistocene was characterized by relatively stable SSTs (E.g. Etourneau et al., 2010), high δ^{15}N values and low productivity. This correlation between the different records might reflect a close relationship between productivity, nutrient supply/utilization and hydrological conditions over the last 3 Ma. However, the global bulk δ^{15}N trends at both EEP sites were surprisingly similar to that recorded along the California, Benguela and Arabian Sea margins (E.g. Muzaka et al., 1991; Liu et al., 2008; Etourneau et al.,

2009) revealing the same $\delta^{15}N$ pattern with a shift from low to high mean values of ~2-3‰ around 2 Ma. This strongly suggests that the bulk $\delta^{15}N$ recorded at both EEP sites might have been primarily overprinted by a global signal instead of reflecting local changes in $\delta^{15}N$ tied to the regional subsurface nutrient pool.

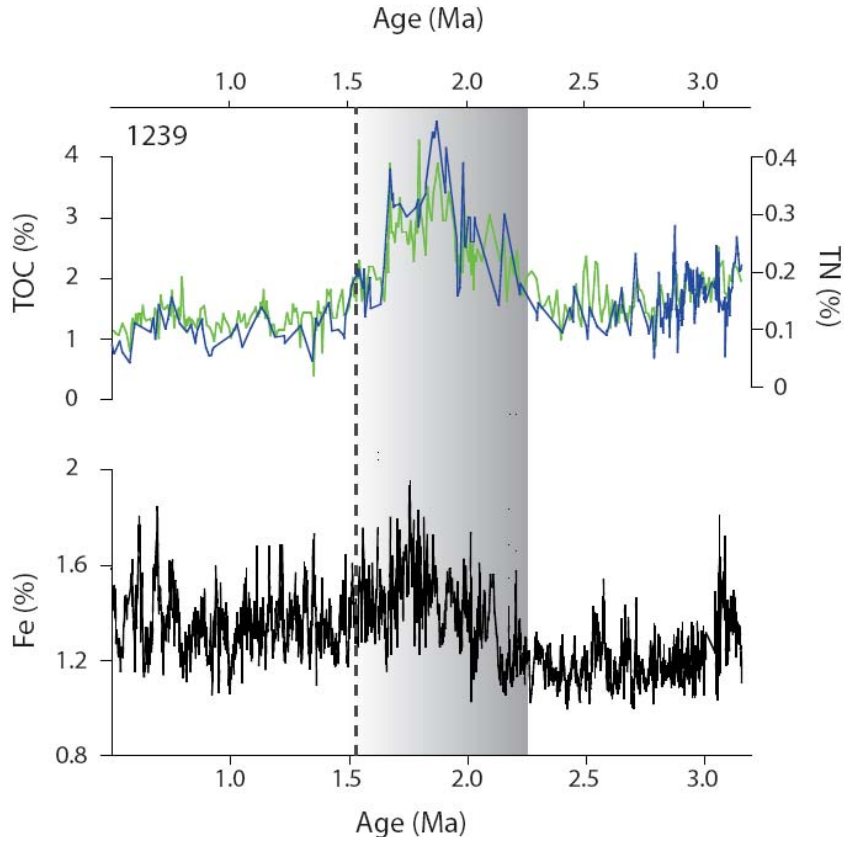

Figure 8. 4 (a) TN contents at the EEP Sites 1239 (green) and 1240 (blue). **(b)** Fe content at Site 1239.

Liu et al. (2008) attributed the $\delta^{15}N$ shift recorded along the California margin 2 Ma ago to the intensification of denitrification in response to the reorganization of the Southern Ocean polar frontal system. The development of the latter would have affected the nature of the upwelled waters in the low latitudes. The resemblance with other records from different denitrifying zones (E.g. Arabian Sea) seems to corroborate this theory as they are influenced by the same water masses originating in the Southern Ocean. Robinson et al. (submitted) recently proposed a new scenario challenging changes in oxygenation of the intermediate and mode waters coming from the polar oceans, export productivity and oxygen demand in the low-latitudes coastal upwelling systems. The establishment of the polar frontal system in the Southern Ocean 2 Ma ago would have driven to a switch from high to poor ventilated intermediate and mode waters, thus feeding by less oxygenated waters the upwelling zones. Synchronously, the latitudinal atmospheric circulation strengthening would have led to the shoaling of the thermocline in the low-latitude upwelling regions. Enhanced nutrient supply associated to increasing upwelling activity would have conducted to enhanced local productivity as well as the oxygen demand. As a result, poorly oxygenated upwelled waters further depleted in oxygen by local productivity, would have driven to the expansion of the denitrifying zones accompanied by heavier isotopic values within the OMZ as observed today (E.g. Altabet et al., 1995).

Given the trend at Sites 1239 and 1240, we assert that the bulk $\delta^{15}N$ likely recorded this transition. Although low $\delta^{15}N$ values over the last 3 Ma could not correspond to local

denitrification processes – the $\delta^{15}N$ values at Sites 1239 and 1240 remained overall too low – they might have rather been affected by an isotopic signal advected from nearby OMZ within the nutricline. In the EEP, recent works associated EEP $\delta^{15}N$ variations and changes in denitrification zones extension along the South American margins. Robinson et al. (2009) and Dubois et al. (2011) demonstrated that the variations in their sedimentary EEP $\delta^{15}N$ records for the last climatic cycles did not reflect local nitrate utilization changes because they were obscured by heavy nitrate transported from the ETSP OMZ to the EEP through the PCC. Denitrification processes offshore Peru can affect sedimentary $\delta^{15}N$ records in far regions like the eastern tropical North Pacific by significantly increasing sedimentary $\delta^{15}N$ values when denitrification in the Peru OMZ strengthens (E.g. Pichevin et al., 2010). We conclude that the general trend in the EEP $\delta^{15}N$ was dominated by changes in denitrification intensity off South America with an expansion of hypoxia and denitrification zones leading to increasing $\delta^{15}N$ values in the EEP since 2 Ma ago.

8.6.3 Regional nutrient utilization

To reconstruct a local signal of nitrate utilization, we subtracted the denitrification signature to the EEP records (see Figure 8.3c) as previously applied by Galbraith et al. (2008) and Robinson et al. (2009). We selected the $\delta^{15}N$ record off California at Site 1012 (Liu et al., 2008) as being the site recording denitrification changes along the eastern Pacific margins, the California margin being known to house one of the most important denitrifying zones of the world ocean. The three records were smoothed to a 25 kyr sampling interval to eliminate potential bias due to age model uncertainties and sampled on the same age scale. The resulting gradient $\Delta\delta^{15}N$ between the EEP and California sites give us a good estimate of changes in the regional subsurface nitrate pool.

The residual $\Delta\delta^{15}N$ draws a slightly different picture than that of the bulk $\delta^{15}N$ records. While the alternance between warm and cold phases as well as differences in amplitude between the two sites records is well preserved, the $\Delta\delta^{15}N$ was similar before and after the productivity maximum, the latter period being characterized by a low $\Delta\delta^{15}N$ gradient at both EEP sites. The interpretation of the $\Delta\delta^{15}N$ as an indicator of nutrient consumption implies that degree of utilization was nearly the same before and after the high productive episode, and was even lower during the productivity maximum event around 2 Ma. The bulk $\delta^{15}N$ constantly exhibited light values (less than 5‰) despite a likely overprinted signal of heavy isotopes related to denitrification changes, and could not therefore be ascribed to high nitrate consumption. During periods of strong productivity, we infer that the $\delta^{15}N$ values indicate even weaker nitrate utilization suggesting that the EEP nitrate pool likely remained overall rich over the last 3 Ma.

The two periods of relatively higher nitrate utilization, similar in $\Delta\delta^{15}N$ variations, corresponded to two distinct hydrologic patterns. The interval between 3 and 2.2 Ma was marked by a cooling period whilst the last 1.5 Ma were represented by relatively stable SSTs (E.g. Lawrence et al., 2006; Dekens et al., 2007; Etourneau et al., 2010). The low $\delta^{15}N$ values indicate a continuous high nutrient supply through upwelled waters, the major source of nitrate in the EEP. It has been recently demonstrated that SST changes in the EEP were not strictly related to changes in upwelling strength - colder waters when upwelling intensifies - but also to changes in the temperature of the upwelled waters themselves (Dekens et al., 2007). The waters shoaling in the EEP mainly comes from both Southern Ocean and North Pacific. During the Pliocene warm period, these waters were warmer at the location where they formed (Martinez-Garcia et al., 2010), in the polar frontal systems, and consequently, when they rose later in the EEP, they would have conducted to warmer SSTs. Thus, SST cooling

between 3 and 2 Ma would not have illustrated a strengthening of the equatorial upwelling system due to trade wind forcing but a cooling of the upwelled waters which is consistent with previous hypotheses asserting the intensification of the upwelling system and the emergence of the cold tongue appeared later (E.g. Etourneau et al., 2010; Martinez-Garcia et al., 2010). We conclude that the equatorial upwelling system in the EEP would have remained likely active since the Pliocene. This assertion matches with our results; the nitrate supply was probably sufficiently high in the EEP through the Plio/Pleistocene climate transition. The upwelled waters, independent of SST changes, would have therefore continuously carried nitrate to the EEP surface waters. The nitrate pool was probably largely supplied to not have been a limiting factor for productivity, which is in sum similar to modern conditions.

8.6.4 Silica supply in the EEP

Today, EEP is a HNLC region because nutrients such as Fe and/or silica limit productivity in this area (Brzezinski et al., 2011). Over the last 3.0 Ma, Fe and silica contents might have changed in concert with climate change, oceanic reorganization and nutrient distribution and thus affected local productivity. According to Cortese et al., (2004), the demise of siliceous productivity in the North Pacific and Southern Ocean together with the reorganization of the global conveyor circulation caused a redistribution of silica in the subsurface and deep-water masses, favoring siliceous plankton productivity to become strongly enhanced in coastal upwelling areas first (~ 3.0 Ma) and later (~ 2.0 Ma) in the Southern Ocean. This might affect the EEP as well. The BSI records revealed overall higher values between 3.0 and 2.0 Ma than during the Pleistocene. Silica was probably more supplied during the late Pliocene/early Pleistocene cooling in response to this silica leakage from North Pacific and Southern Ocean to the low-latitude upwelling systems. Inversely, the mid to late Pleistocene where biogenic opal production strongly declined corresponded to a modern-like system with limited silica in the surface waters due to its strong utilization in the Southern Ocean. However, although silica might have played a role on productivity changes in the EEP, it does not explain the TN and TOC variations. The high global biological production at 2.0 Ma reported at several locations including sites from the center of the cold tongue (Site 846) or at the northern edge of the EF (Sites 1239 and 1240) was likely dictated by another factor.

8.6.5 Fe control on EEP productivity

The comparison between TN, TOC and Fe contents at Site 1239 revealed striking similarities over the last 3 Ma. The parallel variations of those records suggest a strong link between biological production and Fe concentration. We assume here that Fe concentration measured on the particulate fraction reflect changes in bio-assimilable or dissolved iron as recently applied for the Southern Ocean (E.g. Martinez-Garcia et al., 2011); greater particulate Fe reach the surface, greater is its dissolution, thus making it more bio-available for phytoplankton growth. Intervals of increasing Fe concentration should have corresponded to periods of enhanced Fe fertilization, whereas decreasing Fe should instead mirror more Fe limitation. The parallel evolution between Fe, TOC and TN strongly lend support that primary productivity peaks was probably mainly triggered by enhanced Fe fertilization. Given that Fe is the major limiting factor in the modern EEP, we assert that Fe was a limiting factor for biological production all over the Plio/Pleistocene climate transition. The character of HNLC region with Fe as limiting factor for phytoplankton growth conferred to the EEP likely persisted over million years, even for warmer-than-today periods.

Fe entering the EEP might have originated from two major sources: EUC, transporting Fe from the western equatorial Pacific (WEP), and/or terrestrial inputs from South America (or nearby islands such as Galapagos Islands). A recent study stated that the Fe origin in the equatorial

Pacific Ocean since the Pliocene might have been transported by the EUC (Ziegler et al., 2008). It has been demonstrated that the atmospheric circulation switched from a weak to strong Walker circulation after 2 Ma (E.g. Ravelo et al., 2005; Wara et al., 2005; Etourneau et al., 2010). When the Walker circulations is weak, precipitations are mainly located on the eastern Pacific and reciprocally, when the zonal atmospheric circulation is strong, wetter conditions dominate the western Pacific. Extrapolating modern conditions to the Plio-Pleistocene climate, we suppose that more humid conditions should characterize the EEP prior to 2 Ma, which is consistent with recent climate model reporting more precipitation over the EP during the Pliocene warmth (Brierley et al., 2009). The hinterland erosion in the western Pacific due to enhanced rainfalls was probably reduced before 2 Ma and greater after. Fe at Site 1239 was measured on the particulate fraction. It is unlikely that such Fe concentration detected at this site was transferred under its particulate form from the western to the far eastern Pacific. In contrast, atmospheric conditions over the eastern Pacific might cause such changes in Fe supply from the continent. Regarding the weak zonal atmospheric circulation prior to 2 Ma, we exclude the aeolian transport as the main driver of Fe from the continent to the EE surface waters.

Rincon-Martinez et al. (2010) have recently posited that the Ecuadorian rivers mainly provided Fe at Site 1239. This hypothesis was supported by other indicators of terrestrial inputs (E.g. Titanium), which evolved similarly to Fe concentrations. Increased precipitation over the northern part of South America could increase the transport of particulate and dissolved Fe to the EEP and thereby stimulate the phytoplankton productivity. We found that Fe experienced an increase during a short interval of time centered at 2 Ma. Prior to 2 Ma, if wetter conditions dominated the eastern Pacific, it should have corresponded to a continuous high supply of Fe through strong riverine transport as recently reported for the last climatic cycles (E.g. Rincon-Martinez et al., 2010). Reciprocally, the last 2 Ma should have corresponded to reduced Fe supply due to the intensification of the Walker circulation, a progressive switch to drier conditions over the EP. Our results do not support this simple scheme. Since 3 Ma, dry conditions, basically encountered during normal or La Niña-like conditions, mostly dominated the EP. Solely the peak between 2.4 and 1.6 Ma suggests more humid conditions associated to a higher precipitation rate.

8.6.6 ITCZ and EF reconstruction for the last 3 Ma

It has been recently evidenced that increased Fe supply in the EEP during the warmest phases of the last climatic cycles was associated to a northward migration of the ITCZ and EF, as well as a more vigorous cold tongue (Rincon-Martinez et al., 2010). In contrast, some others proposed that they corresponded to a southernmost position of the ITCZ, arguing that Fe supply at Site 1239 was probably only local (Dubois et al., 2011). If true, we should not observe major differences in the productivity records throughout the EEP. However, the response of the primary productivity was not restricted to Site 1239, which is indeed the closest to the South American coast, but was also reported at Sites 1240 and 846, located respectively further west and at the center of the modern cold tongue. We emphasize that the strong Fe supply around 2 Ma likely affected the EEP productivity as a whole. We also suggest that the cold tongue was probably the most vigorous at this time, which is consistent with the period of coolest SSTs and lowest $\delta^{15}N$. Extrapolating a similar scenario to the Plio-Pleistocene climate transition than recently proposed for the last interglacials (Rincon-Martinez et al., 2010), the increasing temperature gradient between the EEP warm pool and cold tongue may have promoted the northward shift of the southeasterly trade winds across the equator, precipitation in the eastern Pacific similar to El Niño-like conditions and therefore displaced northward the ITCZ and EF to reach their northernmost position between 2.4 and 1.6 Ma. However, is still lacking Plio-Pleistocene records from the EEP warm pool to unravel the

evolution of the SST gradients north and south of EF. In contrast, during the late Plio-Pleistocene cooling and from the mid-to-late Pleistocene, decreasing Fe concentration, higher $\delta^{15}N$ values and weak productivity suggest that the ITCZ and EF were probably further south and was accompanied by a contraction of the EEP cold tongue. Reasons explaining why ITCZ and EF were at their northernmost position between 2.4 and 1.6 Ma remain unclear, although it may correspond to a transition period preceding the establishment of the Walker circulation related to the global oceanic reorganization, especially in the Southern Ocean.

8.7. Summary and Conclusions

Here, we used a suite of proxies at two well dated Sites 1239 and 1240 to monitor the evolution of primary productivity, nutrient cycling and oceanic changes in the EEP over the last 3 Ma. As previously described (E.g. Cortese et al., 2004; Lawrence et al., 2006; Dekens et al., 2007), we found that the productivity period maximum in the EEP occurred between 2.4 and 1.6 Ma, while weakened productivity characterized the late Plio/Pleistocene cooling and the mid-to-late Pleistocene. Compared to these two latter periods of time, the maximum productivity corresponded to an important nitrate supply as illustrated by the low nitrogen isotopic values. This was synchronous to a more vigorous cold tongue associated to a strong supply of nutrient-rich cold waters upwelled in the EEP that shifted northward the EF-ITCZ complex. This is supported by the SST record, which revealed coevally the coldest temperatures recorded in the EEP over the last 3 Ma. The northward migration of the ITCZ likely corresponded to more humid conditions in the EEP. Enhanced precipitation increased continental erosion and Fe transport to the surface waters would have fertilized the surface waters and probably triggered the period of maximum biological production. The HNLC character of the EEP with Fe as the major limiting factor was probably the major feature characterizing the EEP since the warm Pliocene. Despite changes in nitrate or silica supply, Fe was needed in this region to stimulate primary productivity, even under warmer-than-today periods. However, is still unknown why precipitation would have been greater around 2 Ma comparatively to previous and following periods of time. Precipitation conditions in the EP likely differed over the Pliocene/Pleistocene transition than previously proposed. This was probably related to the oceanic reorganization occurring in the Southern ocean which might have conducted to contrasted temperature changes in the low-latitudes upwelling system. However, further studies in this region supported by modeling studies are therefore necessary to reconstruct position of the ITCZ position during one of the most important period of time of the EEP.

References

-Altabet, M.A., and Francois, R. (1994), Sedimentary nitrogen isotopic ratio as a recorder for surface ocean nitrate utilization. Glob.Biogeochem.Cycl., *8*, 103-116.

-Altabet, M.A., Francois, R., Murray, D.W., and Prell, W.L. (1995), Climate related variations in denitrification in the Arabian Sea from sediment 15N/14N ratios. Nature, 373, 506-509.

-Altabet, M.A., Higginson, M.J., and Murray, D.W. (2002), The effect of millennial-scale changes in Arabian Sea denitrification on atmospheric CO2.Nature, 415, 159-162.

-Behl, R. J., and Kennett, J.P. (1996), Brief interstadial events in the Santa Barbara basin, NE Pacific, during the past 60 kyr. Nature, 379, 243-246.

-Bolton, C.T., Lawrence, K.T., Gibbs, S.J., Wilson, P.A., Cleaveland, L.C., and Herbert, T. (2010), Glacial-interglacial productivity changes recorded by alkenones and microfossils in late Pliocene eastern equatorial Pacific and Atlantic upwelling zones. Earth Planet. Sci. Lett.,*295*, 401-411.

-Brandes, J. A., and Devol, A.H. (2002), A global marine-fixed nitrogen isotopic budget: Implications for Holocene nitrogen cycling. Glob.Biogeochem.Cycl., 16, doi: 10.1029/2001GB001856.

-Brierley, C.M., Fedorov, A., Liu,Z., Herbert, T.D., Lawrence, K.T., and LaRiviere, J.P. (2009), Greatly expanded tropical warm pool and weakened Hadley circulation in the Early Pliocene. Science, 323, 1714–1718.
-Bruland, K.W., Rue, E.L., Smith, G.J., and DiTullio, G.R. (2005), Iron, micronutrients and diatom blooms in the Peru upwelling regime: brown and blue waters off Peru. Marine Chemestry, 93, 81-103.
-Brzezinski, M.A., Baines, S.B., Balch, W.M., Beucher, C.P., Chai, F., Dugdale, R.C., Krause, J.W., Landry, M.R., Marchi, A., Measures, C.I., Nelson, D.M., Parker, A. E., Poulton, A., Seplph, K.E., Strutton, P.G., Taylor, A.G., Twining, B. (2011), Co-limitation of diatoms by iron and silicic acid in the equatorial Pacific. Deep-Se Res. II, 58, 493-511.
-Cane, M.A. (1986), El Niño. Ann. Rev. Earth Planet. Sci., 14, 43-70.
-Cannariato, K.G., and Ravelo, A.C. (1997), Pliocene-Pleistocene evolution of eastern tropical Pacific surface water circulation and thermocline depth. Paleoceanography, 12, 805-820.
-Chai, F., Lindley, S.T., and Barber, R.T. (1996), Origin and maintenance of a high nitrate condition in the equatorial Pacific, Deep-Sea Res. II, 43, 1031-1064.
-Chavez, F.P., Toggweiler, J.R. (1995), Physical estimates of global new production: the upwelling contribution, In: Summerhayes, CP. (Ed), Upwelling in the Ocean: Modern Processes and Ancient Records. Johan Wiley, Hoboken, N.J, 313-320.
-Cline, J. D., and Kaplan, I. R. (1975), Isotopic fractionation of dissolved nitrate during denitrification in the eastern tropical North Pacific Ocean. Marine Chemistry, 3, 271-299.
-Coates, A.G., and Obando, J.A. (1996), The geologic evolution of the Central American Isthmus.In Jackson, J.B.C., Budd, N., Coates, A.G. Evolution and Environment in Tropical America, U. Chicago Press, 21-56.
-Codispoti, L. A., Yoshinari, T., and Devol, A.H. (2005), Suboxic respiration in the oceanic water column. in Respiration in Aquatic Ecosystems, edited by del Giorgio, P. and Williams, P. J. LeB., 328, Oxford University Press, Cambridge, UK.
-Conte, M.H., Eglinton, G., and Madureira, L.A.S. (1992), Long-chain alkenones and alkyl alkenoates as paleotemperature indicators: their production, flux and early sedimentary diagenesis in the Eastern North Atlantic. Organic Geochemistry, 19, 287-298.
-Cortese, G., Gersonde, R., Hillenbrand, C.-L, and Kuhn, G. (2004), Opal sedimentation shifts in the world over the last 15 Myr. Earth Planet. Sci. Let., 224, 509-527.
-Dekens, P.S., Ravelo, A.C., and McCarthy, M.D. (2007), Warm upwelling regions in the Pliocene warm period. Paleoceanography, 22, doi: 10.1029/2006PA001394.
-De Pol-Holz, R., Ulloa, O., Lamy, F., Dezileau, L., Sabatier, P., and Hebbeln, D. (2007), Late Quaternary variability of sedimentary nitrogen isotopes in the eastern South Pacific Ocean. Paleoceanography, 22, PA2207, doi:10.1029/2006PA001308.
-Dubois, C., and Kienast, M. (2011), Spatial reorganization in the equatorial divergence in the Eastern Tropical Pacific during the last 150 kyr. Geophysical Research Letters, 38, doi:10.1029/2011GL048325.
-Dugdale, R.C., Wilkerson, F.P., Chai, F., and Feely, R. (1995), The role of silicate pump in driving new production. Deep-Sea Res., 42, 697-719.
-Dugdale, R.C., Wishmeyer, A.G., Wilkerson, F.P., Barber, R.T., Chai, F., Jiang, M., and Peng, T.-H. (2002b), Meridional asymmetry of source nutrients to the equatorial Pacific upwelling ecosystem and it's potential impact on ocean-atmosphere CO2 flux; a data and modeling approach. Deep-Sea Research II, 49, 2513-2533.
-Dugdale, R.C., Lyle,M., Wilkerson,F.P., Chai,F., Barber,T., and Peng,T.H. (2004), Influence of equatorial diatom processes on Si deposition and atmospheric CO2 cycles at glacial/interglacial timescales. Paleoceanography, 19, doi: 10.1029/2003PA000929.
-Dwyer, G.S., and Chandler,M.A. (2009), Mid-Pliocene sea level and continental ice volume based on coupled benthic Mg/Ca palaeotemperatures and oxygen isotopes.*Phil. Trans. Royal Soc.A,* 367,157-168, doi:10.1098/rsta.2008.0222.
-Etourneau, J., Martinez,P., Blanz,T., and Schneider,R. (2009), Pliocene–Pleistocene variability of upwelling activity, productivity, and nutrient cycling in the Benguela region.Geology, 37, 871–874.
-Etourneau, J., Schneider,R., Blanz,T., and Martinez,P. (2010), Intensification of the Walker and Hadley atmospheric circulations during the Pliocene–Pleistocene climate transition. Earth Planet. Sci. Lett., 297, 103-110.
-Farrell, J.W., Pedersen,T.F., Calvert,S.E., and Nielsen,B. (1995), Glacial-interglacial changes in nutrient utilization in the equatorial Pacific Ocean.Nature, 377, 514-517.

-Galbraith, E. D., Kienast,M., Pedersen,T.F., and Calvert,S.E. (2004), Glacial-interglacial modulation of the marine nitrogen cycle by high-latitude O2 supply to the global thermocline.Paleoceanography, 19.
-Ganeshram, R.S., Pedersen,T.F., Calvert,S.E., and Francois,R. (2002), Reduced nitrogen fixation in the glacial ocean inferred from changes in marine nitrogen and phosphorus inventories.Nature, 415, 156-159.
-Gripp, A.E., and Gordon,R.G. (1990), Current plate velocities relative to the hotspots incorporating the NUVEL-1 global plate motion model.Geophys. Res. Lett., 17, 1109-1112.
-Hebbeln, D., Marchant,M., Freudenthal,T., and Wefer,G. (2000a), Surface sediment distribution along the Chilean continental slope related to upwelling and productivity.Marine Geology, 164, 119-137.
-Holbourn, A.,Kuhnt,W., Schulz,M., and Erlenkeuser,H. (2005), Impacts of orbital forcing and atmospheric carbon dioxide on Miocene ice-sheet expansion.Nature, 438, doi: 10.1038/nature04123.
-Karas, C., Nürnberg,D., Gupta,A.K., Tiedemann,R., Mohan,K., and Bickert,T. (2009), Mid-Pliocene climate change amplified by a switch in Indonesian subsurface throughflow.Nature Geoscience, doi: 10.1038/NGE520.
-Karl, D., Michales,A.,Bergman, B., Capone,D., Carpentier,E., Letelier,R., Lipschultz,F., Paerl,H., Sigman,D., and Stal,L. (2002), Dinitrogen fixation in the world's oceans.Biogeochemistry, 57/58, 47-98.
-Kessler, W.S. (2006), The circulation of the eastern tropical Pacific: A review.Progr.Oceanogr., 69, 181-217.
-Kraupp, L.J., Measures,C.I., Selph,K.E., and MacKenzie,F.T. (2011), The distribution of dissolved Fe and Al in the upper waters of the Eastern Equatorial Pacific.Deep-Sea Res. II, 58, 296-310.
-Landry, M.R., Selph,K.E., Taylor,A.G., Décima,M., Balch,W., and Bidigare,R.R. (2011), Phytoplankton growth, grazing and production balances in the HNLC Equatorial Pacific.Deep-Sea Res. II, 58, 524-535.
-Lawrence, K.T., Liu,Z., and Herbert,T.D. (2006), Evolution of the eastern tropical Pacific through Plio-Pleistocene glaciation. Science, 312, 79-83.
-Lisiecki, L.E., and Raymo,M.E. (2005), A Pliocene-Pleistocene stack of 57 globally distributed benthic 18O records.Paleoceanography, 20, doi:10.1029/2004PA001071.
-Liu, K.-K., and Kaplan,I.R. (1989), The eastern tropical Pacific as a source of 15N-enriched nitrate in seawater off southern California.Limn. Ocean., 34, 820-830.
-Liu, Z., Altabet,M.A., and Herbert,T.D. (2008), Plio-Pleistocene denitrification in the eastern tropical North Pacific: Intensification at 2.1 Ma.Geochem., Geophys., Geosys., 9, doi: 10.1029/2008GC002044.
-Lunt, D.J., Haywood,A., Schmidt,G.A., Salzmann,U., Valdes,P.J., and Dowsett,H. (2009), Earth system sensitivity inferred from Pliocene modelling and data.Nature Geoscience, 3, 60-64.
-Martinez, P., Lamy,F., Robinson,R.R., Pichevin,L., and Billy,I. (2006), Atypical d15N variations at the southern boundary of the East Pacific oxygen minimum zone over the last 50 ka.Quarternary Sciencie Reviews, 25, 3017-3028.
-Martinez-Garcia, A., Rosell-Melé,A., McClymont,E.L., Gersonde,R., and Haug,G. H. (2010), Subpolar Link to the Emergence of the Modern Equatorial Pacific Cold Tongue.Science, 328, 1550-1553.
-Martinez-Garcia, A., Rosell-Melé,A., Jaccard,S.L., Geibert,W., Sigman,D.S., Haug,G.H. (2011), Southern Ocean dust-climate coupling over the past four million years. Nature, 476, 312-316.
-Medina-Elizalde, M., Lea,D., and Fantle,M.S. (2008), Implications of seawater Mg/Ca variability for Plio-Pleistocene tropical climate reconstruction,Earth Planet. Sci. Lett., 269, 585-595.
-Meyers, P. A. (1997), Organic geochemical proxies of paleoceanographic, paleolimnologic, and paleoclimatic processes,Organic Geochemestry,27, 213-250.
-Mix, A.C., Bard,E., Eglinton,G., Keigwin,L.D., Ravelo,A.C., and Rosenthal,Y. (2000), Alkenones and multiproxy strategies in paleoceanographic studies.Geochim., Geophys., Geosyst., 1, 1033, doi:10.1029/2000GC000056.
-Mix, A.C., Tiedemann,R., and Blum,P. (2003),Site 1239.Proc. Ocean Drill.Progr.Init. Rep.,202, College Station, Tex.
-Müller, P. J., and Schneider,R. (1993), An automated leaching method for the determination of opal in sediments and particulate matter.Deep-Sea Res. I,40, 425-444.
-Müller, P., Cepek,M., Ruhland,G., and Schneider,R. (1997), Alkenone and coccolithophorids species changes in late Quaternary sediments from the Walvis Ridge: Implications for the alkenone paleotemperature method.Palaeogeo.Palaeoclim.Palaeoecol., 135, 1-76.
-Murray, J.W., Barber,R.T., Roman,M.R., Bacon,C.R., and Feely,R.A. (1994), Physical and biological controls on carbon cycling in the equatorial Pacific.Science, 266, 58-65.
-Pagani, M., Liu,Z., LaRiviere,J., Ravelo,A.C. (2009), High Earth-system climate sensitivity determined from Pliocene carbon dioxyde concentrations.Nature Geoscience,3, 27-30.

-Pennington, T.J., Mahoney,K.L., Kuhawara,V.S., Kolber,D.D., Calienes,R., and Chavez,F.P. (2006), Primary production in the eastern tropical Pacific: A review.Progr.Oceanogr., 69, 285- 317.
-Pichevin, L.E., Reynolds,B.C., Ganeshram,R.S., Cacho,I., Pena,L., Keefe,K., and Ellam,R.M. (2009), Enhanced carbon pump inferred from relaxation of nutrient limitation in the glacial ocean.Nature, 459, doi:10.1038/nature08101.
-Pichevin, L. E., Ganeshram,R. S., Francavilla,S., Arellano-Torres,E., Pedersen,T. F., and Beaufort,L. (2010), Interhemispheric leakage of isotopically heavy nitrate in the eastern tropical Pacific during the last glacial period.Paleoceanography, 25, doi:10.1029/2009PA001754.
-Pisias, N.G., Mayer,L.A., and Mix,A.C. (1995), Paleoceanography of the eastern equatorial Pacific during the Neogene: synthesis of Leg 138 drilling results.Proc. Ocean Drill.Progr. Sci. Res.,138, College Station, Tex.
-Prahl, F.G., Dymond,J., and Sparrow,M.A. (2000), Annual biomarker record for export production in the central Arabian Sea.Deep-Sea Res. I, 47, 1581-1604.
-Ravelo, A.C., Andreasen,D.H., Lyle,M., Olivarez Lyle,A., Wara,M. (2004), Regional climate shifts caused by gradual cooling in the Pliocene epoch.Nature, 429, 263-267.
-Raymo, M.E., Lisiecki,L.E., and Nisancioglu,K.H. (2006), Plio-Pleistocene ice volume, Antarctic climate, and the global $d^{18}O$ record.Science, 313, 492-495.
-Reynolds, B.C.,Frank,M., and Halliday,A.N. (2008), Evidence for a major change in silicon cycling in the subarctic North Pacific at 2.73 Ma.Paleoceanography, 23, doi: 10.1029/2007PA001563.
-Rincón-Martinez, D., Lamy,F., Contreras,S., Leduc,G., Bard,E., Saukel,C., Blanz,T., Mackensen,A., and Tiedemann,R. (2010), More humid interglacials in Ecuador during the past 500 kyr linked to latitudinal shifts of the equatorial front and the Intertropical Convergence Zone in the eastern tropical Pacific.Paleoceanography,doi:10.1029/2009PA001868.
-Robinson, R.S., Martinez,P., Pena,L.D., and Cacho,I. (2009), Nitrogen isotopic evidence for deglacial changes in nutrient supply in the eastern equatorial Pacific.Paleoceanography, 24, doi: 10.1029/2008PA001702.
-Rodgers, K.B., Blanke,B., Madec,G., Aumont,O., Ciais,P., and Dutay,J. (2003), Extratropical sources of Equatorial Pacific upwelling in an OGCM.Geophys. Res. Let., 30, doi: 10.1029/2002GL016003.
-Sachs, J., and Repeta,D.J. (1999), Oligotrophy and nitrogen fixation during eastern Mediterranean sapropels events,Science, 286, 2485-2488.
-Sarmiento, J.L., Gruber,N., Brzezinski,M.A., and Dunne,J. (2004), High-latitude controls of thermocline nutrients and low latitude biological productivity.Nature, 427, 56-60.
-Seki, O., Foster,G.L., Schmidt,D.N., McKensen,A., Kawamura,K., and Pancost,R., (2010), Alkenone and boron-based Pliocene pCO2 records.Earth Planet.Sci. Lett., 292, 201-211.
-Schroth, A.W., Crusius,J.,Sholkovitz,E.R., and Bostick,B. (2009), Iron solubility driven by speciation in dust sources to the ocean.Nature Geosciences,2, 337-340.
-Sigman, D.M., Jaccard,S.A., and Haug,G.H. (2004), Polar ocean stratification in a cold climate.Nature, 428, 59-63.
-Sigman, D. M., Altabet,M. A., Michener,R., McCorkle,D. C., Fry,B., and Holmes,R. M. (1997), Natural abundance-level measurement of the nitrogen isotopic composition of oceanic nitrate: an adaptation of the ammonia diffusion method.Marine Chemistry, 57, 227-242.
-Steph, S., Tiedemann,R., Prange,M., Groeneveld,J., Schulz,M., Timmermann,A., Nürnberg,D., Rülhemann,C., Saukel,C., and Haug,G. (2009), Early Pliocene increase in the thermohaline overturning preconditioned the development of the modern equatorial Pacific cold tongue.Paleoceanography, 25,doi: 10.1029/2008PA001645.
-Strub, P.T., Mesias,J.M., Montecinos-Banderet,V., Rutllant,J., and Salinas-Marchant,S. (1998), Coastal ocean circulation off western South America.The Sea, 11, 273-313.
-Takahashi, T., Sutherland,S.C., Sweeney,C., Poisson,A., Metzl,N., Tilbrook,B., Bates,N., Wanninkhof,R., Feely,R.A., Sabine,C., Olafsson,J., and Nojiri,Y. (2002), Global sea-air CO_2 flux based on climatological surface ocean pCO_2, and seasonal biological and temperature effects.Deep Sea Res. II, 49, 1601-1622.
-Thomas, W.H. (1972), Nutrient inversions in the southeastern tropical Pacific Ocean.Fishery Bull., 70, 929-932.
-Toggweiler, J.R., Dixon,D., and Broecker,W.S. (1991), The Peru upwelling and the ventilation of the South Pacific thermocline,Journal of Geophysics Research, 96, 20467-20497.
-Tripati, A.K., Roberts,C.D., and Eagle,R.A. (2009), Coupling of CO_2 and ice sheet stability over major climate transitions of the last 20 millions years.Science, 326, 1394-1397.

-Waddell, L.M., Hendy,I.L., Moore,T.C., and Lyle,M.W. (2009), Ventilation of the abyssal Southern Ocean during the late Neogene: A new perspective from the subantarctic Pacific, Paleoceanography, 24, doi: 10.1029/2008PA001661.

-Wakeham, S.G., Hedges,J.I., Lee,C., Peterson,M.L., and Hernes,P.J. (1997), Compositions and transport of lipid biomarkers through the water column and sufficial sediments of the equatorial Pacific Ocean.Deep-Sea Res. II,*44*, 2131-2162.

-Wara, M., Ravelo,A.C., and Delaney,M.L. (2005), Permanent El Niño-like conditions during the Pliocene warm period.Science, 309, 758-761.

-Ziegler, C.L., Murray,R.W., Plank,T., and Hemming,S.R. (2008), Sources of Fe to the equatorial Pacific Ocean from the Holocene to Miocene.Earth Planet. Sci. Lett., 270, 258-270.

CHAPTER 9

CONCLUDING REMARKS AND FUTURE PERSPECTIVES

9.1. Summary and conclusions

The eastern tropical Pacific is an ideal test bed to explore past background states of the tropical ocean because it is a region with large latitudinal gradients in SSTs and nutrient conditions, and it has the ability to undergo fast dynamic adjustments and remarkably large SST changes with a total amplitude of 10°C or higher due to a strong coupling between the atmosphere and surface ocean in the presence of a shallow and steep thermocline (Mitchell and Wallace, 1992). The main aim of this thesis was to investigate the paleoceanographic evolution of the eastern tropical Pacific cold tongue and its relationship to the climate in western tropical South America using a combination of different organic and inorganic geochemical and mineralogical proxies. This chapter gives a chronological summary of the main results of this thesis and provides some remaining open questions and future research perspectives.

9.1.1. Modern Equatorial Front signature on the oxygen isotopes of recently deposited planktonic foraminifera

In the first part of the thesis (Chapter 4) the spatial pattern of planktonic foraminifera $\delta^{18}O_c$ in the eastern tropical Pacific was studied to determine whether oxygen isotopes of planktonic organisms reflect the regional ocean density patterns and its relationship with the allocation of the modern equatorial front – ITCZ complex. This was based on a set of surface sediment samples located in the Panama and Peru basins, the Carnegie, Cocos and Nazca ridges, and Galapagos Rise (Figure 3.1). Results indicate that similar to the latitudinal pattern of $\delta^{18}O_{pc}$ (see section 4.2), measured $\delta^{18}O_c$ of shallow-dweller species (*G. ruber* ss, *G. ruber* sl, *G. triloba* and *G. sacculifer*) generally increase towards the south of the EF, along with increasing mixed-layer salinity and decreasing mixed layer temperature. The lowest $\delta^{18}O$ values are generally observed in samples located on the Cocos Ridge, while the highest $\delta^{18}O$ values occur over the Carnegie Ridge (Figure 4.3). Since the oxygen isotope composition is a function of salinity and temperature, it seems that at least for the shallowest dweller *G. ruber* ss both, SST and salinity, influence equally its oxygen isotope ratios as predicted by the temperature vs. $\delta^{18}O$ and salinity vs. $\delta^{18}O$ relationships derived from this data set (r^2 = 0.54 and r^2 = 0.47, respectively; n=42).

Although the isotopic signal of the mean foraminiferal population in the sediment can be affected after deposition (I.e. processes such as bioturbation and calcite dissolution), these data show that the spatial variability of ocean's surface density in the eastern tropical Pacific can be transported and identified into the sediment in the ^{18}O signal of shallow dwellers. Moreover, the $\delta^{18}O$ signal of *G. ruber* ss shows a close resemblance to the spatial distribution of U^{K}_{37} values in the eastern equatorial Pacific (Figure 9.1), which exhibit highest values generally restricted to the warm pool north of the equatorial front, and lower values in the cold tongue off Peru (E.g. Kienast et al., 2012).

With exception of *G. ruber*, a proper determination of the apparent calcification depths (ACDs) of planktonic species from our sediment samples was not so simple and we reported wider water depths ranges than other authors have done (see section 5.2). This conflict between core-top and plankton-tow studies might be explained by the fact that foraminiferal shells found in the sediment are generally heavier in $\delta^{18}O$ than those collected alive in the water column (E.g. Vergnaud-Grazzini, 1976; Mulitza et al., 1997; Mulitza et al., 2004). It has also been suggested that under oceanic conditions of low salinity and warm temperature in the mixed layer (as in the Panama Basin), species such as *G. sacculifer* continue to secrete calcite between the base of the mixed layer and up to 200 m, thereby enriching the oxygen-18 (E.g.

Duplessy et al., 1981). Moreover, it is believed that these species experience gametogenic calcification, which implies that adults undergo gametogenesis would extract additional $CaCO_3$ from deeper (cooler) waters than the epipelagic waters where the foraminifera form the bulk of their shells (E.g. Bé, 1980).

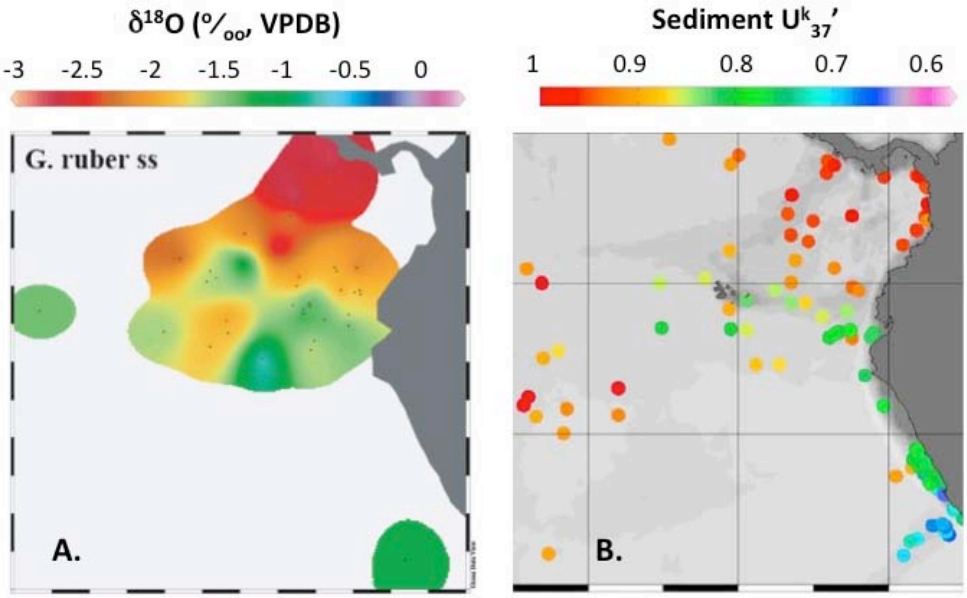

Figure 9. 1 **(a)** Interpolated $\delta^{18}O$ values of the shallow-dweller *G. ruber* ss, compared to **(b)** the surface sediment U^{K}_{37} in the EEP, from Kienast et al. (2012). $\delta^{18}O$ values measured in this study are expressed relative to Pee Dee Belemnite (PDB) standard, based on calibrations directly to National Bureau of Standards 19. U^{K}_{37} data include values reported previously by other investigators.

Maps of the difference between the $\delta^{18}O$ from recent sediments and equilibrium calcite $\delta^{18}O$ computed using regressions established on living foraminifera (Waelbroeck et al., 2005) indicate that this difference is of a regional nature and increases in areas where surface stratification is high, as in low latitudes and in regions of low surface salinity (E.g. area north of the equatorial front). On the other hand, the differences are usually smallest at the lower temperature limit. For example spinose species display the smallest deviation from equilibrium calcite and reported ACD in the eastern tropical Pacific, particularly south of the equatorial front (Figure 5.5). This might either indicate a shallower depth habitat, less stratification or a weighing of the flux towards the warmer season (E.g. Mulitza et al., 1998).

Since planktonic foraminifera live depth-stratified, the oxygen isotope (calcification depth) difference between certain species can be used as a proxy for stratification (E.g. Williams and Healy Williams, 1980; Mulitza et al., 1997; Rühlemann et al., 2001; Spero et al., 2003). According to our dataset, the $\delta^{18}O$ difference between *G. ruber* ss and *G. tumida* and between *P. obliquiloculata* and *G. tumida* show a statistically significant (confidence level 95%) relationship to water column thermal stratification. In this way, strong (weak) stratification in the upper 150 m of the water column is recorded as a large (small) $\Delta\delta^{18}O$. The $\Delta\delta^{18}O_{G.tumida\text{-}G.ruber}$ was tested in the down-core record of core RC11-238, located on the Carnegie Ridge between the coast of South America and the Galapagos Islands (Section 4.5.5) and ODP Site 1239 (Section 5.4.2). In both cases, high interglacial $\Delta\delta^{18}O_{\text{G.ruber-G.tumida}}$ values indicate stratified waters north of the EF, where a strong thermal gradient occurs in the upper 100 m. Low glacial $\Delta\delta^{18}O_{\text{G.ruber-G.tumida}}$ values reflect intensified upwelling linked to a stronger Peru Current and a northward location of the EF-ITCZ complex.

9.1.2. Late Pleistocene source and flux of terrigenous sediments into the eastern equatorial Pacific

The second part of this thesis comprises three case studies (chapters 5, 6, 7) focused on the transport and deposition of terrigenous material in the easternmost Pacific Ocean at different time periods in the Late Pleistocene. These studies used a multi-proxy approach combining inorganic (elements and element ratios) and organic (biomarker) proxies, as well as bulk geochemistry and grain-size analysis. Fluvial and eolian transports are the most important pathways for the transference of terrigenous material into the ocean. One case study therefore deals with the long-term variability in the accumulation of fine-grained sediments that reach the deep sea off the Ecuadorian coast (ODP Site 1239; Chapter 5), while other study investigates on long-term eolian dust deposition in the deep sea off the Peruvian coast (ODP Site 1237; Chapter 7). Besides tracing terrigenous input into these deep-sea environments, the Lima Basin case study (Chapter 6) also reconstructed paleo-conditions on the continent based on specific biomarkers.

Based on the geographical location and oceanographic/atmospheric settings of each site we hypothesized that for ODP Site 1239, drilled close to the eastern crest of Carnegie Ridge (Sections 2.4.1 and 3.1.2; Figure 2.4b), terrigenous sediment supply comes from the mainland delta systems formed around river mouths located along the continental shelf (I.e. Guayas and/or Esmeraldas drainage systems). Although these rivers deposit most of their sediments in the Ecuadorian Trench, the eastern portion of the Carnegie Ridge still receiving a moderate load of continental detritus (Figure 2.13; E.g. Pazmiño, 2005). Additionally, based on ^{232}Th flux measurements Singh et al. (2011) established that in the Panama Basin, included the Carnegie Ridge, the location at which eolian (as opposed to riverine) fluxes dominate the detrital flux occurs at approximately 300 km from the margin. On the other hand, ODP Site 1237, drilled on the easternmost flank of Nazca Ridge, lies below the wind-driven surface currents of the southeast Pacific (Sections 2.4.1 and 3.1.3; Figure 3.2), therefore recording mainly deposition of terrigenous eolian components from the Atacama Desert and the arid coasts of Peru (E.g. Molina-Cruz and Price, 1977; Scheidegger and Krissek, 1982).

Table 9.1. Selection of published Ti/Al and Fe/Al ratios, taken from Plewa et al. (2012).

Material	Ti/Al ratio	Fe/Al ratio	Reference
Upper continental crust	0.037	0.435	(Taylor and McLennan, 1995)
Upper continental crust	0.040	0.399	(Wedepohl, 1995)
Crustal average	0.069	0.68	(Taylor, 1964)
Average shale	0.053	0.55	(Wedepohl, 1971, 1995)
Average shale	0.059	0.61	(Turekian and Wedepohl, 1961)
River suspended matter	0.060	0.51	(Martin and Meybeck, 1979)
Deep-sea clay	0.060	0.63	(Martin and Meybeck, 1979)
Deep-sea clay	0.059	0.83	(Turekian and Wedepohl, 1961)
Basalt average	0.10	0.98	(Vinogradov, 1962)
Basaltic Rocks	0.18	1.11	(Turekian and Wedepohl, 1961)
Morocco	–	0.64	(Guieu et al., 2002)
Sahara	–	0.69	(Guieu et al., 2002)
Dust 30°N, 11°W	0.029	0.23	(Stuut et al., 2005)
Dust 28°N, 13°W	0.060	0.51	(Stuut et al., 2005)
Dust 22°N, 17°W	0.050	0.51	(Stuut et al., 2005)
Dust 19°N, 17°W	0.070	0.45	(Stuut et al., 2005)
Northern Saharan dust	0.091	–	(Ganor et al., 1991)
Moroccan dust	–	0.99–1.24	(Bergametti et al., 1989)
Sahelian dust	–	1.51–1.76	(Bergametti et al., 1989)
Tenerife	–	0.7	(Arimoto et al., 1995)
Surface samples (Realm of the islands)	0.09–0.25	0.59–1.12	This study
Surface samples (rest)	0.05–0.09	0.39–1.01	This study

The Al/Ti, Ti/Al and Fe/Al ratios can be used to further constrain the potential source of the terrigenous material, since different rock types have different ratios (Table 9.1). Regarding the Al/Ti ratio ODP Site 1239 exhibit values in a range from 11 to 25 (mean 17.53 ± 2.78) with no glacial-interglacial pattern, while ODP Site 1237 is slightly higher (mean 20.42 ± 2.51), varying

between 15 and 30. According to Pye (1987), the Al/Ti ratio of windblown material is 21. This points to dust as the most probable terrigenous source at ODP Site 1237. For comparison, the Al/Ti ratio of average continental crust is 15.6, average upper crust is 26.8, granites are even 40 but basalt or oceanic crust are lower than 10 (Taylor and McLennan, 1985). The Fe/Al ratio (0.49 ± 0.07 for ODP Site 1239 and 0.50 ± 0.05 for ODP Site 1237) does not show any significant downcore variations. Hence, by comparing the values reported in Table 9.1 with those from our study sites, the terrigenous matter for ODP Site 1239 (Ti/Al 0.06 ± 0.01) seems to come mainly from river suspended matter, while for ODP Site 1237 (Ti/Al 0.05 ± 0.01) the terrigenous matter could be mainly derived from windblown dust. Besides confirming our initial hypothesis about the source for terrigenous matter, both ratios (Ti/Al and Fe/Al) also validate that the terrigenous source did not change over the last 500 kyr in any of the studied cores.

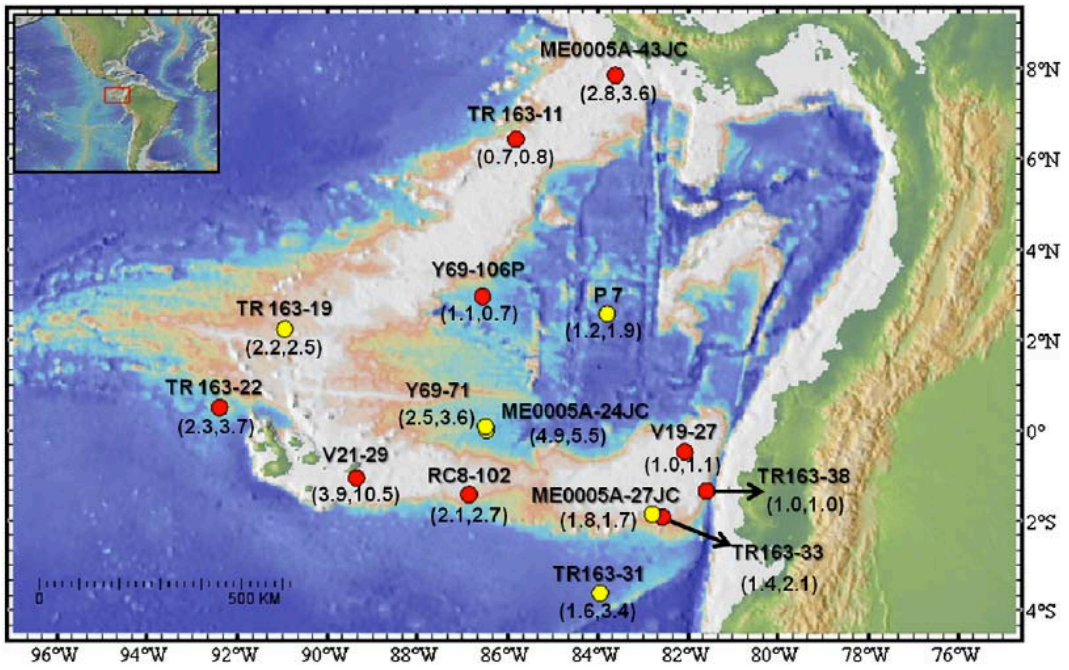

Figure 9. 2 Map showing location of studied cores in the Panama Basin, from Singh et al. (2011). Red circles represent cores analyzed by Singh et al. (2011) and yellow circles represent cores studied by others (Kienast et al., 2007; Loubere et al., 2001). Focusing factors are bracketed next to each core identification (first number in bracket represents Holocene (0–13 ka) focusing factor and second number represents glacial (13–25 ka) focusing factor.

The content and accumulation rates of siliciclastic material, iron (Fe), titanium (Ti), and lipid biomarker taraxerol at ODP Sites 1239 and 1237 exhibit a consistent glacial/interglacial pattern over the past 500 kyr. In the former, sediments are predominantly terrigenous during interglacials, while glacial siliciclastic supplies are substantially lower (Figures 5.3). Further support is provided by the ^{232}Th fluxes calculated by Singh et al. (2011), which demonstrate that at cores V19-27 (close to ODP Site 1239), ME0005-27JC and TR163-38, which are closest to the South American margin, fluxes are higher during the Holocene than those during glacial (Table 9.2). Further to the west ^{232}Th fluxes of non-margin cores are higher in glacial than in the Holocene, implying that as one moves away from the continent, the detrital signal becomes predominantly eolian derived (Singh et al., 2011).

Glacial-interglacial siliciclastic AR variations at Site 1239 (Figure 5.3) are unlikely due to post-depositional processes such as horizontal focusing or winnowing. This part of the Carnegie Ridge is thickly clearly depositional and probably has not supplied much additional sediment to the Panama Basin (Singh et al., 2011). In seismic survey for drilling on ODP Leg 202 (line 6;

Shipboard Scientific Party, 2003a) it is possible to estimate how variable the average sedimentation rates have been based on the depth to the first major seismic horizon compared to its depth at Site 1239. Site 1239 has a sedimentation rate of 4.8 cm/kyr in the upper 50 m. Along line 6, 60% of the profile has a sedimentation rate between 0.5 and 1.5X— that of Site 1239, 15% of the profile has rates >1.5X— that of Site 1239, and a little less than 20% of the profile has sedimentation rates ~0.5X— that of Site 1239 (Singh et al., 2011). Based on this and inspection of the other seismic lines, Singh et al. (2011) concluded that the sedimentation rate on the ridge appears to be uniform. Moreover, for margin cores V19-27 and TR163-38, located on the easternmost Carnegie Ridge, the average focusing factors during the Holocene and glacial are 1 and 1, respectively (Figure 9.2), so glacial focusing factors imply that sediment has not been redistributed at the studied site. Further south, cores TR163-33 and ME0005A-27JC exhibit 1.4 and 1.8 during Holocene, respectively (Figure 9.2), indicating that sediment in excess of what has been delivered vertically has been advected by deep-sea horizontal advection (I.e. focusing) to the studied site.

Table 9.2. Spatio-temporal variability of 232Th flux in the Panama Basin, from Singh et al. (2011). 232Th flux data for the first five cores are from Kienast et al. (2007), while the remaining data are from Singh et al. (2011).

Core ID	Approximate distance from continent (km)	^{232}Th flux (dpm/m^2/a)		
		Holocene	Glacial	Glacial/holocene
ME0005-24JC	600	1.9	2.6	1.3
Y69-71	600	1.8	2.5	1.4
ME0005-27JC	155	6.3	5.4	0.9
TR163-19	1250	0.8	1.2	1.4
TR163-31	250	7.2	8.9	1.2
V19-27	100	29.2	3.9	0.1
RC8-102	650	1.4	1.6	1.2
TR163-11	400	2.9	3.0	1.0
V21-29	900	0.5	0.5	1.1
ME0005A-43JC	100	7.7	8.0	1.0
TR163-22	1300	1.1	2.2	1.9
Y69-106P	850	2.6	3.0	1.2
TR163-38	40	19.8	14.9	0.8
TR163-33	140	5.8	6.8	1.2

Two different methods of calculating accumulation rates at ODP Site 1237 consistently show increased siliciclastic and Fe accumulation rates by factors of 2-3 during glacials compared to interglacials (Figure 7.2). Dust flux analyses based on ^{232}Th data also suggest that there were two-fold increases in eolian fluxes during glacial in the central equatorial (E.g. Anderson et al., 2006; McGee et al., 2007; Winckler et al., 2008) and eastern equatorial Pacific Ocean (E.g. McGee et al., 2007; Winckler et al., 2008). Among those studies, the easternmost cores are located at 110°W, and the dust source is hypothesized to change from northern-sourced (Chinese and North American) to southern-sourced (Africa, Australia and South American) dust between 5°N and 0°N in the equatorial Pacific (McGee et al., 2007). Although our study provides the record of the core furthest to the east (76.37°W) and closest to the South American continent, magnitude of the AR variations is very similar to the Glacial/ Holocene variations at both 110°W (McGee et al., 2007; Winckler et al., 2008) and 140°W (Anderson et al., 2006). Dust fluxes at Site 1237 are >30 times those measured in cores located on the equator at 110°W, which we explained by the proximal position of core 1237 to the continent. Given the large distance between the cores, the coherence of the dust flux records between the two sites is surprisingly good, supporting the hypothesis of a common source. It is clear that the major part of the detrital fractions at these two locations must be eolian.

Focusing factor at ODP Site 1237 average approximately 2, indicating that sediment in excess of what has been delivered vertically has been advected by deep-sea horizontal advection (I.e.

focusing) throughout the time interval in consideration. Sediment focusing could explain the observed 35 - 65 % difference in the accumulation of bulk and constituent sediments at the study site obtained by the two methods. The combined results, however, provide a robust basis for paleoclimate interpretations, since the general trend and the amplitudes of the terrigenous input obtained by the two independent methods compare very well.

As summarized above, results from ODP Sites 1239 and 1237 clearly oppose each other in source and chronological patterns (see Figure 7.3). Sediment and element fluxes to the Pacific seafloor vary considerably and depend upon the background state of the tropical Pacific and its influence in the South American climate. In the next section we conclude on the reasons behind these time-related patterns based on the analysis of the paleoceanography of the tropical Pacific.

9.1.3. The eastern equatorial Pacific mean background state during the Late Pleistocene

Since sediment and element fluxes to the Pacific seafloor vary considerably and depend upon the location of the ITCZ in chapters 5 and 7 we focused on evaluating the tropical Pacific background state response to Late Quaternary glacial-interglacial climate variability. For this purpose we estimated zonal and meridional SST asymmetries.

The zonal SST gradient, estimated from Mg/Ca measurements at ODP Site 806B (Ontong Java Plateau; Medina-Elizalde and Lea, 2005) and Site TR163-19 (north of the EEP cold tongue; Lea et al., 2000), shows a distinct glacial-interglacial pattern, with minima during the interglacials and maxima during glacials (Figure 5.5e). This W-E gradient suggests a weakened Walker circulation (El Niño-like conditions) during interglacials. During these warm periods trade winds are expected to weak along the equator as atmospheric pressure rises in the western Pacific and falls in the eastern Pacific. Also anomalous warming in the central and eastern Pacific should ensue, while the Walker atmospheric circulation across the tropical Pacific is weaken and accompanied by a deepening of the thermocline in much of the eastern tropical Pacific, especially along the equator (see Section 1.3). Such scenario is coincident with results from ODP Site 1239, where we found 1) reduced upwelling activity or intensity, expressed as high $\Delta\delta^{18}O_{G.ruber\text{-}G.tumida}$ values (Figure 5.4c); and 2) an anomalous warming in the easternmost Pacific, revealed by alkenone-derived glacial-interglacial SST amplitudes of up to 3.5°C (Figure 5.5.e). Conversely, during glacials, the W-E gradient suggests an intensified Walker circulation (La Niña-like conditions), characterized by cold surface water in the eastern Pacific, and possibly associated to the cold tongue (Figure 5.5e). During these cold periods trade winds are expected to strength along the equator as a warm pool remains in the west, and an eastern equatorial cold tongue, and associated upwelling, is clearly developed. The warm surface waters of the western Pacific warm pool give rise to atmospheric convection, driving easterly trade winds at the surface, and promoting the Walker circulation.

The meridional gradient was estimated using alkenone-derived SST from ODP Site 1239 (off the coast of Ecuador, see section 3.1.2) and Site MD02-2529 (off the Costa Rican margin, see Section 3.1.5). Systematic glacial-interglacial patterns are also recorded in the meridional SST gradient record (Figures 5.5b and c). Low meridional SST gradients occur during interglacials, while glacials were characterized by a steeper SST gradient, with SST amplitudes of up to 2.6°C. Meridional SST gradients within the cold tongue (ODP Site 1239 – TG7, off southern Peru) change in a glacial-interglacial pacing, the gradient being 4 - 5°C during interglacials and 6 - 7°C during glacials (Figures 7.3g-h). Then, the intensity of equatorward winds, a part of the Hadley atmospheric circulation, was likely increased during glacials. In the modern climate system this intensification is accompanied of displacements of high-pressure cells closer to the continental low, and equatorial upwelling activity (see sections 1.3 and 2.2). The opposite settings are

expected during interglacials.

Taken together, the co-occurrence of weaker meridional and zonal SST gradients suggest an El Niño-like state during interglacial periods, resulting in a reduction of off-shore upwelling, and the spatial extent of the EECT, allowing a southward shift of the EF-ITCZ, reflected in an abnormally heavy rainfall over the ordinarily arid coastal region of southern Ecuador and Peru (E.g. Horel and Cornejo-Garrido, 1986; Hastenrath, 2002; Rossel et al., 1996; Bendix, 2000a; Bendix and Bendix, 2006). Therefore high interglacial fluxes of terrigenous detritus and biogenic material to the eastern Carnegie Ridge, where ODP Site 1239 is located, can be attributed to heavy river discharges of rivers draining the Ecuadorian lowlands, E.g. Guayas and Esmeraldas rivers (Figure 2.4).

The above mentioned scenario contrast with La Niña-like conditions recorded during glacial periods, characterized by stronger meridional and zonal SST gradients, with attendant weakening of the local Hadley circulation and causing the opposite effect on precipitation and productivity patterns. During La Niña-like an EF-ITCZ northward shift is expected (E.g., Rossel et al., 1996; Bendix and Bendix, 2006; Haylock et al., 2006) associated to an expansion of the EECT, and an intensification of the trade winds and off-shore upwelling. The enhanced coastal upwelling and the northward displacement of the EF-ITCZ caused a general aridification of proximal landmasses to the east due to reduced rainfall and lowered water vapor content above cold upwelling zones. These atmospheric and continental settings explain the higher glacial windblown dust fluxes from the Peruvian coastal deserts and the Atacama Desert (recorded at ODP Site 1237), and the decrease in the continental detritus delivery from the mainland delta systems of Ecuador (recorded at ODP Site 1239).

9.1.4. Eastern equatorial Pacific primary productivity during the Pliocene-Pleistocene climate transition

In chapter 8 we reconstructed the evolution of the primary productivity, biogeochemical cycles and oceanic conditions from ODP sites 1239 and 1240, both situated in the equatorial upwelling system, in order to disentangle the different processes regulating the EEP system since 3.2 Ma. Two biogenic sediment components, Alkenone (C_{37}) and biogenic silica (BSi) concentrations, were measured. C_{37} is commonly used as an indicator of past changes in alkenone producers (some specific coccolithophorids), while BSi generally accumulates in sediments when diatom production is high (E.g. Farrell et al. 1995), and therefore the primary signal (related to opal production) is quite relevant in view of the paleoceanographic utilization of opal accumulation data, where emphasis is placed on diatom production rather than on preservation processes.

Throughout the Late Pliocene-Early Pleistocene, both, C_{37} and BSi contents experienced relatively high values between 3 and 2 Ma, a maximum around 2 Ma and lower values afterwards (Figures 8.2b and f). TN and TOC at both Sites 1239 and 1240 decreased values from 3 to 2.4 Ma, followed by an increasing trend towards a maximum achieved between 2.4 and 1.5 Ma, then, exhibited low values, similar to that around 2.5 Ma (Figures 8.2a-d). During the high productivity period of the late Pliocene, between 2.4 and 1.5 Ma, C_{37} and biogenic silica concentrations at Site 1239 reached values up to 20 mg/g and 20% respectively, while TOC and TN contents, increased up to 4% and 0.4%, respectively. On the other hand, during the same time interval, $CaCO_3$ concentrations in the eastern equatorial Pacific experienced a decrease (Farrell et al., 1995; Murray et al., 1995).

Similar productivity records have been reported elsewhere in the central and Eastern tropical Pacific. For instance Farrell et al. (1995) reported elevated opal percentages and AR in

Galapagos region between 3 and 1.5 Ma, with a distinct maximum at about 1.9 Ma. This maximum, as well as in ODP Sites 1239 and 1240, corresponds to a minimum in $\%CaCO_3$ and $CaCO_3$ flux (Figure 9.3). Since the export of carbonate from the surface ocean is a more efficient transporter of organic carbon to the deep sea than diatom silica because of its greater abundance and density (e.g. Armstrong et al., 2002; Francois et al., 2002), carbonate contents decrease might indicate either (1) lower calcareous plankton production or (2) lack of preservation. In the EEP, Murray et al. (1995) examined preservation data to relative influence of dissolution on the alteration of the record of carbonate production. They concluded that the minimum in $CaCO_3$ AR is related to production rather than dissolution hypothesizing that during those intervals of opal accumulation maxima at times of low $CaCO_3$ AR (I.e. 1.5-2.4 Ma) implies that siliceous organisms dominated production, especially because only a small proportion (approx. 10%) of the opal rain is presently preserved at those sites.

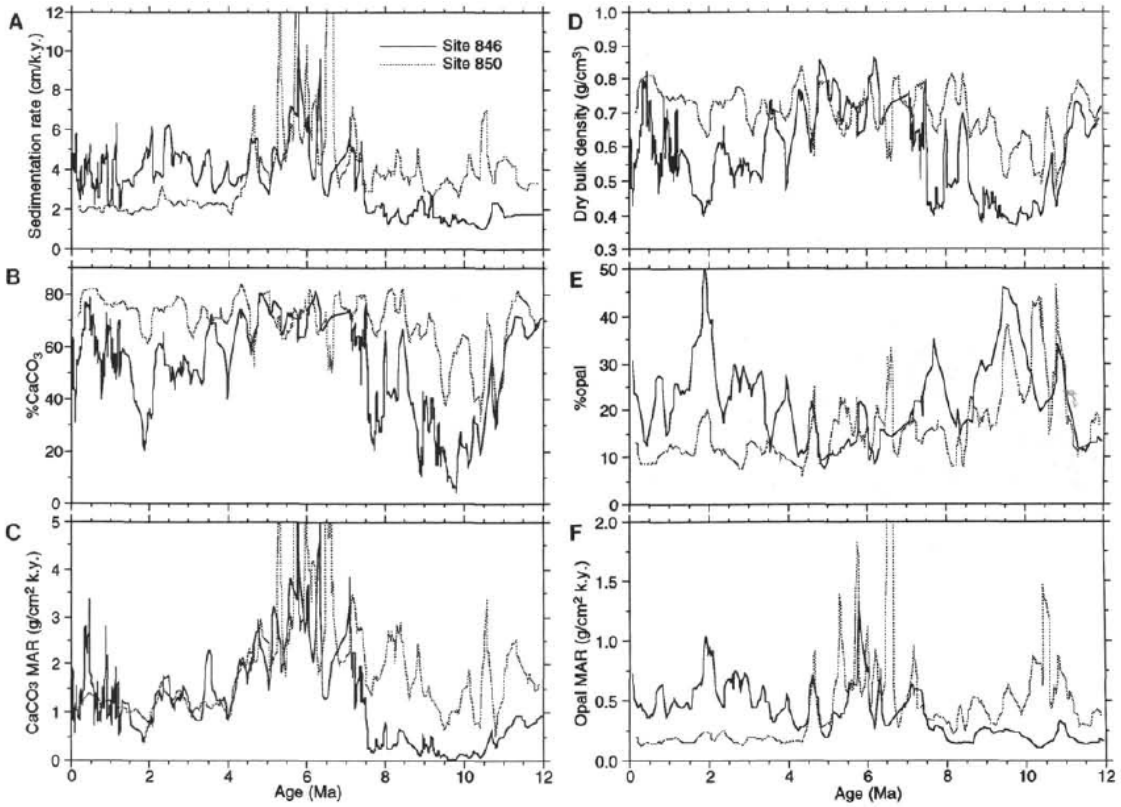

Figure 9. 3 Sedimentary records of ODP Sites 846 and 850, from Farrell et al. (1995). **(f)** Opal AR records from the Galapagos region (Sites 846) and the equatorial zone (Site 850) show the shift in the locus of maximum opal accumulation at 4.4 Ma, associated to the final closure of the Panamanian seaway. Opal AR declined sharply after 4.4 Ma in the Pacific Basin and increased in the Galapagos region. Also shown is a common increase near 2 Ma associated to a **(b)** decrease in $\%CaCO_3$ observed at several EEP sites .

Being coccolithophores one of the most important pelagic calcifying organisms in the present ocean, the high abundance of C_{37} alkenones between, 1.5 and 2.4 Ma (Figure 8.2b), results contrasting with the EEP minima in $\%CaCO_3$ and $CaCO_3$ flux (Figure 9.3). However, The abundance of alkenones in sediments is a function of both the amount of haptophyte export productivity from the overlying water column and organic matter preservation, itself dependent on sediment redox conditions and accumulation rates. Concerning the haptophyte productivity, Bolton et al. (2010) found that for the EEP the Pliocene nannofossil assemblage patterns primarily reflect the nutrient and temperature affinities of the grouped species rather than a preservational signal and that the large-amplitude of Glacial–Interglacial changes in $\%CaCO_3$ during the Pliocene partially result from productivity variations, i.e., the massive

input of biogenic silica during glacials dilutes the $\%CaCO_3$ content of the sediment record.
In summary, the significant correspondence between a regional EEP long-term high biogenic opal content (E.g. Farrell et al., 1995) associated to a long-term increase in alkenone-synthesizing coccolithophores (E.g. Lawrence et al., 2006; Dekens et al., 2007) and TOC between 2.4 and 1.5 Ma provides robust evidence that the Plio-Pleistocene transition pattern are not significantly skewed by dissolution but are rather a clear signal of an enhanced ratio of siliceous to coccolithophore productivity resulting from a common forcing.

After 3 Ma, the closure of the Panama and Indonesia corridors in the tropics (Keigwin et al., 1982; Coates et al., 1992; Haug and Tiedemann, 1998; Cane and Molnar, 2001; Karas et al., 2009) was complete, especially affecting deep thermohaline circulation. A progressive reduction in SST occurred and was accompanied by an increase of the low-latitude zonal and meridional temperature gradients that forced the gradual contraction of the warm pool towards the equator (Figure 1.3; Ravelo, 2010) at the same time that upwelling of the equatorial Pacific and the eastern ocean basin coastal regions intensified (E.g. Marlow et al., 2000; Wara et al., 2005; Lawrence et al., 2006; Dekens et al., 2007; Brierley et al., 2009; Etourneau et al., 2009). However, these assumptions based on productivity and SST-related proxies do not explain the productivity maximum period occurring at the end of the late Pliocene/early Pleistocene cooling, neither the weak biological production during the cooling interval or since the mid-Pleistocene. Moreover, it has been recently shown that the wind-driven upwelling activity in the Pacific likely strengthened since 2 Ma ago due to the intensification of the tropical/subtropical atmospheric circulation (Etourneau et al., 2010). In ODP Sites 1239 and 1240 records, the intensification of the upwelling coincided with a decline in local productivity which is unexpected considering that stronger upwelling should correspond to more nutrient supply to the surface and thereby should support high – no low – local primary productivity.

To elucidate the mechanism behind high productivity we analyzed the nitrogen isotopic composition of bulk sediment ($\delta^{15}N$) and subtracted the denitrification signature of Site 1012 (off California) to the EEP records (see Figure 8.3c) as a proxy to interpret nitrate utilization related to productivity. The interpretation of the $\Delta\delta^{15}N$ as an indicator of nutrient consumption implies that the degree of utilization was nearly the same before and after the high productivity episode of the Plio-Pleistocene transition, and was even lower during the productivity maximum event around 2 Ma. Then, the bulk $\delta^{15}N$, which constantly exhibits light values (less than 5‰), indicates a continuous high nutrient supply through upwelled waters, the major source of nitrate in the EEP. We conclude that the upwelled waters, independent of SST changes, would have therefore continuously carried nitrate to the EEP surface waters. The nitrate pool was probably largely supplied, not being a limiting factor for productivity, which is in sum similar to modern conditions: a High Nutrient Low Chlorophyll (HNLC) region because nutrients such as Fe and/or silica limit productivity in this area.

The BSI records revealed overall higher values between 3 and 2 Ma than during the Pleistocene. Silica was probably more supplied during the late Pliocene/early Pleistocene cooling in response to this silica leakage from North Pacific and Southern Ocean to the low-latitude upwelling systems resulting in the proliferation of fast-growing diatoms. Given that Fe is the major limiting factor in the modern EEP, we assert that Fe was a limiting factor for biological production all over the Plio-Pleistocene climate transition. The comparison between TN, TOC and Fe contents at Site 1239 revealed striking similarities over the last 3 Ma (Figure 8.4). We found that Fe experienced an increase during a short interval of time centered at 2 Ma. Prior to 2 Ma, if wetter conditions dominated the eastern Pacific, it should have corresponded to a continuous high supply of Fe through strong riverine transport as recently reported for the last climatic cycles (see chapter 5). Reciprocally, the last 2 Ma should have

corresponded to reduced Fe supply due to the intensification of the Walker circulation, a progressive switch to drier conditions over the EP. However, our results do not support this simple scheme. Since 3 Ma, dry conditions, basically encountered during normal or La Niña-like conditions, mostly dominated the EP. Solely the peak between 2.4 and 1.6 Ma suggests more humid conditions associated to a higher precipitation rate.

9.2. Outlook and future perspectives

The manuscripts presented as part of this thesis used a cluster of paleoceanographic proxies in order to answer some specific scientific questions for which the project "*The missing link to understand Plio-Pleistocene changes in southeast Pacific oceanography, productivity, and El Niño behavior – SE trade wind strength and its dust transport*" was undertaken. While those questions were to a great extent answered, other issues of topical interest emerged. Mainly as a consequence of the findings reported here. In this context, some future perspectives that may address the newly emerged questions are summarized below.

9.2.1. Oxygen isotopes of planktonic foraminifera

The general pattern of the differences between "equilibrium calcite" and fossil foraminifera $\delta^{18}O$ demonstrates that the relationship between them is complex and depends on local hydrography. From our study, it seems unlikely that a transfer function in form of a simple linear regression equation is the appropriate tool to correct for these distortions in paleoceanographic reconstructions of complex areas such as the eastern tropical Pacific. We realized that the current database of $\delta^{18}O$ of seawater for the eastern Pacific still need to be improved significantly with measurements in the easternmost area and across the equatorial front.

Although several $\delta^{18}O$ gradients between species indeed show changes indicative of variations of ocean stratification across the equatorial front, this approach can be complicated by the fact that foraminifera are not restricted to a certain depth level, but can also change their habitat depth. For example, Sautter and Thunell (1991) have shown that both *N. dutertrei* and *N. pachyderma* follow isothermal ranges, migrating to shallower waters during upwelling and subsequently descending after upwelling. Additionally, the use of sediment samples might be biased since (1) not all the species of foraminifera have the same seasonality; (2) foraminiferal tests are exposed to post-depositional mixing (I.e. bioturbation, winnowing and lateral migration along the ocean floor); and (3) some can experience calcite dissolution. Therefore, further research is clearly needed concerning the isotopic composition in living planktonic foraminifera in order to depict a clearer relationship between the "equilibrium calcite" and foraminiferal $\delta^{18}O$, avoiding artifacts caused by seasonality, sediment mixing and calcite enriching in ^{18}O during ontogenesis or gametogenesis. Furthermore, it is important to develop much more research on the ecology and isotopic composition of living planktonic foraminifera and its distribution across the Equatorial front during different seasons.

9.2.2. Glacial-interglacial terrigenous delivery and continental hydrological balance.

The specific mechanism behind the disproportion in the magnitude of lithogenic supply among interglacials to the EEP (ODP Site 1239) is unknown. Differences in atmospheric CO_2 concentrations, astronomical forcing and glacial ice-volume (see Tzedakis et al., 2009) plausibly fostered variations in moisture advection to the ITCZ and to the continent hence stimulating variations in precipitation, vegetation cover and fluvial suspended loads that are reflected in the variable magnitude between the different interglacials of terrestrial input to the EEP. To

unravel the main climatic triggers affecting interglacial hydrological balance much more research in the area of ocean/atmosphere/lithosphrere is required and necessary.

Researchers studying ocean sediments in the central equatorial Pacific have tended to emphasize the importance of Chinese and North American dust sources (E.g. Nakai et al., 1993; Rea et al., 1994), others suggest Australia and New Zealand as additional important sources (E.g. Stancin et al., 2006), while the dust deposited in the eastern equatorial Pacific is dominantly derived from sources in northern South America (E.g. Nakai et al., 1993; Rea et al., 1994; Stancin et al., 2006). On a general level, existing Nd and Pb isotope and clay mineralogy data, as well as dust models, suggest a change from northern-sourced to southern-sourced dust between 5°N and 0°N in the equatorial Pacific (McGee et al., 2007). We provisionally accept these basic findings, which suggest that ODP Site 1237 provides a record of dust production and deposition, while acknowledging the need for more detailed provenance studies of deep sea terrigenous fraction. Appropriate regional mapping of the dust AR at different time frames will provide a comprehensive picture of changes in the intensity of the dust cycle, including source, transport and deposition.

9.2.3. Paleoceanography of the Plio-Pleistocene climatic transition

Extrapolating a similar scenario to the Plio-Pleistocene climate transition than proposed in chapter 5 for the last interglacials, the increasing temperature gradient between the EEP warm pool and cold tongue may have promoted the northward shift of the southeasterly trade winds across the equator, precipitation in the eastern Pacific similar to El Niño-like conditions and therefore displaced northward the ITCZ and EF to reach their northernmost position between 2.4 and 1.6 Ma. However, it is still lacking Plio-Pleistocene records from the EEP warm pool to unravel the evolution of the SST gradients north and south of EF. In contrast, during the late Plio-Pleistocene cooling and from the mid-to-late Pleistocene, decreasing Fe concentration, higher $\delta^{15}N$ values and weak productivity suggest that the ITCZ and EF were probably further south and was accompanied by a contraction of the EEP cold tongue. Reasons explaining why ITCZ and EF were at their northernmost position between 2.4 and 1.6 Ma remain unclear, although it may correspond to a transition period preceding the establishment of the Walker circulation related to the global oceanic reorganization, especially in the Southern Ocean.

REFERENCES

Abrantes, F., Lopes, C., Mix, A., and Pisias, N. (2007). Diatoms in Southeast Pacific surface sediments reflect environmental properties. Quaternary Science Reviews 26, 155–169.

-Aceituno, P. (1988) .On the functioning of the Southern Oscillation in the South American Sector. Part I: Surface climate. Monthly Weather Review 116, 505-524.

-Alexander, M.A., Bladé, I., Newman, M., Lanzante, J. R., Lau, N.C., and Scott, J.D. (2002). The Atmospheric Bridge: the Influence of ENSO Teleconnections on Air-Sea Interaction Over the Global Oceans. Journal of climate 15 (16), 2205–2231.

-Alexander, M.A., and Scott, J.D. (2002).The influence of ENSO on air-sea interaction in the Atlantic. Geophysical research letters 29 (14), 10.1029/2001GL014347.

-Allmendinger, R. W., Jordan, T. E., Kay, S. M., and Isacks, B. L. (1997). The evolution of the Altiplano-Puna Plateau of the Central Andes. Annual Review of Earth and Planetary Sciences25, 139–174.

-Alpers, C.N., and Brimhall, G.H. (1988). Middle Miocene climate change in the Atacama Desert, northern Chile: evidence from supergene mineralization at La Escondida. Geological Society of America Bulletin 100, 1640–1656.

-Altabet, M.A., and Francois, R. (1994).Sedimentary nitrogen isotopic ratios asa recorder for surface ocean nitrate utilization, Global Biogeochemical Cycles 8, 103–116. doi: 10.1029/93GB03396.

- Anderson, R.F., Fleisher, M.Q., and Lao, Y. (2000). Glacial-interglacial variability in the delivery of dust to the central equatorial Pacific Ocean. Earth and Planetary Science Letters, 242, 406, doi:10.1016/j.epsl.2005.11.061.

-Andreasen, D. J. and Ravelo, A. C. (1997).Tropical Pacific Ocean thermocline depth reconstructions for the last glacial maximum. Paleoceanography 12(3), 395-413.

- Armstrong, R. A., Lee, C., Hedges, J. I., Honjo, S., and Wakeham, S. G. (2002). A new mechanistic model for organic carbon fluxes in the ocean based on the quantitative association of POC with ballast minerals. Deep-Sea Research, Part 2, Topical Studies in Oceanography, 49, 219–236.

-Babeyko, A., Sobolev, S., Vietor, T., Oncken, O., and Trumbull, R. (2006). Numerical study of weakening processes in the central Andean backarc. In: Oncken, O. et al. (Eds).The Andes – Active Subduction Orogeny. Berlin: Springer-Verlag. 495–510.

-Bakun, A., Nelson, C.S., (1991). The seasonal cycle of wind stress curl in sub-tropical boundary current regions. Journal of Physical Oceanography 21, 1815–1834.

-Ballantyne, A. P., Rybczynski, N., Baker, P. A., Harington, C. R., and White, D. (2006).Pliocene Arctic temperature constraints from the growth rings and isotopic composition of fossil larch. Palaeogeography, Palaeoclimatology and Palaeoecology 242, 188–200, doi:10.1016/j.palaeo. 2006.05.016.

-Ballantyne, A.P., Greenwood, D.R., Sinninghe Damsté, J.S., Csank, A.Z., Eberle, J.J. and Rybczynski, N. (2010).Significantly warmer Arctic surface temperatures during the Pliocene indicated by multiple independent proxies. Geology38, 603-606. doi: 10.1130/G30815.1.

-Bareille, G., Grousset, F., Labracherie, M., Labeyrie, L., and Petit, J. -R. (1994). Origin of detrital fluxes in the Southeast Indian Ocean during the last climatic cycles. Paleoceanography 9(6), 799-819.

-Bartoli, G., Sarnthein, M., Weinelt, M., Erlenkeuser, H., Garbe-Schönberg, D., and Lea, D. (2005).Final closure of Panama and the onset of northern hemisphere glaciation. Earth and Planetary Science Letters 237, 33–44.doi:10.1016/j.epsl.2005.06.020.

-Bassinot, F. C. (2007).Oxygen isotope stratigraphy of the oceans. In: Scott A. E. (Ed) Encyclopedia of Quaternary Science, Elsevier, Oxford, 1740-1748.

- Bé, A. W. H. (1980). Gametogenic calcification in a spinose planktonic foraminifer, Globigerinoides sacculifer (Brady). Marine Micropaleontology 5, 283-310.

-Beaufort, L. (2002). Cruise Report MD 126 MONA (Marges Ouest Nord-Américaines) - IMAGES VIII: Leg 1, Vancouver (Canada), 30-05-2002 to San Diego (USA), 06-06-2002; Leg 2, San Diego (USA), 08-06-2002 to Panama, 24-06-2002.Les rapports de campagnes à la mer. Institut polaire français Paul-Émile Victor., 186 p.

-Beck, M., Burmester, R., Cembrano, J., Drake, R., García, A., Hervé, F., and Munizaga, F. (2000). Paleomagnetism of the North Patagonian Batholith, southern Chile. An exercise in shape analysis. Tectonophysics 326 (1–2), 185–202.

-Beltran, C., Flores, J. A., Sicre, M. A., Baudin, F., Renard, M., and de Rafélis, M. (2011).Long chain alkenones in the early Pliocene Sicilian sediments (Trubi Formation–Punta di Maiata section),

Implications for the alkenone paleothermometry, Palaeogeography, Palaeoclimatology, Palaeoecology 308, 253–263. doi:10.1016/j.palaeo.2011.03.017.
-Bemis, B. E., Spero, H. J., Bijma, J., and Lea, D. W. (1998). Reevaluation of the oxygen isotopic composition of planktonic foraminifera: Experimental results and revised paleotemperature equations. Paleoceanography 13, 150-160.
-Bendix, J. (2000a).PA comparative analysis of the major El Niño events in Ecuador and northern Peru over the las two decades. Zbl. Geol. Palaeont.Teil I 7-8, 1119-1131.
-Bendix, J. (2000b).Precipitation dynamics in Ecuador and northern Peru during the 1991/92 El Niño: a remote sensing perspective. International Journal of Remote Sensing 21 (3), 533–548.
-Bendix, A., and Bendix, J., (2006).Heavy rainfall episodes in Ecuador during El Niño events and associated regional atmospheric circulation and SST patterns. Advances in geosciences 6, 43-49.
- Berger, W.H. (1976). Biogenous deep-sea sediments: production, preservation, and interpretation. In: Treatise on Chemical Oceanography, edited by J.P. Riley and R. Chester, Academic Press, New York, 265–388 pp.
-Berger, W. H., Killingley, J. S., and Vincent, E. (1978). Stable isotopes in deep-sea carbonates: Box Core ERDS-92 west equatorial Pacific. Oceanologica Acta 1, 203-216.
-Best, B. J. and Kessler, M. (1995) Biodiversity and conservation in Tumbesian Ecuador and Peru. Cambridge, U.K.: Birdlife International.220 p.
-Betancourt, J. L., Latorre, C., Rech, J. A., Quade, J., and Rylander, K. A. (2000).A 22,000-year record of monsoonal precipitation from northern Chile's Atacama Desert. Science 289, 1542-1546.
-Bijma, J., Altabet, M., Conte, M., Kinkel, H., and Versteegh, G. J. M. (2001). Primary signal: Ecological and environmental factors - Report from working group 2.Geochemistry Geophysics Geosystems 2, 2000GC000051.
-Bird, M. I., Summons, R. E., Gagan, M. K., Roksandic, Z., Dowling, L., Head, J., Fifield, L. K., Cresswell, R. G., Johnson, D. P. (1995). Terrestrial vegetation change inferred from n-alkane $\delta^{13}C$ analysis in the marine-environment. Geochimica et Cosmochimica Acta 59, 2853– 2857.
-Bjerknes, J., (1969).Atmospheric teleconnections from equatorial Pacific. Monthly Weather Review, 97, 163-172.
-Blisniuk, P. M., Stern, L. A., Chamberlain, C. P., Zeitler, P. K., Ramos, V. A., Sobel, E. R., Haschke, M. Strecker, M. R., and Warkus, F. (2006).Links between mountain uplift, climate, and surface processes in the southern Patagonian Andes. pp. 429–440 in: Oncken, O., Chong, G., Franz, G., Giese, P., Götze, H.-J. Ramos, V. A., Strecker, M. R., and Wigger P.(editors). The Andes: Active Subduction Orogeny. Frontiers in Earth Sciences. Springer Verlag, Berlin.
-Bolton, C. T., Lawrence, K. T., Gibbs, S. J., Wilson, P. A., Cleaveland, L. C., Timothy, D., and Herbert, T. D. (2010).Glacial-interglacial productivity changes recorded by alkenones and microfossils in late Pliocene eastern equatorial Pacific and Atlantic upwelling zones. Earth and Planetary Science Letters 295, 401–411. doi:10.1016/j.epsl.2010.04.014.
-Bookhagen, B., and Strecker, M. R. (2008).Orographic barriers, high-resolution TRMM rainfall, and relief variations along the eastern Andes. Geophysical Research Letters 35, L06403, doi: 10.1029/2007GL032011.
-Boot C. S., Ettwein V. J., Maslin M. A., Weyhenmeyer C. E., and Pancost R. D. (2006).A 35,000 year record of terrigenous and marine lipids in Amazon Fan sediments. Organic Geochemistry 37, 208-219.
-Boss, C. B., and Fredeen, K. J. (1997).Concepts, Instrumentation and Techniques in Inductively Coupled Plasma Optical Emission Spectrometry. Perkin-Elmer Corporation, USA, 125 p.
-Brand, L. E. (1991).Minimum iron requirements of marine phytoplankton and the implications for the biogeochemical control of new production. Limnology and Oceanography 36, 1756–1771.
-Brand, L. E. (1994).Physiological ecology of marine coccolithophores. In: Winter, A. and Siesser, W. G. (Eds.) Coccolithophores. Cambridge University Press, Cambridge, UK, pp. 39–49.
-Brandes, J. A., and Devol, A. H., (1997). Isotopic fractionation of oxygen and nitrogen in coastal marine sediments, Geochimica et Cosmochimica Acta 61, 1793–1801. Doi: 10.1016/S0016-7037(97)00041-0.
-Brassell, S. C., Eglinton, G., Marlowe, I. T., Pflaumann, U., and Sarnthein, M. (1986). Molecular stratigraphy: A new tool for climatic assessment. Nature 320, 129–133.
-Brassell S. C., Eglinton G., and Howell V. J. (1987).Palaeo-environmental assessment for marine organic-rich sediments using molecular organic geochemistry. In: Fleet, A. J., and Brooks, J. (Eds.) Marine Petroleum Source Rocks. Blackwell, London, pp. 79–98.
-Brierley, C. M. Fedorov, A. V., Liu, Z., Herbert, T. D., Lawrence, K. T., and LaRiviere, J. P. (2009).Greatly

expanded tropical warm pool and weakened Hadley circulation in the early Pliocene. 323 (5922), 1714-1718. *Doi:* 10.1126/science.1167625.
-Broccoli, A. J., Dahl, K. A., and Stouffer, R. J. (2006).Response of the ITCZ to Northern Hemisphere cooling. Geophysical Research Letters 33, L01702, doi: 10.1029/2005GL024546.
-Brocks J. J., and Summons R. E. (2004).Sedimentary hydrocarbons, biomarkers for early life. In: Schlesinger W. H. (Ed.) Treatise on Geochemistry. Pergamon Press, Oxford, 63-115.
-Brocks J. J., and Pearson A.(2005).Building the biomarker tree of life. Reviews in Mineralogy and Geochemistry 59, 233-258.
- Broecker, W. S. (1971). Calcite accumulation rates and glacial to interglacial changes in oceanic mixing. In: Late Cenozoic Glacial Ages, edited by K. K. Turekian, Yale Univ. Press, New Haven, Conn., 239 – 265 pp.
-Broecker, W. S. (1986).Oxygen isotope constraints on surface temperatures. Quaternary Research 26, 121-134.
-Brzezinski, M.A., Dumousseaud, C., Krause, J.W., Measures, C.I., Nelson, D. M. (2008). Iron and silicic acid concentrations together regulate Si uptake in the equatorial Pacific Ocean. Limnology and Oceanography 53, 875–889.
-Brzezinski, M.A., Baines, S.B., Balch, W.M., Beucher, C.P., Chai, F., Dugdale, R. C., Krause, J.W., Landry, M.R., Marchi, A., Measures, C.I., Nelson, D.M., Parker, A. E., Poulton, A., Seplph, K.E., Strutton, P.G., Taylor, A.G., and Twining, B. (2011). Co-limitation of diatoms by iron and silicic acid in the equatorial Pacific. Deep-Sea Research Part II 58, 493-511.
-Burton, K.W., Ling, H.-F., and O'Nions, R.K. (1997). Closure of the Central American isthmus and its effect on deep-water formation in the North Atlantic, Nature 386 (6623), 382–385. Doi: 10.1038/386382a0.
-Bush, W. H., and Keller, G. H. (1981).The physical properties of Peru-Chile continental margin sediments – The influence of coastal upwelling on sediment properties. Journal of Sedimentary Petrology 51(3), 705-719.
-Cáceres, L., Gómez-Silva, B., Garró, X., Rodríguez, V., Monardes, V., and McKay, C. P. (2007). Relative humidity patterns and fog water precipitation in the Atacama Desert and biological implications. Journal of Geophysical Research 112, G04S14.Doi: 10.1029/2006JG000344.
-Calvert, S. E., and Pedersen, T. F. (2007). Elemental proxies for palaeoclimatic and palaeoceanographic variability in marine sediments: interpretation and application. In: Hillarie, C., and de Vernal, A. (Eds.).Proxies in Late Cenozoic Paleoceanography. Developments in Quaternary Research 1, Elsevier Science, Amsterdam, 567–644.
-Calienes, R., Guillen, O., Lostanau, N., (1985). Variabilidad espacio temporal de clorofila, produccion primaria y nutrients frente a la costa peruana. IMARPE bolletin, Callao. 44.
-Cannariato, K.G, and Ravelo, A.C. (1997) Pliocene–Pleistocene evolution of eastern tropical Pacific surface water circulation and thermocline depth. Paleoceanography 12(6), 805–820.
-Cane, M.A., and Molnar, P., (2001).Closing of the Indonesian Seaway as a precursor to east African aridification around 3 to 4 million years ago, Nature, 411, 157–162. Doi: 10.1038/35075500.
-Cantalamessa, G., Di Celma, C., and Ragaini, L. (2005). Sequence stratigraphy of the Punta Ballena Member of the Jama Formation (Early Pleistocene, Ecuador): insights from integrated sedimentologic, taphonomic and paleoecologic analysis of molluscan shell concentrations. Palaeogeography, Palaeoclimatology, Palaeoecology 216, 1– 25. doi:10.1016/j.palaeo.2004.09.012.
-Cereceda, P., Osses, P., Larrain, H., Farías, M., Lagos, M., Pinto, R., and Schemenauer, R. S. (2002). Advective, orographic and radiation fog in the Tarapacá region, Chile. Atmospheric Research 64, 261–271.
-Chelton, D. B., Esbensen, S. K., Schlax, M. G., Thum, N., Freilich, M. H., Wentz, F. J., Gentemann, C. I., McPhaden, M. J., Schopf, P. S. (2001).Observations of Coupling between Surface Wind Stress and Sea Surface Temperature in the Eastern Tropical Pacific. Journal of Climate 14(7), 1479-1498.
-Chiang, J. C. H., and Bitz, C. M. (2005). Influence of high-latitude ice cover on the marine intertropical convergence zone. Climate Dynamics 25, 477–496.
-Clapperton, C. (1993).Quaternary Geology and Geomorphology of South America. Elsevier, Amsterdam.
-Clark, P. U., Archer, D., Pollard, D., Blum, J. D., Rial, J. A., Brovkin, V., Mix, A. C., Pisias, N. G, Roy, M. (2006). The middle Pleistocene transition: characteristics, mechanisms, and implications for long-term changes in atmospheric pCO2. Quaternary Science Reviews 25, 3150–3184. doi:10.1016/j.quascirev.2006.07.008.
-Clarke, J. D. A. (2006). Antiquity of aridity in the Chilean Atacama Desert. Geomorphology 73, 101-114.

-Clemens, S. (1998). Dust response to seasonal atmospheric forcing: Proxy evaluation and calibration. Paleoceanography 13(5), 471–490.
-Coale, K.H., Fitzwater, S.E., Gordon, R.M., Johnson, K.S., Barber, R.T., (1996).Control of community growth and export production by upwelled iron in the equatorial Pacific Ocean. Nature 379, 621–624.
-Coates, A. G., Jackson, J. B. C., Collins, L. S., Cronin, T. M., Dowsett, H. J., Bybell, L. M., Jung, P., and Obando,J. A. (1992). Closure of the Isthmus of Panama: The near-shore marine record of Costa Rica and western Panama. Geological Society of America Bulletin 104, 814–828.
-Cobbold, P. R., Rosello, E. A., Roperch, P., Arriagada, C., Gómez, L. A., and Lima, C. (2007). Distribution, timing and causes of Andean deformation across South America. Geological Society of London 272, 321–343.
-Collot, J. –Y., Michaud, F., Alvarado, A., Marcaillou, B., Sosson, M., Ratzov, G., Migeon, S., Calahorrano, A., and Pazmino, A. Visión general de la morfología submarina del margen convergente de Ecuador-Sur de Colombia: implicaciones sobre la transferencia de masa y la edad de la subducción de la Cordillera de Carnegie. En: Collot, J. –Y., Salares, V., and Pazmino, A. (Eds). GEOLOGÍA Y GEOFÍSICA MARINA Y TERRESTRE DEL ECUADOR. Comisión Nacional del Derecho del Mar (CNDM) - Institut de Recherche pour le Développement (IRD) - Instituto Oceanográfico de la Armada (INOCAR), 47-74.
-Coltorti, M., and Ollier, C. D. (2000).Geomorphic and tectonic evolution of the Ecuadorian Andes. Geomorphology 32, 1–19.
-Conte, M. H., Sicre, M. –A., Rühlemann, C., Weber, J. C., Schulte, S., Schulz-Bull, D., and Blanz, T. (2006).Global temperature calibration of the alkenone unsaturation index (U^{K}_{37}) in surface waters and comparison with surface sediments. Geochemistry, Geophysics, Geosystems 7(2), doi: 10.1029/2005GC001054.
-Conte, M. H., and Weber, J. C., (2002). Plant biomarkers in aerosols record isotopic discrimination of terrestrial photosynthesis. Nature 417, 639–641.
-Cordani, U.G., Milani, E.J., Filho, A.T., and Campos, D.A. (editors).(2000).Tectonic Evolution of South America.31st International Geological Congress, Rio de Janeiro, 6–17 August 2000.Geological Society of America, Boulder.
-Cranwell, P. A. (1981).Diagenesis of free and bound lipids in terrestrial detritus deposited in lacustrine sediment. Organic Geochemistry 3 (3), 79– 89.
-Crowley, T. J. (1996). Pliocene climates: the nature of the problem. Marine Micropaleontology 27, 3–12. Doi: 10.1016/0377-8398 (95)00049-6.
-Dekens, P. S., Ravelo, A. C., and McCarthy, M. D. (2007). Warm upwelling regions in the Pliocene warm period. Paleoceanography 22, PA3211. Doi: 10.1029/2006PA001394.
-De Mendiola, B.R., (1981).Seasonal phytoplankton distribution along the Peruvian coast. In, Richards, F.A.(Ed.), Coastal Upwelling. American Geophysical Union, Washington, DC, pp. 348–356.
-Dehairs, F., Chesselet, R., and Jedwab, J. (1980). Discrete suspended particles of barite and the barium cycle in the open ocean. Earth and Planetary Science Letters 49, 528-550.
-Dengo, C.A., and Covey, M.C. (1993).Structure of the Eastern Cordillera of Colombia: Implications for trap styles and regional tectonics, American Association of Petroleum Geologists Bulletin 77, 1315–1337.
-Deser, C., and Wallace, J. M. (1990). Large-scale atmospheric circulation features of warm and cold episodes in the tropical Pacific. Journal of Climate 3, 1254-1281.
-DiTullio, G. R., Geesey, M. E., Maucher, J. M., Alm, M. B., Riseman, S. F., and Bruland, K. W. (2005). Influence of iron on algal community composition and physiological status in the Peru upwelling system. Limnol.Oceanogr., 50(6), 2005, 1887–1907.
-Dowsett, H.J., Cronin, T.M., Poore, R.Z., Thompson, R.S., Whatley, R.C., and Wood, A.M. (1992).Micropaleontological evidence for increased meridional heat transport in the North Atlantic Ocean during the Pliocene. Science 258, 1133–1135. Doi: 10.1126/science.258 .5085.1133.
-Duce, R., and Tindale, N. (1991). Chemistry and biology of iron and other trace metals. Limnological Oceanography 36(8), 1715-1726.
-Dumont, J. F., Santana, S., Vilema, W., Pedoja, K., Ordoñez, M., Cruz, M., Jiménez, N., and Zambrano, I. (2005).Morphological and microtectonic analysis of Quaternary deformation from Puná and Santa Clara Islands, Gulf of Guayaquil, Ecuador (South America).Tectonophysics 399 (2005) 331– 350. doi:10.1016/j.tecto.2004.12.029.
-Dumont, J. F., Santana, S., and Vilema, W. (2005).Morphologic evidence of active motion of the Zambapala Fault, Gulf of Guayaquil (Ecuador).Geomorphology 65,223–239. doi:10.1016/j.geomorph.2004.09.003
- Duplessy, J. C., Bé, A. W. H. and Blanc, P.L. (1981). Oxygen and carbon isotopic composition and

biogeographic distribution of planktonic foraminifera in the Indian Ocean. Palaeogeography, Palaeoclimatology, Palaeoecology 33, 9-46.
-Dymond, J. (1981). Geochemistry of Nazca plate surface sediments: An evaluation of hydrothermal, biogenic, detrital and hydrogenous sources. In: Kulm, L. D., Dymond, J., Dasch, E. J., Hussong, D. M., and Roderick, R. (Eds.), Nazca Plate: Crustal Formation and Andean Convergence. Memoir Geological Society of America154, 133–173.
-Dymond, J., Suess, E., and Lyle, M. (1992). Barium in deep-sea sediment: a geochemical proxy for paleoproductivity. Paleoceanography 7(2): 163-181.
-Echevin, V., Aumont, O., Ledesma, J., and Flores, G. (2008). The seasonal cycle of surface chlorophyll in the Peruvian upwelling system: A modelling study. Progress in Oceanography 79 (2008) 167–176. doi:10.1016/j.pocean.2008.10.026.
-Egbue, O., and Kellogg, J. (2010).Pleistocene to Present North Andean "escape". Tectonophysics 489, 248–257. doi:10.1016/j.tecto.2010.04.021
-Eglinton, G., and Hamilton, R. J. (1967).Leaf epicuticular waxes. Science 156, 1322– 1334.
-Eglinton, T. I., and Eglinton, G. (2008).Molecular proxies for paleoclimatology. Earth and Planetary Science Letters 275, 1-16. doi:10.1016/j.epsl.2008.07.012.
-Elger, K., Oncken, O., and Glodny, J. (2005). Plateau-style accumulation of deformation; southern Altiplano. Tectonics 24, TC4020.Doi: 10.1029/2004TC001675.
-Etourneau, J., Martinez, P., Blanz, T., Schneider, R., (2009). Pliocene–Pleistocene variability of upwelling activity, productivity, and nutrient cycling in the Benguela region. Geology 37, 871–874.
-Etourneau, J., Schneider, R., Blanz, T., and Martinez, P. (2010).Intensification of the Walker and Hadley atmospheric circulations during the Pliocene–Pleistocene climate transition. Earth and Planetary Science Letters 297, 103-110. doi:10.1016/j.epsl.2010.06.010.
-Evans, C. D. R., and Whittaker, J. E. (1982).The geology of the western part of the Borbón Basin, North-west Ecuador. Geological Society of London, Special Publications10, 191-198. Doi: 10.1144/ GSL.SP.1982.010.01.12.
-Fairbanks, R. G., Wiebe, P. H., and Bé, A. W. H. (1980).Vertical distribution and isotopic composition of living planktonic foraminifera in the western North Atlantic. Science 207, 61-63.
- Farrell, J. W., Raffi, I., Janecek, T. C., Murray, D. W., Levitan, M., Dadey, K. A., Emeis, K. -C., Lyle, M., Flores, J. -A., and Hovan, S. (1995). Late Neogene sedimentation patterns in the eastern equatorial Pacific Ocean. In: Proceedings of the Ocean Drilling Program, Scientific Results, 138, edited by Pisias, N. G., Mayer, L. A., Janecek, T. R., Palmer-Julson, A., and van Andel, T. H., College Station, TX (Ocean Drilling Program), 717–756 pp. doi:10.2973/odp.proc.sr.138.143.1995
-Fedorov, A., Dekens, P., McCarthy, M., Ravelo, A. C., deMenocal, P. B., Barreiro, M., Pacanowski, R. C., and Philander, S. G. (2006).The Pliocene Paradox (Mechanisms for a permanent El Niño).Science, 312, 5779, doi:10.1126/science.1122666.
-Feldberg, M. J. and Mix, A. C. (2003). Planktonic foraminifera, sea surface temperatures, and mechanisms of oceanic change in the Peru and south equatorial currents, 0-150 ka BP. Paleoceanography 18(1), 1016, doi: 10.1029/2001PA000740.
-Fiedler, P. C., and Talley, L. D. (2006). Hydrography of the eastern tropical Pacific: A review. Progress in Oceanography 69 (2006) 143–180. doi:10.1016/j.pocean.2006.03.008.
-Field, D. B. (2004).Variability in vertical distribution of planktonic foraminifera in the California Current: Relationships to vertical ocean structure. Paleoceanography 19, PA2014.
Doi: 10.1029/2003PA000970.
-Filipelli, G. M., and Flores, J. A. (2009). From the warm Pliocene to the cold Pleistocene: A tale of two oceans. Geology 37, 959-960. doi:10.1130/focus102009.1.
- Francois, R., Honjo, S., Krishfield, R., and Manganini, S. (2002). Factors controlling the flux of organic carbon to the bathypelagic zone of the ocean. Global Biogeochemical Cycles 16, Art. No. 1087.
-Fung, I. Y., S. K. Meyn, I. Tegen, S. C. Doney, J. G. John, and J. K. B. Bishop (2000), Iron supply and demand in the upper ocean, Global Biogeochem. Cycles, 14(2), 697 – 700.
-Ganeshram, R. S., Pedersen, T. F., Calvert, S. E., McNeill, G. W., and Fontugne, M. R. (2000). Glacial-interglacial variability in denitrification in the world's oceans: Causes and consequences, Paleoceanography 15, 361–376. Doi: 10.1029/1999PA000422.
-Garcés, J. (2005). Procesos que afectan la termoclina y la TSM en el Pacifico ecuatorial oriental con enfasis en el borde costero ecuatoriano. Tesis doctoral en Oceanografia. Departamento de Oceanografia, facultad de Ciencias Naturales y Oceanograficas, Universidad de Concepcion, 71 p.

-Garreaud, R. D. (1999). A multiscale analysis of the summertime precipitation over the central Andes. Monthly Weather Review 127, 901 – 921.
-Garreaud, R. D., Vuille, M., and Clement, A. C. (2003). The climate of the Altiplano: observed current conditions and mechanisms of past changes. Palaeogeography, Palaeoclimatology, Palaeoecology 194, 5-22. Doi: 10.1016/S0031-0182(03)00269-4.
-Garreaud, R. D., Molina, A., Farias, M. (2010). Andean uplift, ocean cooling and Atacama hyperaridity: A climate modeling perspective. Earth and Planetary Science Letters 292, 39–50. doi:10.1016/j.epsl.2010.01.017.
-Garzione, C. N., Hoke, G. D. Libarkin, J. C., Withers, S., Mac Fadden, B., Eiler, J., Ghosh, P., and Mulch, A.(2008).Rise of the Andes. Science 320, 1304-1307. doi:10.1126/science.1148615.
-Ghosh, P., Garzione, C.N., and Eiler, J.M. (2006). Rapid uplift of the Altiplano revealed through $^{13}C–^{18}O$ bonds in paleosol carbonates. Science 311, 511–515.
-Gillan, F. T., Hogg, R. W., and Drew, E. A. (1984).The sterol and fattyacid compositions of 7 tropical seagrasses from North Queensland, Australia. Phytochemistry 23, 2817 – 2821.
-Gingele, F., and Dahmke, A. (1994).Discrete barite particles and barium as tracers of paleoproductivity in south Atlantic sediments. Paleoceanography 9(1), 151-168.
-Gómez, E., Jordan, T. E., Allmendinger, R. W., Hegarty, K., Kelley, S., and Heizler, M. (2001).Controls on architecture of the Late Cretaceous to Cenozoic southern Middle Magdalena Valley Basin, Colombia. Geological Society of America Bulletin115, 131–147.
-Gómez, E., Jordan, T. E., Allmendinger, R. W., and Cardozo, N. (2005).Development of the Colombian foreland-basin system as a consequence of the diachronous exhumation of the northern Andes. Geological Society of America Bulletin117, 1272–1292.
-Gonzalez, C, Urrego. L. E and Martinez, J. I. Late Quaternary vegetation and climate change in the Panama Basin: Palynological evidence from marine cores ODP 677B and TR 163-38. Palaeogeography, Palaeoclimatology, Palaeoecology 234 (2006) 62–80. doi:10.1016/j.palaeo.2005.10.019.
-Gough, M. A., Fauzi, R., Mantoura, C., and Preston, M. (1993).Terrestrial plant biopolymers in marine sediments. Geochimica et Cosmochimica Acta 57, 945– 964.
-Gregory-Wodzicki, K.M. (2000).Uplift history of the Central and Northern Andes; a review. Geological Society of America Bulletin 112, 1091–1105.
-Grimalt, J. O., and Lopez, J. F. (2007).Alkenone paleothermometry from coccoliths. In: Scott A. E. (Ed) Encyclopedia of Quaternary Science 1610-1625.
-Gutscher, M. –A., Malavieille, J., Lallemand, D., and Collot, J. –Y. (1999). Tectonic segmentation of the North Andean margin: Impact of the Carnegie collision. Earth and Planetary Science letters 168, 255-270.
-Halpern, D., and Hung, C.-W., (2001): Satellite observations of the southeast Pacific intertropical convergence zone during 1993–1998. *J. Geophys. Res.,* 106 ,28 107–28 112.
-Hamilton, K., and Garcia, R. R., (1986).El Nino/Southern Oscilllation events and their associated midlatitude teleconnections 1531-1841. Bulletin American Metereological Society 67(11), 1354-1361.
-Harada, N., Handa, N., Harada, K., and Matsuoka, H. (2001). Alkenones and particulate fluxes in sediment traps from the central equatorial Pacific. Deep-Sea Research Part I, Oceanographic Research Papers 48, 891–907.
-Hartley, A. J., and Chong, G. (2002). Late Pliocene age for the Atacama Desert: Implications for the desertification of western South America. Geology 30 (1), 43–46.
-Hartley, A. J., Chong, G., Houston, J., Mather, A. E. (2005). 150 million years of climate stability: Evidence from the Atacama Desert, northern Chile. Geological Society of London Journal 162, 421–441. Doi: 10.1144/0016-764904-071.
-Hastenrath, S. (2002). The Intertropical Convergence Zone of the eastern Pacific revisited, International Journal of Climatology, *22*, 347-356, doi:10.1002/joc.739.
-Haug, G.H., and Tiedemann, R. (1998).Effect of the formation of the Isthmus of Panama on Atlantic Ocean thermohaline circulation. Nature 393, 673– 676. Doi: 10.1038/31447.
-Haug, G., Sigman, D., Tiedemann, R., Pedersen, T., and Sarnthein, M. (1999).Onset of permanent stratification in the subarctic Pacific Ocean. Nature 401 (6755), 779-782.
-Haug, G. H., Hughen, K. A., Sigman, D. M., Peterson, L. C., and Röhl, U. (2001a).Southward migration of the Intertropical Convergence Zone through the Holocene, Science, 293, 1304–1308, doi:10.1126/science.1059725.
-Haug, G.H., Tiedemann, R., Zahn, R., and Ravelo, A.C. (2001b).Role of Panama uplift on oceanic freshwater balance, Geology 29, 207–210. Doi: 10.1130/0091 7613(2001)029<0207: ROPUOO>2.0.CO;2.
-Haylock, M. R., Peterson, T. C., Alves, L. M., Ambrizzi, T., Anunciação, Y. M. T., Baez, J., Barros, M. R.,

Berlato, M. A., Bidegain, M., Coronel, G., Corradi, V., Garcia, V. J., Grimm, A. M., Karoly, D., Marengo, J. A., Marino, M. B., Moncunill, D. F., Nechet, D., Quintana, J., Rebello, E., Rusticucci, M., Santos, J. L., Trebejo, I., and Vincent, L. A., (2006). Trends in Total and Extreme South American Rainfall in 1960–2000 and Links with Sea Surface Temperature. Journal of climate 19, 1490 - 1512.

-Hays, J. D. and Perruzza, A. (1972).The significance of calcium carbonate oscillations in eastern equatorial Atlantic deep-sea sediments for the end of the Holocene warm interval. Quaternary Research2, 335-362.

-Hays, S. P., McPhaden, M. J., and Wallace, J. M. (1989).The influence of sea-surface temperatures on surface wind in the eastern equatorial Pacific, Weekly to monthly variability. Journal of Climate 2, 1500-1507.

-Haywood, A. M., and Valdes, P. J. (2004), Modelling Pliocene warmth: Contribution of atmosphere, oceans, and cryosphere, Earth and Planetary Science Letters, 218, 363–377, doi: 10.1016/S0012-821X (03)00685-X.

-Haywood, A.M., Dekens, P., Ravelo, A.C., Williams, M. (2005).Warmer tropics during the mid-Pliocene? Evidence from alkenone paleothermometry and a fully coupled ocean-atmosphere GCM, Geochem Geophys Geosys 6, doi: 10.1029/s2004GC000799.

-Haywood, A.M., Chandler, M.A., Valdes, P.J., Salzmann, U., Lunt, D.J., and Dowsett, H.J., (2009a). Comparison of mid-Pliocene climate predictions produced by the HadAM3 and GCMAM3 General Circulation Models. Global and Planetary Change66, 208-224. doi:10.1016/j.gloplacha.2008.12.014.

-Haywood, A. M., Dowsett, H. J., Valeds, P. J., Lunt, D. J., Francis, J. E., and Sellwood, B. W., (2009b).Introduction Pliocene climate, processes and problems, Philosophical Transanctions of the Royal Society a 367, 3–17. doi:10.1098/rsta.2008.0205.

-Hedges, J. I., and Parker, P. L. (1976).Land-derived organic matter in surface sediments from the Gulf of Mexico. Geochimica et Cosmochimica Acta 40, 1019– 1029.

-Hedges, J. I., Keil, R. G., and Benner, R. (1997). What happens to terrestrial organic matter in the ocean? Organic Geochemistry 27, 195–212.

-Herbert, T. D. (2003).Alkenone paleotemperature determinations. In: Elderfield, H. (Ed.) Treatise on Geochemistry, Volume 6. pp. 625. Elsevier, p.p. 391-432.

-Herbert, T.D., and Shuffert, J.D. (1998). Alkenone unsaturation estimates of late Miocene through late Pliocene sea-surface temperature at site 958. In: Proceedings of the Ocean Drilling Program, 17–21.

-Herbert, T.D., Peterson, L.C., Lawrence, K.T., Liu, Z.H. (2010).Tropical ocean temperatures over the past 3.5 million years. Science 328, 1530–1534.

-Hernandez, F., and Zambrano, E. (2009). Relación entre la temperatura superficial del mar del océano pacífico oriental y las precipitaciones en la costa del ecuador, durante 1981-2006. Acta oceanográfica del pacífico 15 (1).

-Heusser, L. E., and Shackleton, N. J., (1994). Tropical climatic variation on the Pacific slopes of the Ecuadorian Andes based on a 25,000-year pollen record from deep-sea sediment core Tri 163-31B. Quaternary Research42:222-225.

-Hinrichs K. -U., and Rullkötter, J. (1997). Terrigenous and marine lipids in Amazon Fan sediments: Implications for sedimentological reconstructions. In: Proceedings of the Ocean Drilling Program, Scientific Results 155 (Flood R. D., Piper D. J. W., Klaus A., Peterson L. C. (Eds.), College Station, TX (Ocean Drilling Program), 539-553.

-Hoefs, M. J. L., Versteegh, G. J. M., Rijpstra, W. I. C., de Leeuw, J. W., and Sinninghe Demste, J.S. (1998).Postdepositional oxic degradation of alkenones: implications for the measurement of Paleo Sea surface temperatures. Paleoceanography 13, 42–49.

-Hoke, G. D., Isacks, B .L. Jordan, T. E., Blanco, N., Tomlinson, A. J., and Ramezani, J. (2007). Geomorphic evidence for post-10 Ma uplift of the western flank of the central Andes 18°30'–22°S. Tectonics 26, TC5021, doi: 10.1029/2006TC002082.

-Hoke, G.D., Isacks, B.L., Jordan, T.E., and Yu, J.S. (2004). Groundwater-sapping origin for the giant quebradas of northern Chile, Geology 32, 605–608.

-Holmgren, M., Stapp P., Dickman, C. R., Gracia, C., Graham, S., Gutiérrez, J. R., Hice, C., Jaksic, F., Kelt, D. A., Letnic, M., Lima, M., López, B. C., Meserve, P. L., Milstead, W. B., Polis, G. A., Previtali, M. A., Richter, M., Sabaté, S., and Squeo, F. A. (2006). A synthesis of ENSO effects on drylands in Australia, North America and South America, Advances in Geosciences 6, 69–72.

-Holtvoeth J., Wagner T., and Schubert C. J. (2003). Organic matter in river-influenced continental margin sediments: The land-ocean and climate linkage at the Late Quaternary Congo fan (ODP Site 1975). Geochemistry, Geophysics, Geosystems 4, 1109-1135.

-Holz, C., Stuut, J.-B. W., Henrich, R. (2004) terrigenous sedimentation processes along the continental margin off NW Africa: implications from grain-size analysis of seabed sediments. Sedimentology 51, 1145-1154.
-Hooghiemstra, H., Wijninga, V. M., and Cleef, A. M. (2006). The paleobotanical record of Colombia: implications for biogeography and biodiversity. Annals of the Missouri Botanical Garden 93, 297–324.
-Hoorn, C. (1994a).Fluvial palaeoenvironments in the intracratonic Amazonas Basin (early Miocene-early middle Miocene, Colombia), Palaeogeogr. Palaeoclimatol. Palaeoecol.109: 1–54.
-Hoorn, C. (1994b).An environmental reconstruction of the Palaeo-Amazon River system (middle-late Miocene, NW Amazonia). Palaeogeogr.Palaeoclimatol.Palaeoecol. 112:187–238.
-Houston, J. (2006). Evaporation in the Atacama Desert: An empirical study of spatio-temporal variations and their causes, Journal of Hydrology (2006) 330, 402– 412. doi:10.1016/j.jhydrol.2006.03.036.
-Houston, J., and Hartley, A. J. (2003).The central Andean west-slope rain shadow and its potential contribution to the origin of hyper-aridity in the Atacama Desert. International Journal of Climatology 23, 1453-1464. doi:10.1002/joc.938.
-Hovan, S. A. (1995). Late Cenozoic atmospheric circulation intensity and climatic history recorded by eolian deposition in the eastern equatorial pacific ocean. In Pisias, N. G., Janecek, T. R., Palmer-Julson, A., and van Andel, T. H., editors, Proceedings of the Ocean Drilling Program, Scientific Results, volume 138, pages 615 – 625.
-Hovius, N., (1998). Controls on sediment supply by large rivers, Relative Role of Eustasy, Climate, and Tectonism in Continental Rocks, Society of Sedimentary Geology. Special Publication No. 59. pp 3–16.
-Hu, J., Peng, P., and Chivas, A.R. Molecular biomarker evidence of origins and transport of organic matter in sediments of the Pearl River estuary and adjacent South China Sea. Applied Geochemistry 24 (2009) 1666–1676. doi:10.1016/j.apgeochem.2009.04.035.
-Insel, N., Poulsen, C. J., Ehlers, T. A. (2009). Influence of the Andes Mountains on South American moisture transport, convection, and precipitation. Climate Dynamics
Doi: 10.1007/s00382-009-0637-1.
-Itambi, A. C., von Dobeneck, T., Mulitza, S., Bickert, T., and Heslop, D. (2009). Millennial-scale
Northwest African droughts related to Heinrich events and Dansgaard-Oeschger cycles: Evidence in marine sediments from offshore Senegal. Paleoceanography24, PA1205. Doi>10.1029/2007PA001570.
-Ivanova, E. B., Beaufort, L., Vidal, L., and Kucera, M. (2012).Precession forcing of productivity in the Eastern Equatorial Pacific during the last glacial cycle. Quaternary Science Reviews 40, 64-77.
-Jaillard, E., Ordoñez, M., Benítez, S., Berrones, G., Jiménez, N., Montenegro, G., Zambrano, I., (1995). Basin development in an accretionary, oceanic-floored forearc setting: southern coastal Ecuador during late Cretaceous to late Eocene times. In: Tankard, A.J., Suarez, S.R., Welsink, H.J. (Eds.), Petroleum Basins of South America, A.A.P.G. Memoir, vol. 62.pp. 597– 613.
-Jickells, T. D., An, Z. S., Andersen, K. K., Baker, A. R., Bergametti, G., Brooks, N., Cao, J. J., Boyd, P. W., Duce, R. A., Hunter, K. A., Kawahata, H., Kubilay, N.,laRoche, J., Liss, P. S., Mahowald, N., Prospero, J. M., Ridgwell, A. J., Tegen,I., and Torres, R. (2005).Global iron connections between desert dust, ocean biogeochemistry, and climate. Science, 308(5718):67–71.
-Karas, C., Nürnberg, D., Gupta, A. K., Tiedemann, R., Mohan, K., and Bickert, T. (2009). Mid-Pliocene climate change amplified by a switch in Indonesian subsurface through flow. Nature Geosciences 2, 434-438. Doi: 10.1038/NGEO520.
-Keigwin, L. D. (1982). Isotopic paleoceanography of the Caribbean and east Pacific: Role of Panama uplift in late Neogene time. Science 217, 350-353.
-Keller, G., Adatte, T., Hollis, C., Ordóñez, M., Zambrano, I., Jiménez, N., Stinnesbeck, W., Aleman, A., and Hale-Erlich, W. (1997). The Cretaceous/Tertiary boundary event in Ecuador: reduced biotic effects due to eastern boundary current setting. Marine Micropaleontology, 31(3-4), 97–133.
-Killops, S. D., and Frewin, N. L. (1994).Triterpenoids diagenesis and cuticular preservation. Organic Geochemistry 21, 1193–1209.
-Kirst G., Schneider R. R., Muller P. J., von Storch I., and Wefer G. (1999). Late quaternary temperature variability in the Benguela current system derived from alkenones. Quaternary Research 52, 92–103.
-Klein, S.A., and Hartmann, D.L., (1993): The seasonal cycle of low stratiform clouds. Journal of Climate, 6, 1587-1606.
-Kleinert K., and Strecker, M. R. (2001).Climate change in response to orographic barrier uplift; Paleosol and stable isotope evidence from the late Neogene Santa Maria Basin, northwestern Argentina. Geological Society of America Bulletin 113, 728–742.
-Kolla, V., Biscaye, P.E., Hanley, A.F. (1979).Distribution of quartzin late Quaternary Atlantic sediments in

relation to climate. Quaternary Research 11, 261– 277.
-Krissek, L. A., Scheidegger, K. F., and Kulm, L. D. (1980).Surface sediments of the Peru-Chile continental margin and the Nazca Plate. Geological Society of America Bulletin 91, 321-331.
-Kukowski, N., Hampel, A., Hoth, S., and Bialas, J. (2008). Morphotectonic and morphometric analysis of the Nazca plate and the adjacent offshore Peruvian continental slope — Implications for submarine landscape evolution. Marine Geology 254, 107-120. doi:10.1016/j.margeo.2008.05.017
-Koutavas, A. and Lynch-Stieglitz, J. (2003). Glacial-interglacial dynamics of the eastern equatorial Pacific cold tongue –Intertropical Convergence Zone system reconstructed from oxygen isotope records. Paleoceanography 18(4), 1089, doi: 10.1029/2003PA000894.
-Koutavas, A., Lynch-Stieglitz, J., Marchitto, T. M. and Sachs, J. (2002).El-Niño-like pattern in Ice Age tropical Pacific sea surface temperature. Science 297, 226-230.
-Ku, T.L., Luo, S.D., Kusakabe, M., Bishop, J.K.B., (1995). Ra-228-derived nutrient budgets in the upper equatorial pacific and the role of new silicate in limiting productivity. Deep-Sea Research Part II 42 (2-3), 479–497.
-Kujau, A., Nürnberg, D., Zeilhofer, C., Bahr, A., and Röhl, U. (2010).Mississippi River discharge over the last ~560.000 years – Indications from X-ray fluorescence core-scanning. Palaeogeography, Palaeoclimatology and Palaeoecology 298, 311-318.doi:10.1016/j.palaeo.2010.10.005
-Lamb, S., and Davis, P., (2003).Cenozoic climate change as a possible cause for the rise of the Andes. Nature 425, 792–797.
-Landry, M.R., Ondrusek, M.E., Tanner, S.J., Brown, S.L., Constantinou, J., Bidigare, R.R., Coale, K.H., Fitzwater, S., (2000).Biological response to iron fertilization in the eastern equatorial Pacific (IronEx II). I. Microplankton community abundances and biomass. Marine Ecology-Progress Series 201, 27–42.
-Latrubesse, E. M., Stevaux, J. C and Sinha, R. (2005).Tropical Rivers. Geomorphology 70 (2005) 187–206.
-Lawrence, K. T., Liu, Z., and Herbert, T.D. (2006).Evolution of the eastern tropical Pacific through Plio-Pleistocene glaciation. Science312, 79–83. doi:10.1126/science.1120395.
-Laws, E. A., Popp, B. N., Bidigare, R. R., Riebesell, U., Burkhardt, S., and Wakeham, S. G. (2001).Controls on the molecular distribution and carbon isotopic composition of alkenones in certain haptophyte algae. Geochemistry, Geophysics, Geosystems 2, 2000GC000057.
-Lea, D. W., Pak, D. K. and Spero, H. J. (2000).Climate impact of late Quaternary equatorial Pacific sea surface temperature variations. Science 289, 1719-1724.doi:10.1126/science.289.5485.1719.
-Lea, D. W., Pak, D. K., Peterson, L. C., and Hughen, K. A. (2003). Synchroneity of tropical and high latitude Atlantic temperaturas over the last glacial termination.Science301, 1361–1364.
-Lea, D. W., Pak, D. K., Belanger, C. L., Spero, H. J., Hall, M. A. and Shackleton, N. J. (2006). Paleoclimate history of Galápagos surface waters over the last 135,000 yr. Quaternary Science Reviews 25, 1152-1167.
-Leduc, G., Vidal, L., Tachikawa, K., Rostek, F., Sonzogni, C., Beaufort, L. and Bard, E. (2007). Moisture transport across Central America as a positive feedback on abrupt climatic changes. Nature 445, 908-911.doi:10.1038/nature05578.
-Leduc, G., Vidal, L., Tachikawa, K. and Bard, E. (2010), Changes in Eastern Pacific ocean ventilation at intermediate depth over the last 150 kyr BP, Earth and Planetary Science Letters 298, 217–228. doi:10.1016/j.epsl.2010.08.002.
-Lenters, J.D., and Cook, K. H. (1995). Simulation and diagnosis of the regional summertime precipitation climatology of South America.Journal of Climate 8, 2988–3005.
-Leynaert, A., Treguer, P., Lancelot, C., Rodier, M., (2001). Silicon limitation of biogenic silica production in the Equatorial Pacific. Deep-Sea Research Part I 48, 639–660.
-Li, L., Li, Q., Tian, J., Wang, P., Wang, H., and Liu, Z. (2011).A 4-Ma record of thermal evolution in the tropical western Pacific and its implications on climate change. Earth and Planetary Science Letters 309, 10–20. doi:10.1016/j.epsl.2011.04.016
-Lisiecki, L. E., and Raymo, M. E. (2005). A Pliocene–Pleistocene stack of 57 globally distributed benthic $\delta^{18}O$ records. Paleoceanography 20, PA1003. doi:10.1029/2004PA001071.
-Lisitzin A. P. (1996) Oceanic sedimentation. Lithology and geochemistry. AGU, Washington D.C.,400 pp.
-Liu, Z., Altabet, M. A., and Herbert, T. D. (2008). Plio-Pleistocene denitrification in the eastern tropical North Pacific: Intensification at 2.1 Ma. Geochemistry, Geophysics, Geosystems 9.doi: 10.1029/2008GC002044.
-Logan, G. A., Smiley, C. J., and Eglinton, G. (1995). Preservation of fossil leaf waxes in association with their source tissues, Clarkia, northern Idaho, USA. Geochimica et Cosmochimica Acta 59,751– 763.
-Lunt, D. J., Foster, G. L., Haywood, A. M., and Stone, E. J. (2008). Late Pliocene Greenland glaciation controlled by a decline in atmospheric CO2 levels. Nature 454, 1102–1105, doi:10.1038/nature07223.

-Lyle, M. (1992). Composition maps of surface sediments of the Eastern Tropical Pacific Ocean. Proceedings of the Ocean Drilling Program, Initial Reports Part 1(138), edited by Sondra K. Stewart, pp. 101-115, National Science Foundation and Joint Oceanographic Institutions, Inc., College Station, TX, Ocean Drilling Program.
-Ma, C. -C., Mechoso, C., Robertson, A. W., Arawa, A. (1996). Peruvian stratus clouds and the tropical Pacific circulation: A coupled ocean-atmosphere GCM study. Journal of Climate 9, 1635-1645.
-Machare, J. and Ortlieb, L. (1992). Plioquaternary vertical motions and the subduction of the Nazca Ridge, Central Coast of Peru. Tectonophysics, 205, 97–108.
-Maher, B.A., Prospero, J.M., Mackie D., Gaiero D., Hesse, P.P., and Balkanski, Y. (2010). Global connections between aeolian dust, climate and ocean biogeochemistry at the present day and at the last glacial máximum. Earth-Science Reviews 99 (2010) 61–97. doi:10.1016/j.earscirev.2009.12.001
-Malfait, B. T., and Van Andel, T. H. (1980). Amodern oceanic hardground on the Carnegie Rifge in the eastern Equatorial Pacific. Sedimentology 27, 467-496.
-Marchitto, T. M. (2007). Nutrient proxies.In: Scott A. E. (Ed) Encyclopedia of Quaternary Science 1732-1740.
-Marlow, J.R., Lange, C.B., Wefer, G., Rosell-Melé, A. (2000). Upwelling intensification as part of the Pliocene-Pleistocene climate transition.Science 290, 2288–2291.
-Marlowe, I. T., Brassell, S .C., Eglinton, G., and Green, J. C., (1990). Long-chain alkenones and alkyl alkenoates and the fossil coccolith record of marine sediments. Chemical Geology 88, 349–375.
-Martin. J. -M., and Meyback, M. (1979).Elemental mass-balance of material carried by major world rivers. Marine Chemistry 7, 173-206.
-Martínez, I., Keigwin, L., Barrows, T.T., Yokoyama, Y. and Southon, J. (2003). La Niña-like conditions I the eastern equatorial Pacific and a stronger Choco Jet in the northern Andes during the last glaciation. Paleoceanography 18(2), 1033, doi:10.1029/2002PA000877.
- McGee, D., Marcantonio, F., and Lynch-Stieglitz, J., (2007), Deglacial changes in dust flux in the eastern equatorial Pacific, Earth and Planetary Science Letters, 257, 215p.,0012-821X, doi: 10.1016/j.epsl.2007.02.033.
-McManus, D.A., (1970). Criteria of climatic change in the inorganiccomponents of marine sediments.Quat. Res. 1, 72–102.
-McPhaden, M. J., Zebiak, S. E., and Glantz, M. H. (2006). ENSO as an IntegratingConcept in Earth Science.Science 314, 1740-1745. doi: 10.1126/science.1132588.
-Meschede, M., and Barckhausen, U. (2001). The relationship of the Cocos and Carnegie ridges> Age constraints from paleogeographic reconstructions. International Journal of Earth Sciences 90, 386-392.
-Mikolajewicz, U., and Crowley, T.J., (1997), Response of a coupled ocean/energy balance model to restricted fl ow through the central American isthmus, Paleoceanography 12, 429–441. doi: 10.1029/96PA03542.
-Miller, K. G., Wright, J. D., Browning. J. V., Kulpecz, A., Kominz, M., Naish, T. R., Cramer, B. S., Rosenthal, Y., Peltier, W. R., and Sosdian, S. (2012). High tide of the warm Pliocene: Implications of global sea level forAntarctic deglaciation. Geology.doi: 10.1130/G32869.1
-Milliman, J.D., Meade, R.H., (1983). World-wide delivery of riversediment to the oceans. J. Geol. 91, 1–21.
-Milliman, J.D., Syvitski, P.M., (1992). Geomorphic/tectonic controlof sediment transport to theocean: the importance of smallmountainous rivers. Journal of Geology 100, 525–544.
-Mitchell, T. P., and Wallace, J, M. (1992). The annual cycle in equatorial convection and sea surface temperature. Journal of Climate 5, 1140-1156.
-Mix, A., Tiedemann, R., and Blum, P. (2003). Southeast pacific paleoceanographictransects sites 1232 - 1242. In Mix, A., Tiedemann, R., and Blum, P. (Editors), InitialReports Leg 202, volume 202 of Proceedings of the Ocean Drilling Program,College Station, TX. IODP, IODP.
-Moberly, R., Sheperd, G.L., Coulbourn, W.T., (1982). Forearc andother basins, continental margin of northern and southern Peruand adjacent Ecuador and Chile. In: Leggett, J.K. (Ed.), Trench–Forearc Geology: Sedimentation and Tectonics on Modern andAncient Plate Margins, Geological Society of London, Spec.Publs., vol. 10, pp. 171–189.
-Molina-Cruz, A., and Price, P. (1977). Distribution of opal and quartz on the ocean floor of the subtropical southeastern Pacific. Geology 5, 81-84.
-Molnar, P., and Cane, M. A. (2002).El Niño's tropical climate and teleconnections as a blueprint for pre-Ice Age climates. Paleoceanography 17(2), doi: 10.1029/2001PA000663.
-Molnar, P., and England, P. (1990). Late Cenozoic uplift of mountain ranges and global climatic change:

Chicken or egg?, Nature 346, 29-34.
-Montgomery, D. R., Balco, G., and Willett, S. D. (2001). Climate, tectonics, and the morphology of the Andes, Geology 29, 579-582.
-Mortimer, C. (1973), The Cenozoic history of the southern Atacama Desert, Chile, Journal of the Geological Society of London 129, 505–526.
-Mortimer, C. (1980).Drainage evolution in the Atacama Desert of northernmost Chile. Revista Geológica de Chile 11, 3–28.
-Müller, P. J. and Schneider, R. (1993). An automated leaching method for the determination of opal in sediments and particulate matter.Deep Sea ResearchPart I: Oceanographic Research Papers 40(3), 425.
-Müller, P. J., Cepek, M., Ruhland, G., and Schneider, R. R. (1997). Alkenone and coccolithophorid species changes in late Quaternary sediments from the Walvis Ridge: Implications for the alkenone paleotemperature method. Palaeogeography, Palaeoclimatology, Palaeoecology 135, 71–96. Doi: 10.1016/S0031-0182(97)00018-7.
-Müller, P. J., Kirst, G., Rulhand, G., von Storch, I., and Rosell-Melé, A. (1998).Calibration of the alkenone paleotemperature index U^{K}_{37}based on core-tops from the eastern South Atlantic and the global ocean (60°N–60°S). Geochimica et Cosmochimica Acta 62(10), 1757–1772. doi:10.1016/S0016-7037(98)00097-0.
-Mulitza, S., Donner, B., Fischer, G., Paul, A, Pätzold, J., Rühlemann, C., and Segl, M. (2004). The South Atlantic oxygen-isotope record of planktic foraminifera. In: The South Atlantic in the Late Quaternary: Reconstruction of Mass Budget and Current Systems, edited by G. Fischer and G. Wefer, Springer, NY, 121-142 pp.
-Mulitza, S., Dürkoop, A., Hale, W., Wefer, G., and Niebler, H. S. (1997). Planktonic foraminifera as recorders of past surface-water stratification. Geology 25 (4), 335–338.
-Mulitza, S., Prange, M., Stuut, J. -B., Zabel, M., von Dobeneck, T., Itambi, A. C., Nizou, J., Schulz, M., and Wefer, G. (2008). Sahel megadroughts triggered by glacial slowdowns of atlantic meridional overturning. Paleoceanography, 23(4),PA4206.doi:10.1029/2008PA001637
- Mulitza, S., Wolff , T., Pätzold, J., Hale, W., and Wefer, G. (1998). Temperature sensitivity of planktic foraminifera and its influence on the oxygen isotope record. Marine Micropalaeontology 33, 223–240.
-Murray, D. W., Farrell, J. W., and McKenna, V. (1995). Biogenic sedimentation at Site 847, eastern equatorial Pacific Ocean during the past 3 m.y. In: Proceedings of the Ocean Drilling Program, Scientific Results, 138, edited by Pisias, N. G., Mayer, L. A., Janecek, T. R., Palmer-Julson, A., and van Andel, T. H., College Station, TX (Ocean Drilling Program), 429–459 pp. doi:10.2973/odp.proc.sr.138.122.1995
-Murray, R., and Leinen, M. (1996).Scavenged excess aluminum and its relationship to bulk titanium in biogenic sediment from the central equatorial Pacific Ocean. Geochimica et Cosmochimica Acta 60(20), 3896-3878.
-Murray, R., Leinen, M. and Isern, A. (1993). Biogenic flux of Al to sediment in the central equatorial Pacific Ocean: Evidence for increased productivity during glacial periods. Paleoceanography 8(5), 651-670.
-Naafs, B. D. A., Stein, R., Hefter, J., Khélifi, N., De Schepper, S., and Haug, G. H. (2010). Late Pliocene changes in the North Atlantic Current. Earth and Planetary Science Letters.doi:10.1016/j.epsl.2010.08.023.
-Nakai, S., Halliday, A. N., Rea, D. K. (1993). Provenance of dust in the Pacific Ocean. Earth and Planetary Science Letters 119, 143–157.
-Nizou, J., Hanebuth, T. J. J., Heslop, D., Schwenk, T., Palamenghi, L., Stuut, J. –B., and Heinrich, R. (2010). The Senegal River mud belt: A high-resolution archive of paleoclimatic change and coastal evolution. Marine Geology 278, 150-164. doi:10.1016/j.margeo.2010.10.002.
-Oncken, O., Hindle, D., Kley, J., Elger, K., Victor, P., and Schemmann, K. *(*2006). Deformation of the Central Andean Upper Plate System –facts, fiction, and constraints for plateau models. In: Oncken, O.et al. (Eds). The Andes – Active Subduction Orogeny. Berlin: Springer-Verlag, 3–27.
-Pagani, M., Freeman, K.H., Arthur, M.A., (2000). Isotope analyses of molecular and total organic carbon from Miocene sediments. Geochimica et Cosmochimica Acta 64, 37–49.
-Pagani, M., Liu, Z., LaRiviere, J., and Ravelo, A.C. (2010). High Earth-system climate sensitivity determined from Pliocene carbon dioxide concentrations. Nature Geoscience 3 (1), 27–30. doi: 10.1038/NGEO724.
-Pak, H. and Zaneveld, J. R. V. (1974). Equatorial Front in the Eastern Pacific Ocean. Journal of Physical Oceanography 4, 570-578.
-Pancost, R. D., Baas, M., van Geel, B., and Sinninghe Damsté, J. S. (2002). Biomarkers as proxies for

plant inputs to peats: an example from a sub-boreal ombrotrophic bog. Organic Geochemistry33, 675–690.
-Pancost, R. D and Boot, C. S. (2004). The paleoclimatic utility of terrestrial biomarkers in marine sediments. Marine Chemistry 92, 239-261.
-Pattan, J. N. Parthiban, G., Gupta, S.M., and Mir, I.A. Fe speciation and Fe/Al ratio in the sediments of southeastern Arabian Sea as anindicator of climate change.Quaternary International 250 (2012) 19e26. doi:10.1016/j.quaint.2011.08.007.
-Pazmiño, N. A. (2005). Sediment distribution and depositional processes on the Carnegie Ridge.Master of Science Thesis, Texas A&M University, 136 p.
-Pearson, A., and Eglinton, T. I., (2000). The origin of n-alkanes in Santa Monica Basin surface sediment: a model based on compound-specific $\Delta^{14}C$ and $\delta^{13}C$ data. Organic Geochemistry31, 1103– 1116.
-Pena, L. D., Cacho, I., Ferreti, P. and Hall, M. A. (2008). El Niño-Southern Oscillation –like variability during glacial terminations and interlatitudinal teleconnections. Paleoceanography 23, PA3101, doi:10.1029/2008PA001620.
-Pennington, J. T., Mahoney, K. L., Kuwahara, V. S., Kolber, D. D., Calienes, R., and Chavez, F. P. (2006). Primary production in the eastern tropical Pacific: A review. Progress in Oceanography 69 (2006) 285–317. doi:10.1016/j.pocean.2006.03.012
-Peters K. E., Walter C. C., and Moldowan J. M. (2004). The Biomarker Guide: Volume I: Biomarkers and isotopes in the environments and human history. Cambridge University Press, Cambridge, 490 pp.
-Philander, S. G. H., Gu, D., Halpern, D., Lambert, G., Lau, N.-C., Li, T., and Pacanowski, R. C. (1996). Why the ITCZ is mostly northof the equator. Journal of Climate9, 2958–2972.
-Philander, S. G. H. (2010). Tilting at connections, from Pole to Equator.Science 328, 1488-1489. doi:10.1126/science.1189748
-Pinto, L., Hérail, G., Fontan, F., de parseval, P. (2007).Neogene erosion and uplift of the western edge of the Andean Plateau as determined by detrital heavy mineral analysis. Sedimentary Geology 195, 217–237. doi:10.1016/j.sedgeo.2006.08.001
-Pinto, L., Hérail, G., Moine, B., Fontan, F., Charrier, R., and Dupré, B. (2004). Using geochemistry to establish the igneous provenances of the Neogene continental sedimentary rocks in the Central Depression and Altiplano, Central Andes. Sedimentary Geology 166, 157–183. doi:10.1016/j.sedgeo.2003.12.002
-Pisias, N. G. and Mix, A. C. (1997). Spatial and temporal oceanographic variability of the eastern equatorial Pacific during the late Pleistocene: Evidence from radiolaria microfossils. Paleoceanography 12(3), 381-393.
-Plewa, K., Meggers, H., Kuhlmann, H., Freudenthal, T., Zabel, M., and Kasten, S. (2012). Geochemical distribution patterns as indicators for productivity and terrigenous input off NW Africa. Deep-Sea Research I 66, 51-66.
-Pourrut, P., Gómez, G., Bermeo, A., and Segovia, A. (1995ª). Factores condicionantes de los regímenes climáticos e hidrológicos. In: Pourrut, P. (Ed). El Agua en el Ecuador: Clima, precipitaciones y escorrentía. Corporación Editora Nacional, Quito, Ecuador, 7-12.
-Pourrut, P., Róvere, O., Romo, I., and Villacres, H. (1995b). El Clima del Ecuador. In: Pourrut, P. (Ed). El Agua en el Ecuador: Clima, precipitaciones y escorrentía. Corporación Editora Nacional, Quito, Ecuador, 13-29.
-Pourrut, P., and Nouvelot, J. –F. (1995). Anomalías y fenómenos climáticos extremos. In: Pourrut, P. (Ed). El Agua en el Ecuador: Clima, precipitaciones y escorrentía. Corporación Editora Nacional, Quito, Ecuador, 67-76.
-Prahl, F. G., and Wakeham, S. G. (1987). Calibration of unsaturation patterns in long-chain ketone comositions for paleotemperature assessment. Nature 330, 367-369.
-Prahl, F. G., de Lange, G. J., Lyle, M., and Sparrow, M. A., (1989). Post-depositional stability of long-chain alkenones under contrasting redox conditions. Nature 341, 434–437.
-Prahl, F. G., Muehlhausen, L. A., and Zahnle, D. L. (1998). Further evaluation of long-chain alkenones as indicators of paleoceanographic conditions. Geochimica et Cosmochimica Acta 52, 2303–2310.
-Prahl, F. G., Wolfe, G. V., and Sparrow, M. A. (2003). Physiological impacts on alkenone paleothermometry. Paleoceanography 18, 1025.doi:10.1029/2002PA000803.
-Prins, M. A. andWeltje, G. J. (1999). End-Member Modelling of Siliciclastic Grain-Size Distributions: The Late Quaternary Record of Eolian and Fluvial SedimentSupply to the Arabian Sea and Its Paleoclimatic Significance, volume 62 of SepmSpecial Publication. Geological Society Publishing House, London.

-Prospero, J.M., Uematsu, M., and Savoie, D.L. (1989). Mineral Aerosol transport to the Pacific Ocean. Chemical oceanography, Academic Press Limited, Chapter 58, 187-218.
- Pye, K. (1987). Aeolian dust and dust deposits. Academic Press, London, 334 pp.
-Quinn, W. H., and Burt, W. (1970). Prediction of abnormally heavy precipitation over the Equatorial Pacific Dry Zone. Journal of Applied Meteorology 9, 20-28.
-Ravelo, A. C. (2006). Walker circulation and global warming, lessons from the past. Oceanography 19(4), 114-122.
-Ravelo, A. C. (2010). Warmth and glaciation. Nature Geoscience3, 672-673.
-Ravelo, A.C., Andreasen, D., Lyle, M., Olivarez, L., and Wara, M.W. (2004). Regional climate shifts caused by gradual global cooling in the Pliocene Epoch. Nature 429, 263–267.
-Raymo, M. E., and Huybers, P. (2008). Unlocking the mysteries of the ice ages, Nature451(7176), 284-285.
-Raymond, D. J., Esbensen, S. K., Paulson, C., Gregg, M., Bretherton, C. S., Petersen, W. A., Cifelli, R., Shay, L. K., Ohlmann, C., and Zudeima, P. (2004), EPIC2001 and the coupled ocean-atmosphere system of the tropical east Pacific, Bulletin of the American Meteorological Society, 85(9), 1341-1354, doi:10.1175/BAMS-85-9-1341.
-Rea, D. K. (1994), The paleoclimatic record provided by eolian depositionin the deep sea, The geologic history of wind, Rev. Geophys., 32(2),159– 195.
-Rech, J.A., Currie, B.S., Michalski, G., and Cowan, A.M. (2006). Neogene climate change and uplift in the Atacama Desert, Chile. Geology 34, 761–764.
-Richter, T., van der Gaast, S., Koster, B., Vaars, A., Gieles, R., De Stigter, H., De Haas, H., and van Weering, T. (2006). The avaatech xrf core scanner: technical description and applications to NE atlantic sediments. In Rothwell, R. (Ed) editor, New Techniques in Sediment Core Analysis.Special Publications 267, Geological Society of London, 39–50.
-Rickaby, R. and Halloran, P. (2005). Cool La Niña during the warmth of the Pliocene? Science 307, 1948–1952.
-Rieley, G., Collier, R.J., Jones, D.M., and Eglinton, G. 1991. Thebiogeochemistry of Ellesmere Lake, U.K.: I. Source correlation of leaf wax inputs to the sedimentary lipid record. Organic
Geochemistry 17, 901– 912.
-Robinson, M. M. 2009. New quantitative evidence of extreme warmth in the Pliocene Arctic. Stratigraphy 6 (4), 265–275.
-Robinson, M. M., Dowsett, H. J., Dwyer, G. S., Lawrence, K. T. 2008. Reevaluation of mid-
Pliocene North Atlantic sea surface temperatures. Paleoceanography 23, PA3213
doi:3210.1029/2008pa001608.
-Robinson, R. S., Mix, A., and Martinez, P. 2007. Southern Ocean control on the extent of denitrification in the southeast Pacifi cover the last 70 ka. Quaternary Science Reviews 26, 201–212. doi: 10.1016/j.quascirev.2006.08.005.
-Rohling, E. J. 2007. Oxygen isotopic composition of seawater. In: Scott A. E. (Ed) Encyclopedia of Quaternary Science, Elsevier, Oxford, 1748-1756.
-Rossel, F.R., Cadier, E., Gomez, G., 1996. Las inundaciones en la zona costera ecuatoriana: Causas , obras de proteccion existentes y previstas.Bull. Inst. Fr. Etudes andines 25(3), 399-420.
- Rühlemann, C., Diekmann, B., Mulitza, S., and Frank, M. (2001). Late Quaternary changes of western equatorial Atlantic surface circulation and Amazon lowland climate recorded in Ceara Rise deep-sea sediments. Paleoceanography 16 (3), 293–305.
-Sachs, J. P., Pahnke, K., Smittenberg, R., and Zhang, Z. 2007. Biomarkers.In: Scott A. E. (Ed) Encyclopedia of Quaternary Science 2, 1627-1633.
-Saillard, M. 2008. Dynamique du soulèvement côtier Pléistocène des Andes centrales : Etude de l'évolution géomorphologique et datations (10Be) de séquences de terrasses marines (Sud Pérou – Nord Chili). THÈSEEn vue de l'obtention du DOCTORAT DE L'UNIVERSITÉ DE TOULOUSE III - Paul Sabatier.Sciences de la Terre et Environnement. 314 p.
-Sansom, H. W., 1965: The structure and behavior of the ITCZ. The WorldMeteorological Organization Technical Note, No. 69, Geneva, 91-108
-Sarnthein, M., Winn, K., Duplessy, J.-C., and Fontugne, M. (1988). Global variations of surface ocean productivity in low and mid latitudes: Influence on CO2 reservoirs of the deep ocean atmosphere during the last 21,000 years.Paleoceanography, 3(3), 361–399.
-Sarthou, G., et al. (2003), Atmospheric iron deposition and sea-surface dissolved iron concentrations in the east Atlantic.Deep Sea Res., PartI, 50, 1339– 1352.

-Saukel, C. 2011. Tropical southeast pacific continent-ocean-atmosphere linkages since the Pliocene inferred from eolian dust.Dissertation zur Erlangung des Doktorgrades der Naturwissenschaften am Fachbereich Geowissenschaften der Universität Bremen, 174 p.
-Sautter, L. R., and Thunnel, R. C. 1991. Seasonal variability in the d18O and d13C of planktonic foraminifera from an upwelling environment; sediment trap results from the San Pedro Basin, Southern California. Paleoceanography 6, 307-334.
-Schefuß E., Versteegh G. J. M., Jansen J. H. F., and Sinninghe Damsté J. S. 2004. Lipid biomarkers asmajor source and preservation indicators in SE Atlantic surface sediments. Deep SeaResearch Part I: OceanographicResearch Papers 51, 1199-1228.
-Scheidegger, K. F., and Krissek, L. A. 1982. Dispersal and deposition of eolian and fluvial sediments off Peru and northern Chile. Geological Society of America Bulletin 93, 150-162.
-Shipboard Scientific Party, 1988. Site 681.In: Suess, E., von Huene, R., et al., Proceedings of Ocean Drilling Program, Initial Reports 112: College Station. TX (Ocean Drilling Program), 305–362. doi:10.2973/odp.proc.ir.112.112.1988
-Shipboard Scientific Party, 2003a. Site 1239.In: Mix, A.C., Tiedemann, R., Blum, P., et al., Proceedings of Ocean Drilling Program, Initial Reports 202: College Station. TX (Ocean Drilling Program), 1–93. doi:10.2973/odp.proc.ir.202.110.2003
-Shipboard Scientific Party, 2003b. Site 1237.In: Mix, A.C., Tiedemann, R., Blum, P., et al., Proceedings of Ocean Drilling Program, Initial Reports 202: College Station. TX (Ocean Drilling Program), 1–93. doi:10.2973/odp.proc.ir.202.110.2003
-Shipboard Scientific Party, 2003c. Site 1229.In: D'Hondt, S. L., Jørgensen, B.B., Miller, D.J., et al., Proceedings of Ocean Drilling Program, Initial Reports 201: College Station. TX (Ocean Drilling Program), 1–78. doi:10.2973/odp.proc.ir.201.110.2003
-Sigman, D.M., Altabet, M.A., Francois, R., McCorkle, D. C., and Fischer, G. 1999. The $\delta^{15}N$ of nitrate in the Southern Ocean: Consumption of nitrate in surface waters.Global Biogeochemical Cycles 13, 1149–1166. doi:10.1029/1999GB900038.
-Simoneit, B.R. T. 1986. Cyclic terpenoids of the geosphere. In: Johns,R. B. (Ed.) Biological Markers in the Sedimentary Record. Elsevier,Amsterdam, pp. 43–99.
-Singh, A. K., Marcantonio, F., and Lyle, M. (2011). Sediment focusing in the Panama Basin, eastern equatorial Pacific Ocean. Earth and Planetary Science Letters 309, 33-44. doi:10.1016/j.epsl.2011.06.020
-Skilbeck, C. G., and Fink, D. 2006. Data report: Radiocarbon dating and sedimentation rates for Holocene–upper Pleistocene sediments, Eastern equatorial Pacific and Peru continental margin.Proceedings of Ocean Drilling Program, Initial Reports201, doi:10.2973/odp.proc.sr.201.108.2006.
-Smetacek, V., 1998. Biological oceanography—diatoms and the silicate factor. Nature 391, 224–225.
-Spero, H. J., Bijma, J., Lea, D. W., and Bemis, B. E. 1997. Effect of seawater carbonate concentration on foraminiferal carbon and oxygen isotopes. Nature 390, 497-500.
-Spero, H. J., Mielke, K. M., Kalve, E. M., Lea, D. W. and Pak, D. K. 2003. Multispecies approach to reconstructing eastern equatorial Pacific thermocline hydrography during the past 360 kyr. Paleoceanography 18 (1), 1002, doi:10,1029/2002PA000814.
-Spero, H. J., and Lea, D. W. 1993. Intraspecific stable isotope variability in the planktic foraminifera *Globigerinoides sacculifer*: Results from laboratory experiments. Marine Micropaleontology 22, 221-234.
-Spikings, R.A., Winkler, W., Hughes, R.A., and Handler, R. 2005. Thermochronology of allochthonous terranes in Ecuador: unravelling the accretionary and post-accretionary history of the Northern Andes. Tectonophysics 399, 195-220.
-Srinivasan, M. S., and Sinha,D. K. 1998. Early Pliocene closing of the Indonesian Seaway: Evidence from north–east Indian Ocean and tropical Pacific deep sea cores. Journal of Asian Earth Sciences 16, 29 – 44, doi :10.1016/S0743-9547(97)00041-X.
-Stancin, A. M., Gleason, J. D., Rea, D. K., Owen, R. M., Moore, J., Blum, T. C., and Hovan, J. D. (2006). Radiogenic isotopic mapping of late Cenozoic eolian and hemipelagic sediment distribution in the east-central Pacific. Earth and Planetary Science Letters 248, 840–850.
-Starck D., and Anzotegui, L. 2001.The late-Miocene climate change—persistence of a climate signal through the orogenic stratigraphic record in northwestern Argentina. Journal of South American Earth Sciences 14, 763–774.
-Stuut, J.-B. W., Prins, M. A., Schneider, R. R., Weltje, G. J., Jansen, J. H. F., Postma, G. (2002) A 300-kyr record of aridity and wind strength in southwestern Africa: inferences from grain-size distributions of sediments on Walvis Ridge, SE Atlantic. Marine Geology 180, 221-233.

-Takahashi, K., and Battisti, D. S. 2007. Processes Controlling the Mean Tropical Pacific Precipitation Pattern: I. The Andes and the Eastern Pacific ITCZ.Journal of Climate20, 3434–3451.
-Takahashi, T., Sutherland, S. C., Sweeney, C., Poisson, A., Metzl, N., Tilbrook, B., Bates, N., Wanninkhof, R., Feely, R. A., Sabine, C., Olafsson, J., and Nojiri, Y. 2002. Global sea–air CO2 flux based on climatological surface ocean pCO2, and seasonal biological and temperature effect.Deep-Sea Research II 49, 1601–1622.
-Tans, P. P.,Fung, I. Y., and Takahashi, T. 1990 Observational constraints on the global atmospheric CO2 budget. Science 247, 1431–1438.
- Taylor, S., and Mc Lennan, S. (1985). The Continental Crust: Its Composition and Evolution. Blackwell, Oxford, 312 pp.
-Thomsen, H. A., Buck, K. R., and Chavez, F. P. 1994. Haptophytes as components of marine phytoplankton. In: Green, J. C., and Leadbeater, B. S. C. (Eds.) The Haptophyte Algae. Clarendon Press, Oxford, pp. 187–208.
-Thouret, J.–C., Wörner, G., Gunell, Y., Singer, B., Zhang, X., and Souriot, T. 2007. Geochronologic and stratigraphic constraints on canyon incision and Miocene uplift of the Central Andes in Peru. Earth and Planetary Science Letters 263, 151–166. doi:10.1016/j.epsl.2007.07.023
-Thunell, R. C., Keir, R., and Honjo, S. 1982. Calcite dissolution: An in situ study in the Panama Basin.Science212, 659–661.
-Tjallingii, R. 2006. Application and quality of X-Ray Fluorescence core scanning in reconstructing late Pleistocene NW African continental margin sedimentation patterns and paleoclimate variations.Dissertation zur Erlangung des Doktorgrades der Naturwissenschaften am Fachbereich Geowissenschaften der Universität Bremen, 114 p.
-Tiedemann, R., and Mix, A., 2007. Leg 202 synthesis: southeast Pacific paleoceanography. In: Tiedemann, R., Mix, A. C., Richter, C., and Ruddiman, W. F. (Eds.), Proceedings of Ocean Drilling Program, Scientific Results, 202: College Station. TX (Ocean Drilling Program), 1–56. doi:10.2973/odp.proc.sr.202.201.2007
-Tiedemann, R., Sarnthein, M., and Shackleton, N.J. 1994. Astronomic timescalefor the Pliocene Atlantic $\delta^{18}O$ and dust flux records of Ocean Drilling Programsite 659. Paleoceanography 9, 619–638. doi: 10.1029/94PA00208.
-Tiedemann, R., Sturm, A., Steph, S., Lund, S. P., and Stoner, J. S. 2007. Astronomically calibrated time scales from 6–2.5 Ma and benthic isotope stratigraphies of sites 1236, 1237, 1239 and 1241, In Tiedemann, R., Mix, A. C., Richter, C., and Ruddiman, W. F. (Eds.), Proceedings of the Ocean Drilling Program. Scientific Results 202, 1–69. doi:10.2973/odp.proc.sr.202.210.2007.
-Twilley, R. R., Cardenas, W., Rivera-Monroy, V. H., Espinoza, J., Suescum, R., Armijos, M. M., and Solorzano, L. 2001. The Gulf of Guayaquil and the Guayas River Estuary, Ecuador. In: Seeliger, U., and Kjerfve, B. (Eds). Coastal marine Ecosystems of Latin America. Springer-Verlag Berlin, 245-263.
-Twilley, R. R, Lugo, A. E, and Patterson-Zucca, C. 1986. Production,standing crop, and decomposition of litter in basin mangroveforests in southwest Florida. Ecology 67, 670-683
-Uba, C.E., Heubeck, C., and Hulka, C. 2005. Facies analysis and basin architecture of the Neogene Subandean synorogenic wedge, southern Bolivia.Sedimentary Geology 180, 91–123.
-Uba, C.E., Heubeck, C., and Hulka, C. 2006. Evolution of the late Cenozoic Chaco foreland basin, southern Bolivia.Basin Research 18, 145–170.
-Vallejo, C., Spikings, R.A., Luzieux, L., Winkler, W., Chew, D., and Page, L. 2006. The early interaction between the Caribbean plateau and the NW South American Plate.Terra Nova 18, 264-269.
-Vera, C., Baez, J., Douglas, M., Emmanuel, C. B., Marengo, J., Meitin, J., Nicolini, M., Nogues-Paegle, J., Paegle, J., Penalba, O., Salio, P., Saulo, C., Silva-Dias, P. L., and Zipser, E. 2006. The South American lowlevel jet experiment. Bulletin of American Meteorological Society 87, 63–77.
-Verganud-Grazzini, C. (1976). Non-equilibrium isotopic composition of shells of planktonic foraminifera in the Mediterranean Sea. Palaeogeography, Palaeoclimatology, Palaeoecology 20, 263-276.
-Versteegh, G.J.M., Schefuß, E., Dupont, L., Marret, F., Sinninghe Damsté, J.S., Jansen, J.H. F. 2004. Taraxerol and Rhizophora pollen asproxies for tracking past mangrove ecosystems.Geochimica et Cosmochimica Acta 68, 411–422.
-Virji, H. 1981. A preliminary study of summertime tropospheric circulation patterns over South America estimated from cloud winds. Monthly Weather Review 109, 599–610.
-Volkman, J. K. 1986. A review of sterol markers for marine andterrigenous organic matter. Organic Geochemistry 9, 83–99.
-Vuille, M. 1999. Atmospheric circulation over the Bolivian Altiplano during dry and wet periods and

extreme phases of the Southern Oscillation.International Journal of Climatology19, 1579–1600.
-Vuille, N., Bradley, R. S., and Keimig, F. 2000. Interannual climate variability in the Central Andes and its relation to tropical Pacific and Atlantic forcing. Journal of Geophysical Research 105, 12447-12460.
-Waelbroeck, C., Mulitza, S., Spero, H., Dokken, T., Kiefer, T., and Cortijo, E. (2005). A global compilation of late Holocene planktonic foraminiferal d18O: relationship between surface water temperature and d18O. Quaternary Science Reviews 25, 853-868. doi:10.1016/j.quascirev.2003.10.014
-Waliser, D. E., and Gautier, C. 1993. A satellite derived climatology of the ITCZ.Journal of Climate 6, 2162-2174.
-Wang, C., Enfield, D.B., 2001. The tropical Western Hemisphere warm pool. Geophysical Research Letters 28, 1635–1638.
-Wang, C., and Fiedler, P. C. 2006. ENSO variability and the eastern tropical Pacific: A review. Progress in Oceanography 69, 239–266. doi:10.1016/j.pocean.2006.03.004
-Wannigama, G.P., Volkman, J.K., Gillan, F.T., Nichols, P.D., and Johns,R.B. 1981. A comparison of lipid components of the fresh anddead leaves and pneumatophores of the mangrove Avicennia-Marina. Phytochemistry 20, 659–666.
-Wara, M.W., Ravelo, A.C., and Delaney, M.L. 2005. Permanent El Niño-like conditions during the Pliocene warm period. Science 309, 758–761. doi: 10.1126/science.1112596.
-Waylen, P., and Poveda, G. 2002. El Niño–Southern Oscillation and aspects of western South American.Hydro-climatology 16, 1247–1260.doi: 10.1002/hyp.1060
-Weaver, P. P. E., Chapman, M. R., Eglinton, G., Zhao, M., Rutledge, D., andRead,G. 1999. Combined coccolith, foraminiferal, and biomarkerreconstruction of paleoceanographic conditions over the past 120 kyrin the northern North Atlantic (59°N, 23°W). Paleoceanography14, 336–349. doi:10.1029/1999PA900009.
-Wedepohl, K. 1971. Environmental influence on the chemical composition of shales and clays. In: Ahrens, L., Press, K., Runcorn, S., and Urey, H. (Eds.) Physics and chemistry of the Earth. Pergamon Press, Oxford, pp. 307-333.
-Weltje, G. J. and Tjallingii, R. 2008. Calibration of xrf core scanners for quantitative geochemical logging of sediment cores: Theory and application.Earth and Planetary Science Letters 274(3-4), 423–438.
-Willams, D.F., and Healy Williams, N. (1980). Oxygen isotopic-hydrographic relationships among recent planktonic foraminifera from the Indian Ocean. Nature 283, 848–852.
-Winckler, G., Anderson, R.F., Fleisher, M.Q., McGee, D., and Mahowald, N. (2008). Covariant Glacial-Interglacial Dust Fluxes in the Equatorial Pacific and Antarctica, Science, 320, 93p., doi:10.1126/science.1150595.
-Wipf, M., Zeilinger, G., Seward, D., and Schlunegger, F. 2008. Focused subaerial erosion during ridge subduction: impact on the geomorphology in south-central Peru.Terra Nova 20(1), 1–10. doi: 10.1111/j.1365-3121.2007.00780.x
-Witt, C., Bourgois, J., Michaud, F., Ordoñez, Jiménez, N., and Sosson, M. 2006. Development of the Gulf of Guayaquil (Ecuador) during the Quaternary as an effect of the North Andean block tectonic escape. Tectonics 25, TC3017, doi:10.1029/2004TC001723.
-Witt, C., and Bourgois, J. 2010.Forearc basin formation in the tectonic wake of a collision-driven, coastwisemigrating crustal block: The example of the North Andean block and the extensional Gulf of Guayaquil-Tumbes Basin (Ecuador-Peru border area).Geological Society of America Bulletin122, 89-108. doi: 10.1130/B26386.1
-Wyrtki, K. 1975. El Nino – The dynamic response of the Equatorial Pacific Ocean to atmospheric forcing. Journal of Physical Oceanography 5, 572-584.
-Wyrtki, K. 1981. An estimate of equatorial upwelling in the Pacific.Journal of Physical Oceanography 11, 1205-1214.
-Xie, S.-P. 1994. On the genesis of the Equatorial Annual cycle. Journal of Climate 7, 2008-2013.
-Xie,S.-P., Miyama, T., Wang,_Y., Xu, H., De Szoeke, S. P., Small, R. J. O., Richards, J. K., Mochizuki, T., and Awaji, T. 2007., A Regional Ocean–Atmosphere Model for Eastern Pacific Climate: Toward Reducing Tropical Biases.Journal of climate 20, 1504-1522.doi: 10.1175/JCLI4080.1
-Xu, H., Wang, Y., and Xie, S.-P., 2004: Effect of the Andeson eastern Pacific climate: A regional atmospheric modelstudy. Journal of Climate 17, 589-602.
-Yu, J.-Y., and Mechoso, C. R. 1999. Links between Annual Variations of Peruvian Stratocumulus Clouds and of SST in the Eastern Equatorial Pacific.Journal of climate 12, 3305-3318.
-Zhang, R., and Delworth, T. L. 2005.Simulated tropical response to a substantial weakening of the Atlantic thermohaline circulation.Journal of Climate 18, 1853–1860.

-Zhou, J., and Lau, K.-M. 2002. Principal modes of interannual and decadal variability of summer rainfall over South America, variability of summer rainfall over south america.International journal of climatology21: 1623–1644. Doi: 10.1002/joc.700

APPENDIX 1

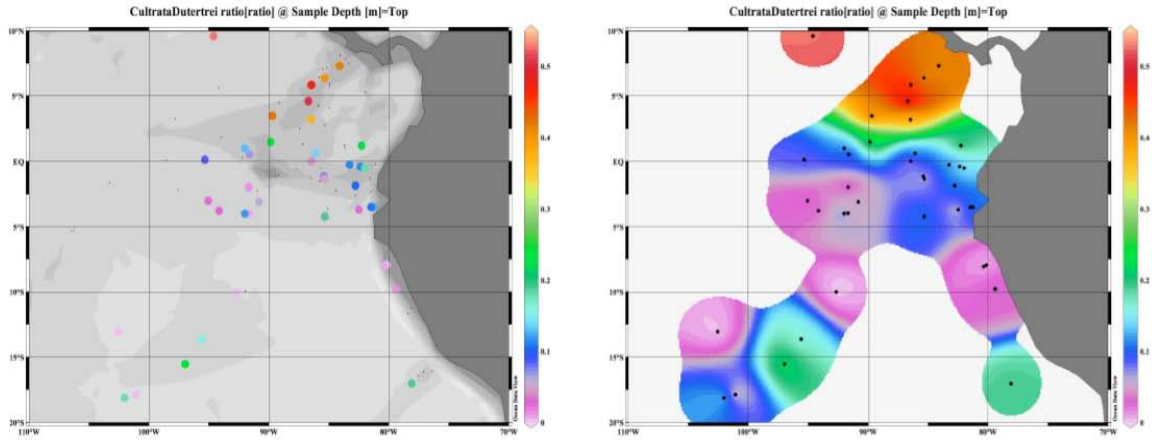

Supplementary Figure 4.1. Distribution pattern of the ratios between *G. cultrata* and *N. dutertrei* ($R_{c/d}$). On the right panel individual core-top $R_{c/d}$ values and on the left panel, interpolated values are shown.

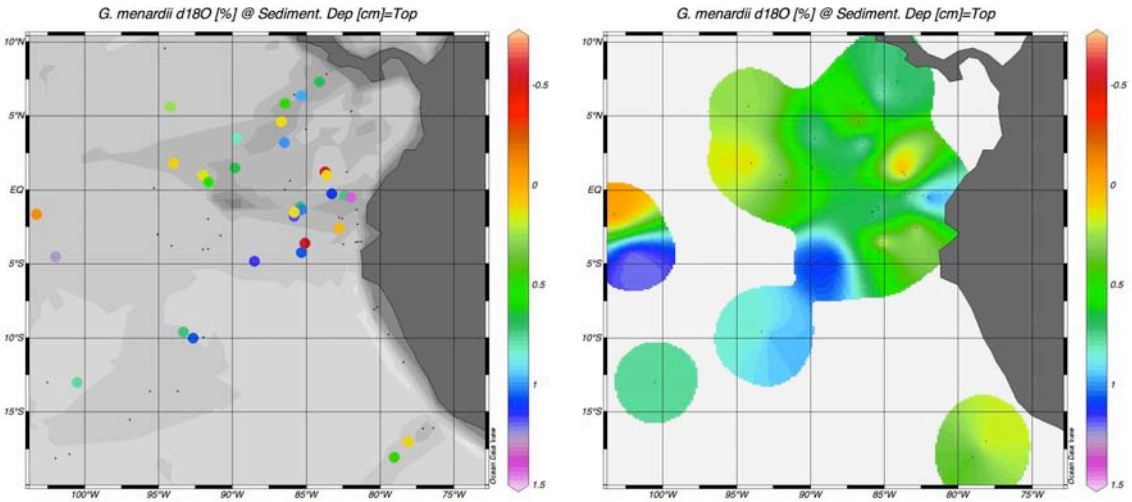

Supplementary Figure 4.2. On the left side panel, the distribution pattern of measured $d^{18}O$ values of *Globorotalia menardii* plotted vs. a simplified bathymetric chart of the eastern equatorial Pacific. On the right side, $\delta^{18}O$ values interpolated. $\delta^{18}O$ values measured in this study are expressed relative to Pee Dee Belemnite (PDB) standard, based on calibrations directly to National Bureau of Standards 19. Visualization done using Ocean Data View (R. Schlitzer, 2005; available at http://odv.awi-bremerhaven.de/)

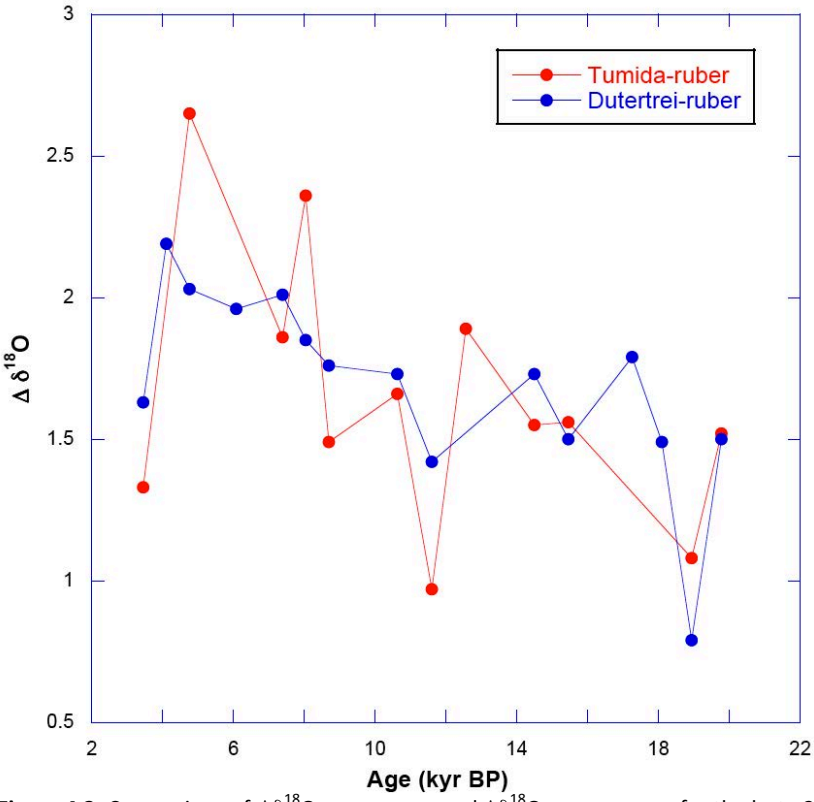

Supplementary Figure 4.3. Comparison of $\Delta\delta^{18}O_{\textit{G.ruber-G.tumida}}$ and $\Delta\delta^{18}O_{\text{G.ruber-N.dutertrei}}$ for the last ~20 kyr. Data from Site RC11-238 (1.52°S; 85.82°W; 2573 m) in the eastern tropical Pacific (Faul et al. 2000). Although the correlation coefficient between $\Delta\delta^{18}O_{\text{G.ruber-N.dutertrei}}$ and the vertical temperature gradient (20-100 m water depth) is not significant in our core-top dataset (r^2= 0.17), it seems to show a similar trend to the one obtained using *G. ruber* and *G. tumida*, confirming the obtained pattern and the potential influence of changes in SST rather than thermocline properties.

APPENDIX 2

Age model

Our stratigraphic framework was established by correlating the magnetic susceptibility from Site 1229E to 681B (Supplementary Figure 6.1.). The age model was improved between 5 and 9 meters by tuning our SST record with the one of Site TR163-19 (2.27°N; 90.95°W) (Lea et al., 2000; Supplementary Figure 6.2.), and for the upper Holocene section, ^{14}C data were used (Supplementary Table 6.1). Radiocarbon ages were obtained from the organic carbon fraction extracted from bulk sediments samples (Skilbeck and Fink, 2006). Thus, we have confidence in the allocation of both the LIG and the LH.

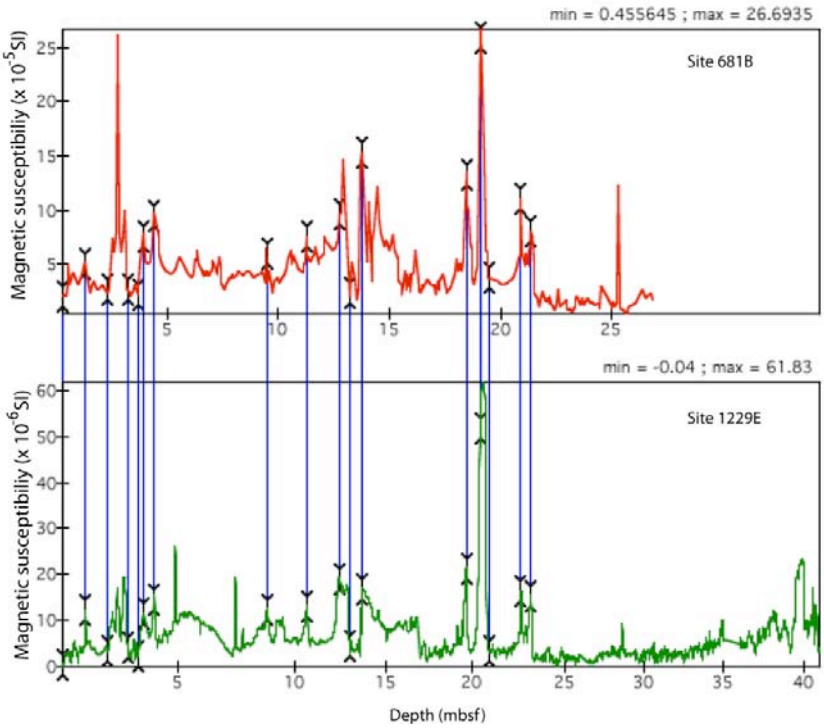

Supplementary Figure 6.1. Magnetic susceptibility correlation between ODP Sites 1229E and 681B (Magnetic susceptibility vs. depth).

Supplementary Table 6.1. Calibrated ^{14}C dates (1 sigma error) and tie points resulting from magnetic susceptibility and SST tunings .^{14}C data taken from Skilbeck and Fink, 2006). Mbsf= meters below sea floor

Site 681B (mbsf)	Site 1229E (mbsf)	14C Age (cal kyr BP) (Skilbeck and Fink, 2006)	Age (kyr) (Schrader, 1992)	Age (kyr) (Lea et al., 2000)
	0.2	0.65 (0.06)		
	0.61	0.79 (0.07)		
	1.09	1.20 (0.06)		
	1.39	1.65 (0.07)		
	1.86	1.87 (0.08)		
	2.3	2.88 (0.08)		
	4.05	* 37.4 (0.02)		
	4.2			37.77
	4.95			64.09
	5.6			86.28
	6.81			107.16
9.27	9		129	
10.4	11.3		143.6	

11.4	12.8		161.7	
12	13.2		173.9	

Stratigraphy

We made every possible attempt to base our stratigraphic framework on oxygen isotopes of benthic foraminifers. We examined 125 samples at 20-cm depth resolution but found that the foraminiferal content was not continuous throughout the sediment core and thus not suitable for reaching a proper age model. Our comparisons are deliberately limited to the last interglacial and late Holocene, two time intervals for which we have a reliable age control (the Holocene is radiocarbon-dated, and the correlations of Site 1229 with core TR163-19 and ODP site 681 nicely supports the allocation of the last interglacial).

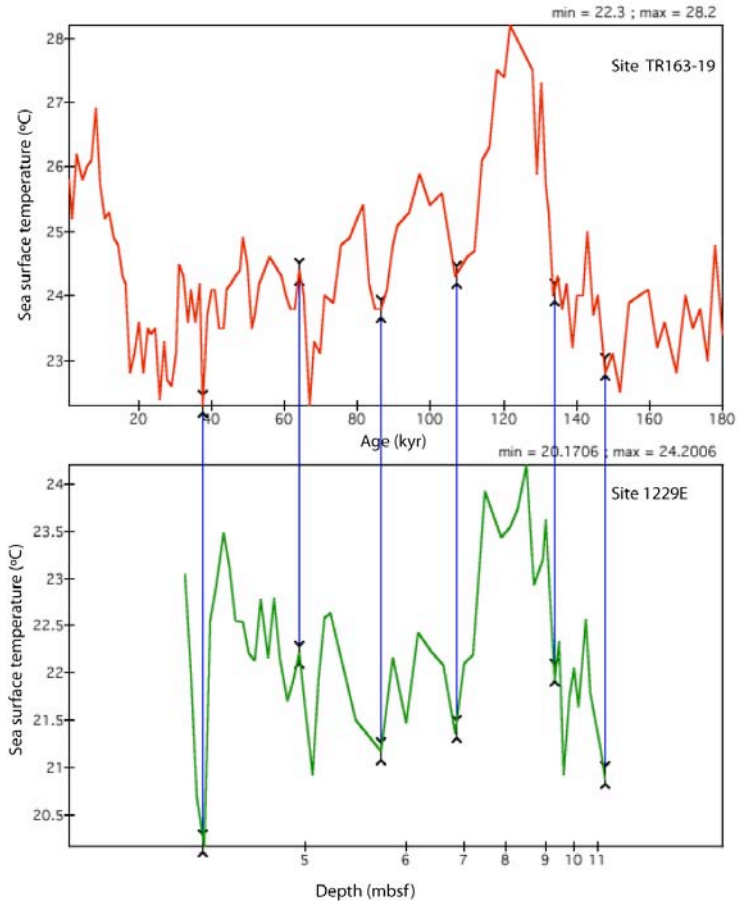

Supplementary Figure 6.2. Sea surface temperature match between core TR163-19 (upper panel, in age scale), vs. SST at ODP Site 1229E (lower panel, in depth scale). Please note that the tuning points at 9 and 11.3 mbsf from the Schrader record (see Table 6.1) fit within the SST match between cores.

Sedimentation rates during the late Holocene

The LH (last 3kyr) was characterized by elevated sedimentation rates (70-100 cm/kyr) and low sediment compaction. Very high sedimentation rates for the last 2-3 kyr have been reported not only for the Site 1229 but also for nearby ODP Site 1228 from Leg 201 (Skilbeck and Fink, 2006; Makou et al., 2010). Moreover, farther south Rein et al. (2004) reported sedimentation rates of 110 cm/kyr (around 12°S; 180m water depth) during the LH (<3 kyr).

The sedimentary record of the LH in the area (Sites 1229 and 1228) is characterized by non-consolidated diatom-rich clays, high organic-carbon content, and the lack of a small calcitic

component, related to the absence of nannofossils that are present in older times (Shipboard Scientific Party, 2003). One explanation for the high sedimentation rates was given by Wefer et al. (1990) and Shipboard Scientific Party (2003) as the effect of lack of compaction, compared to older sediments. However, porosity and water content estimations (Shipboard Scientific Party, 2003) do not show significant differences between LIG and LH values. Another explanation could be winnowing and reworking. However, radiocarbon dating from organic matter of the LH (<3 kyr) in this record (Site 1229) and Site 1228 (located at < 5 km of distance) do not show evidence of reworking or winnowing (Skilbeck and Fink, 2004; Makou et al., 2010). Considering above the most plausible explanation for the elevated sedimentation rates of LH would be enhanced sediment focusing (I.e. syndepositional sediment redistribution by bottom currents) and high TOC exportation from surface waters due to increased upwelling strength.

Although a detailed explanation of the sediment accumulation during the late Holocene is beyond the scope of our study, elevated sedimentation rates might affect the export productivity proxy and enhance preservation of lipid biomarkers. In this respect, high primary productivity inferred from high TOC values during late Holocene is also supported by paleo-productivity estimates based on marine planktonic diatoms (same ODP site) and benthic foraminifer assemblages (Figure 6.2g). Moreover, a strengthened productivity during the late Holocene was recently reported by Makou et al. (2010) using lipid biomarkers at ODP Site 1228. Therefore, we are confident that the increase in TOC during the late Holocene reflects higher export marine productivity in the area.

TOC content and lipid analysis

Total organic carbon (TOC) contents were determined with a Carlo Erba NA-1500 elemental analyzer. Freeze-dried sediments (1-1.5 g) were ultrasonically extracted twice with methanol, dichloromethane:methanol [1:1(vol/vol)], and dichloromethane to obtain the total lipid extract. Aliquots of the total extracts were separated into non-polar and polar fractions by column chromatography after the addition of an internal standard (a mixture of 1-nonadecanol, nonadecanoic acid, 5 alfa-cholestane, and hexatriacontane). The total lipid fractions were methylated with diazomethane and silylated with N,O-bis(trimethylsilyl) trifluoroacetamide in pyridine and then analyzed by GC and GC-MS (Trace GC-MS; Thermo Finnigan) for lipid identification and quantification. All lipid abundances were normalized by TOC (microg g-1 TOC). Repeated concentration measurements were within ±10%.

The alkenone unsaturation index (Uk'_{37}) was calculated with the peak areas of the di- and triunsaturated C37 methyl alkenones using the ratio (C37:2)/(C37:2 + C37:3) (Prahl et al., 1988). To reconstruct the sea surface temperatures, we used the global calibration derived by Müller et al. (1998); Uk'_{37}= 0.033T + 0.044.

The (lycopane+n-C35)/n-C31 ratio was calculated to asses past oxygen exposure during sediment deposition and its effect on biomarker preservation (Table 6.2). Lycopane is preserved under suboxic conditions and is highly prone to oxic degradation in Peruvian surface sediments (Sinninghe Damste et al., 2003a). Lycopane has a higher abundance relative to terrestrial n-alkanes under suboxic conditions and coelutes with the n-C35 alkane. Therefore, its presence was confirmed by GC-MS.

Diatom community analysis

About 1 g of wet sediment was treated according to the technique described by Schrader and Gersonde (1978). Permanent slides of acid-cleaned material were prepared by placing a defined sample volume (0.2 ml) onto a microscope slide, air-drying, and mounting with

Naphrax mounting medium. Two permanent slides were prepared per sample using this method. Diatoms were identified and counted at magnifications of 400 X and 1000 X using a Zeiss-Axioscope 2 plus microscope with phase-contrast illumination. Several transects across each cover slip were examined, depending on microorganism abundances. At least two cover slips per sample were examined in this way. About 300 valves were counted for each cover slip. The counting procedure and definition of counting units for diatoms followed those of Schrader and Gersonde (1978). The freshwater diatom community included the following species: *Cymbella affinis*, *Diploneis subovalis*, *Staurosira construens*, *Rhopalodia musculus*, *Nitzschia paleacea*, and *Nitzschia fonticula*.

Multiple Regression Analysis

Multiple regressions were calculated (Supplementary Table 6.2) on the raw data in the Statistica 6.0 program to identify sources (i.e. marine and terrestrial) and variability between bulk and lipid biomarker data.

Supplementary Table 6.2. Multiple correlations among marine and terrigenous biomarkers between 145 and 35 kyr; significant correlations ($p < 0.05$) are marked with (*) and the highest (>0.5) correlations with (**).

				Marine				Terrigenous			
n = 49	TOC	Lycopane Ratio	Alkenone SST	Alkenone $C_{37:2+C37:3}$	1.15-C_{30} diol	1.14-C_{28} Alkyl diol	C_{27}-12-hydroxy Methyl alkanoate	n-alkanes C_{25} to C_{35}	n-alcohols C_{24} to C_{28}	Alfa-amyrin	Taraxerol
TOC											
Lycopane Ratio	0.44*										
Alkenone SST	0.04	-0.24									
Alkenone $C_{37:2+C37:3}$	0.57**	0.28	0.29*								
1.15-C_{30} diol	0.21	0.39*	0.15	0.23							
1.14-C_{28} Alkyl diol	0.13	-0.04	0.61**	0.34*	0.31*						
C_{27}-12-hydroxy Methyl alkanoate	0.01	-0.07	0.61**	0.23	0.26	0.91**					
n-alkanes C_{25} to C_{35}	0.08	-0.08	0.62**	0.57**	0.36*	0.68**	0.64**				
n-alcohols C_{24} to C_{28}	0.33*	0.21	0.44*	0.65**	0.63*	0.47**	0.33*	0.69**			
Alfa-Amyrin	-0.14	-0.23	0.60**	0.31*	0.39*	0.73**	0.72**	0.82**	0.61**		
Taraxerol	0.06	-0.02	0.48*	0.12	0.34*	0.59**	0.58**	0.43*	0.32*	0.58**	

Interpretation of multiple correlations among terrigenous and marine biomarkers

The highest Pearson correlation coefficient (r = 0.91) among marine biomarkers was found between 1,14-C28 alkyl diol and 12-hydroxy methyl alkanoate relative abundances because both marine biomarkers derive from the same source, the *Proboscia* diatoms (Sinninghe Damste et al., 2003b). The high positive and significant correlations among terrestrial biomarkers confirmed their common origin (i.e. river transported organic matter) in the area (Volkman et al., 1987).

The lack of significant correlations of 1,14-C28 alkyl diol and C27-12-hydroxy methyl alkanoate with TOC and with the lycopane ratio indicates that the downcore variations in *Proboscia* biomarker abundances are not the result of changes in past oxygen exposure and/or organic carbon accumulation. Instead, there is significant positive correlation with alkenone-derived SST (>0.60) and terrigenous biomarker abundance (e.g. alfa-amyrin: >0.70 and n-alkanes: >0.60) indicating that higher *Proboscia* diatom abundances are related to higher SSTs and terrigenous input during the LIG.

Detailed discussion and interpretation of non-TOC normalized biomarker abundances and accumulation rates.

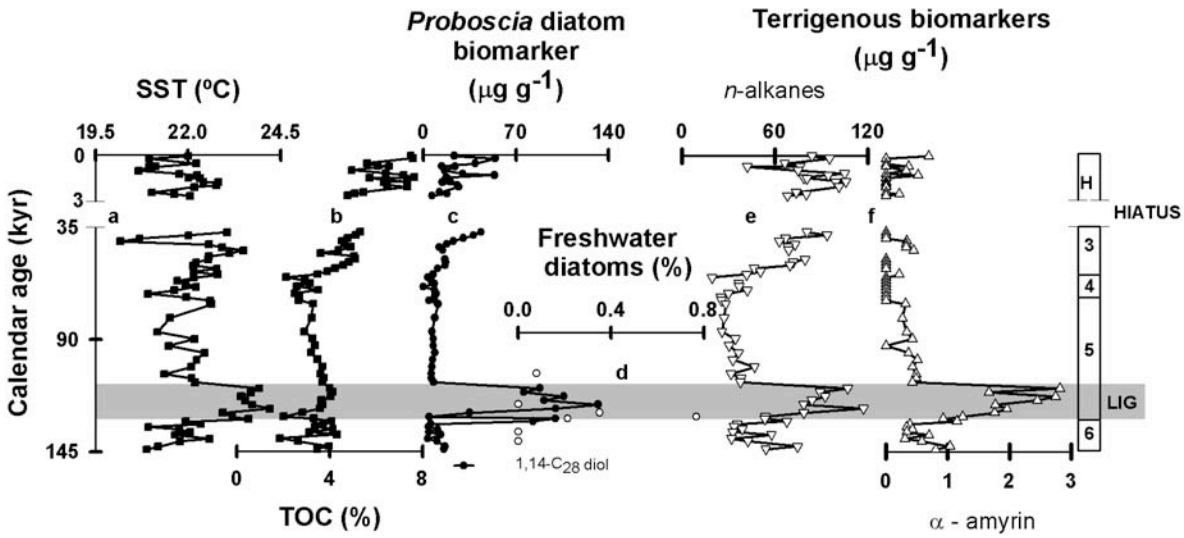

Supplementary Figure 6.3. In Figure 6.2, all biomarker abundances were normalized by TOC in order to deduce changes in biomarker concentration that are not governed primarily by organic matter delivery or preservation. To complement this information, we also show the non-TOC normalized biomarker data on this figure.

Although enhanced TOC and export productivity with elevated sedimentation rate (about 75 cm/kyr) in the late Holocene may hide changes in the lipid biomarker abundances, *Proboscia* biomarker abundance (1,14 C_{28} diol) (Supplementary Figure 6.3c) does not follow the TOC record (Supplementary Figure 6.3b) and never reaches the high values of the LIG. *Proboscia* biomarkers were major components of the total lipid extracts during the entire LIG interval and that was not the case for the sediments deposited during the late Holocene.In fact, the few enhanced values in the late Holocene might be related to sporadic events involving water column stratification in the area, but never as prolonged as for the LIG. Late Holocene accumulation rates (2601 ± 1990 μg/m.kyr) of *Proboscia* biomarkers (E.g. 1,14 C_{28} alkyl diol) were similar to LIG accumulation rates (1134 ± 583 μg/m.kyr) if we consider the high standard deviation, the 10 times higher sedimentation rates and elevated TOC values during LH compared with LIG.

The non-TOC normalized long-chain n-alkanes (terrigenous biomarker) (Figure A3e) follow the trend of TOC (Supplementary Figure 6.3b), increasing after the end of MIS 5 and with values in the LH as high as the LIG. The high values during the LH (Supplementary Figure 6.3e) could be wrongly interpreted as high fluvial input. However, as mentioned above, n-alkanes have a dual source (eolian and fluvial) and they should not be interpreted as fluvial input solely without considering the alfa-amyrin and taraxerol trends. The highest alfa-amyrin abundances (Figure A3f), indicating wetter conditions, are found during the LIG and do not follow the TOC record. In addition, taraxerol was absent in late Holocene samples. Wetter conditions during the LIG are not only supported by increased abundances of mainly fluvial transported biomarkers (alfa-amyrin and taraxerol) but also by the abrupt occurrence of freshwater diatoms indicating river runoff close to the Site 1229 (Supplementary Figure 6.3d).

We also estimated accumulation rates given the different sedimentation regimes between the LIG and the LH. Higher accumulation rates of n-alkanes (9955 μg/m.kyr) characterize the late Holocene compared with the LIG (1145 μg/m.kyr). Alfa-amyrin was present in only a few samples during the LH with an average accumulation rate lower (11 μg/m.kyr) than the LIG (25 μg/m.kyr). We interpret the more pronounced accumulation of n-alkanes during the late Holocene as a response of higher eolian rather than fluvial input. This fits with the scenario proposed for the late Holocene of colder SSTs due to strengthing of the cold coastal wind

driven upwelling and concomitant increase in primary productivity. Thus, drier conditions during the late Holocene than the LIG are supported not only by low alfa-amyrin abundance and accumulation rate but also by the lack of taraxerol in the Holocene record.

APPENDIX 3

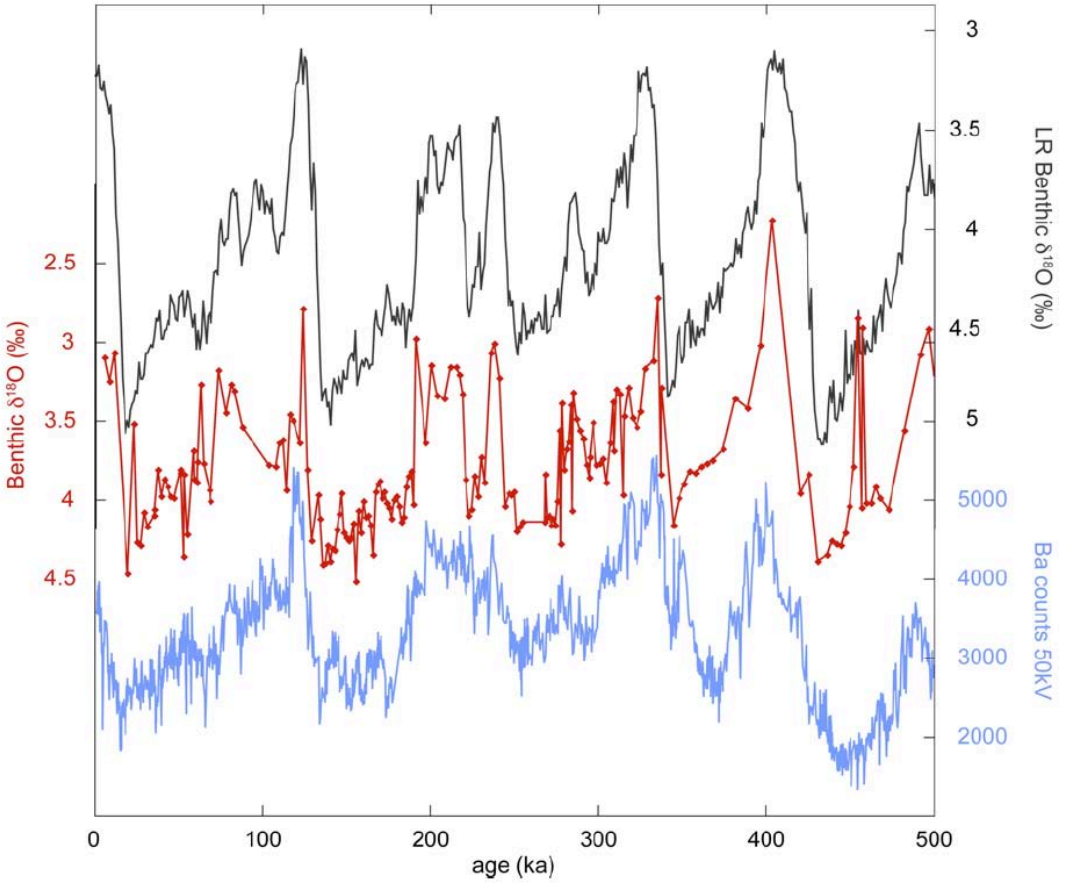

Supplementary Figure 7.1. Age model of ODP Site 1237. Alignment of the benthic $\delta^{18}O$ record from ODP site 1237 (red) to the LR04 stack (black), both in (‰), as refined with the Ba-counts (blue) of ODP Site 1237 XRF scans. For the benthic $\delta^{18}O$ record from ODP site 1237 different species had to be used: *Cibicidoides wuellerstorfi*, *Uvigerina peregrina*, *Uvigerina hispida*. The values obtained for the Uvigerina species were adjusted to *C. wuellerstorfi* by subtracting 0.64.

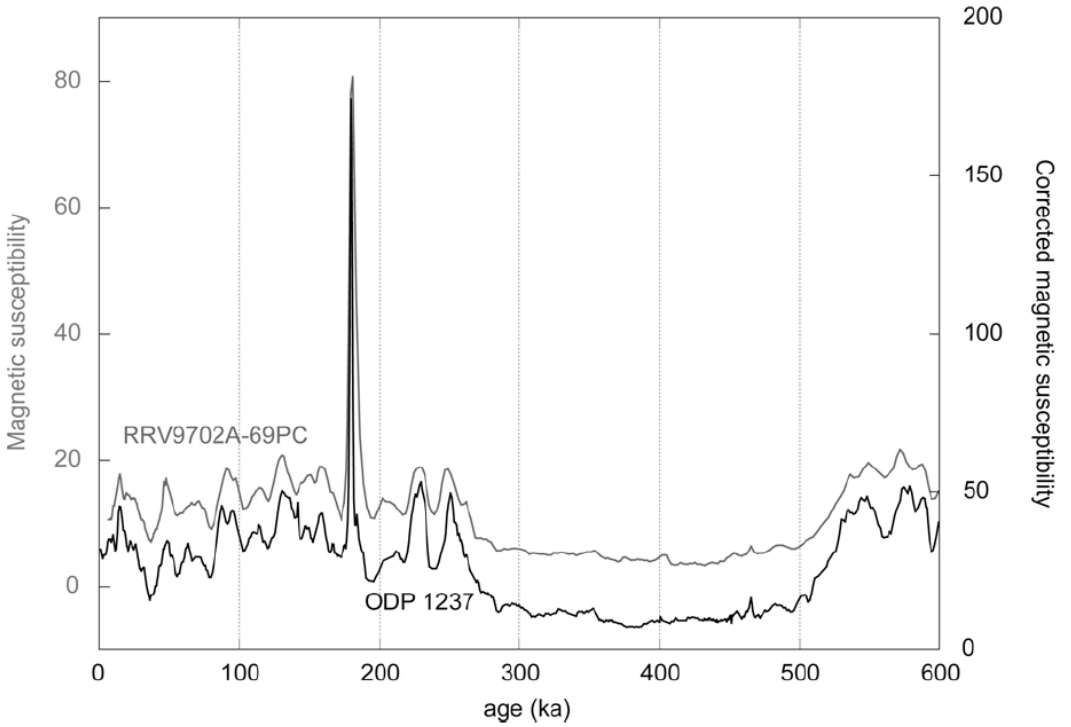

Supplementary Figure 7.2. Alignment of sediment cores investigated in this study. Magnetic Susceptibility of ODP Site 1237 (black) and RRV9702A-69PC (grey). The age model of ODP Site 1237 was thus used for pre-site survey core RRV9702A-69PC. The peak at ~180 ka represents an ash layer present in ODP 1237 boreholes A and C, as well as RRV9702A-69PC.

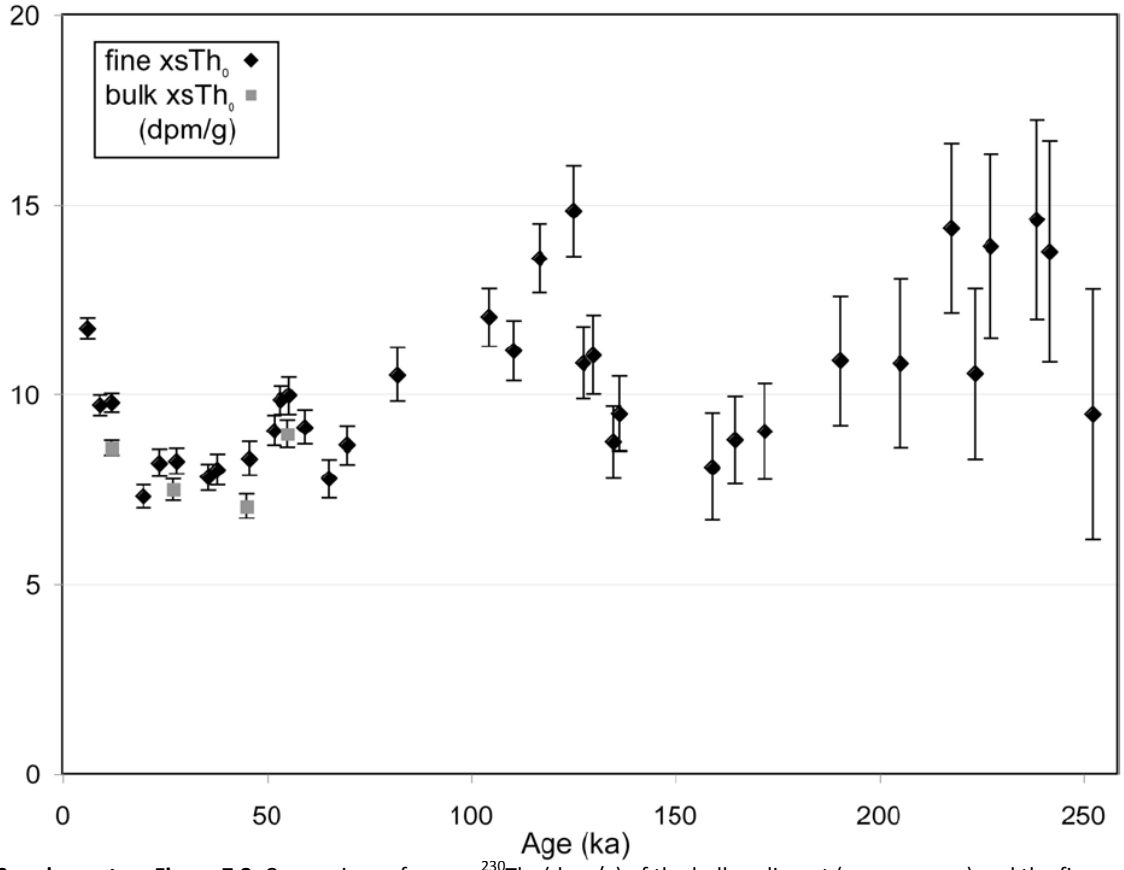

Supplementary Figure 7.3. Comparison of excess $^{230}Th_0$ (dpm/g) of the bulk sediment (grey squares) and the fine fraction (black diamonds). Error bars are shown for both, representing propagated errors associated with the calculation of the initial unsupported ^{230}Th concentration.

Methodology: Th-profiling

Due to a lack of sample material, the fine fraction collected after washing the samples over 63µm – meshes was collected to analyze them for their excess $^{230}Th_0$ and ^{232}Th concentrations. Most of the Thorium sinks to the ocean floor attached to the fine fraction <20µm (cf. Kretschmer et al. 2010). The values for the bulk fraction are thus slightly decreased compared to the fine fraction, as the concentration in the bulk fraction is lower as expected, in our case by about 10%. However, we consider the disparity negligible for our interpretations.

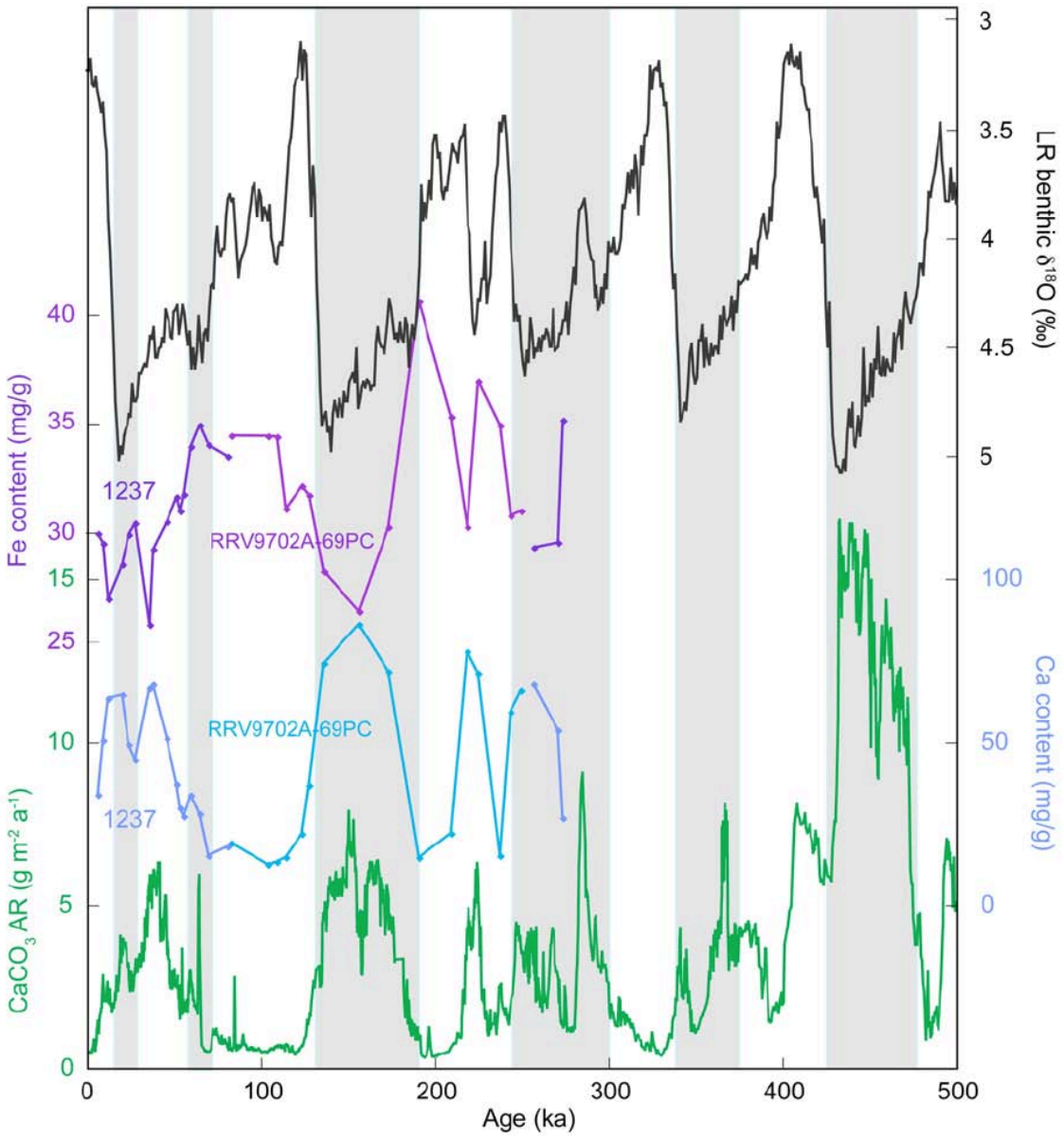

Supplementary Figure 7.4. **a** LR04 stack (black), **b** Iron (Fe) content (mg/g) (purple), **c** Calcium (Ca) content (mg/g) (blue) and **d** $CaCO_3$ mass accumulation rates (mg cm^{-2} ka^{-1}) (green) of ODP site 1237. Glacials are indicated with light blue bars. Ca-contents agree very well with $CaCO_3$ ARs, while Fe-contents are in anti-phase to both Calcium records. This is due to the $CaCO_3$ dissolution effect. Where $CaCO_3$ is well preserved, it dilutes the terrigenous sediment components, in this case Fe.